https://ntrs.nasa.gov/search.jsp?R=19710027897 2020-03-11T21:41:53+00:00Z

General Disclaimer

One or more of the Following Statements may affect this Document

- This document has been reproduced from the best copy furnished by the organizational source. It is being released in the interest of making available as much information as possible.

- This document may contain data, which exceeds the sheet parameters. It was furnished in this condition by the organizational source and is the best copy available.

- This document may contain tone-on-tone or color graphs, charts and/or pictures, which have been reproduced in black and white.

- This document is paginated as submitted by the original source.

- Portions of this document are not fully legible due to the historical nature of some of the material. However, it is the best reproduction available from the original submission.

Produced by the NASA Center for Aerospace Information (CASI)

N71-37373
(ACCESSION NUMBER)
185
(PAGES)
CR-72887
(NASA CR OR TMX OR AD NUMBER)
FACILITY FORM 602
(THRU)
63
(CODE)
28
(CATEGORY)

PRECEDING PAGE BLANK NOT FILMED

FOREWORD

The program described herein was conducted by the Pratt & Whitney Aircraft Division of United Aircraft Corporation, East Hartford, Connecticut. Roger M. Hawkins was Project Manager for Pratt & Whitney Aircraft. The work was performed under management of NASA Project Manager Mr. D.P. Townsend from June 1965 to November 1968, and was completed under NASA Project Manager Mr. L.P. Ludwig of the Fluid System Components Division at Lewis Research Center.

Because of the quantity of data assembled in the course of this program, it has been necessary to prepare the report in two parts. Part I (NASA CR-72819)contains the analytical work performed on compressor end and interstage seals. Part II describes the results of testing the compressor seals, an analysis of two improved self-acting compressor seal designs, and the analysis and testing of the stator pivot seals.

The authors wish to express their appreciation to Messrs. C.A. Knapp, H.L. Northup, P.E. Nicholich, H. Schaffer, P.R. Lawell, R.E. Turley, P.A. Rubenstein, and W.J. Walker for their assistance in the preparation of material for this report. Appreciation is also expressed to Mechanical Technology Incorporated for their assistance in conducting an analytical program contributing to the feasibility analyses of the seals developed under this contract.

CR-72887
PWA-4059

FINAL REPORT

DEVELOPMENT OF COMPRESSOR END SEALS STATOR INTERSTAGE SEALS, AND STATOR PIVOT SEALS IN ADVANCED AIR BREATHING PROPULSION SYSTEMS

PART II

by

R. M. Hawkins and A. H. McKibbin

PRATT & WHITNEY AIRCRAFT
EAST HARTFORD, CONNECTICUT

prepared for
NATIONAL AERONAUTICS AND SPACE ADMINISTRATION

November 24, 1970

NASA LEWIS RESEARCH CENTER
CONTRACT NAS3-7605
Cleveland, Ohio
L.P. Ludwig, Project Manager

Air-Breathing Engine Procurement Center

PRECEDING PAGE BLANK NOT FILMED

ABSTRACT

The results of the program are reported in two volumes. Part I covers screening studies and analysis on 28-inch diameter seals (rotating), and Part II covers experimental work on the 28-inch diameter seals and on small vane pivot seals (oscillatory). Analysis on 28-inch diameter seals revealed that flexible surfaces or high gas film stiffness was necessary to accommodate expected thermal and mechanical deformations. Mathematical models of general usefulness to seal design were developed. Dynamic testing of the four seals selected for evaluation was limited by failure attributed to loss of dimensional tolerances. Based on results two self-acting seals were designed to obtain reduced sensitivity to seal deformation. Stator pivot seals were designed, fabricated and evaluated at temperatures to 1000°F. Lower leakage rates than possible with current seal design were obtained. Actuation torque was greater than anticiapted.

PRECEDING PAGE BLANK NOT FILMED

TABLE OF CONTENTS

TABLE OF CONTENTS (Cont'd)

LIST OF ILLUSTRATIONS

LIST OF ILLUSTRATIONS (Cont'd)

LIST OF ILLUSTRATIONS (Cont'd)

LIST OF ILLUSTRATIONS (Cont'd)

LIST OF ILLUSTRATIONS (Cont'd)

LIST OF ILLUSTRATIONS (Cont'd)

LIST OF ILLUSTRATIONS (Cont'd)

LIST OF ILLUSTRATIONS (Cont'd)

LIST OF ILLUSTRATIONS (Cont'd)

LIST OF TABLES

SUMMARY

This report presents the work accomplished under Contract NAS3-7605 from its initiation on 25 June 1965 to completion of the technical program on 23 October 1970. Specific objectives of the program were to demonstrate the feasibility of gas-film riding compressor end and interstage seals and to demonstrate satisfactory stator pivot sealing. The results of this program are reported in two volumes: Part I is entitiled Screening Studies and Analysis and Part II is entitled Experimental Data and Analysis. The pivot seal work is reported in Part II.

Task I was a concept feasibility analysis program for compressor end seals and interstage seals. The work of Task I was divided into a screening study and two sets of feasibility analyses. The screening study determined the most promising concepts and the feasibility analyses examined the better concepts in some detail. At the end of the first set of feasibility analyses it was recognized that seal tracking was of critical importance. Estimates at that time indicated that the combined effects of manufacturing tolerances, thermal distortions and mechanical distortions would produce a maximum runout of 5 mils in the seal runner, while gas film thickness was estimated to be a nominal 1 mil. These conditions implied that the seal would have to be extremely flexible to conform to runner waviness, or that the gas-film stiffness would have to be extremely high to support the seat at the high points of the runner. The analyses revealed that the combined hydrostatic-hydrodynamic (hybrid) gas film provided the highest stiffness for the operating range. Therefore, variation of the hydrostatic-hydrodynamic concept was used in all selected designs.

In the course of this program it was necessary to identify and analyze seal problem areas which had received little attention in previously published work on seal technology.

Mathematical models that have general usefulness in seal technology were developed and analyzed for the following problem areas:

1. Primary ring tracking of seat face runout
2. Self-acting seal geometries
3. Seal dynamic axial motion (vibration)
4. Minimum gas film thickness as related to deformation and dynamic effects
5. Leakage and pressure distribution over a narrow seal dam.

Much of the above mathematical analysis is in the form of computer programs and are reported in detail in the semi-annual reports. In particular, the self-acting seal computer program is now being used by various seal manufacturers.

Analysis revealed that the segmented (floated-shoe) seals provided the highest degree of flexibility. Two concepts were recommended and accepted for final design and testing. These two concepts were termed the one side floated shoe end seal and one side floated shoe interstage seal.

Two continuous ring seals were also recommended and accepted for final design and testing. These concepts were termed the OC diaphragm end seal, and the semirigid interstage seal.

The four seal concepts recommended were subjected to a final design study and fabricated. These seals were 27 to 28 inches in diameter and therefore suitable for application to compressors in large engines. Static and dynamic test rigs were also designed and fabricated for experimental evaluation of the seals. Static tests covered overall seal leakage rates, secondary-seal leakage rates, static lift-off characteristics, and the dimensional stability of seal components under representative pressure loadings. In addition, the effects of actual manufacturing tolerances on seal behavior were evaluated.

Dynamic testing of the seals was limited by mechanical failures of the seals resulting from difficulties in obtaining and preserving the necessary dimensional tolerances. Since the basic design analysis techniques developed under the program have been applied successfully in smaller seals, it was concluded that the feasibility of large gas-film seals depends on the following: (a) decreasing seal deformation and tolerance variation through improvements in seal design, manufacturing and material dimensional stability; (b) decreasing seal sensitivity to face deformation.

In the final part of the program two self-acting seal concepts were designed and analyzed for performance. The self-acting concepts were selected because testing on mainshaft seals revealed: (a) that the self-acting concept was far less sensitive to face deformation than hydrostatic seals and (b) that it had a performance capability far greater than conventional face seals currently used. (This analysis is reported in Part II.) Rotors for these self-acting seals were fabricated and manufacturing of the remaining seal structure is under Contract NAS3-14409.

Task III was a feasibility analysis of stator pivot bushing and seal concepts. Twelve different concepts were screened, but ten of these were discarded because of excessive leakage, the effects of dirt, the effects of load deflection, inherent reliability, weight, space, design simplicity, and other considerations. Feasibility analyses were conducted for a single-bellows concept and a spherical-seat concept: the results showed that both had the potential to provide substantial improvement over the baseline seal. Both concepts were approved for final design and testing under Task IV.

Task IV provided for final design and procurement of two seals of each design, design and fabrication of a test rig, and experimental evaluation of the seal assemblies. The seals were subjected to a test program which simulated takeoff for 20 hours and cruise for 20 hours. Later, the seals were subjected to a cyclic endurance run of 40 hours. The takeoff and cruise simulations provided conditions typical of advanced engine designs. Both the single-bellows seal and the spherical-seat performed well, but the spherical-seat seal produced somewhat higher leakage and was more subject to wear. It was found that both designs required a rather high actuation torque, and further development to reduce the torque is recommended.

I. STATIC TEST FIXTURES

Two static test fixtures were designed and fabricated to perform room-temperature static tests on the compressor end and interstage seals. One fixture was provided for the interstage seals (see Figure 1) and the other fixture was provided for the end seals (Figure 2). The fixtures allowed visual examination of the bore of each seal, and permitted measurement of pressures in the seal cavities. Adapter rings were provided with the fixtures to allow air leakage past the secondary piston rings to be measured separately from all other leakage paths. The static fixture back plates (simulating the seal runner) were manufactured flat and true within practical manufacturing tolerances to represent the best practice expected in an aircraft engine. Photographs of the static fixtures are shown in Figures 3 and 4.

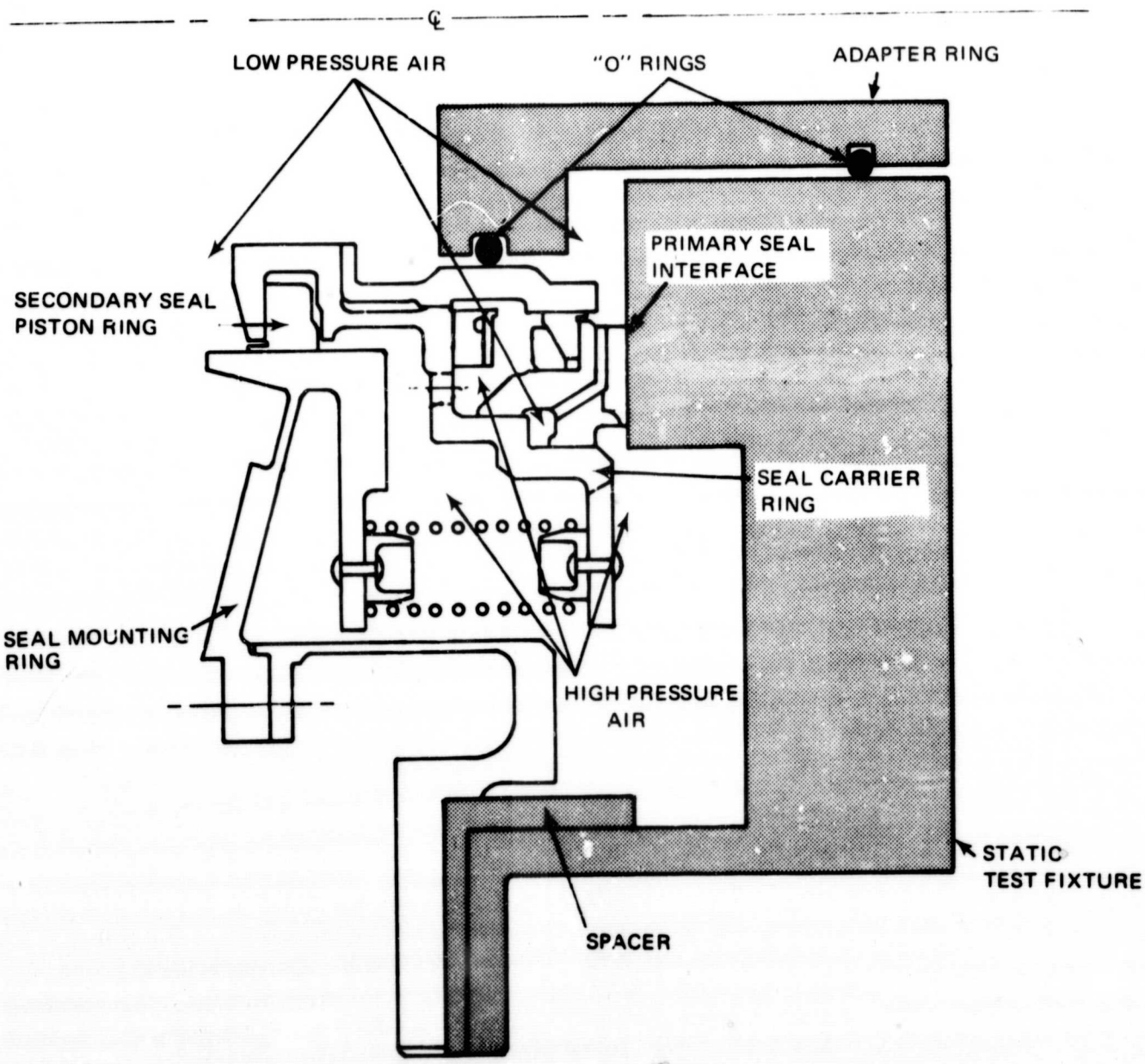

Figure 1 Cross Section of Fixture for Static Test of the One-Side Floated-Shoe Interstage Seal

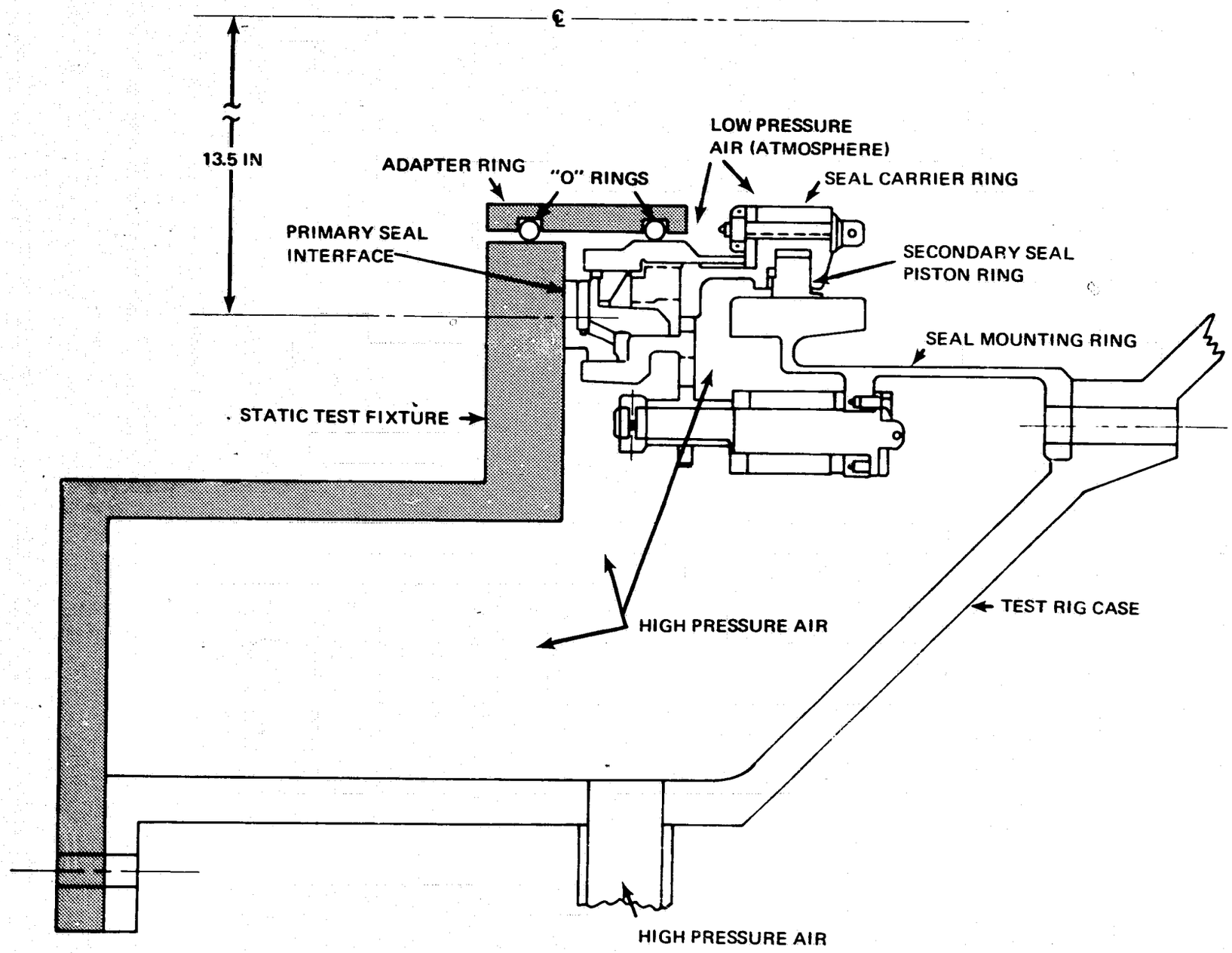

Figure 2 Cross Section of Fixture for Static Test of the One-Side Floated-Shoe End Seal

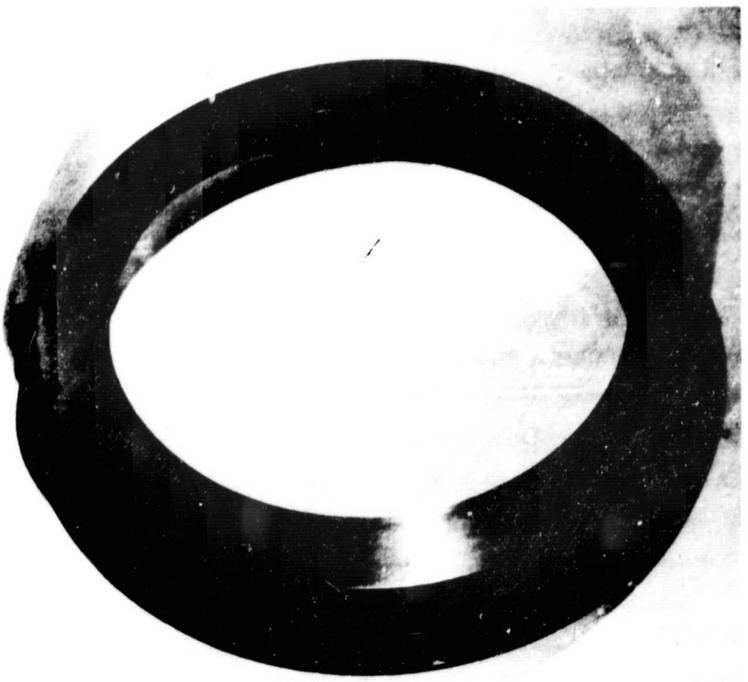

Figure 3 End Seal Static Fixture (XPN-14195)

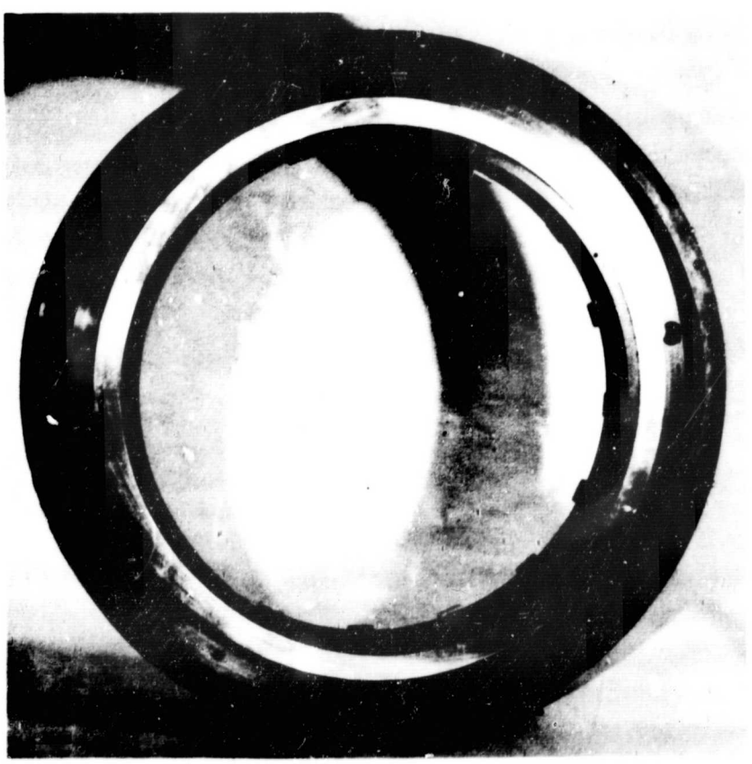

Figure 4 Interstage Seal Static Fixture (XPN-14193)

PRECEDING PAGE BLANK NOT FILMED

II. COMPRESSOR SEAL TESTING IN STATIC FIXTURES

Task VII of the program provided for room-temperature static tests of the four compressor seals designed and manufactured under Tasks I and II of this contact. Pratt & Whitney Aircraft investigated overall seal leakage rates, secondary-seal leakage rates, static lift-off characteristics, and the dimensional stability of seal components under representative pressure loadings. In addition, the effects of practical manufacturing tolerances on seal behavior were evaluated, providing a basis for judgements as to the tolerances and inspection techniques required for successful compressor seals of the gas-film type. The static test fixtures for this work were provided under Task VI of this contract.

A. ONE-SIDE FLOATED-SHOE END SEAL

The design and fabrication of the one-side floated-shoe end seal are described in Part I of this report. Under Task VI, the static fixture was fabricated to permit several checks on the test seal which could not be performed in the test rig. The static test fixture was designed to allow visual examination of the bore of the seal (including the seal shoe segments) and to allow the measurement of pressures and pressure drops in various regions of the seal. An adapter ring was designed for the fixture to allow a separate measurement of the leakage past the secondary seal piston ring. The fixture was also supplied with internal illumination to allow visual checks to ensure that there were no gross leakage paths past the primary or secondary seals.

For the first test of the one-side floated-shoe end seal in the static test fixture (Figure 2) ambient air calibration runs were made to determine whether the fixture would duplicate the rig conditions. The results, which are compared with rig results in Figure 5, show that the fixture provided data very similar to that from the full-scale test rig. Figure 5 also shows the corresponding apparent air-film thickness as measured by the proximity probes.

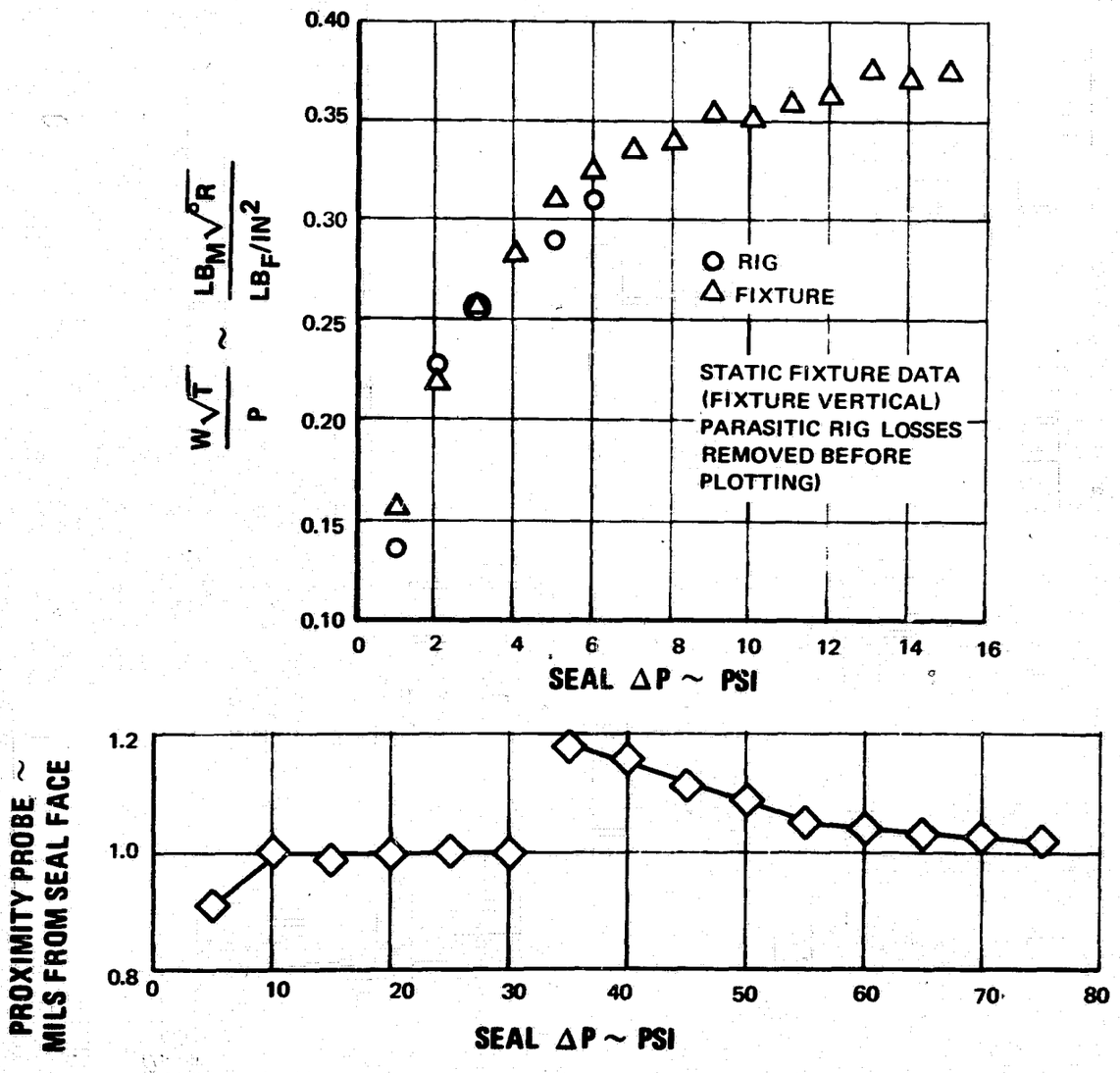

Figure 5 One-Side Floated-Shoe End Seal, Ambient Air Calibration at Static Conditions, Seal in As-Received Condition

As pressure was gradually increased, the seal carrier ring suddenly moved axially about 1/8 inch away from the seal runner. A corresponding jump occurred in the reading of the proximity probes. This jump is illustrated in Figure 5. Because the seal segments were not attached rigidly to the carrier, their movement was much less than the carrier's. When pressure was reduced, the carrier returned to its normal position. The jump away from the seal runner was explained as the result of excessive leakage, causing a pressure imbalance resulting in a new force pushing the seal carrier ring back.

A 2-mil feeler gauge was used to check the separation between the shoe seal segments and the seal runner. The gauge could be inserted at the inner edge of the shoes and pushed halfway across the shoe toward the outer edge, indicating that the shoes were tilted An attempt was made to observe the tilt by shining a light on the outer edge of the shoe and observing the slit light pattern at the inner edge. However, no definitive conclusions could be drawn from the light patterns because of slight surface irregularities and edge diffraction effects.

Tactile examination of the leakage flow indicated excessive flow through the shoe low-pressure vent holes, and a lesser flow through the primary seal interface. The secondary seal piston ring with the rectangular cross-section had no discernible leakage.

The seal was removed from the fixture and disassembled. As shown in Figure 6, dust imprints of the shoe seal segments were clearly outlined on the fixture, with a heavy concentration about the outer edge. These dust imprints confirmed that the shoes were tilting in such a manner that a gap was created between the inner edge of the shoes and the seal runner.

Figure 6 Dust Imprints on the Seat from the One-Side Floated-Shoe End Seal (CN-16704)

To alleviate the tilting, a segmented thrust ring was fabricated to replace the one-piece ring formerly in use (see Figure 34, p. 27). The new segments allowed the beveled thrust rings to align themselves with greater precision. This change also allowed the spring radial load component against the shoe to be directed more positively toward the two secondary seal pads. In addition, eight low pressure vent holes were added to the existing three low-pressure

vent holes in each of the 24 shoes, 96 high-pressure bleed holes were added to the seal carrier ring, and the existing 48 high-pressure bleed holes were enlarged. However, a second test in the static fixture revealed that these modifications did not result in any significant reduction in static leakage (see Figure 7).

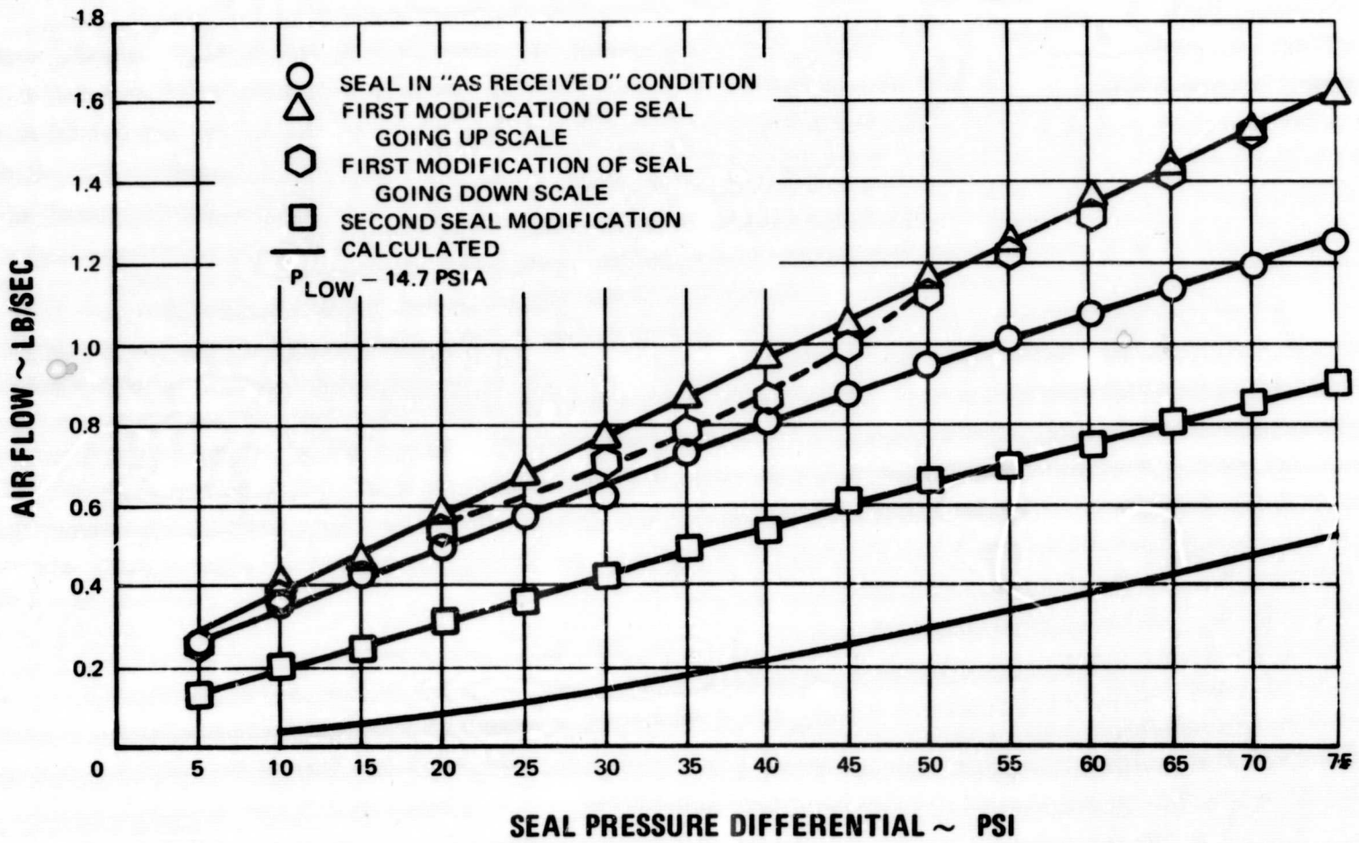

Figure 7 Ambient Air Calibrations of the One-Side Floated-Shoe End Seal

After the second test in the static fixture the seal was disassembled; inspection showed that key dimensions of the floated shoes were out of tolerance. At the same time, analysis of the seal showed that the widths of the secondary seal pads should be reduced to improve moment stability. Individual moment balances were calculated for each shoe, and the secondary sealing pads on the shoes were nickel plated and machined to achieve the calculated balance. This rework was planned so that minimum number of surfaces were remachined and so that machining the hardcoated surfaces was avoided, since the hardcoat was susceptible to chipping.

Figure 8 is a plot of the shoe's residual moment as a function of seal differential pressure. With the range of tolerances specified for the shoe rework, the residual moment on the shoes was between 0 and 0.005 in-lb/in at a seal pressure differential of 80 psi. At lower seal pressures, the residual moment became more positive, causing the primary seal film angles to increase in the convergent direction. Higher seal pressures cause divergent film angles. Con-

vergent film angles increase the opening force on the seal so small convergent angles are more desirable than small divergent angles. However, high film angles in either direction are detrimental to seal performance.

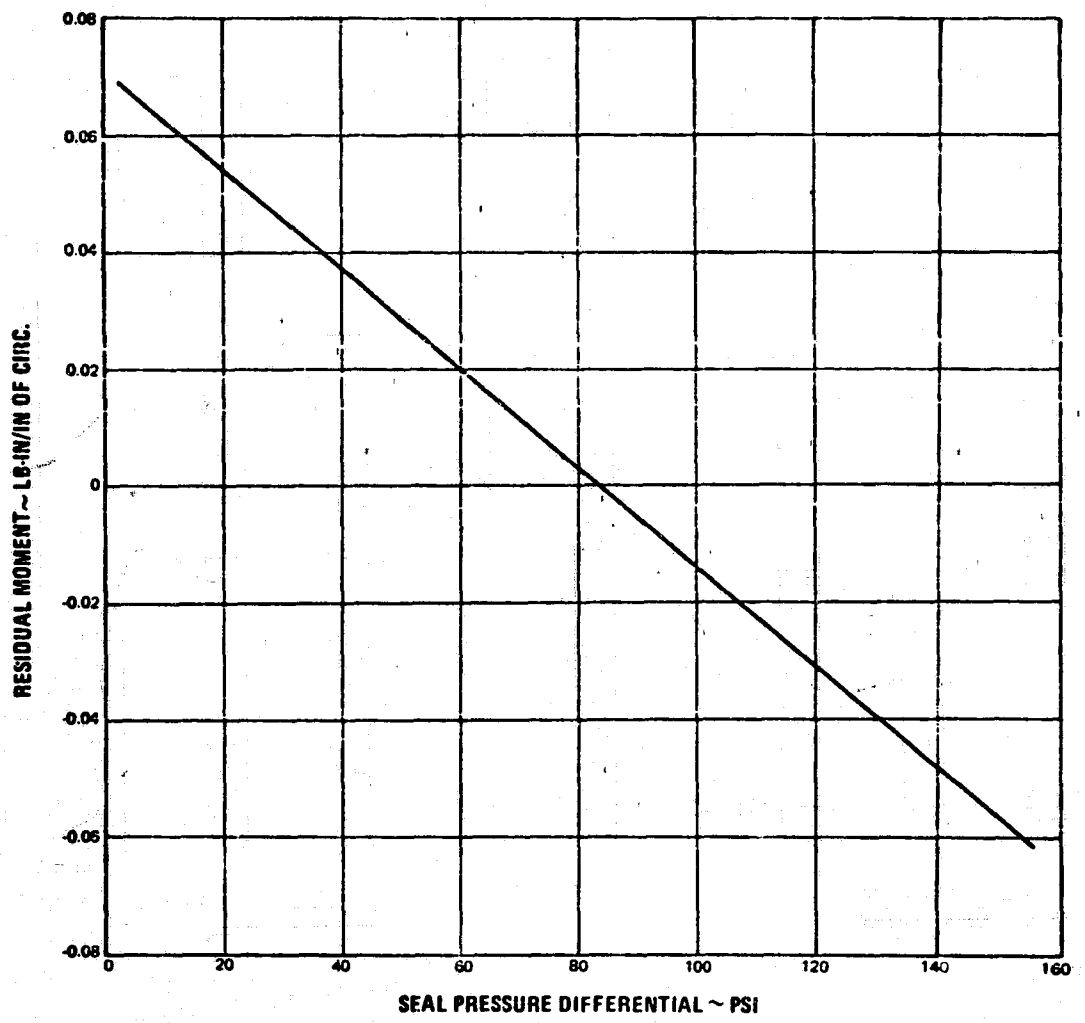

Figure 8 Residual Moment in the One-Side Floated-Shoe End Seal

The magnitude of the primary film angle can be estimated from a curve of restoring moment versus secondary seal film angle (or shoe rotation). Such a curve is shown in Figure 9 for a seal pressure differential of 80 psi, which corresponds to cruise power at altitude. The restoring moment increases linearly with shoe rotation to a point where the edge of the secondary seal is in contact with the carrier. This contact occurs at an angle of 0.59 milliradian and a moment of 0.006 in-lb/in. At higher shoe angles, the moment stiffness is much greater, as indicated by the curve labelled "Restoring Moment with Secondary Step Seal Edge Contact" in Figure 9. The slope of this curve varies with pressure across the seal, so that Figure 9 does not represent shoe angles at any other pressure. The moment stiffness varies linearly with pressure; however, the shoe angles at sea-level idle and sea-level take-off conditions were estimated to be 0.89 and -0.61 milliradian, respectively. The edge contact force will be 0.2 lb/in at both conditions. This level of edge contact load was not considered to be excessive for limited periods of operation.

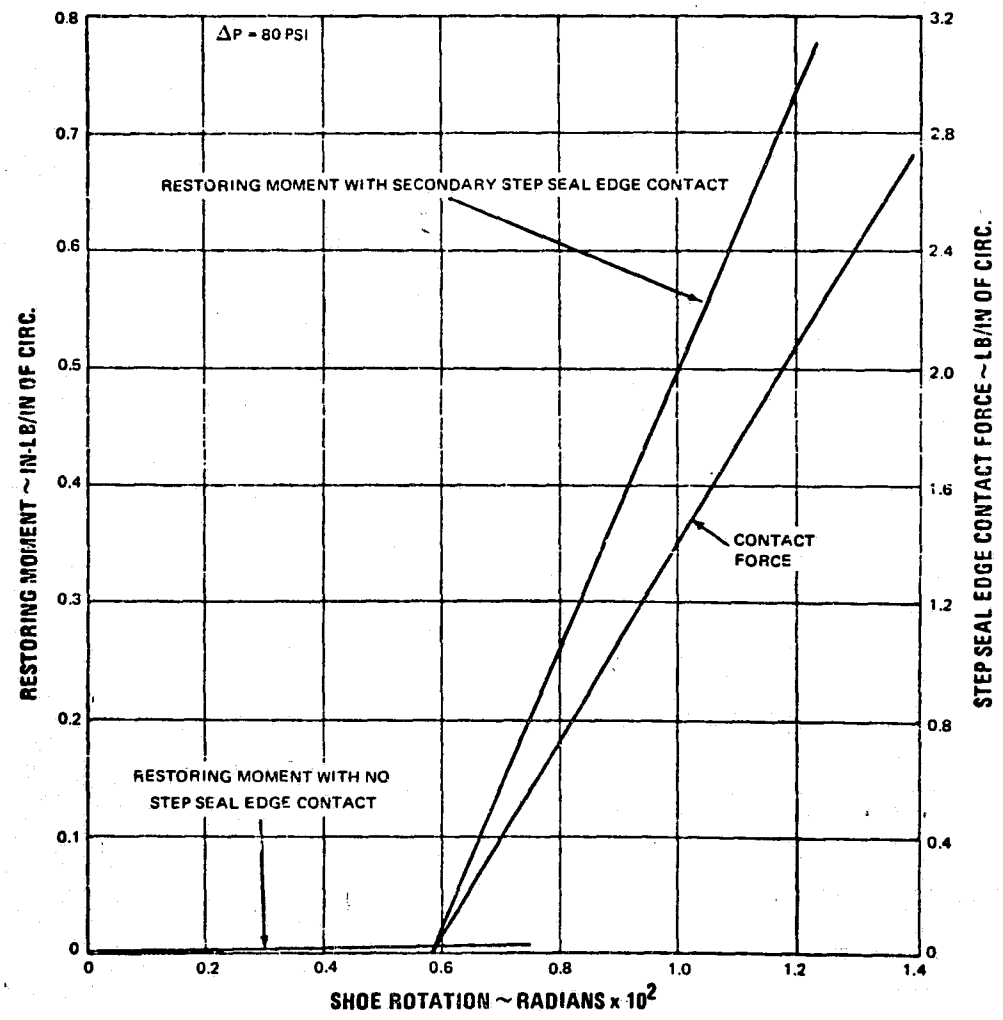

Figure 9 Secondary Step Seal Restoring Moment and Edge Contact Force in the One-Side Floated-Shoe End Seal

The refinishing was successful in reducing air leakage past the seal by an appreciable amount, as shown in Figure 7. An adapter ring was used to determine the leakage rate of the secondary piston-ring seal by sealing off all other leakage paths through the seal. Data from this test showed that the leakage rate past the piston ring was greater than the calculated value, but not of such magnitude as to adversely affect seal performance. The results of this test are shown in Figure 10. Following the test, the seal was prepared for installation in the full-scale test rig.

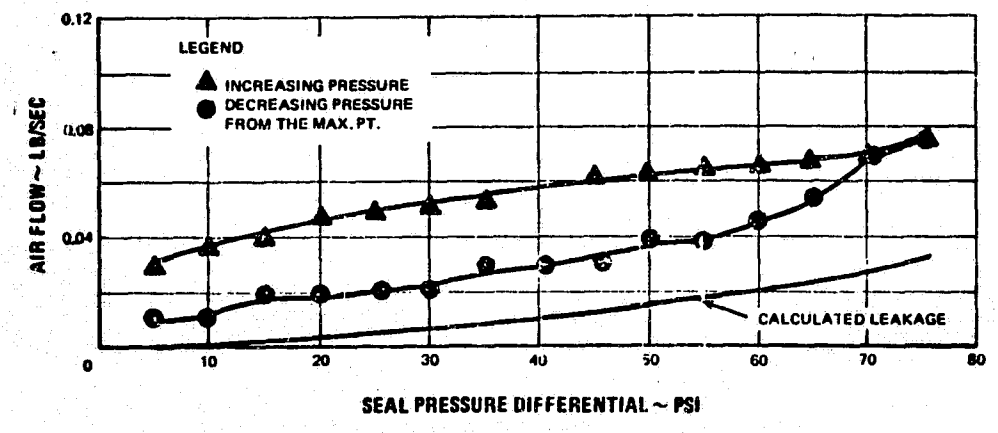

Figure 10 One-Side Floated-Shoe End Seal Secondary Piston Ring Static Calibration

B. ONE-SIDE FLOATED-SHOE INTERSTAGE SEAL

A schematic drawing of the one-side floated-shoe interstage seal is shown in Figure 79, p. 56. Like the end seal, static leakage past the one-side floated-shoe interstage seal in the as-received condition was too high to permit dynamic testing. To reduce the high static leakage, the interstage seal was modified in much the same way as the end seal: the thrust ring was segmented, vent holes were added to the shoes, existing bleed holes in the seal ring holder were enlarged, and additional holes were machined in the holder. Unlike the end seal, these modifications succeeded in substantially reducing static leakage, as shown in Figure 11. However, the improvement was not sufficient to reduce static leakage to the predicted level.

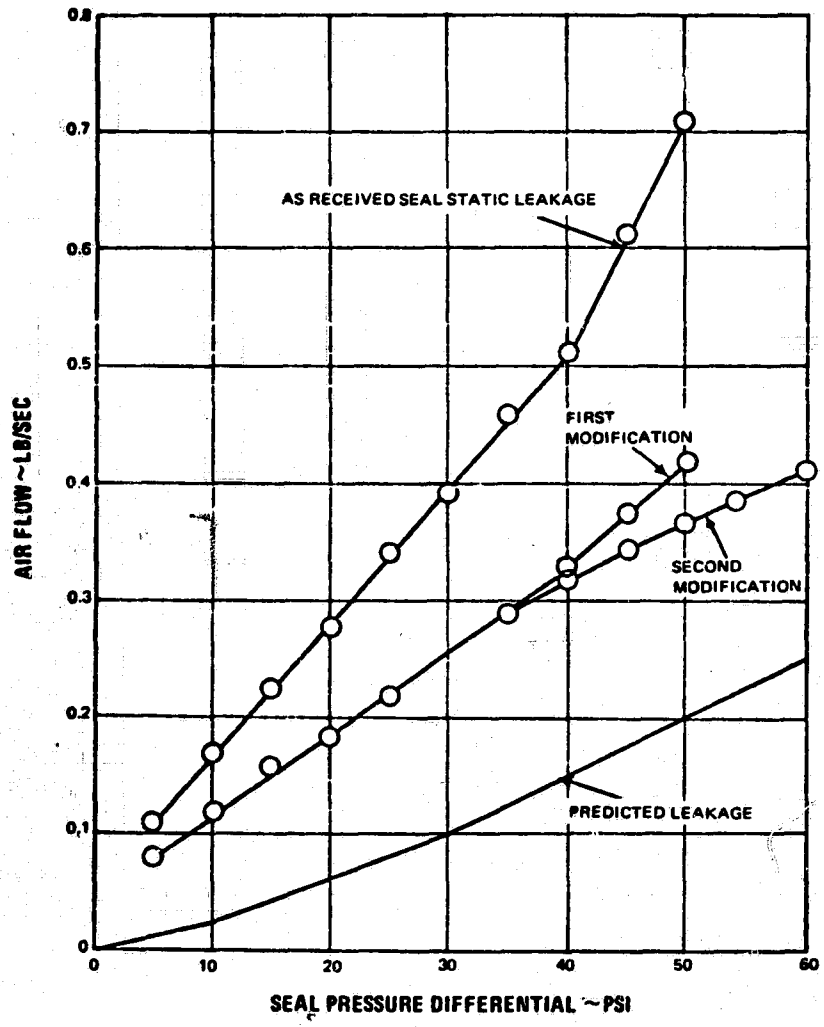

Figure 11 Room-Temperature Static Calibration of the One-Side Floated-Shoe Interstage Seal in the Static Fixture

In order to increase the moment stability of the seal, it was decided to reduce the width of the 24 secondary sealing pads (Reference 15). To improve the moment balance, the critical dimensions of each of the 24 seal shoes were measured and they were individually moment balanced. Moment corrections were made by adjusting the axial positions of the secondary sealing surfaces. In performing the required machining, shoe slopes were held to 0.5 milliradian or less. In addition, the outer seal carrier ring was measured and found to be out of tolerance. It was plated and ground to the correct dimenions.

After reassembly of the seal, testing in the static fixture showed that leakage had not changed materially from that shown on the curve labelled "Modified Seal Static Leakage" in Figure 11. At that time, it was decided that the seal was acceptable for dynamic testing.

C. SEMIRIGID INTERSTAGE SEAL

After receipt of the semirigid interstage seal, the proximity probes were installed in the seal at Pratt & Whitney Aircraft and the seal was subjected to static testing. Leakage was found to range from 0.008 to 0.012 lb/sec higher than predicted, as shown in Figure 12. The calculated static film thickness at room temperature was 0.46 mil at a seal pressure differential of 50 psi and the corresponding calculated total leakage was 0.024. Actual leakage at 50 psi was 0.038 lb/sec, and the proximity probes indicated that the seal was not lifting off the seal plate. Feeler stock 1 mil thick could not be inserted between the primary sealing surfaces at the inner edge.

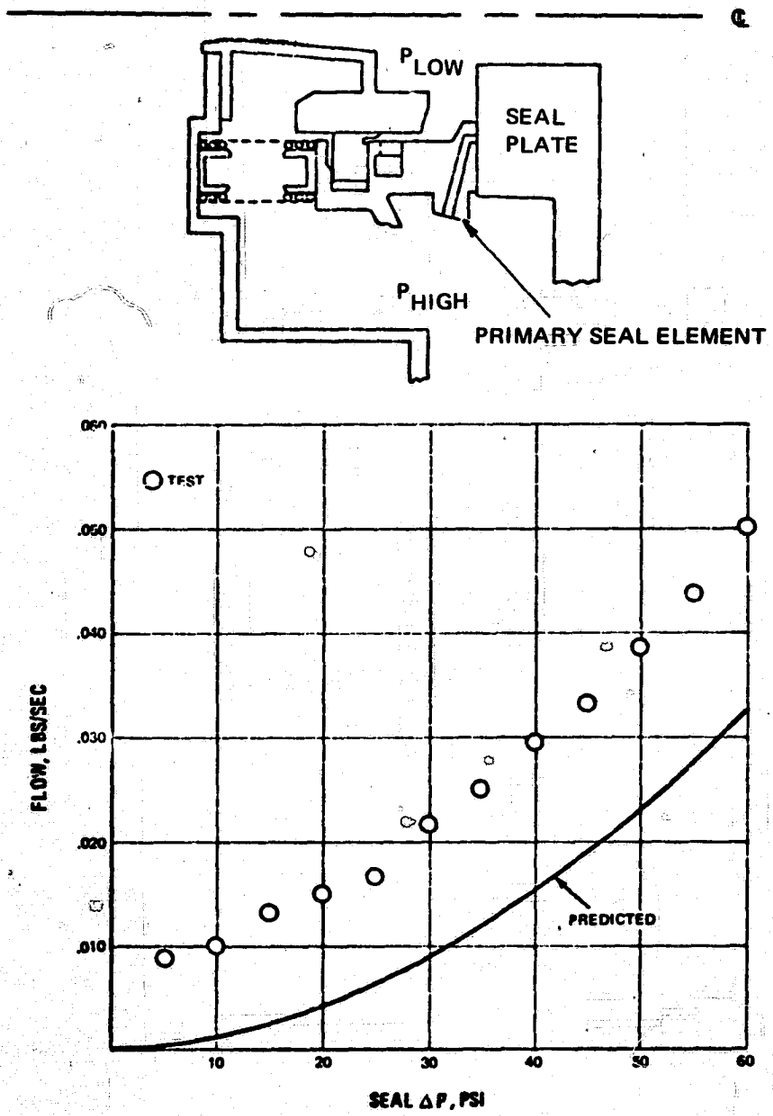

Figure 12 Semirigid Interstage Seal Static Test

The surface waviness of the non-rotating primary seal element was measured with the seal fully assembled: when the springs forced the primary element against the four retaining collars on the anti-torque pins they produced a 4-lobe 4-mil FIR wave in the face of the primary seal element (see Figure 13). The retaining collars were removed so that the primary element

floated on the springs, and a second measurement for waviness indicated no significant change in the wave shape or magnitude. The similarity is evident in Figures 13 and 14.

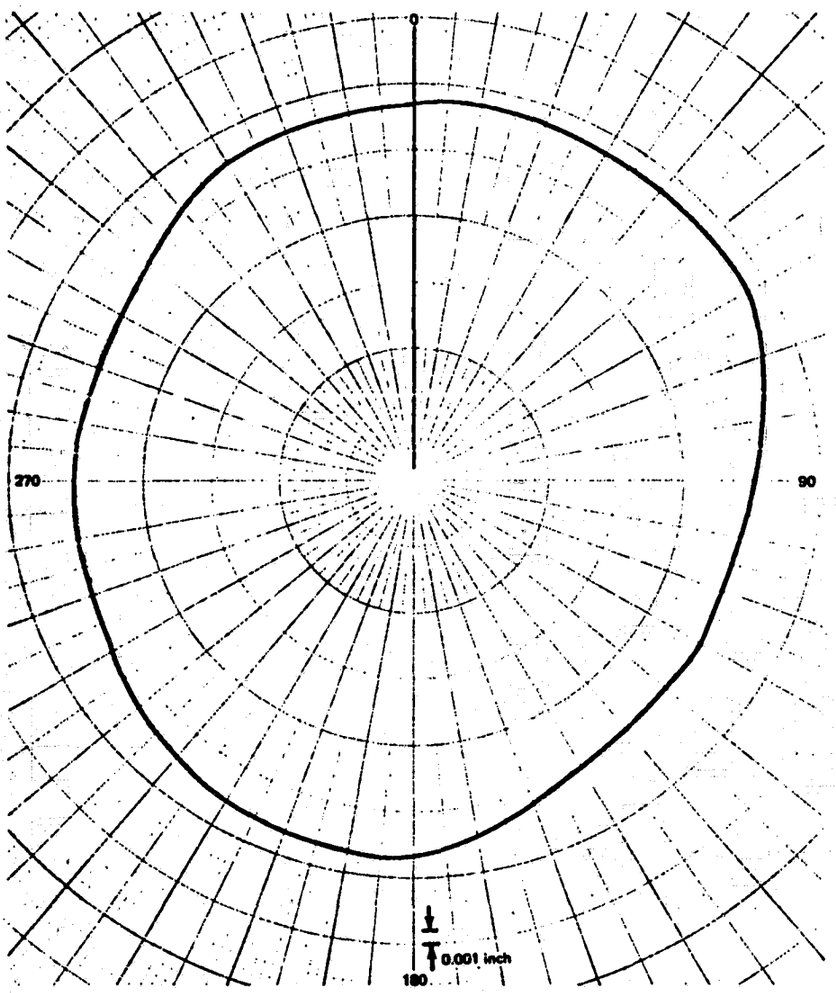

Figure 13 Semirigid Interstage Seal Sealing Face Runout, Restrained

In an effort to reduce waviness, weights of approximately 11.2 ounces each were set on the primary seal element at 24 equally spaced locations. The total weight compressed the springs to an operating length of approximately 0.904 inch. Three equally spaced points on the seal surface were used to define a reference plane, and seal surface runout was plotted with respect to that plane. The original runout (or waviness) is shown in Figure 15. A number of trials were made with the springs in different locations. In each case the seal runout varied, with the maximum and minimum points being displaced around the circumference of the seal face, indicating that the seal runout was sensitive to the spring locations and loads. Several spare coil springs were shortened to replace springs which produced localized high loads in areas of maximum runout. As shown in Figure 16, it was possible to reduce primary seal element face runout from its original value of 4 mils FIR to 2 mils FIR.

A surface inspection of the seal plate from the static fixture revealed a high runout of 4 mils within a small area of the surface. This area was reground to produce a total runout of 0.7 mil FIR.

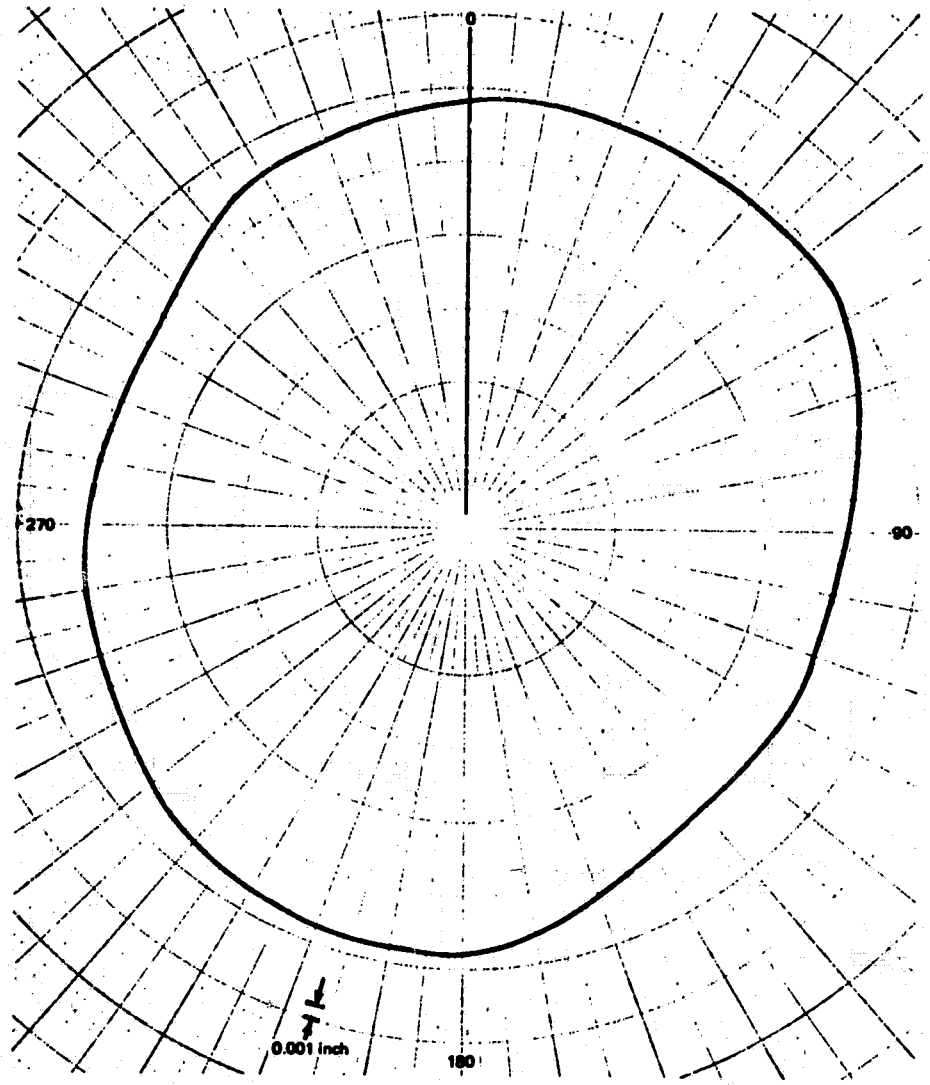

Figure 14 Semirigid Interstage Seal Sealing Face Runout, Unrestrained

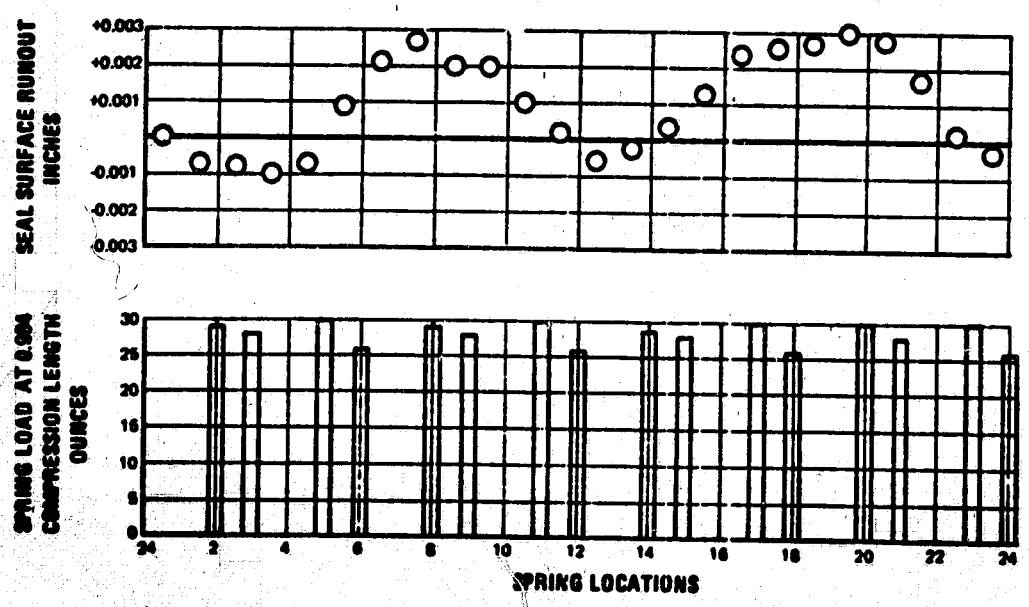

Figure 15 Original Semirigid Seal Runout

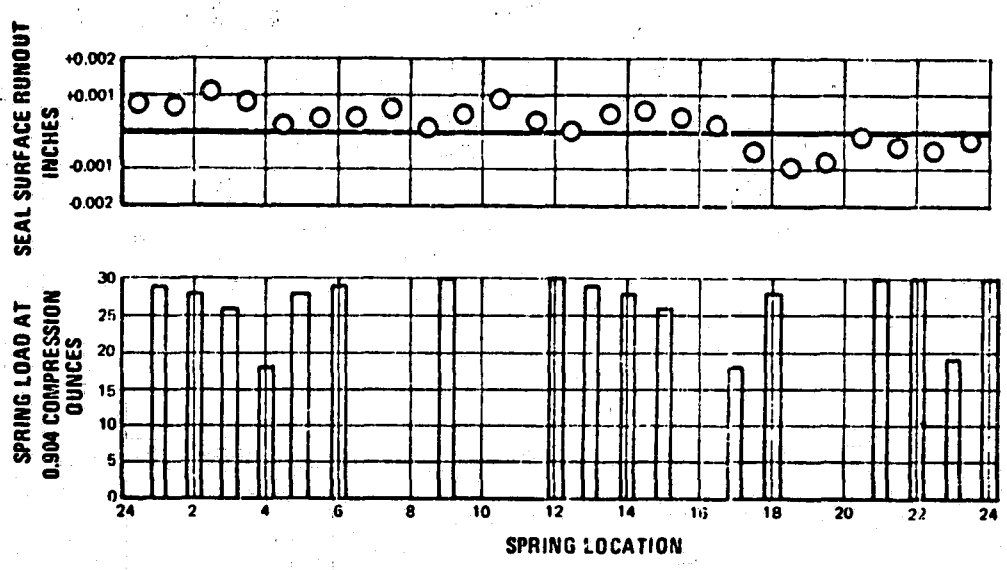

Figure 16 Semirigid Seal Runout After Adjustments

A second test of the semirigid interstage seal in the static fixture showed that the reductions in seal runout had not materially affected seal leakage. Dial indicators were used in conjunction with the proximity probes, and both indicated that lift-off had not been achieved, although the static testing covered the full design range of pressure differentials.

The failure to achieve seal lift-off in the static fixture was apparently caused by waviness in the primary seal element and the seal plate. At the time of the static testing it was recognized that the waviness could lead to destructive rubbing contact of the mating surfaces when the seal was tested dynamically. Contact forces in the wavy seal increase with increasing pressure drop until the air-film stiffness becomes great enough to reduce seal distortion and return the contact force to zero. The maximum contact force and the pressure at which that force occurs vary directly with wave height and inversely with wave length of the seal distortion. However, it was judged that testing at relatively high rotational speeds (a predominantly hydrodynamic regime) would provide a seal closing force primarily due to spring loading (not hydraulic loading), and that this load could be supported by the air-film load capacity.

Figure 17 describes the dimensionless load capacity ($\bar{W}$) of the seal air film as a function of film thickness and surface speed at a pressure drop of 10 psi. The theoretical film thickness for perfectly parallel seal faces is determined by calculating the dimensionless closing force from the balance geometry, pressure drop, and spring load and equating it to the film load capacity from Figure 17. At a pressure drop of 10 psi and a spring load of 31 pounds, the dimensionless load capacity is 0.90 and the film thickness varies from 0.53 mil at 100 ft/sec to 1.03 mil at 850 ft/sec. The minimum film thickness, however, depends on the waviness of the seal surfaces, and is at least 0.5 mil less than the average film thickness. On this basis, it was decided to proceed with dynamic testing of the semirigid interstage seal.

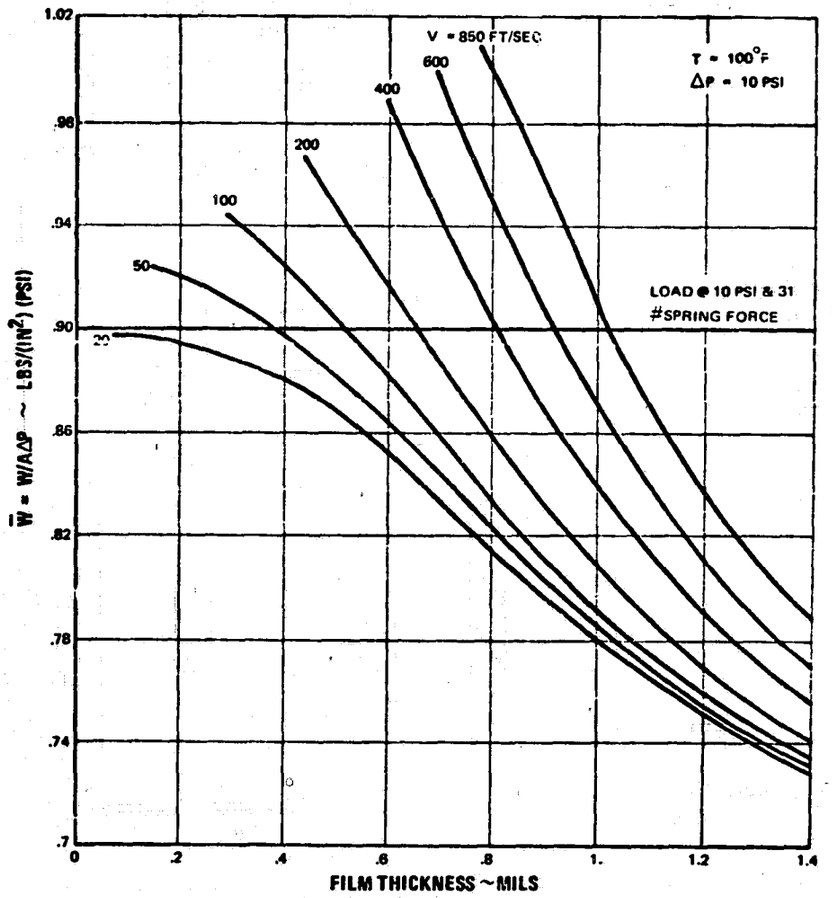

Figure 17 Theoretical Semirigid Interstage Seal Dimensionless Load Capacity

D. OC DIAPHRAGM END SEAL

After receipt of the OC diaphragm end seal, proximity probes were installed and calibrated by Pratt & Whitney Aircraft. The primary OC subassembly was removed from the carrier and axial runouts of the seal face were measured as shown in Figure 18. The seal was reassembled and installed in the static fixture. Testing in the static fixture showed that the air leakage rates at seal pressure differentials up to 150 psi were approximately twice the calculated values, as shown in Figure 19. Readings from proximity probes showed that the air film thickness increased to 0.8 mil as seal pressure differential was increased to 150 psi. These readings indicated the possibility that the seal had lifted off the mating surface of the fixture. Feeler gauge measurements revealed that the thin-strip primary seal face achieved good conformity to the fixture surface: at a pressure differential of 20 psi it was impossible to insert a 1-mil feeler gauge between the seal face and the mating surface.

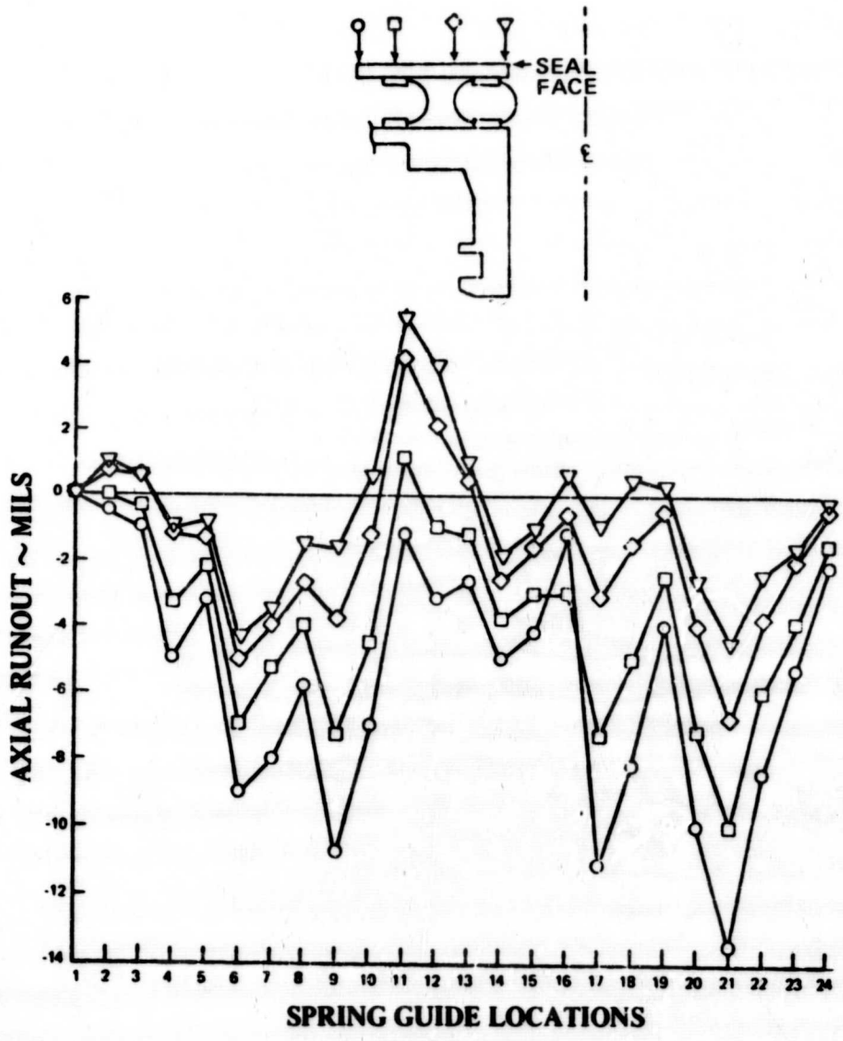

Figure 18 Axial Runout on the Face of the OC Diaphragm End Seal

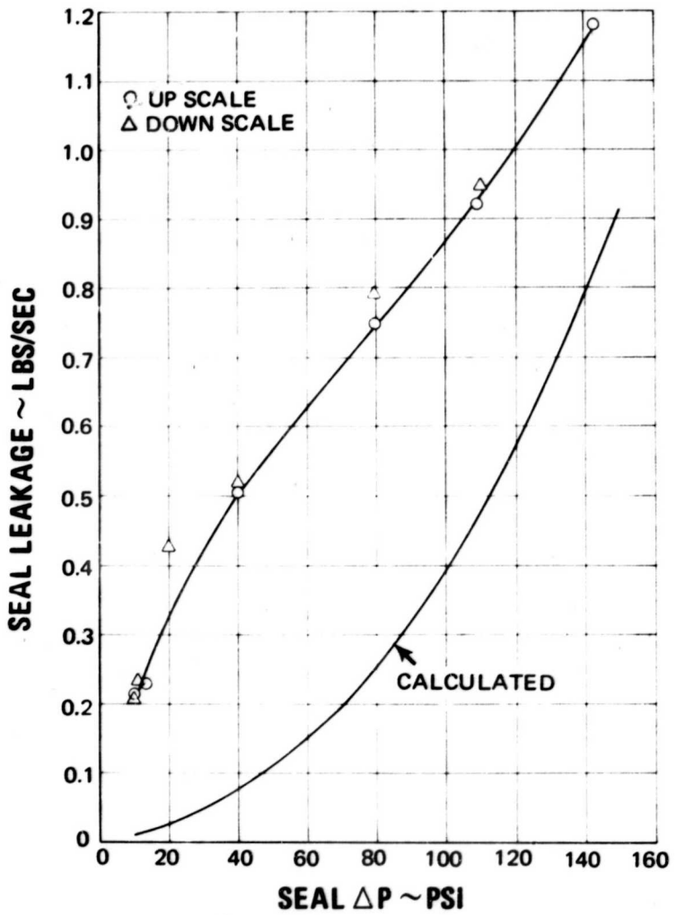

Figure 19 Static Calibration of the OC Diaphragm End Seal

III. FULL-SCALE DYNAMIC TEST RIG

A full-scale test rig was designed and fabricated to evaluate the four selected end and interstage seals under simulated engine conditions. The rig is shown mounted on the rig transporter in Figure 20 and installed in the test stand in Figure 21. It simulates the last stages of a full-scale compressor, including the supporting members, bearing system, and thermal gradients.

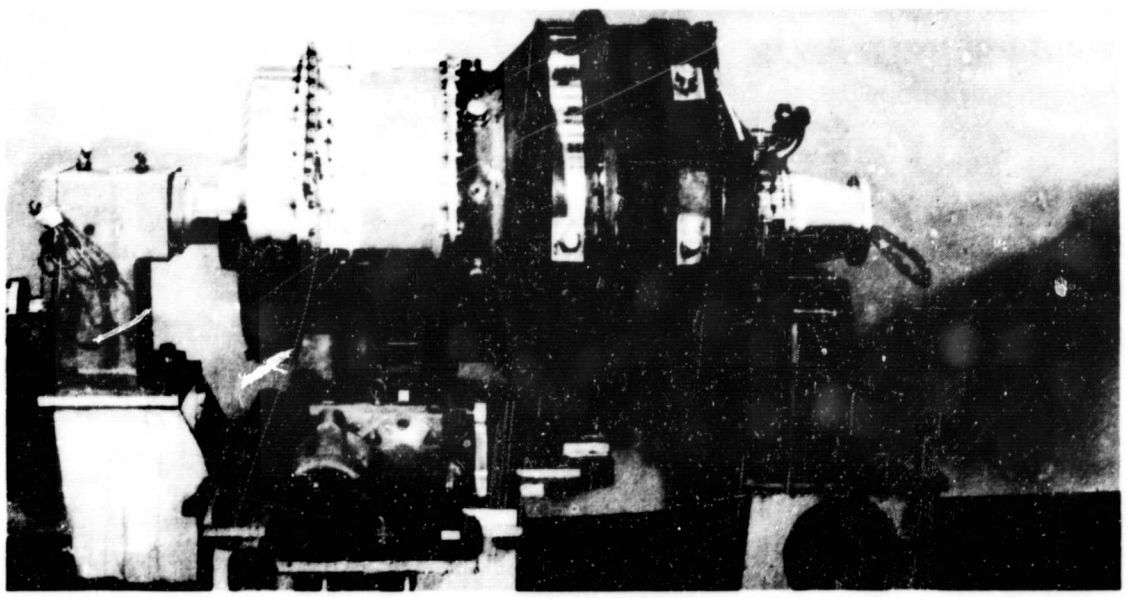

Figure 20 Compressor Seal Test Rig Mounted on Rig Transporter (CN-13744)

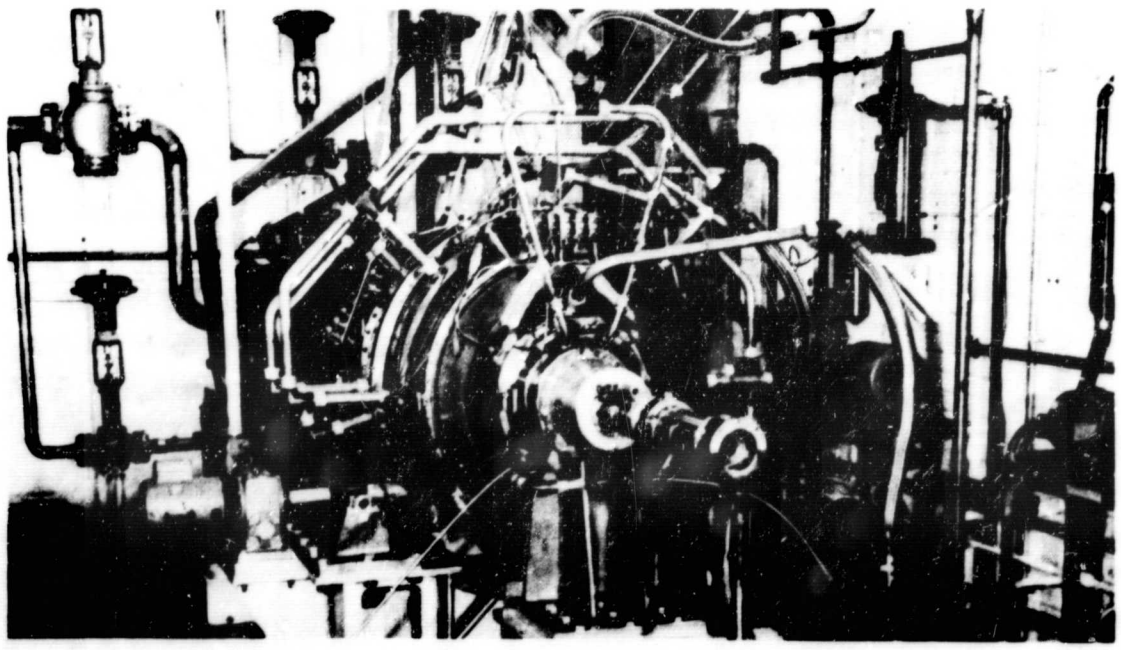

Figure 21 Compressor Seal Test Rig Mounted in Stand (CN-14690)

A. FRONT BEARING COMPARTMENT

The front bearing compartment was designed to provide easy access to the test seal without compromising the simulation of the compressor. For example, the oil scavenge system was designed so that the oil lines would not interfere with the removal of the outer case for seal measurements. A heat shield was provided to protect the carbon rig seal (see Figure 22) from the high temperatures anticipated in the test compartment. The function of the rig seal is to force cooling air through the rotor after it enters the rig. The front bearing supports for the main rig thrust bearing are shown in Figure 23. A 24-channel slip-ring assembly adjacent to the front bearing compartment was used to monitor hub, primary ring and disk temperatures. The disk is shown in Figure 24. A deflection adapter for the cantilevered section of the slip ring was incorporated into the design, with provisions made for alignment.

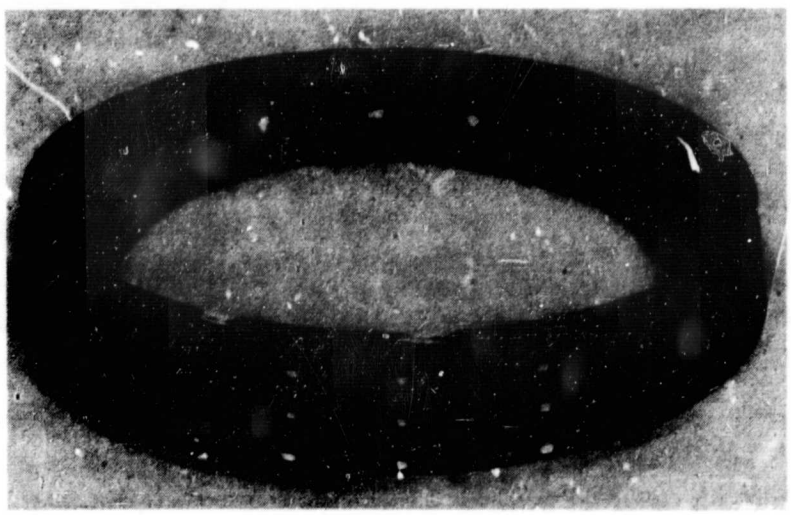

Figure 22 Test Rig Seal (XP-82832)

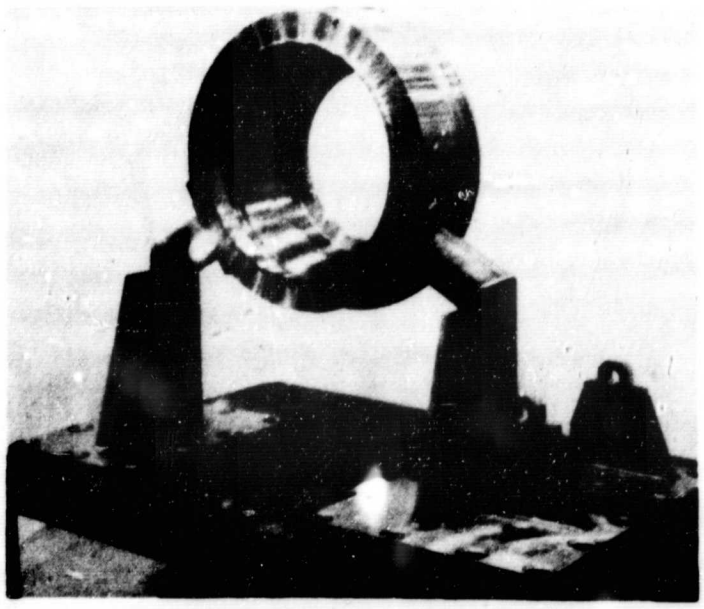

Figure 23 Front Bearing Support for Main Rig Thrust Bearings (XP-84232)

Figure 24 Test Rig Front Disk (XP-82832)

B. THRUST BEARING COMPARTMENT

The seal rig thrust-bearing compartment was an adaptation of an existing duplex bearing and seal configuration which had been very reliable in experimental testing and field service. The bearing compartment and gearbox were designed with a common oil supply, eliminating the need for a carbon face seal to separate the two areas. The common oil system included both scavenge and breather systems. The rig face seal was replaced by an O-ring.

The design also incorporated a double-acting piston arrangement on the rear set of thrust bearings to compensate for the high thrust loads from unbalanced rotor forces. This device used air from a rig compartment, eliminating any need for a separate air supply and regulator. Because of high operating loads, bearing temperatures were monitored through thermocouples at the outer races. Figure 25 is a frontal view of the rear disk, and shows the spacer element of the disk with its instrumentation grooves. Figure 26 is a rear view of the interdisk spacer. The surface of the interstage seal runner can also be seen in this photograph.

C. ROTOR

The rig rotor was designed to accommodate the runners of any of the four test seals. The rig design accounted for thermals, thrust loads, Poisson's effect, and the elastic growth of the members.

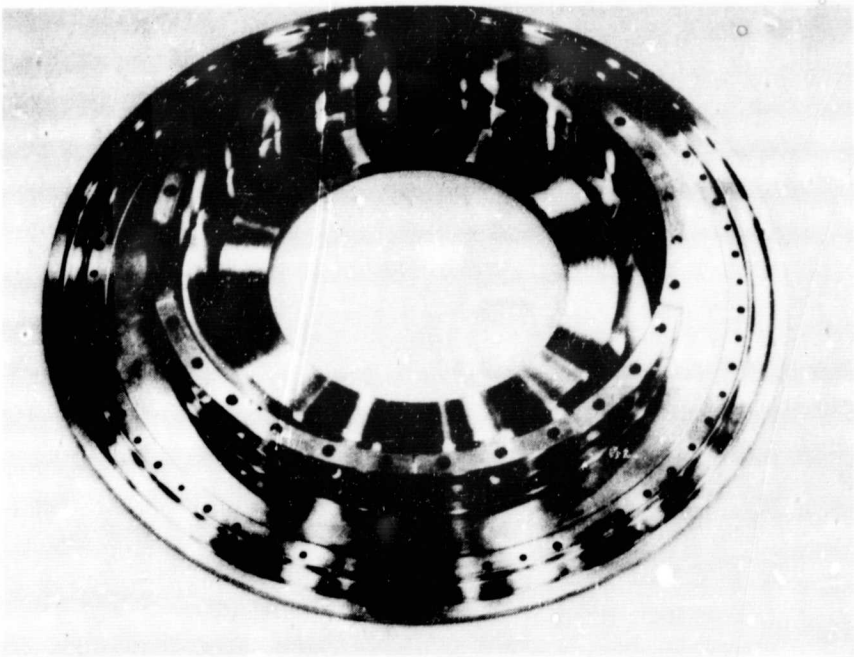

Figure 25 Test Rig Rear Seal (XP-82833)

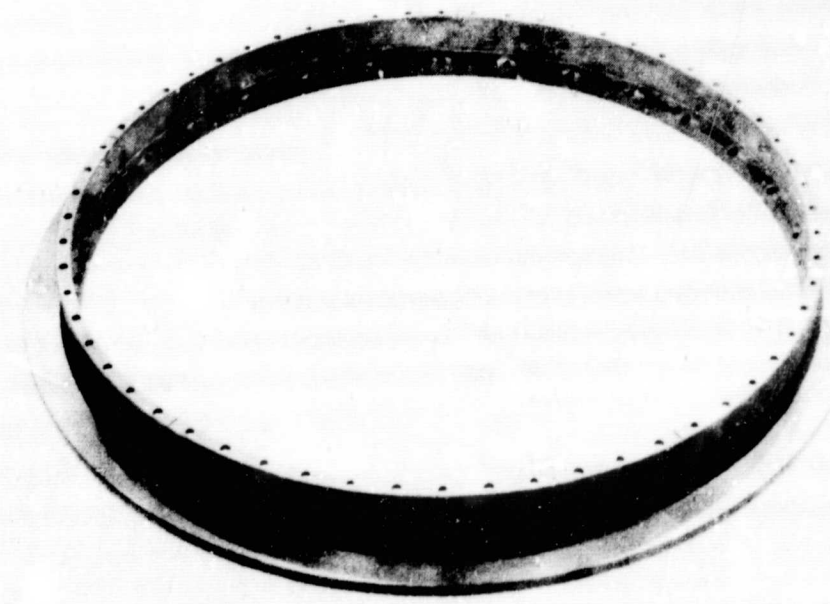

Figure 26 Test Rig Interdisk Spacer (XP-82834)

Each rotor part underwent an individual detail balance. The disks were balanced by end drilling at the outer circumference, while weights were added to hubs and spacers for balance purposes. The front hub of the rotor is shown in Figure 27 with the rig air seal attached. Figure 28 shows the rear hub with balance weights attached. Figure 29 presents a view of the end seal disk with the seal face up, while Figure 30 shows the same part with the seal down.

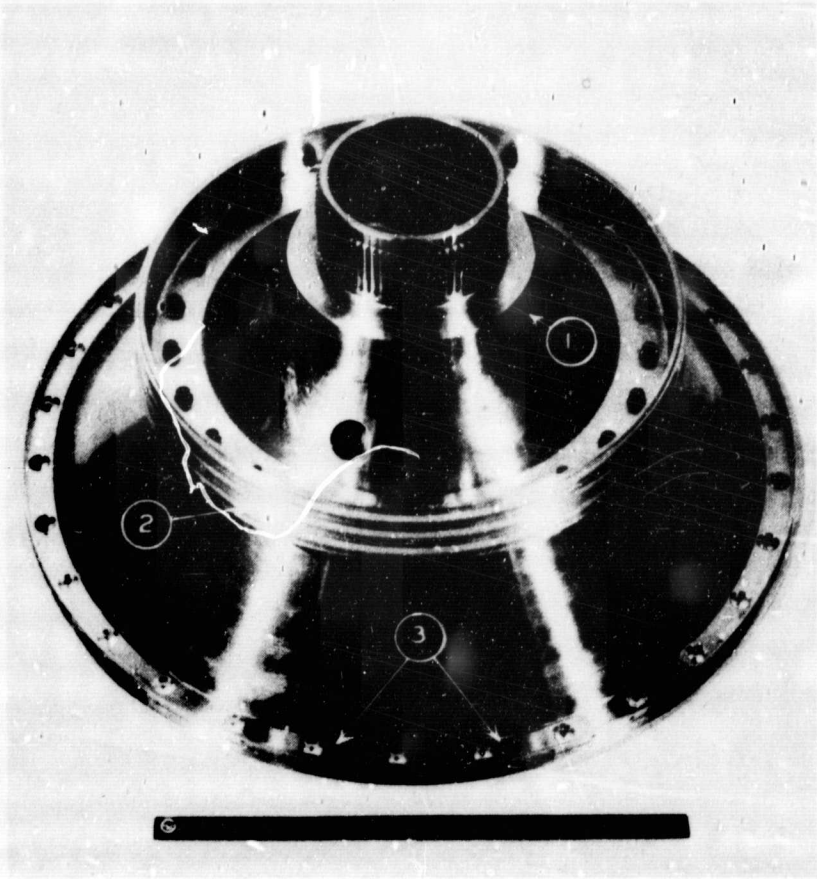

Figure 27

Test Rig Front Assembly
1. Front Hub
2. Rig Seal
3. Counterweight

(XP-83360)

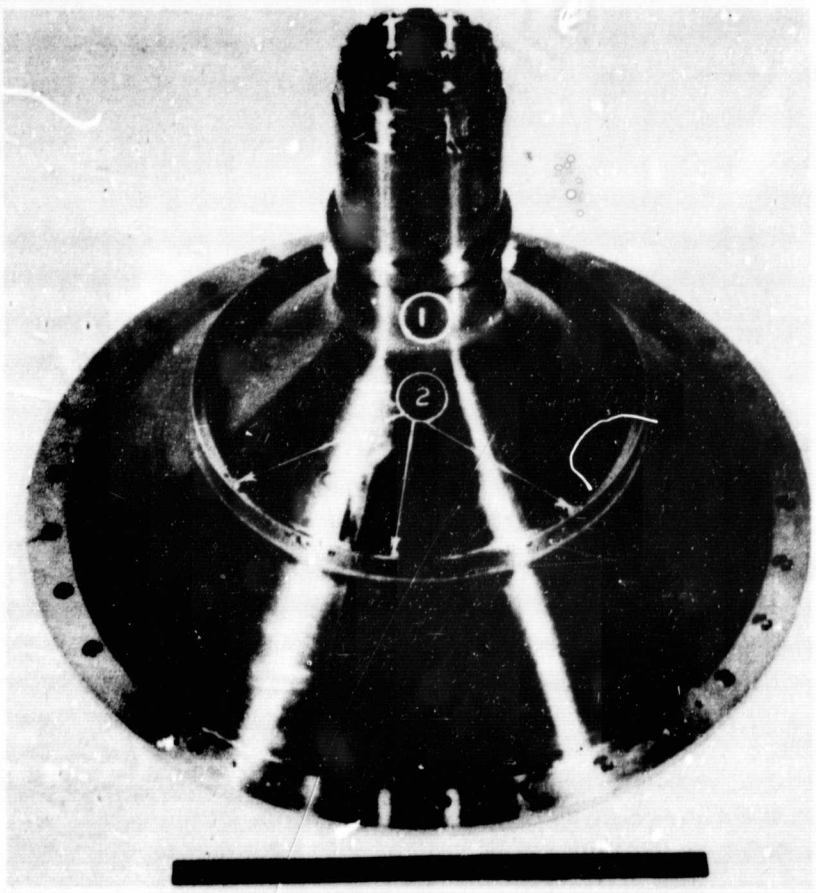

Figure 28

Test Rig Rear Assembly
1. Rear Hub
2. Counterweight

(XP-83361)

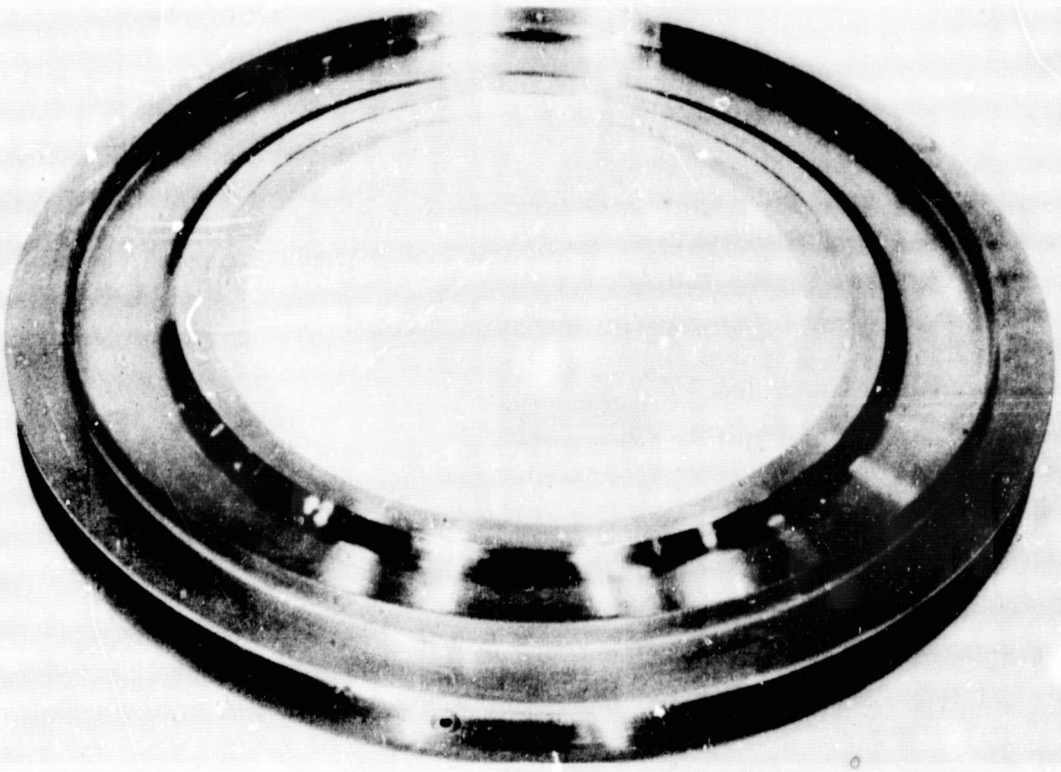

Figure 29 Test Rig End Seal Disk with Seal Face Up (XP-83362)

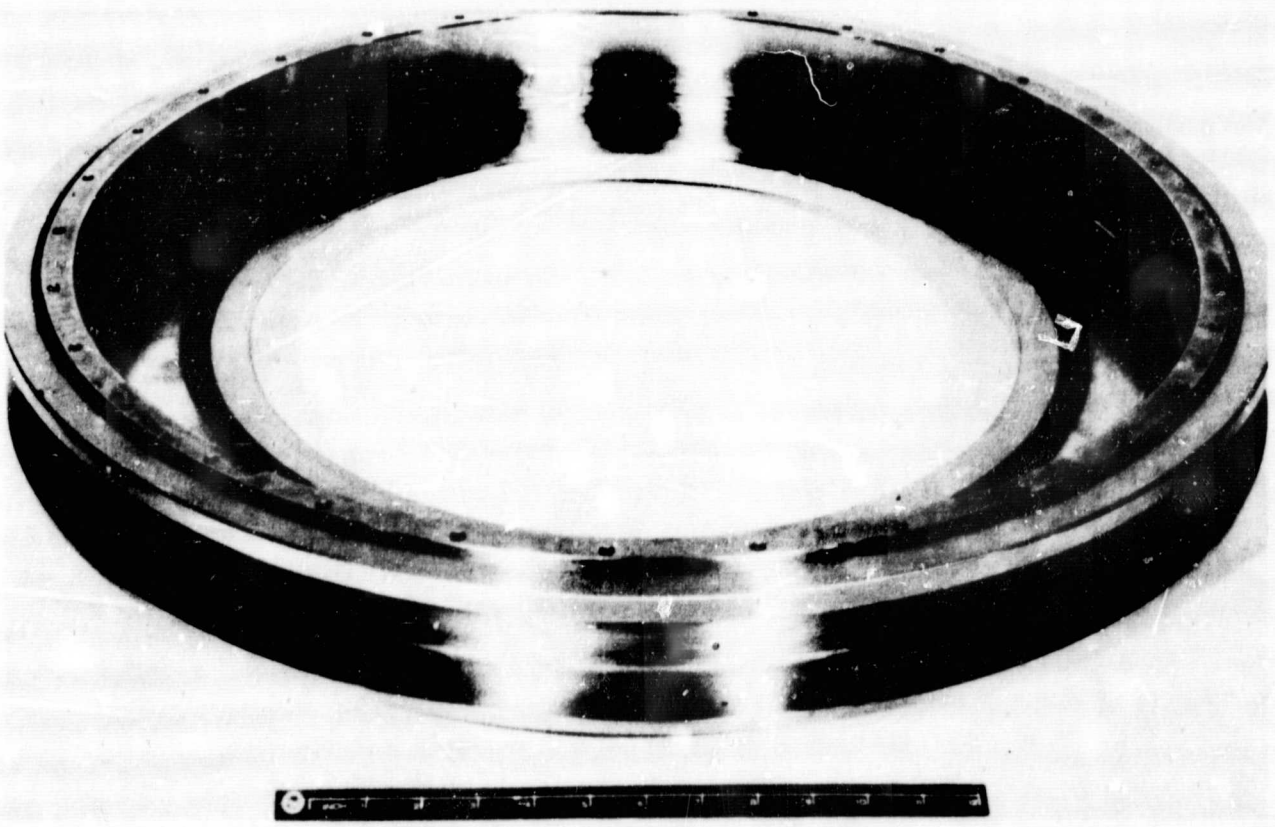

Figure 30 Test Rig End Seal Disk with Seal Face Down (XP-83363)

In order to control vibration in the test rig, the rotor was assembled in three stages. In the first stage, the individual parts were statically balanced, and the location and magnitude of the residual imbalance was marked on the parts. In the second stage, the parts were assembled vectorially in order to ensure that all or most of the residual imbalance would not be stacked up in the same direction. This step was intended to reduce the size of the final dynamic balance correction and to reduce the dynamic loads within the rotor, since such loads would tend to force the rotor out of shape at operating speed. In the third stage, the assembled rotor was dynamically balanced, bringing the residual imbalance to an amount considered acceptable by design analytical studies.

D. OUTER CASE

The rig outer case was designed to withstand the rig operating pressures, temperatures, deflections and loads. It was fabricated from Inconel-718 rings (AMS 5662), and welded together. A gooseneck configuration was designed into the case support to provide constant contact with the bearings that allow the required axial travel of the case with respect to the rotor. The axial travel actuator consisted of a mounting ring attached to the outer race of a bearing supported outside the rig case. The cutouts for the supports are shown in Figure 31. The rear case and sliding support are shown in Figures 32 and 33.

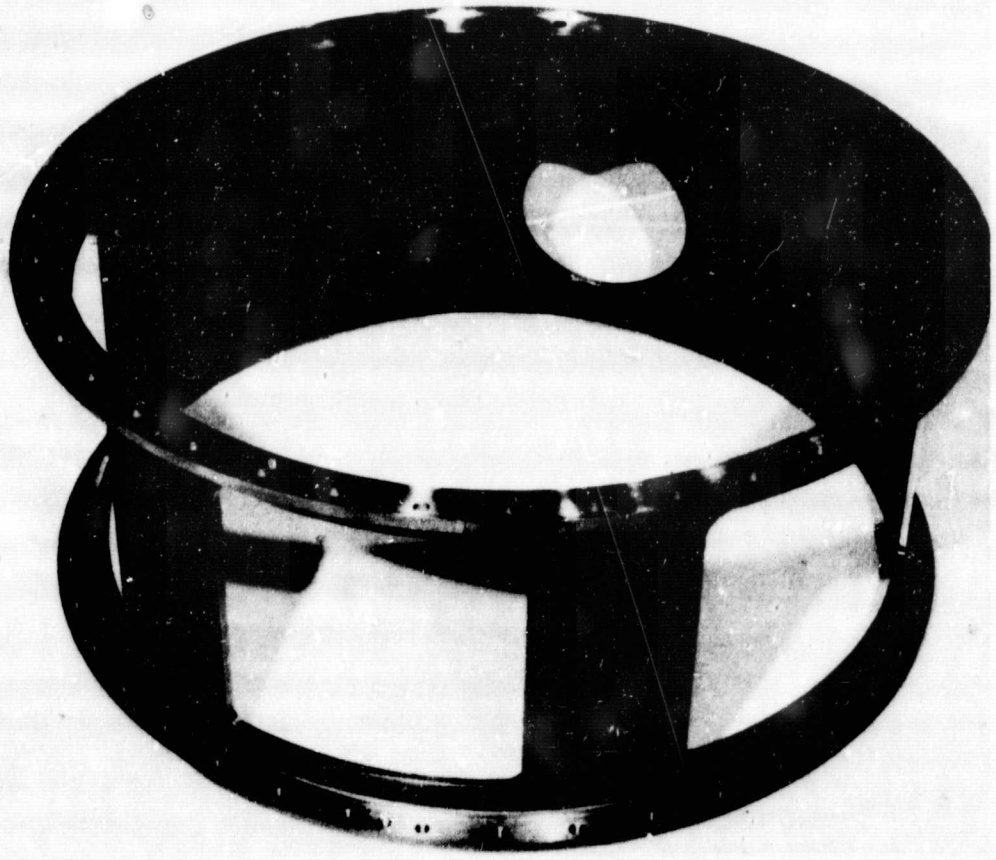

Figure 31 Test Rig Front Case (XP-83364)

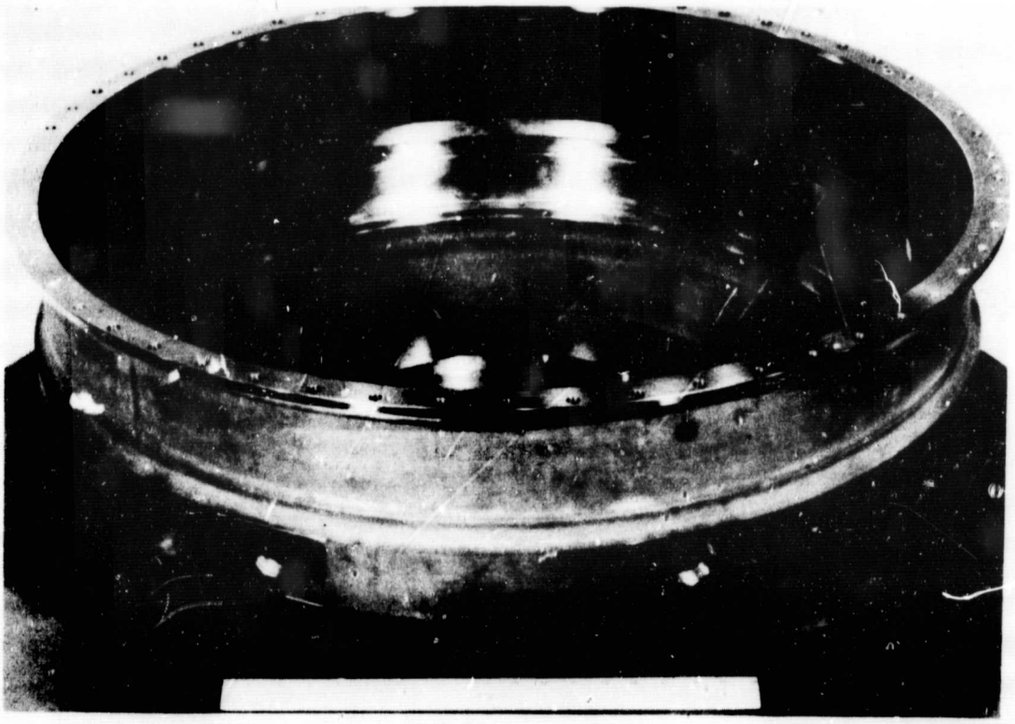

Figure 32 Test Rig Rear Case (XP-83876)

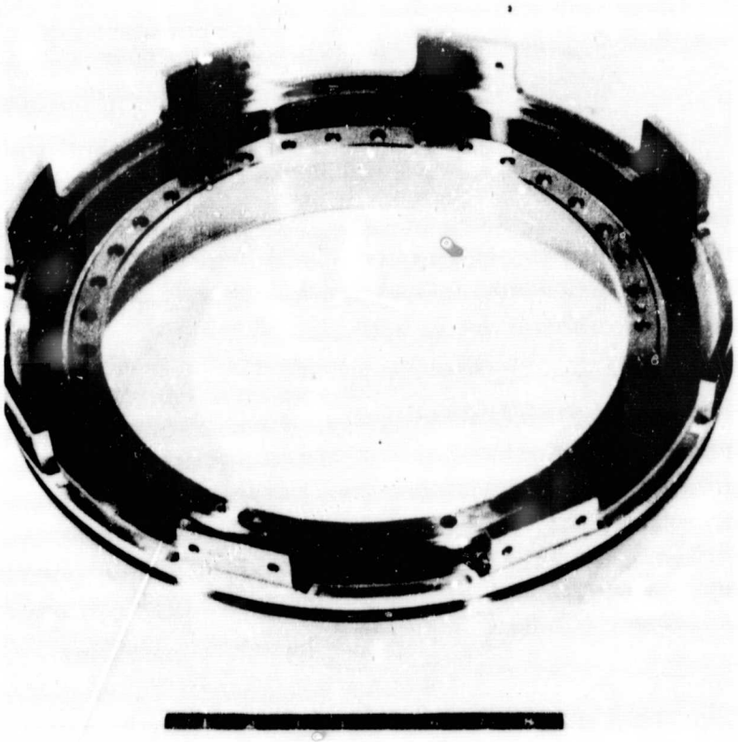

Figure 33 Sliding Support for Test Rig Case (XP-83871)

IV. COMPRESSOR SEAL TESTING IN THE FULL-SCALE DYNAMIC TEST RIG

A. TESTING OF THE ONE-SIDE FLOATED-SHOE END SEAL

The one-side floated-shoe end seal is a face seal consisting of a ring of 24 seal shoe segments acting against a rotating surface (the seal runner) attached to the compressor rotor. Figure 34 is a schematic drawing of the seal. The surface of the seal runner was flat. The primary seal interface was between the nonrotating ring of shoes and the runner surface, and the leakage flowed radially inward through the seal. Secondary seals were provided between the shoes and the carrier ring at the secondary seal pads and the one-piece thrust ring. Another secondary seal was provided between the seal carrier ring and the seal mounting ring at the location of the secondary seal piston ring. The assembled seal unit is shown in Figures 35 and 36.

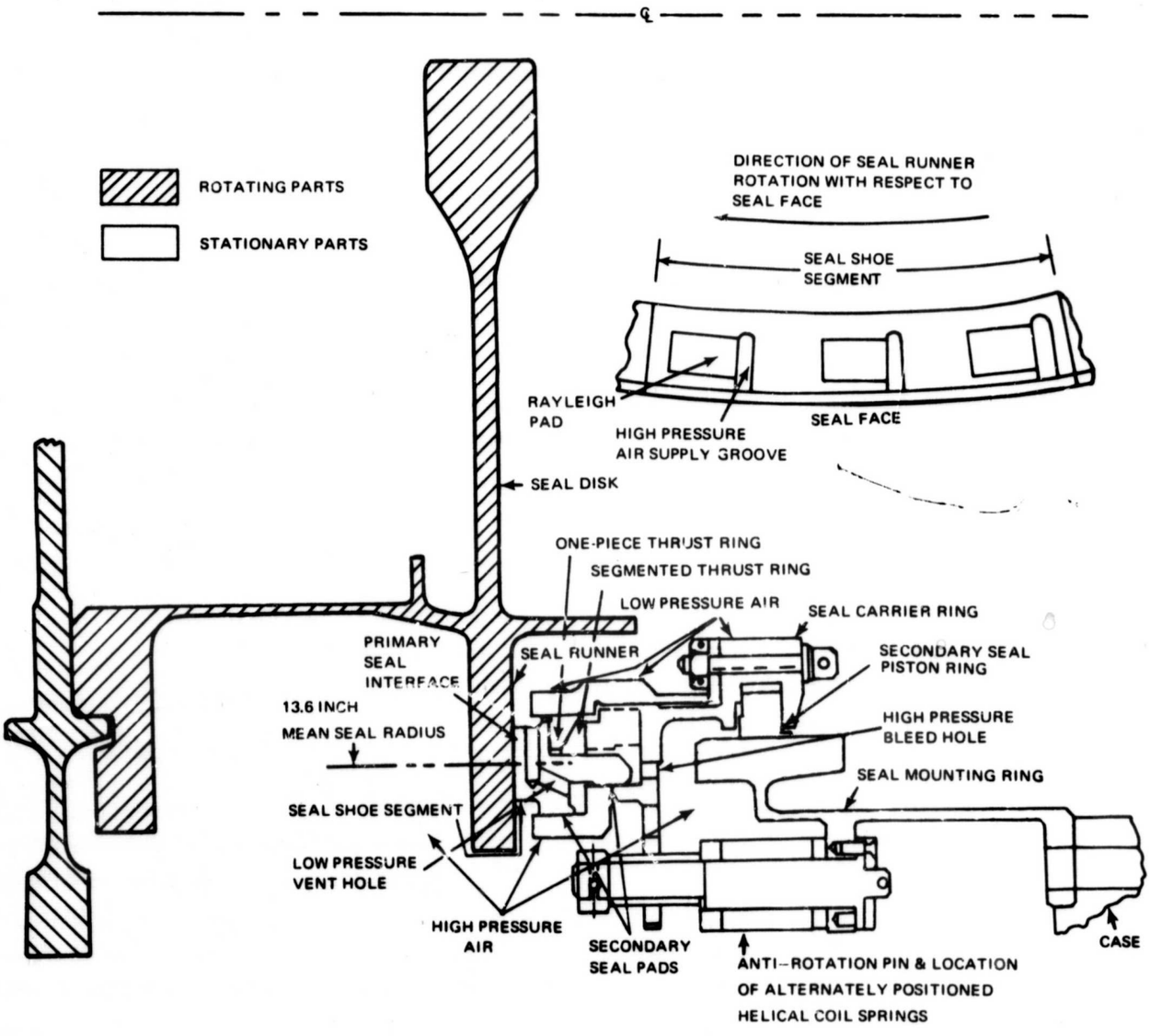

Figure 34 Schematic of the One-Side Floated-Shoe End Seal

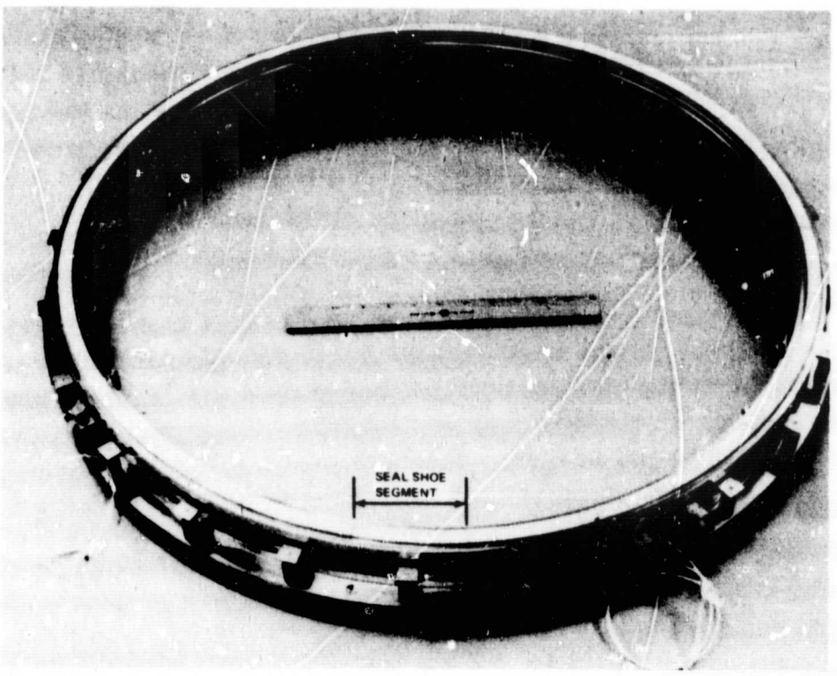

Figure 35 One-Side Floated-Shoe End Seal (CN-14385)

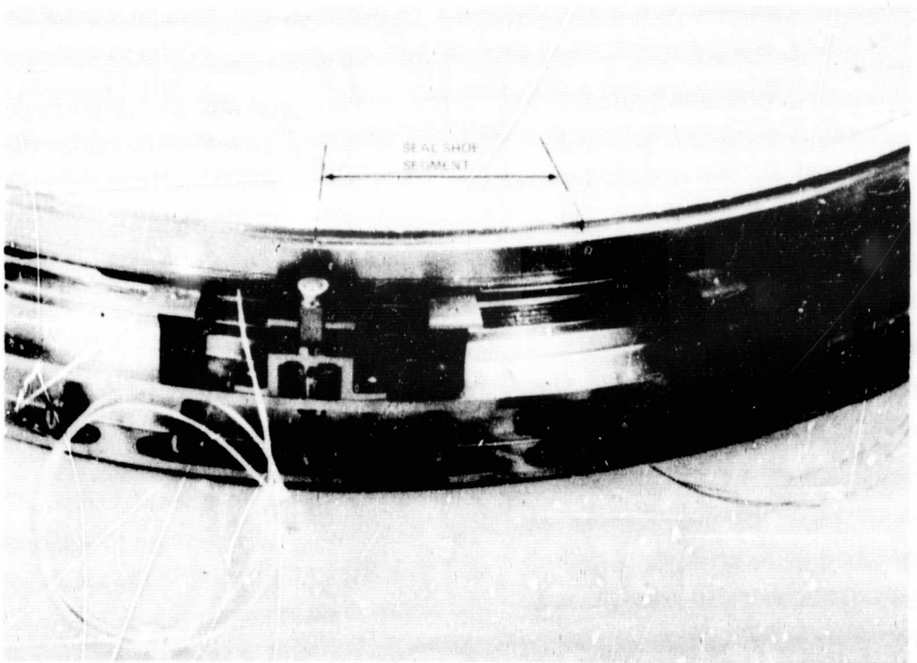

Figure 36 Side View of the One-Side Floated-Shoe End Seal (CN14386)

1. ROOM TEMPERATURE DYNAMIC TESTING

At the test stand, the seal's breakaway torque was measured. It was found to be 200 in-lbs with no pressure differential across the seal. Breakaway torque is the amount of torque required to overcome the friction force between the seal and the seal runner at startup. The capacitance probes were calibrated. The calibration curves are shown in Figure 37.

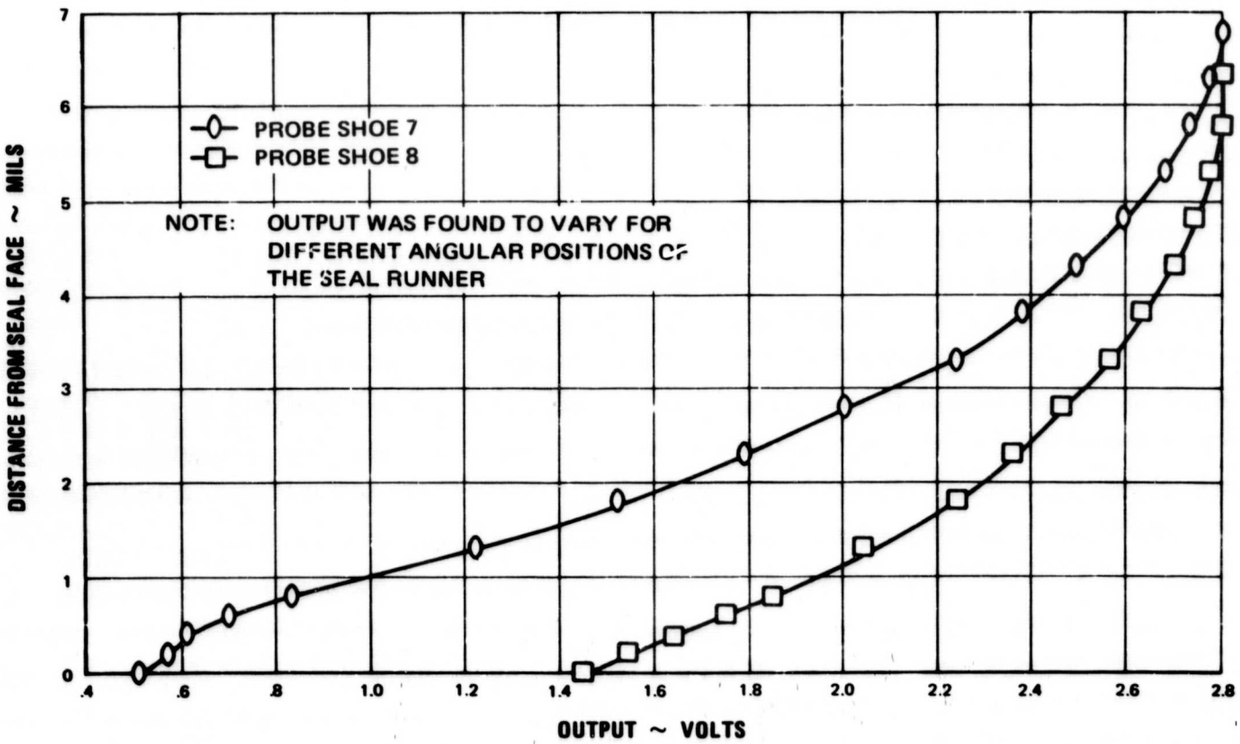

Figure 37 Calibration of the Capacitance Probes

The seal was tested at speeds up to 3400 rpm (400 ft/sec) with a pressure differential of 65 to 70 psi across the seal. Visual observations made during the test included an oscilloscope display of the capacitance probe signal. The display was photographed at intervals of 100 revolutions of the seal runner.

The test was conducted by accelerating slowly from zero speed to near idle speed with a constant 65 to 70 psi pressure drop across the seal. At 3400 rpm the rig was shut down because of an abnormal rise in temperature at the primary seal face and because of the failure of one of the two capacitance probes used to monitor separation between the rotor and the seal shoes. Visual inspection of the seal through an open air-hose fitting revealed extensive damage to the mating surface of the primary ring and the runner. Further dynamic testing of the seal was suspended.

Examination of the data recorded automatically during the test revealed several rapid temperature excursions that resulted from heavy rubbing contacts. As Figures 38 and 39 indicate, the seal appeared to be running satisfactorily for the first 199 seconds of the run. At that point in time, the seal runner was rotating at 2993 rpm, and the body thermocouples in the runner head began to show very rapid local temperature fluctuations and a general temperature rise. The temperature of the shoes started to increase approximately 12 seconds later. Photographs of the oscilloscope display of the capacitance-probe signals (Figures 40 through 43) indicate shoe separation from the runner at the probe location and show the effects of rotation on film thickness. (Note that the probe output varied at different positions of the runner).

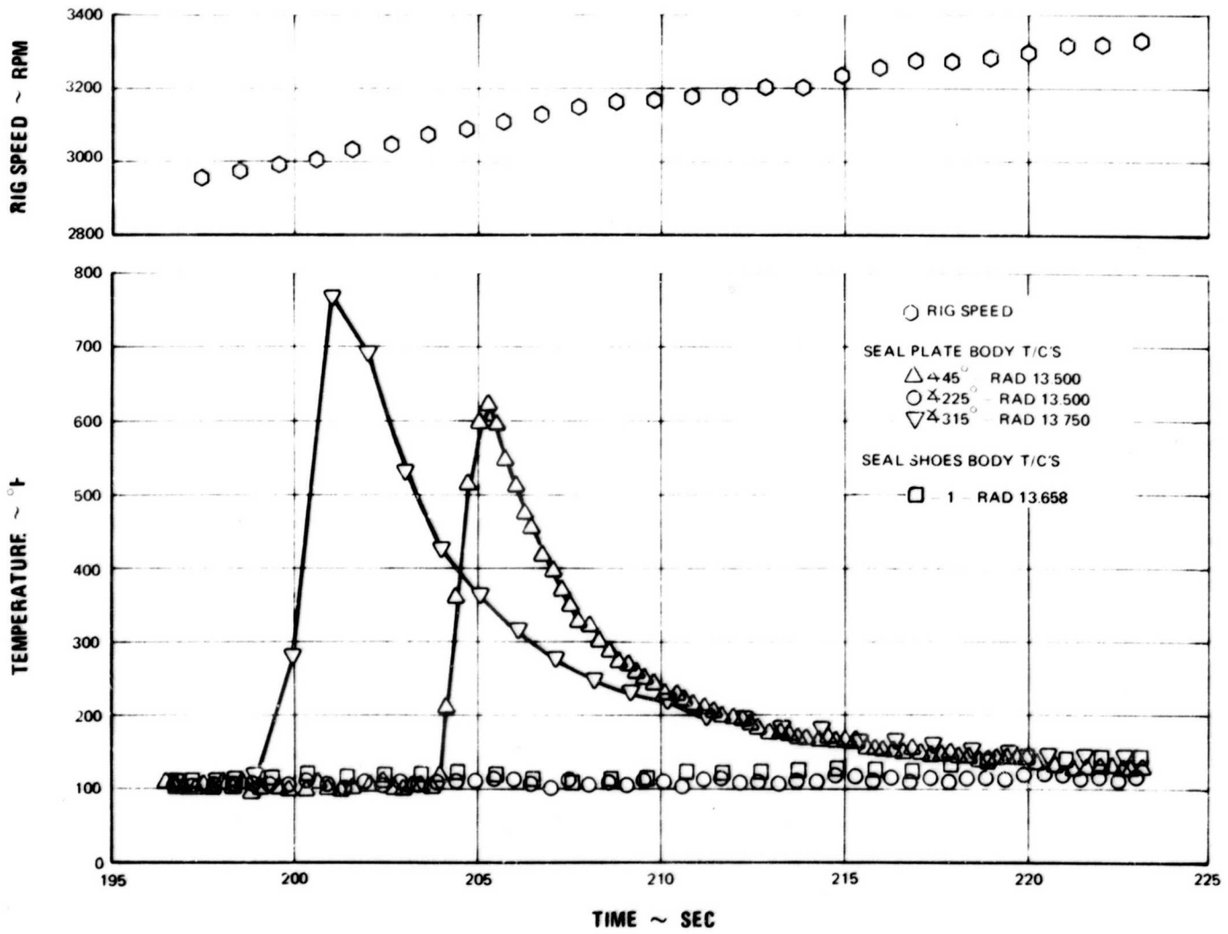

Figure 38 Dynamic Calibration of the One-Side Floated-Shoe End Seal, Last 24 Seconds of Test Run

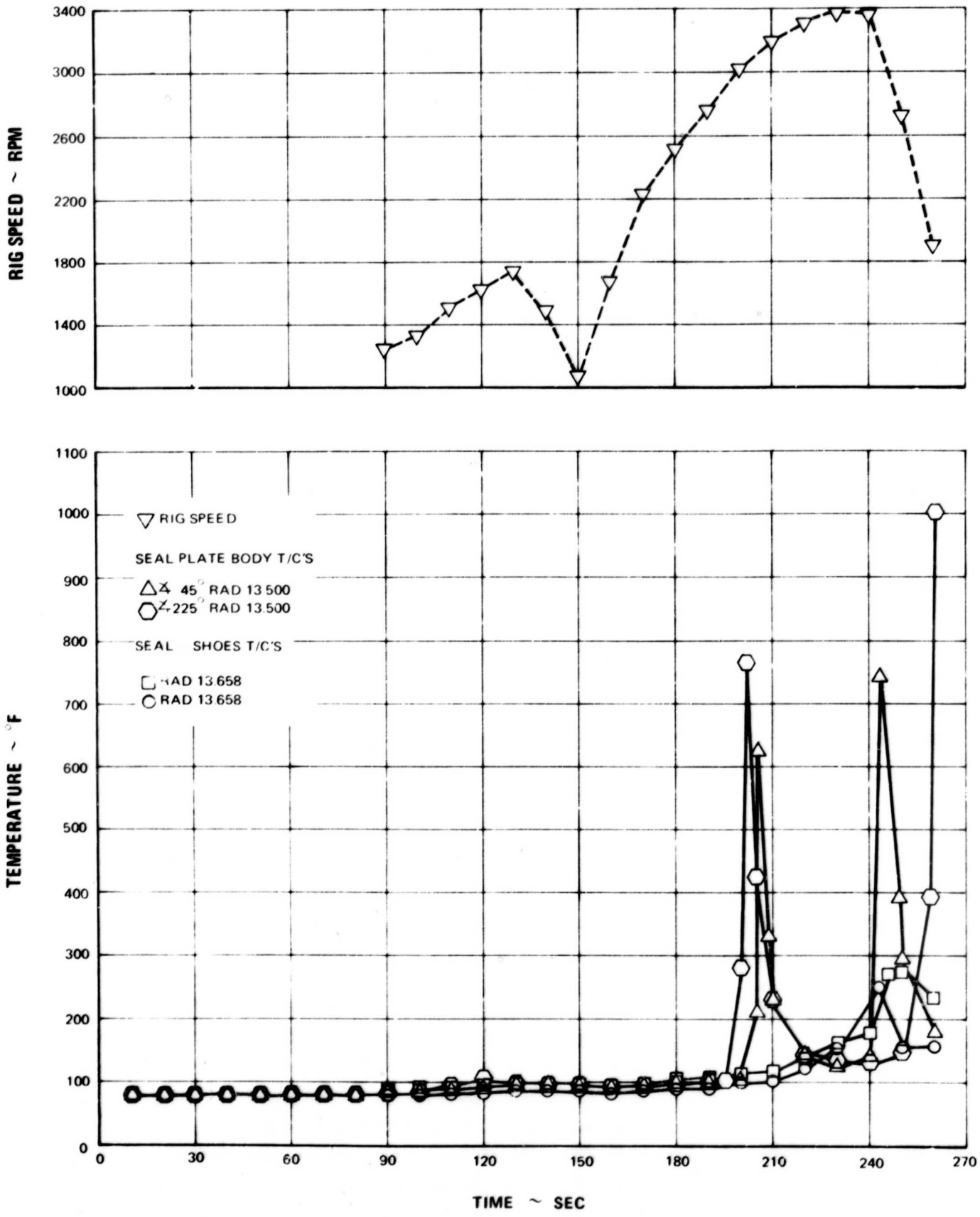

Figure 39 Dynamic Calibration of the One-Side Floated-Shoe End Seal, Complete Test Run

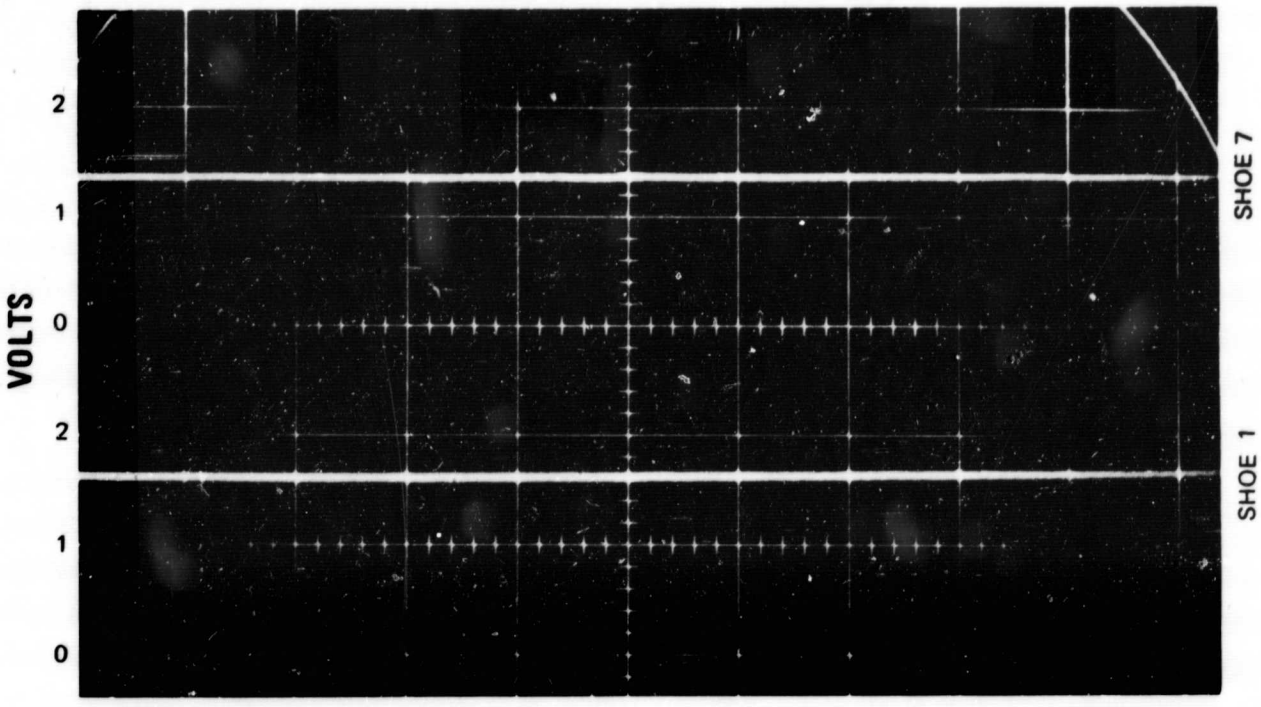

Figure 40 One-Side Floated-Shoe End Seal: Capacitance Probe Outputs, 0 RPM, Seal Pressure Differential 70 PSI (XP-98590)

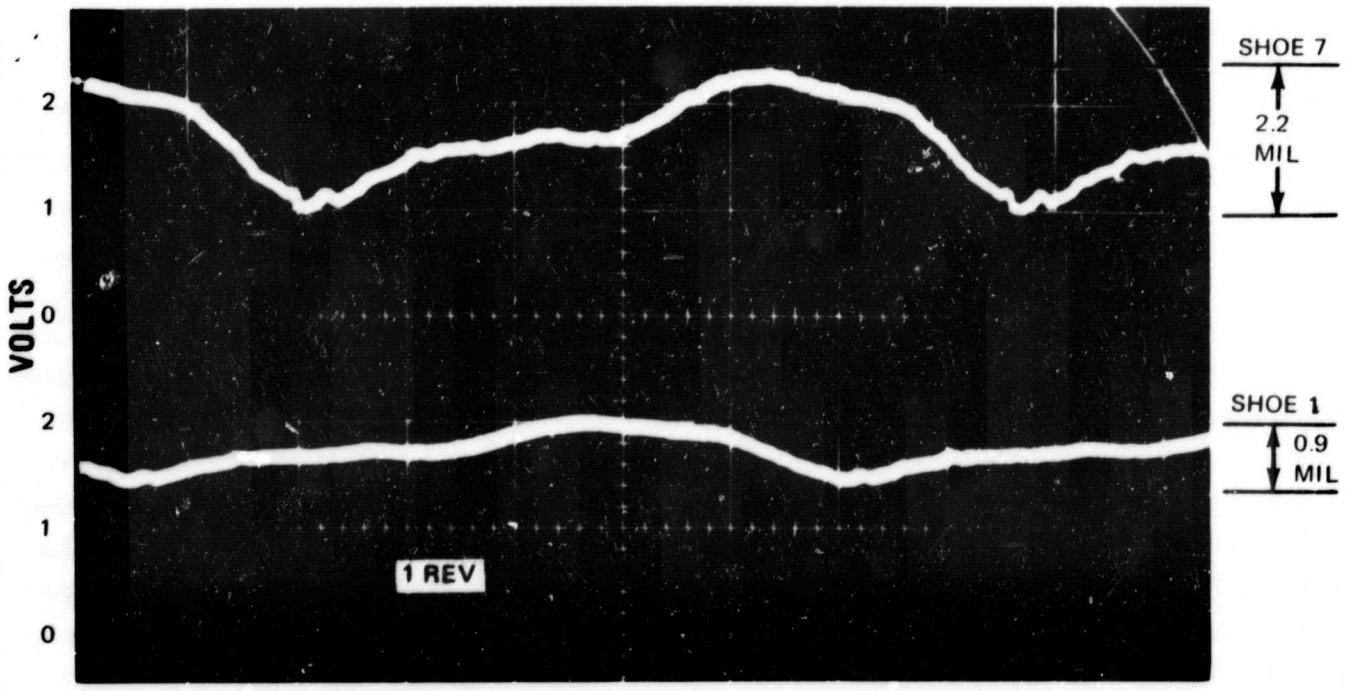

Figure 41 One-Side Floated-Shoe End Seal: Capacitance Probe Outputs, 950 RPM, Seal Pressure Differential 70 PSI, Sweep Time 10 Milliseconds/cm (XP-98593)

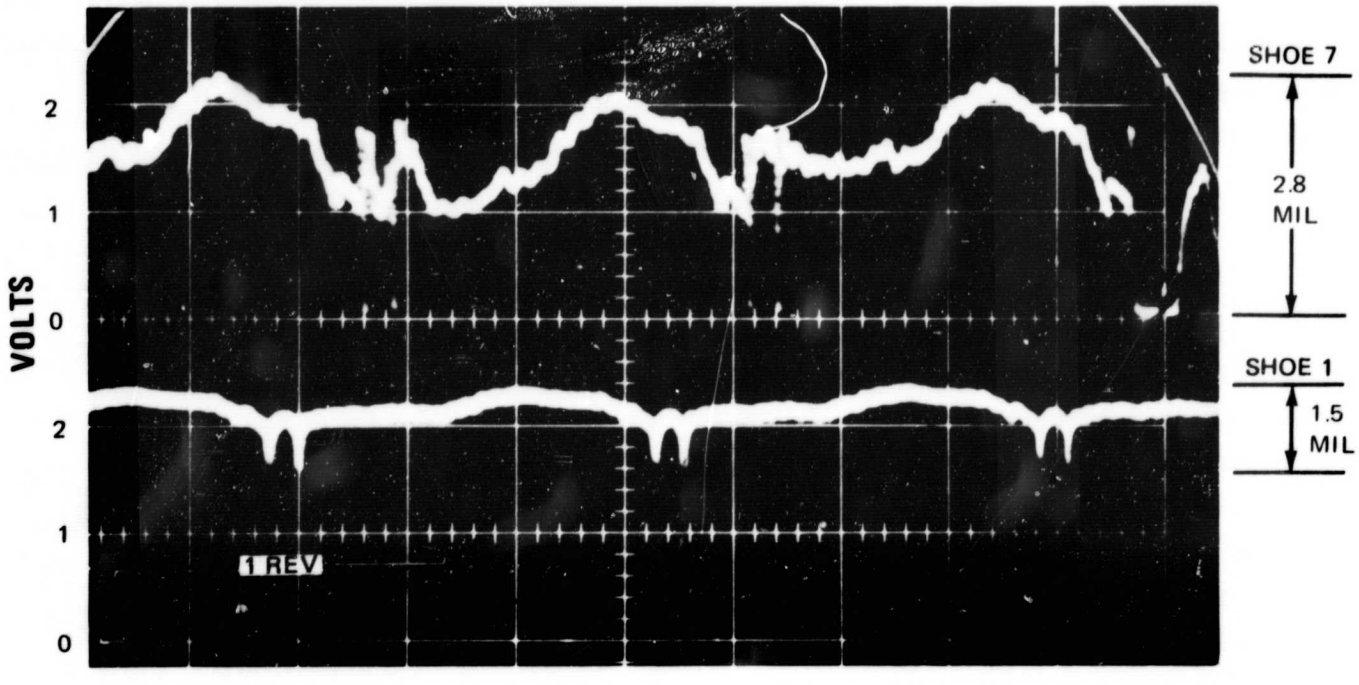

Figure 42 One-Side Floated-Shoe End Seal: Capacitance Probe Outputs, 1700 RPM, Seal Pressure Differential 70 PSI, Sweep Time 10 Milliseconds/cm (XP-98591)

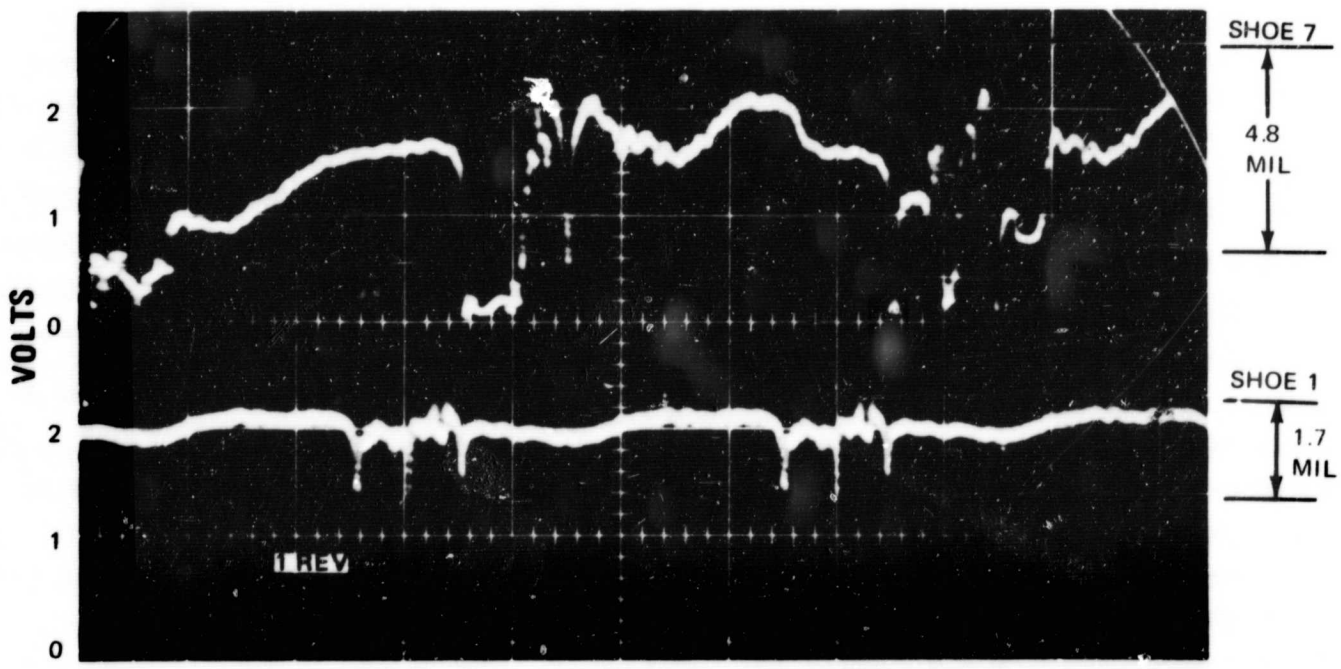

Figure 43 One-Side Floated-Shoe End Seal: Capacitance Probe Outputs, 3000 RPM, Seal Pressure Differential 70 PSI, Sweep Time 5 Milliseconds/cm (XP-98592)

2. POST-TEST INSPECTION

When the seal had been removed from the rig and inspected, it was found that the aluminum oxide hardcoat on the seal shoes had worn to the bottom of the Rayleigh pads or beyond at 60 percent of the pad locations. The wear is shown in Figures 44 through 46. The probe in shoe segment Number 7 failed by shorting out at approximately 200 seconds into the run. Upon inspection, the tip of the probe was found to be heavily smeared.

The chrome carbide hardcoat on the seal runner exhibited an uneven wear track. In some locations there was almost no wear, while in others the hardcoat had worn to a depth of approximiately 0.006 inch. Wear on the runner is shown in Figures 47 through 49. After the test, the mounted runner surface was found to have an axial runout of 0.012 inch, a value larger than that which the seal's dynamic characteristics could tolerate. The runner wear and axial runout measurements in a free state are shown in Figure 50. The high degree of rotor face waviness and out-of-flatness can probably be explained by localized heating incurred during the dynamic test. The subsequent local material removal could have aggravated the deformation by relaxing the residual stresses present from the chrome-carbide hardcoating operation. Before the test, the runner surface was found to be parallel to surface E (see Figure 50) within 0.0005 inch, and the axial runout of the runner mounted in the rig was found to be 0.0035 inch.

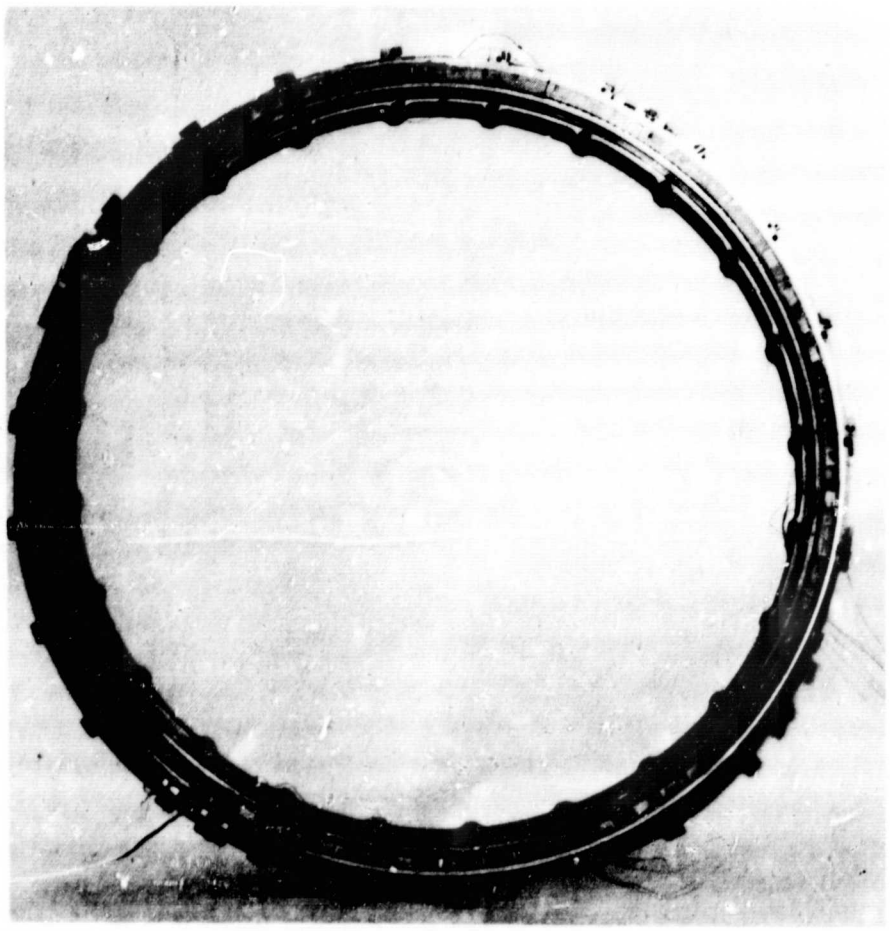

Figure 44 One-Side Floated-Shoe End Seal After Dynamic Calibration (CN-20328)

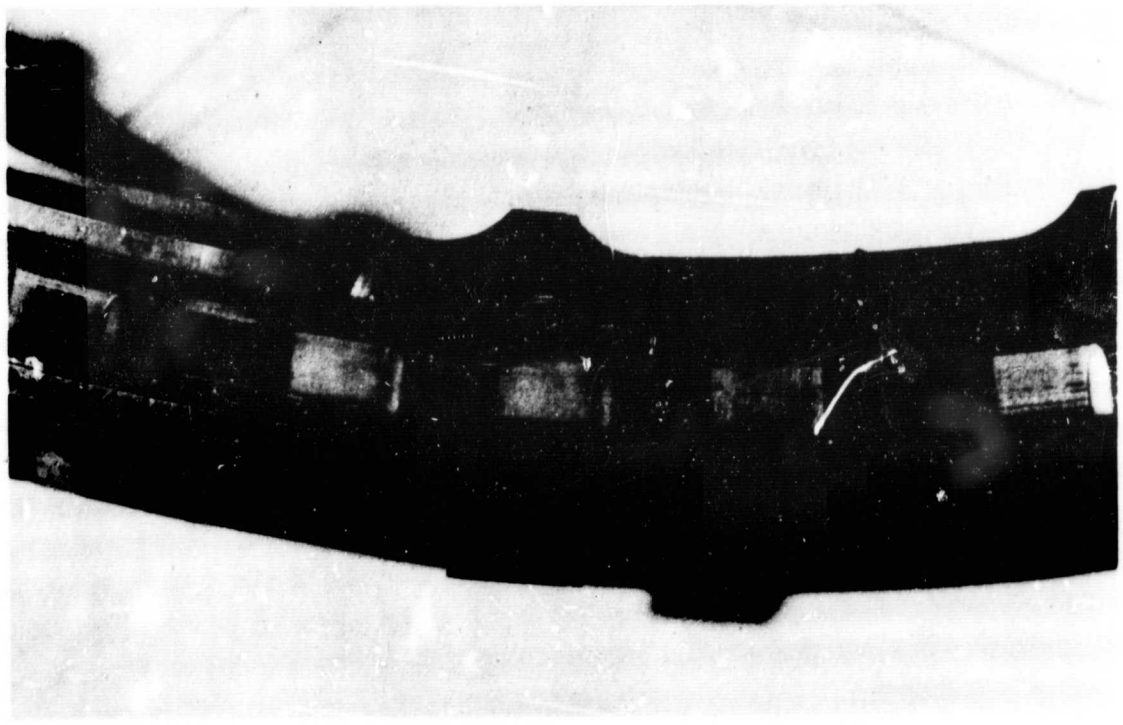

Figure 45 Close-up of Relatively Undamaged Seal Shoe after Dynamic Calibration of One-Side Floated-Shoe End Seal (CN-20329)

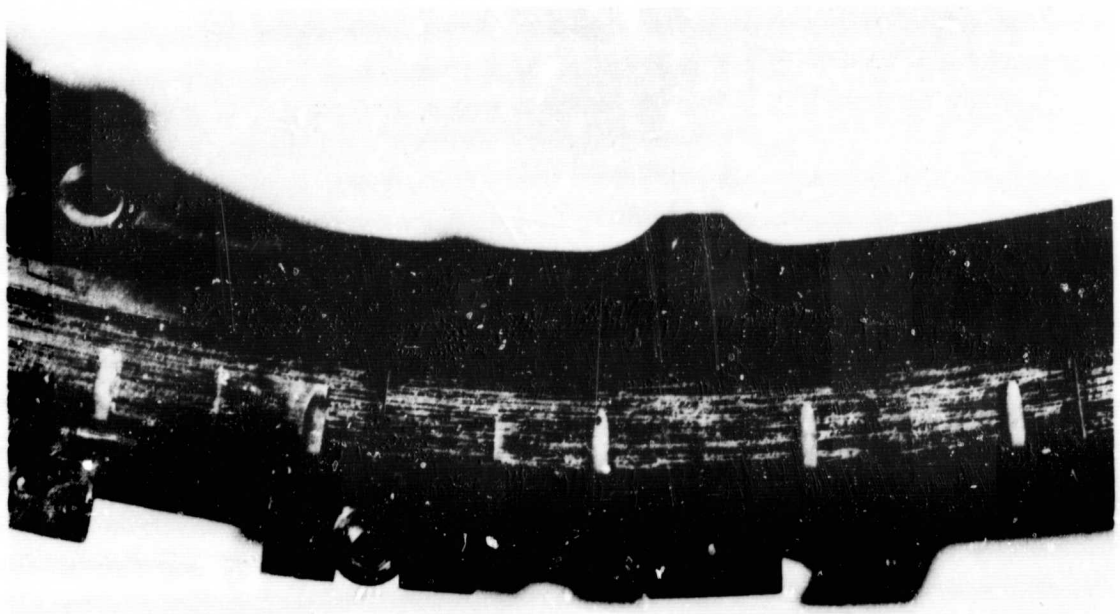

Figure 46 Close-up of Badly-Worn Seal Shoe after Dynamic Calibration of One-Side Floated-Shoe End Seal (CN-20330)

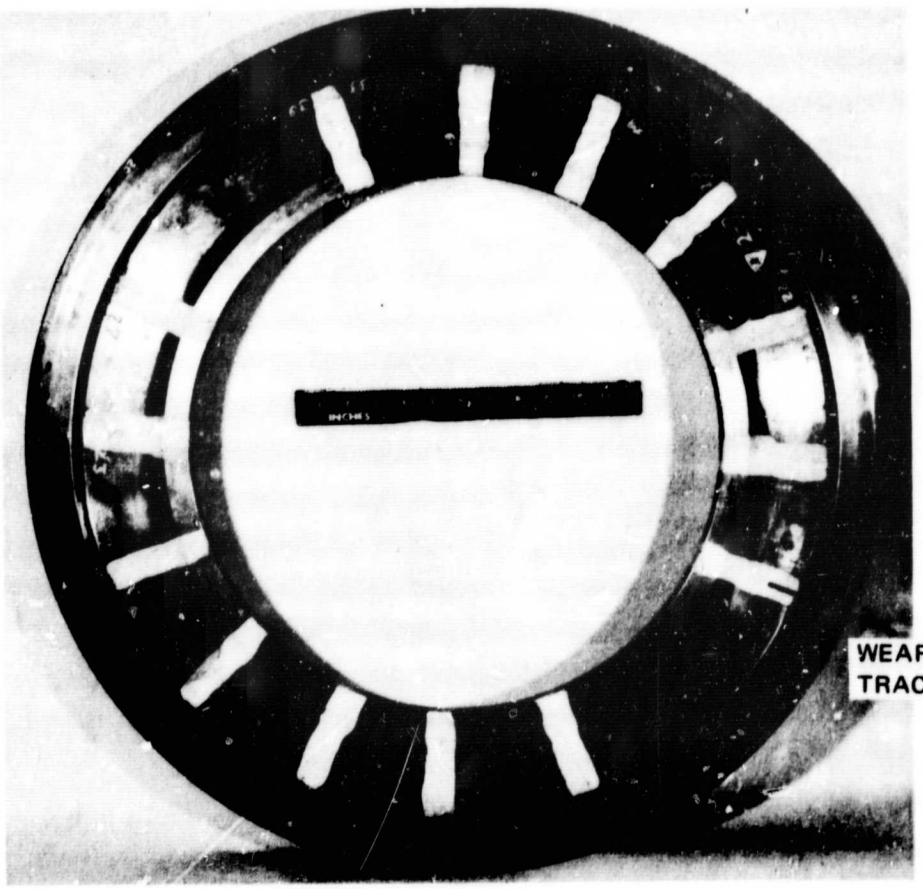

Figure 47

One-Side Floated-Shoe End Seal Runner after Dynamic Calibration

(CN-20333)

Figure 48

Close-up of Lightly-Scored Area on Seal Runner after Dynamic Calibration of One-Side Floated-Shoe End Seal

(CN-20331)

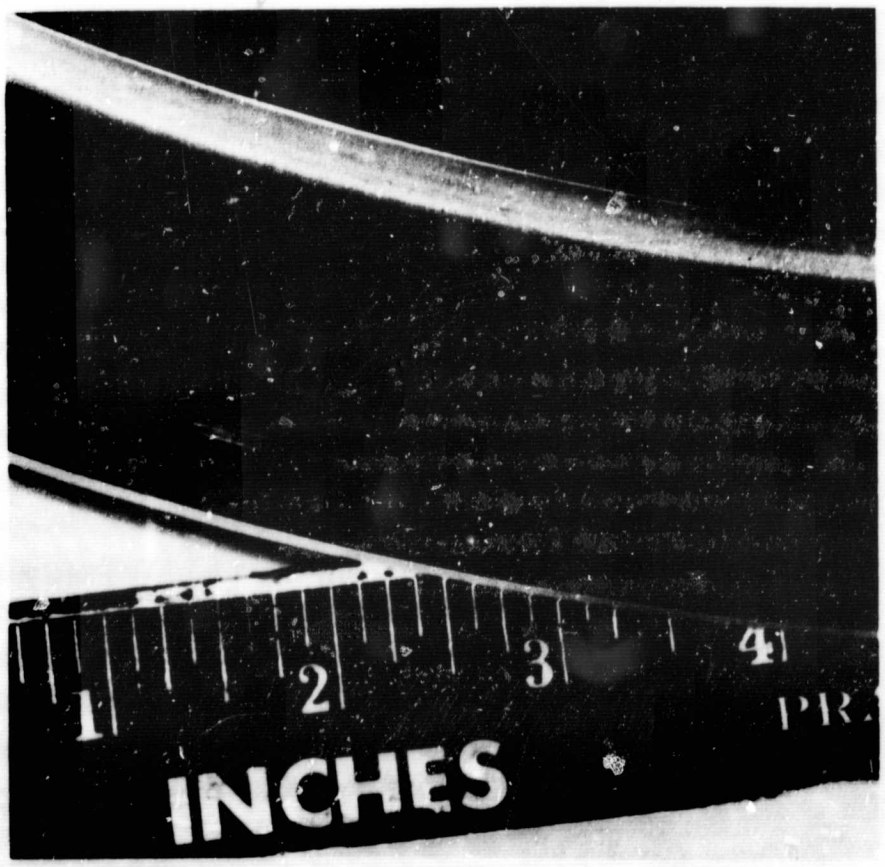

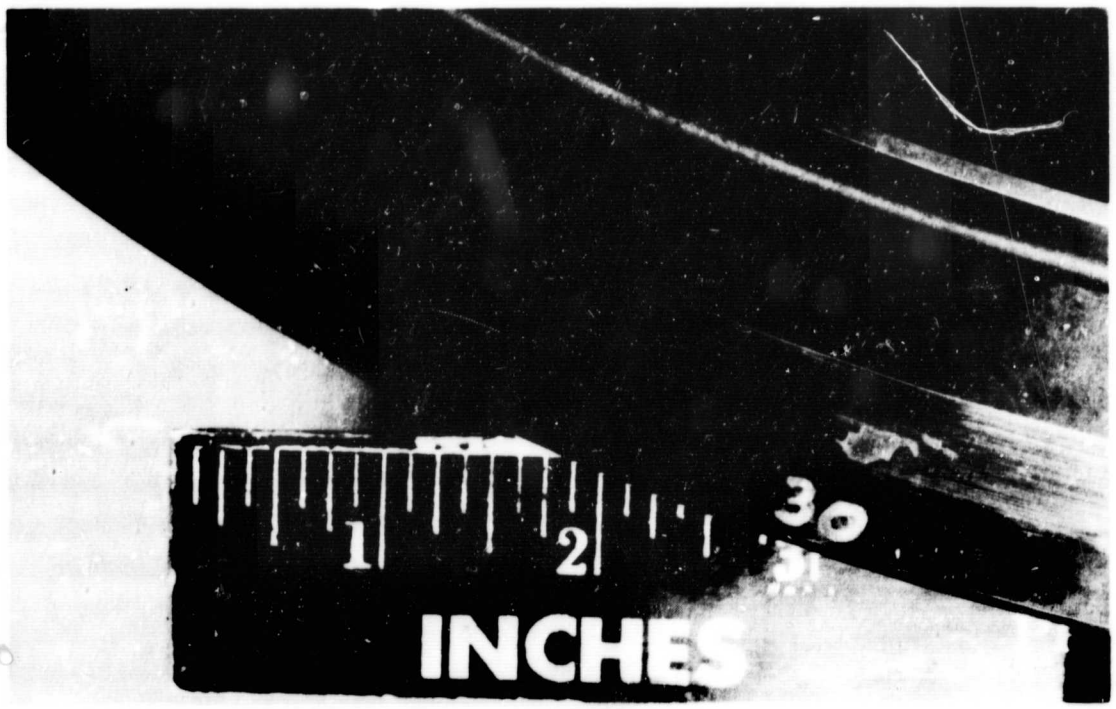

Figure 49 Close-up of Badly-Worn Area on Seal Runner after Dynamic Calibration of One-Side Floated-Shoe End Seal (CN-20332)

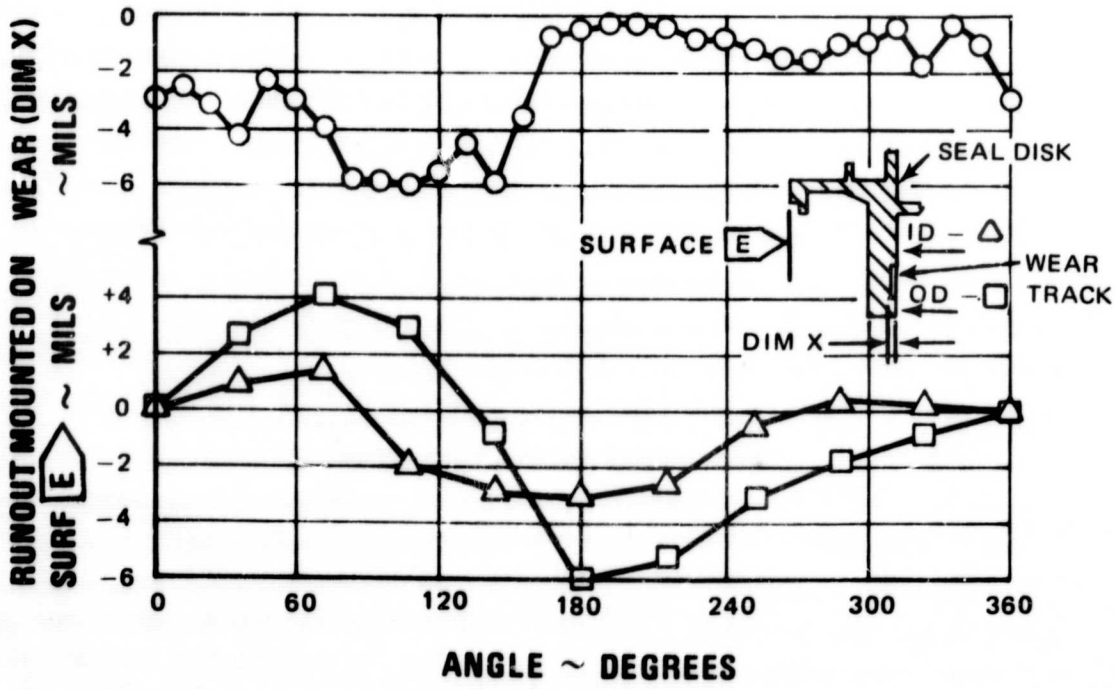

Figure 50 Wear and Runout on the Runner of the One-Side Floated-Shoe End Seal after Dynamic Calibration

B. TESTING OF THE ONE-SIDE FLOATED-SHOE INTERSTAGE SEAL

The one-side floated-shoe interstage seal is similar to the end seal except for structural differences needed to adapt the seal specifically to the interstage position. The seal face consists of a ring of 24 shoe segments acting against a rotating surface (the seal runner) attached to the compressor seal rotor (Figure 51). The primary seal interface was between the nonrotating ring of shoes and the rotating runner surface, and the leakage flowed radially inward through the seal. Secondary seals were provided between the shoes and the carrier ring at the secondary seal pads and the one-piece thrust ring. There was another secondary seal between the carrier ring and the seal mounting ring at the secondary-seal piston ring. The assembled unit is shown in Figures 52 and 53.

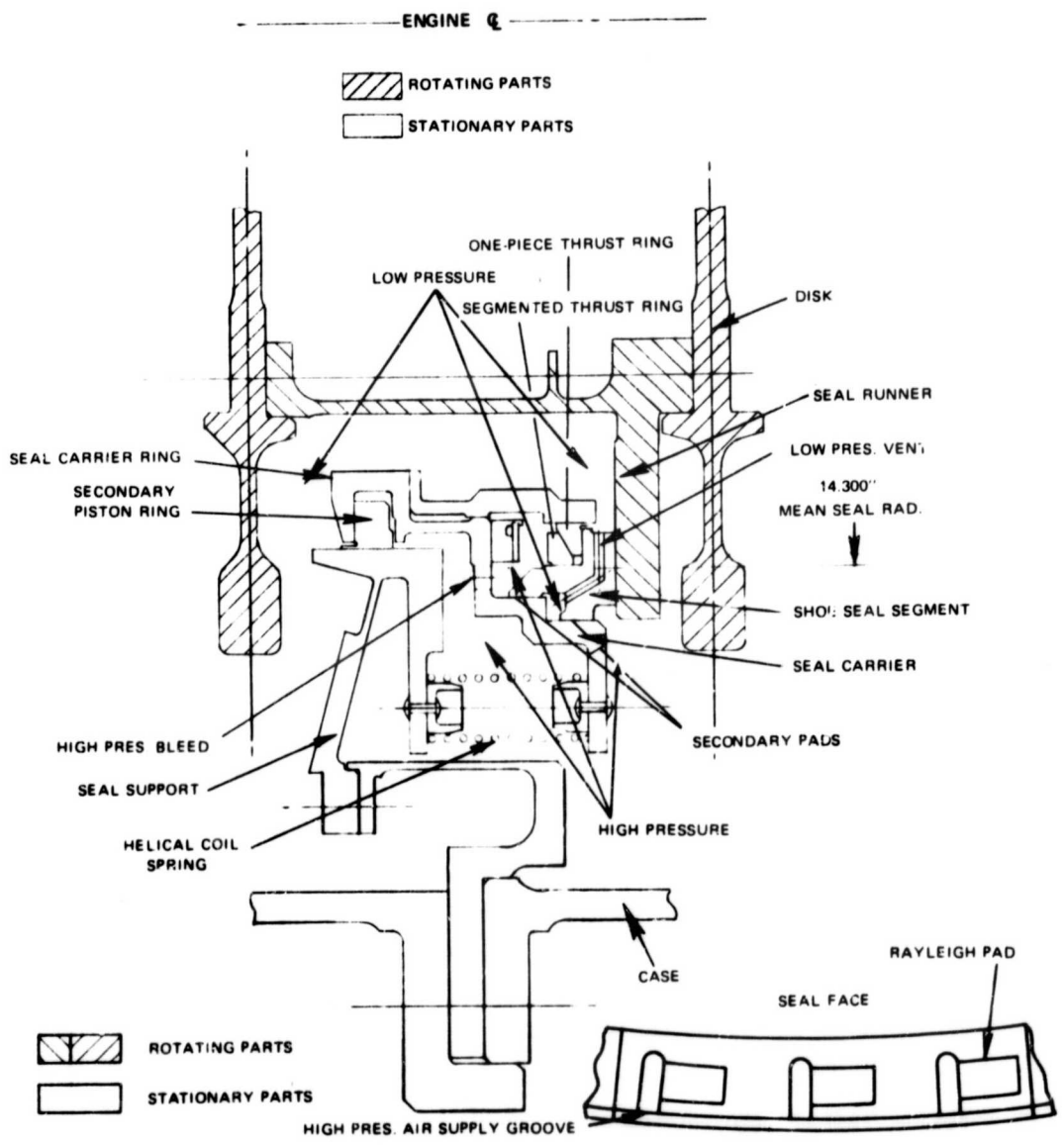

Figure 51 Schematic of One-Side Floated-Shoe Interstage Seal

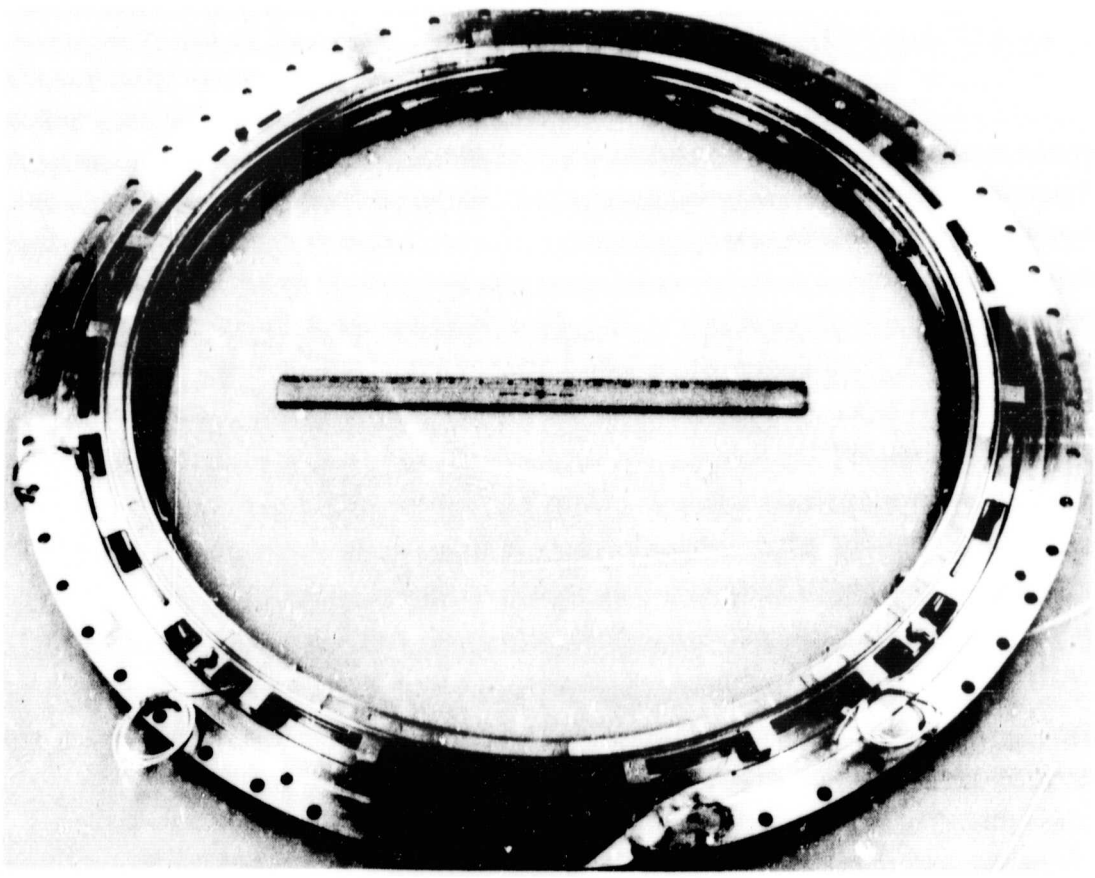

Figure 52 Overall View of Air-Film-Riding Sealing Face of One-Side Floated-Shoe Interstage Seal (WCN-48)

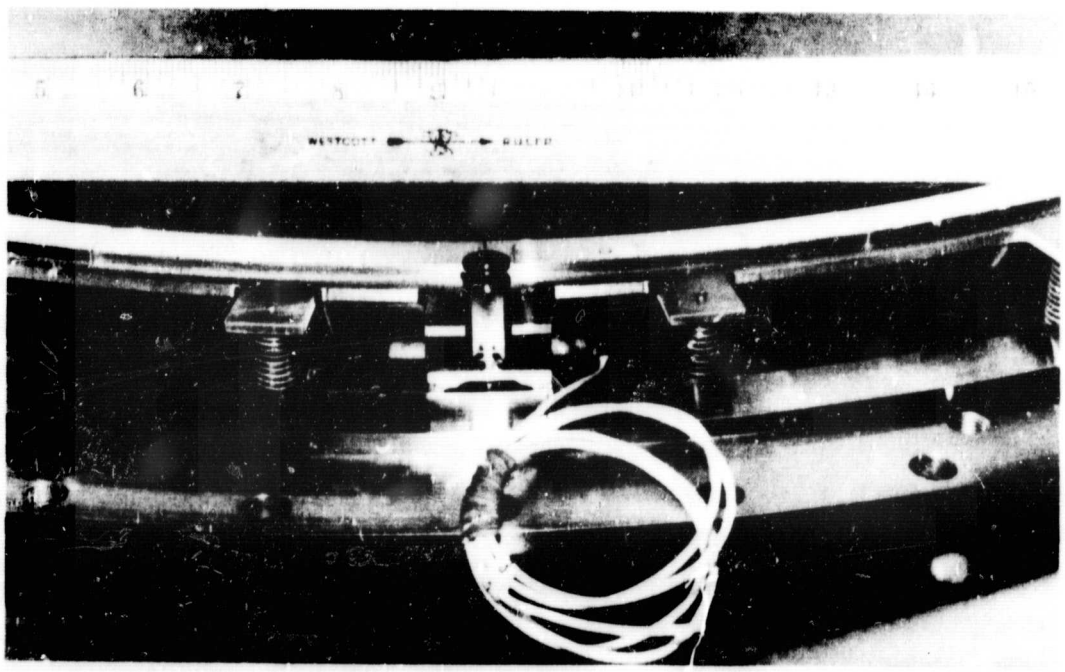

Figure 53 Close-up View of Front of One-Side Floated-Shoe Interstage Seal, Showing Proximity Probe and Anti-Torque Pin with Indexing Slots (WCN-50)

1. ROOM TEMPERATURE DYNAMIC TESTING

Axial surface runouts of the runner were measured and the seal was installed in the full-scale rig for dynamic testing. The surface was flat but was not square with the rotor centerline, producing a one-mode wave form (Figure 54). The rotor was installed in the rig and a seal compression of 0.124 inches was set.

Breakaway-torque measurements made at the rig during static testing indicated that hydrostatic lift-off was not achieved, since no drop in torque was noted when the seal pressure differential was increased. At a seal pressure differential of zero psi, the breakaway torque was 65 inch-pounds.

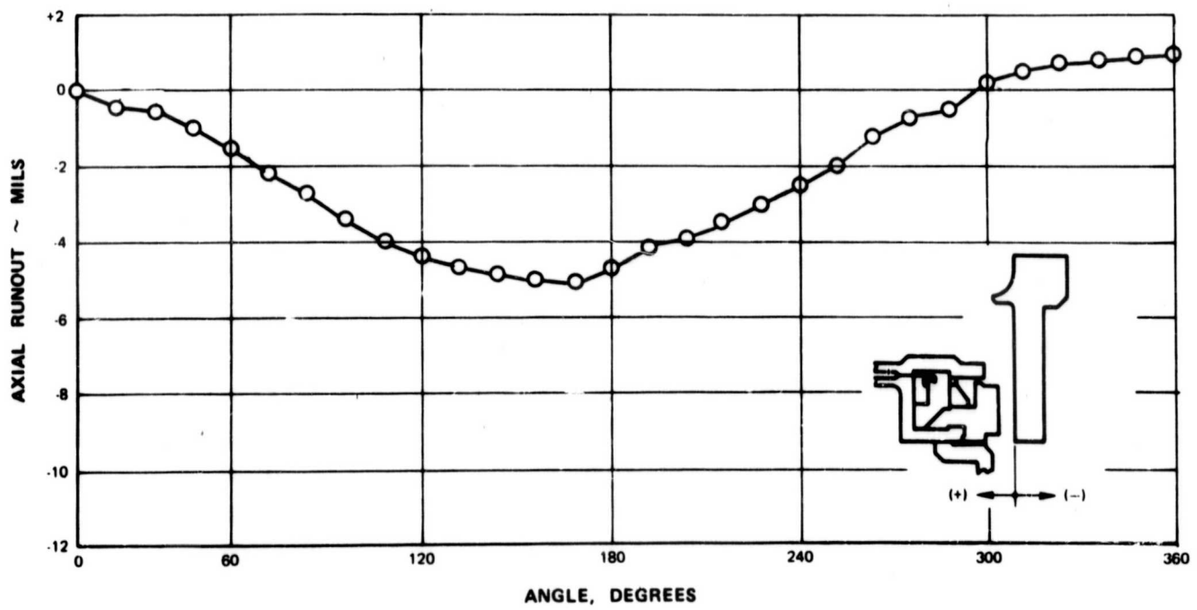

Figure 54 Pre-Test Axial Runout of One-Side Floated-Shoe Interstage Seal

During the room-temperature dynamic testing, a pressure differential of approximately 5 psi was maintained. This pressure was selected in order to provide hydrostatic lift at the secondary seal pads without locking the primary seal face against the runner. Rotor speed was increased rapidly to lift the shoes off of the runner hydrodynamically. Rotor temperatures increased during acceleration and the run was discontinued after reaching 6200 rpm (770 ft/sec), when the temperatures spiked to levels in excess of 500°F. Figures 55 through 58 are photographs of the oscilloscope display of the capacitance probe signal. Since the rotor temperatures were caused by bbing, the gap which the probe seemed to indicate was probably caused by tilting of the shoe. After a short period of running the probe shorted out. Figure 59 is a calibration curve for the probe.

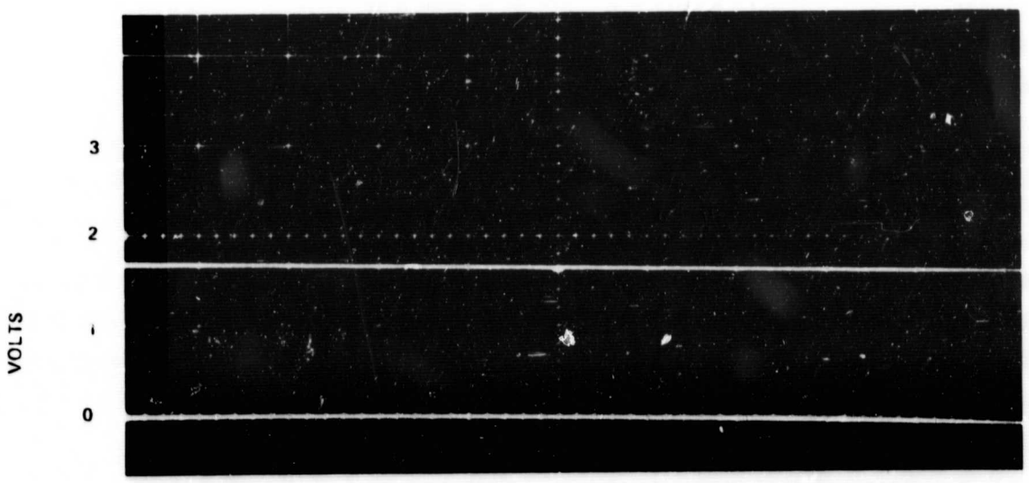

Figure 55 One-Side Floated Shoe Interstage Seal: Capacitance Probe Outputs 0 RPM, Seal Pressure Differential 4.6 PSI

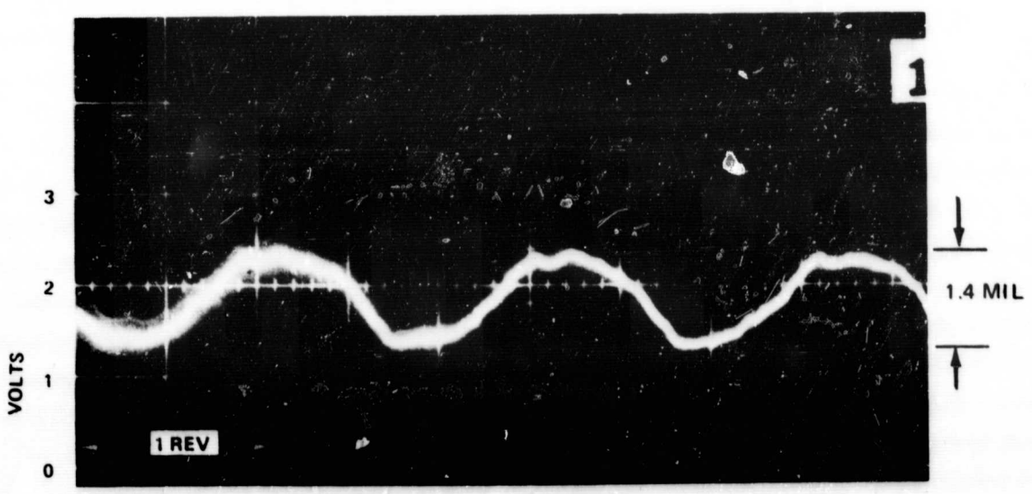

Figure 56 One-Side Floated-Shoe Interstage Seal: Capacitance Probe Outputs, 1910 RPM, Sweep Time 10 Milliseconds/cm

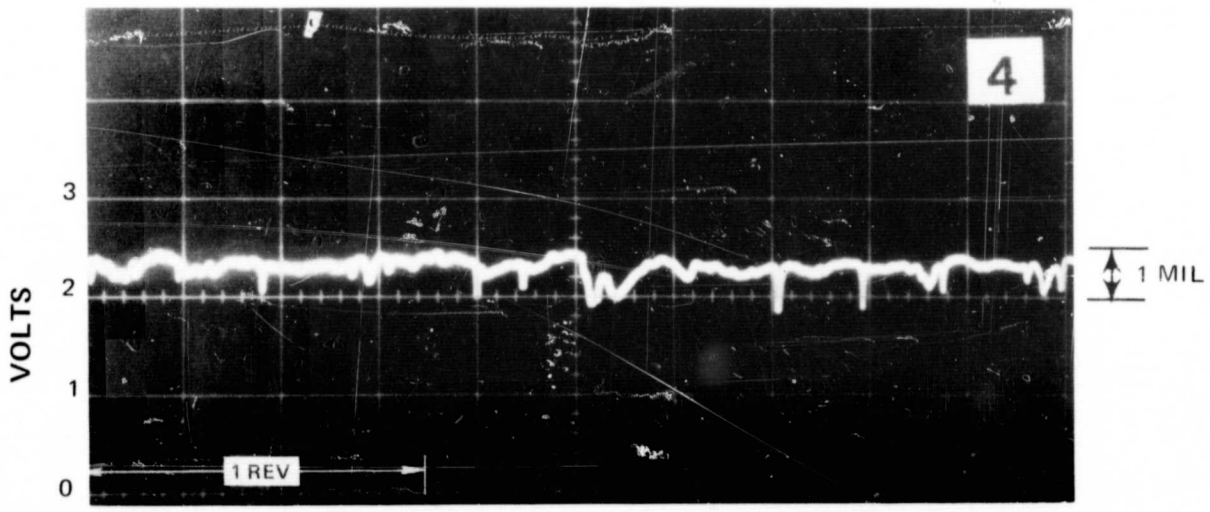

Figure 57 One-Side Floated-Shoe Interstage Seal: Capacitance Probe Outputs, 3500 RPM, Sweep Time 5 Milliseconds/cm

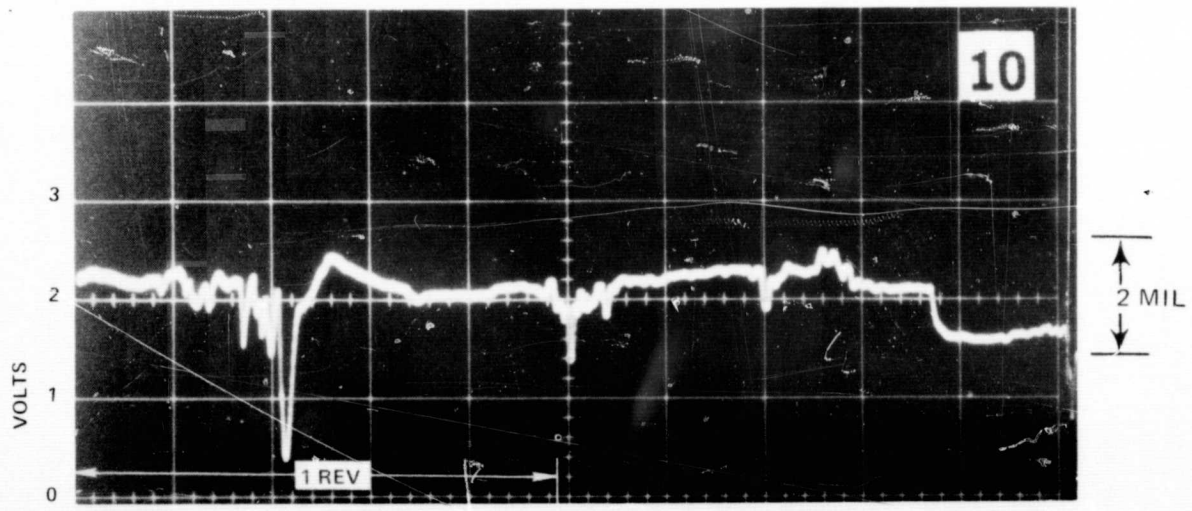

Figure 58 One-Side Floated-Shoe Interstage Seal: Capacitance Probe Outputs, 6200 RPM, Sweep Time 2 Milliseconds/cm

20

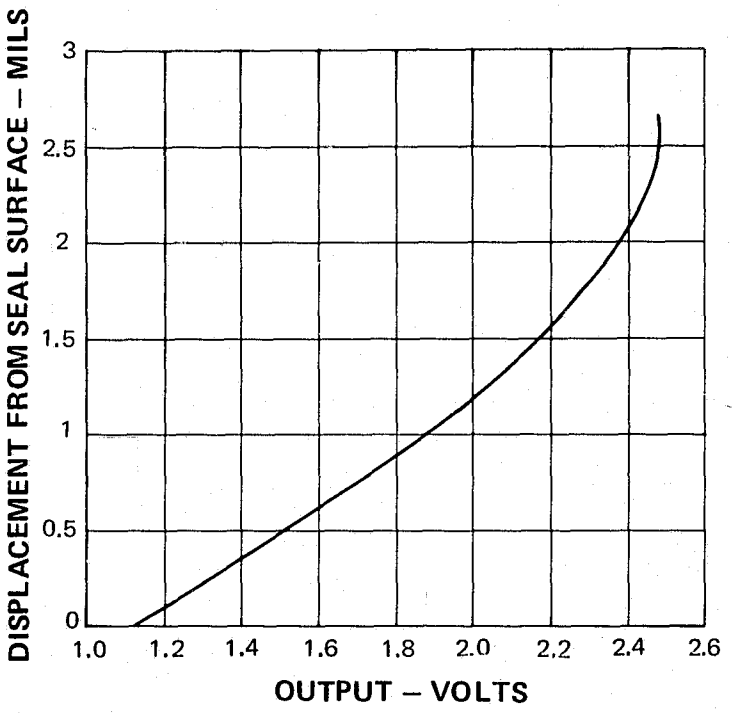

Figure 59 Calibration of the Capacitance Probe in the One-Side Floated-Shoe Interstage Seal

Reduction of the automatically recorded data showed that there were several rapid temperature excursions above 2000 rpm and that the seal pressure differential dropped from the initial 4.6 psi to 0.8 psi. An apparent voltage surge in the recorder supply line caused the recorder to be inoperative for thirty seconds. This occurred approximately 60 seconds into the run and about the same time as the first temperature excursion. Figure 60 is a chronology of the test run.

2. POST-TEST INSPECTION

The wear pattern of the interstage seal was very similar to the wear pattern of the one-side floated-shoe end seal. The primary sealing face on all shoes was worn down to or below the Rayleigh pads, which were one mil deep. Figure 61 shows two views of the seal after testing. Wear at the outer edge was from zero to two mils deep and wear at the inner edge was four four to seven mils deep, indicating that the shoes had tilted. Axial runouts of the runner after testing are shown in Figure 62.

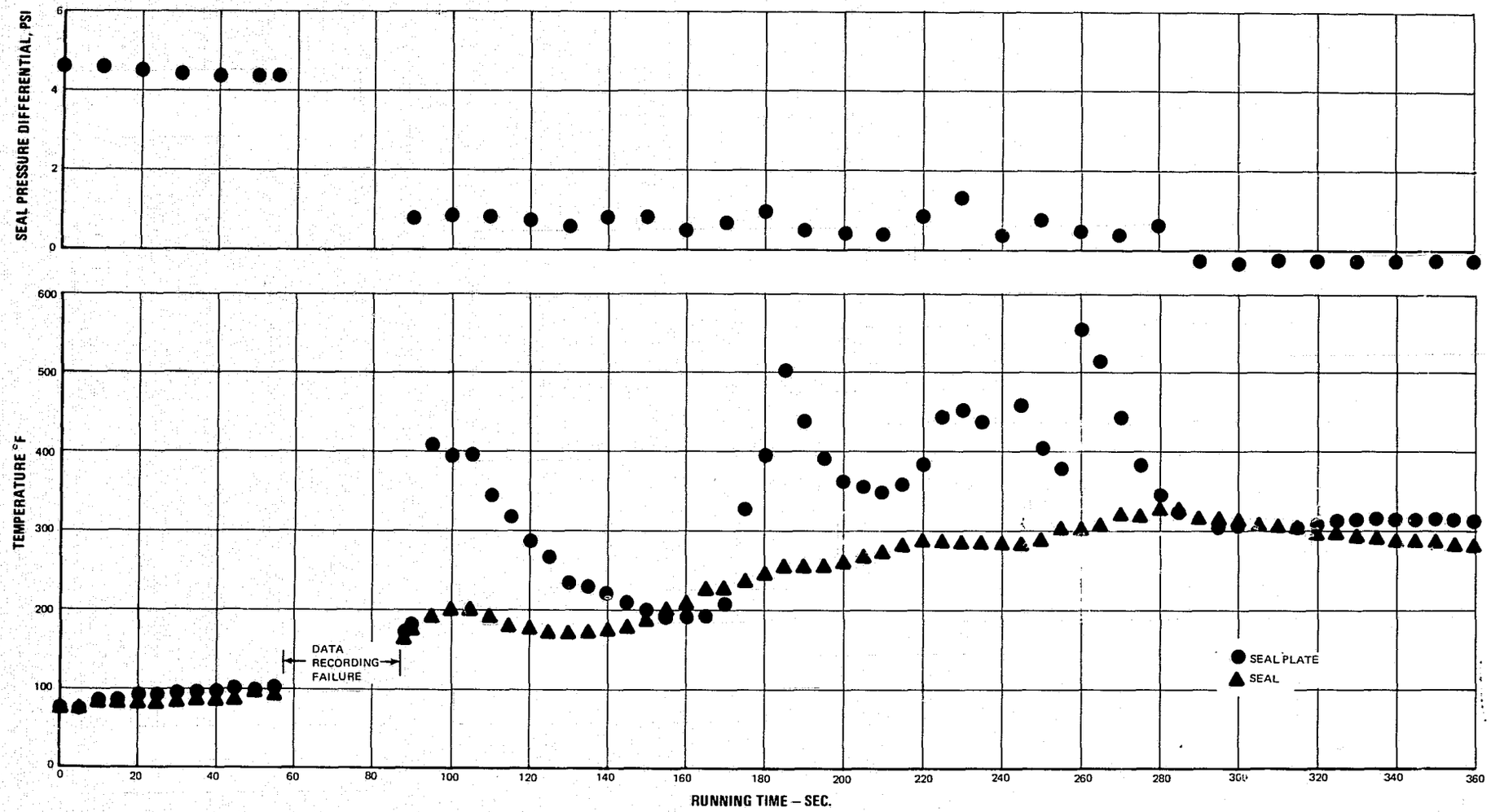

Figure 60 One-Side Floated-Shoe Interstage Seal Dynamic Calibration

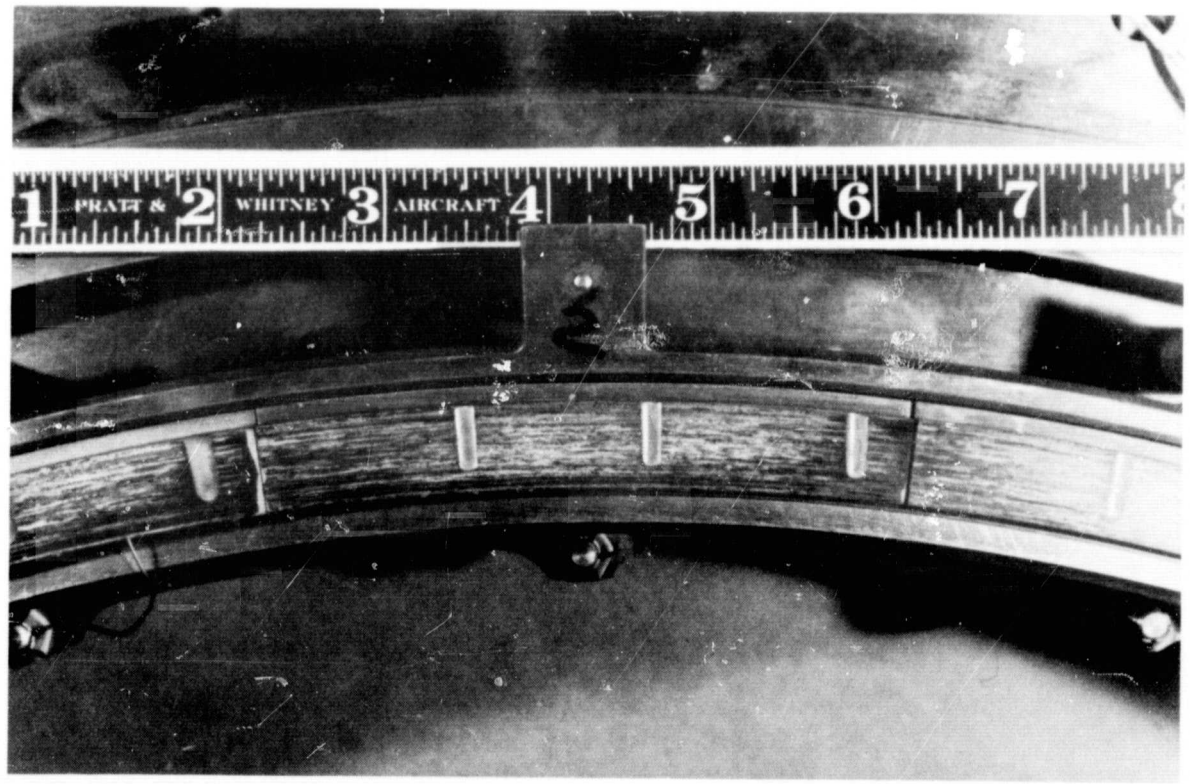

SEAL SURFACE

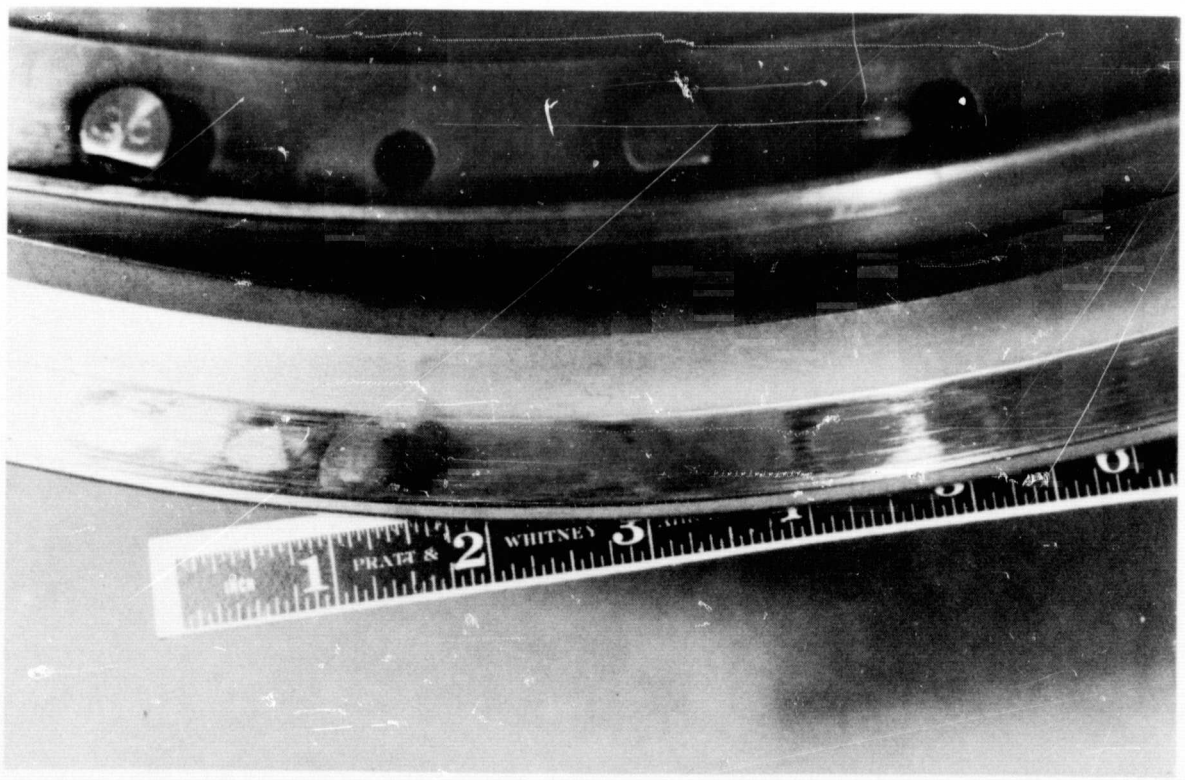

RUNNER SURFACE

Figure 61 One-Side Floated-Shoe Interstage Seal after Dynamic Run (CN-27095, 27097)

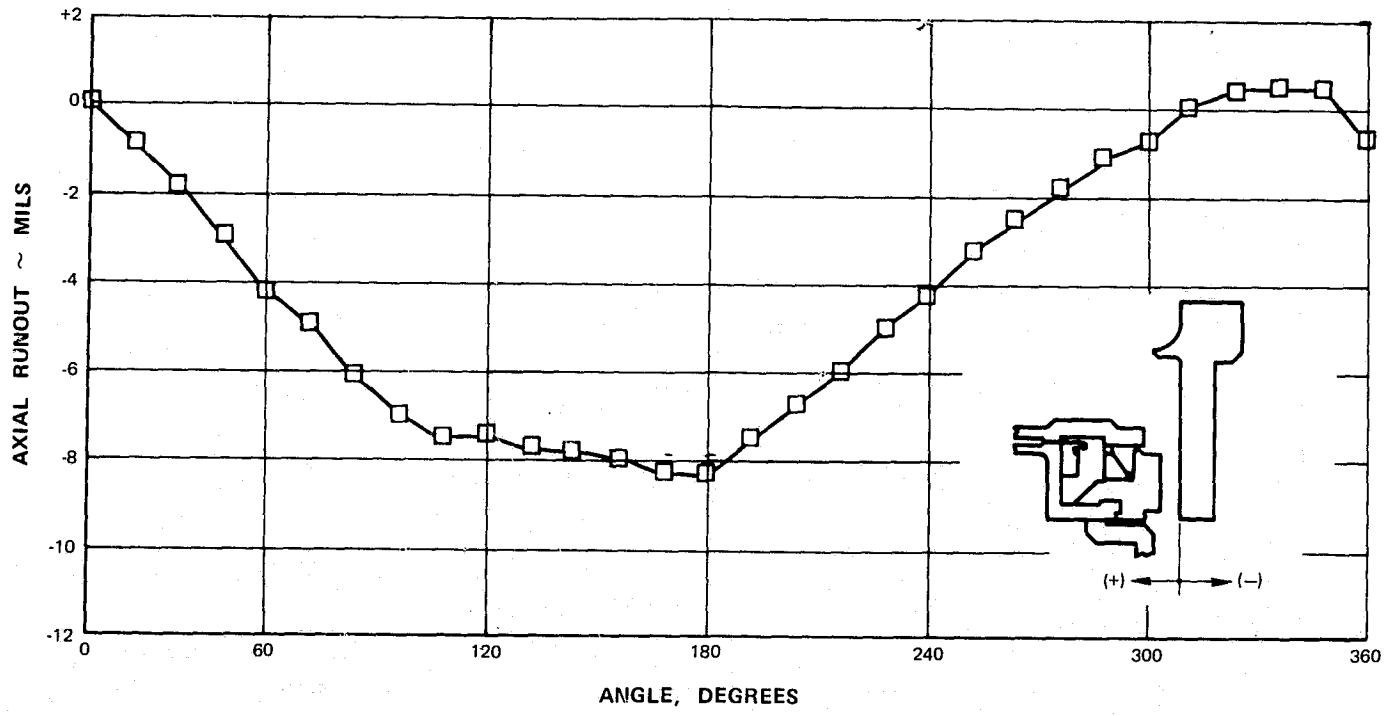

Figure 62 Post-Test Axial Runout of One-Side Floated-Shoe Interstage Seal

C. TESTING OF THE OC DIAPHRAGM END SEAL

The OC diaphragm end seal (Figures 63 and 64) employed a thin, flexible, one-piece strip as the primary seal element, providing a high degree of conformity to runner distortion. The primary seal ring was supported by three C-shaped semitoroidal diaphragms mounted on a floating seal carrier ring. This carrier ring provided for axial travel relative to the main engine structure, and a secondary seal piston ring was used between the carrier and the seal mounting ring. One of the C diaphragms formed a seal between the high-pressure and low-pressure areas. The other two C diaphragms faced each other and formed a chamber to which high-pressure air was admitted. This design permitted direct balancing of the moments on the thin strip. Thickness could be decreased with this design, and flexibility and tracking capability could be increased. Compared to other thin-strip designs, low residual-moment imbalance was easier to achieve because the moment balance was achieved with methods which were more nearly independent of angular displacements of the strip.

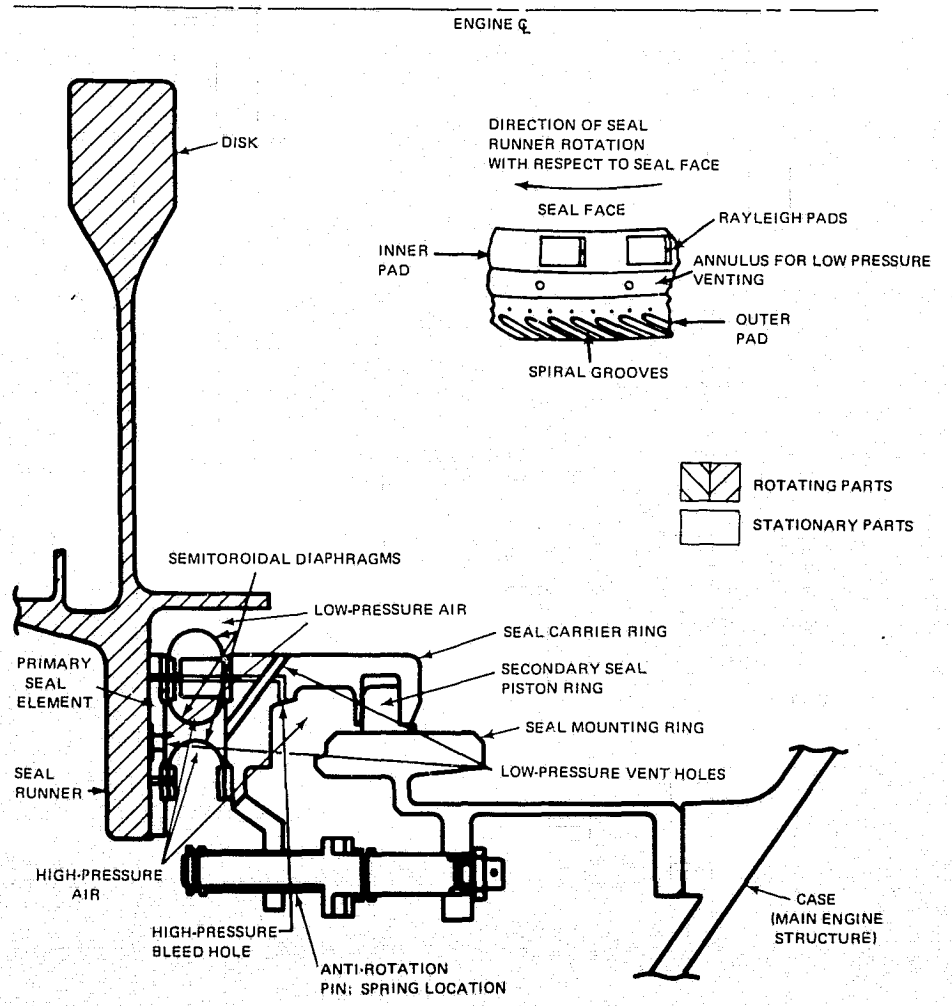

Figure 63 Schematic of OC Diaphragm End Seal

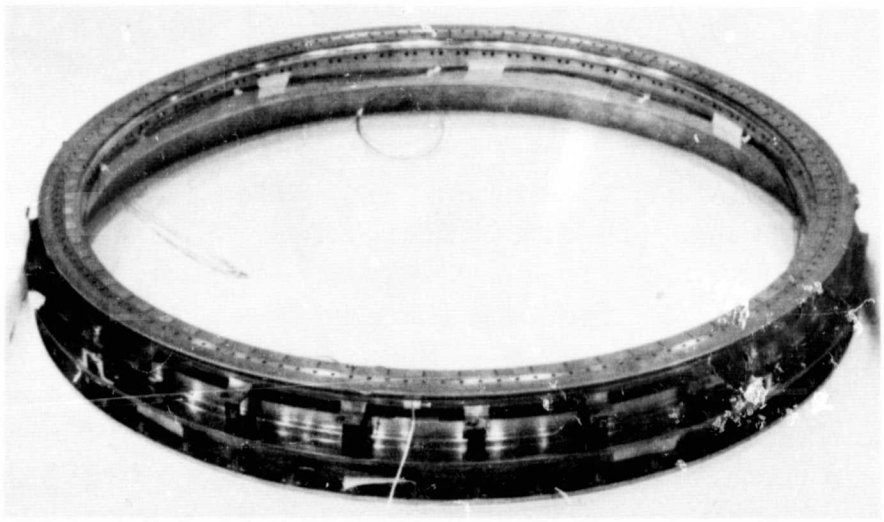

Figure 64 OC Diaphragm End Seal (XPN-12493)

1. ROOM TEMPERATURE DYNAMIC TESTING

Axial runout of the runner was measured (Figure 65) and the seal was installed in the rig. A compression of 0.200 inch was established on the seal at the test stand. Seal breakaway torque was determined to be 100 inch-pounds at a zero pressure differential. Pressure differentials were applied, and additional checks were made to determine if static seal lift-off was achieved. These checks were made by calibrating rig bearing start-up torque from seal breakaway torque. If lift-off had occurred, there would have been a significant drop in torque, but the rotor could not be rotated by applying 1035 inch-pounds of torque at pressure differentials from 10 psi to 120 psi. It was apparent that the seal had hydraulically locked against the rotor and had to be tested at low pressure differentials to prevent damage to the seal antirotation devices.

The seal pressure differential was set at 5 psi and the rig was accelerated to about 6000 rpm (710 ft/sec) to take advantage of the hydrodynamic features of the seal. Pressure differential dropped to 1.5 psi shortly after starting. When rotor temperatures approached 300°F, the rig was decelerated and the test run was terminated after approximately 130 seconds. The rotor came to a stop after 210 seconds. Data were automatically recorded (Figure 66) and oscilloscope displays of the voltage outputs of the proximity probes used to measure the gap between the runner and seal face were photographed (Figures 67 through 72). Both probes had already been bench-calibrated (Figures 73 and 74). The probe, when installed in the seal, were slightly recessed from the seal surface. The second vertical scale indicates the displacement of the seal surface accounting for the amount of probe recess.

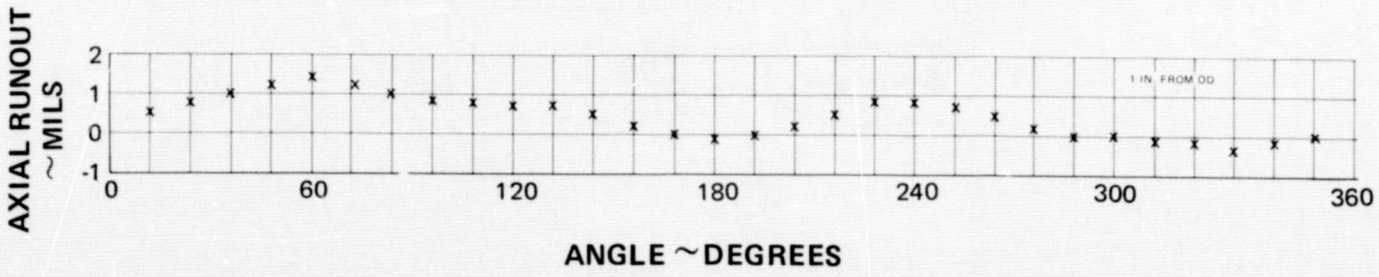

Figure 65 Pre-Test Axial Runout of OC Diaphragm End Seal

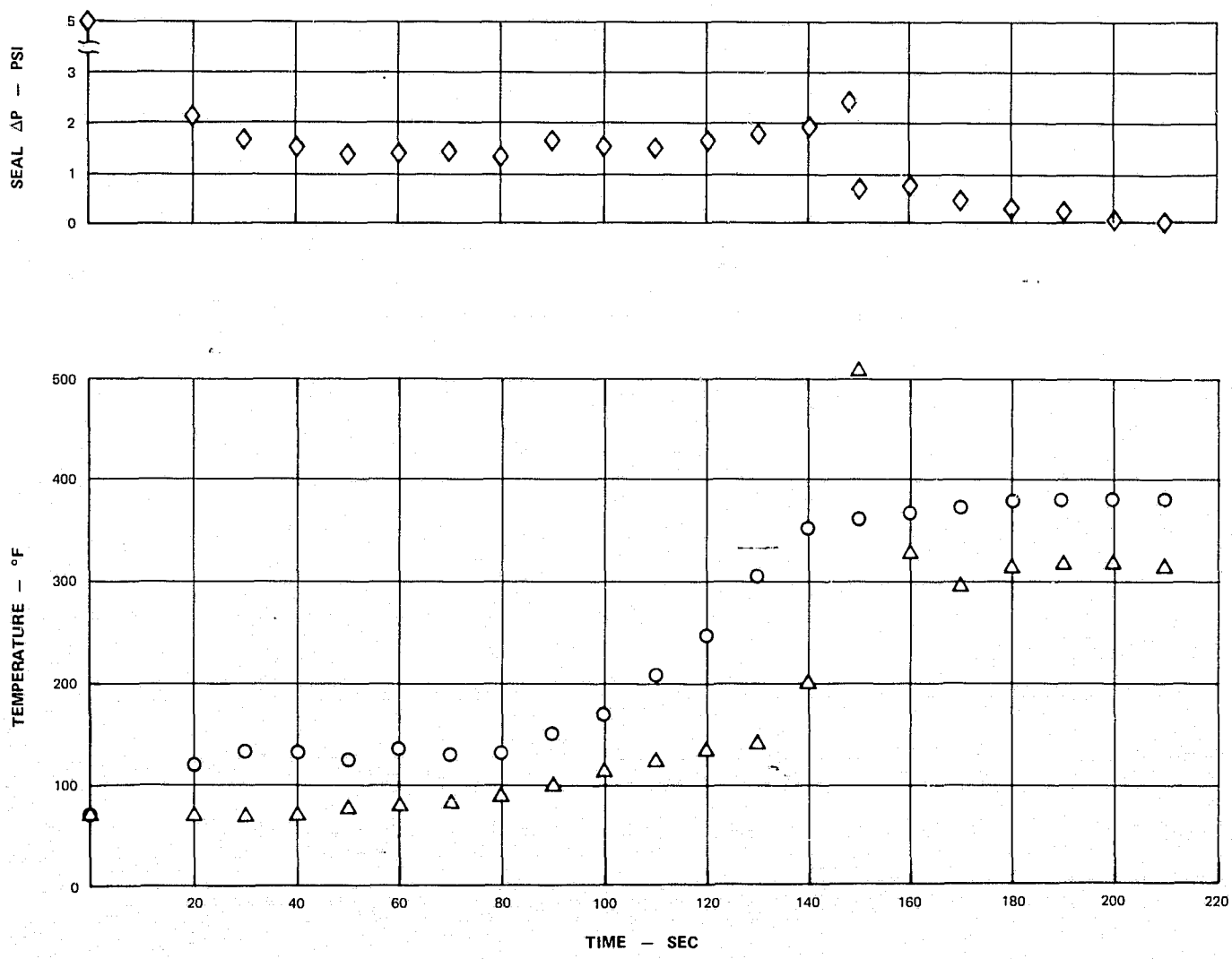

Figure 66 Chronology of OC Diaphragm End Seal Dynamic Run

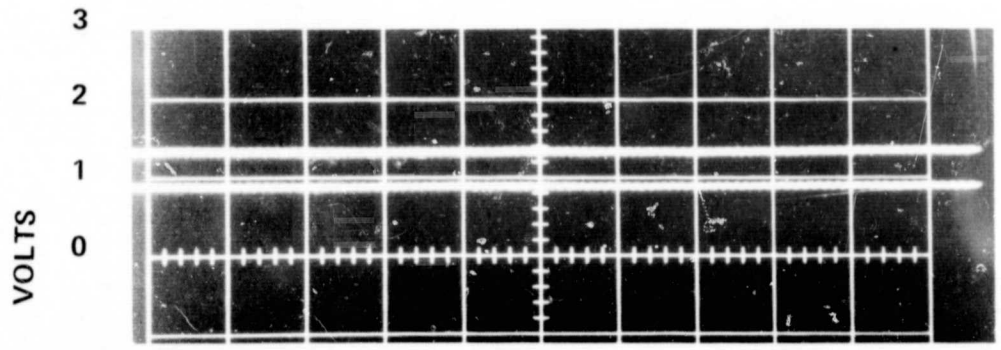

Figure 67 OC Diaphragm End Seal, Capacitance Probe Outputs at 0 RPM, Pressure Differnetial 0 PSI

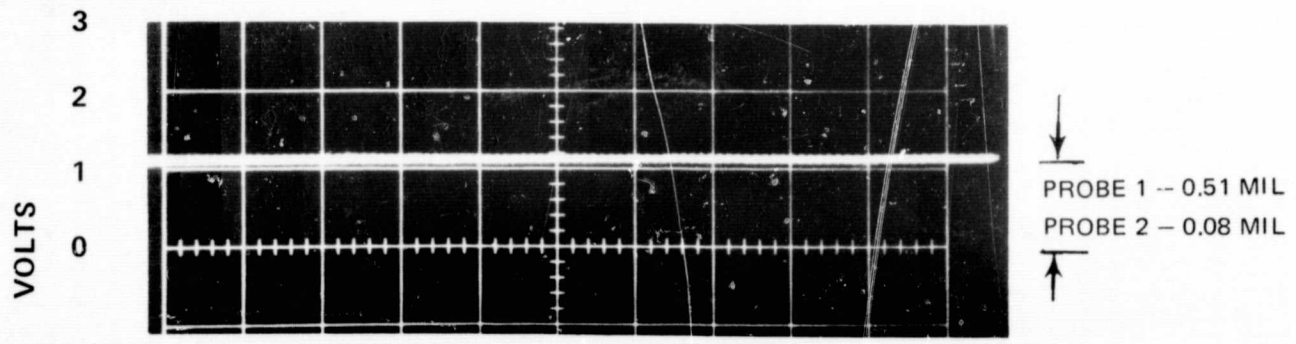

Figure 68 OC Diaphragm End Seal, Capacitance Probe Outputs at 0 RPM, Pressure Differential 5.0 PSI

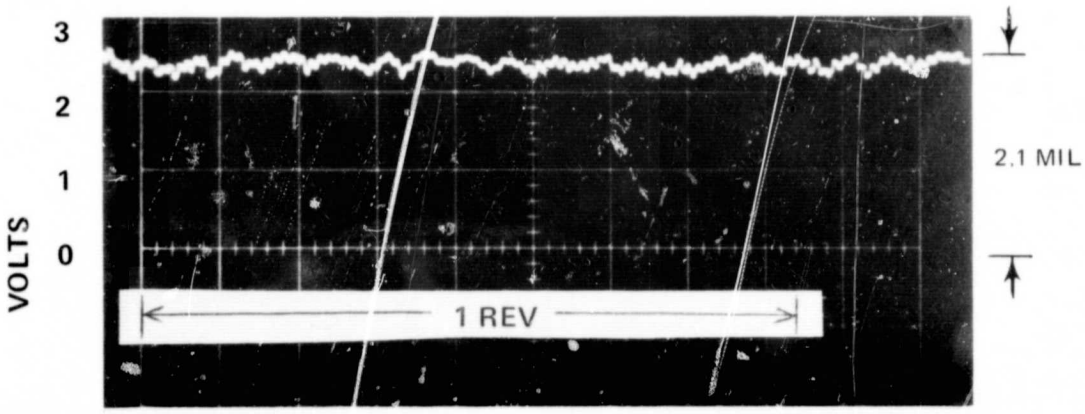

Figure 69 OC Diaphragm End Seal, Capacitance Probe No. 1 Output at 1430 RPM, Pressure Differential Approximately 2.0 PSI

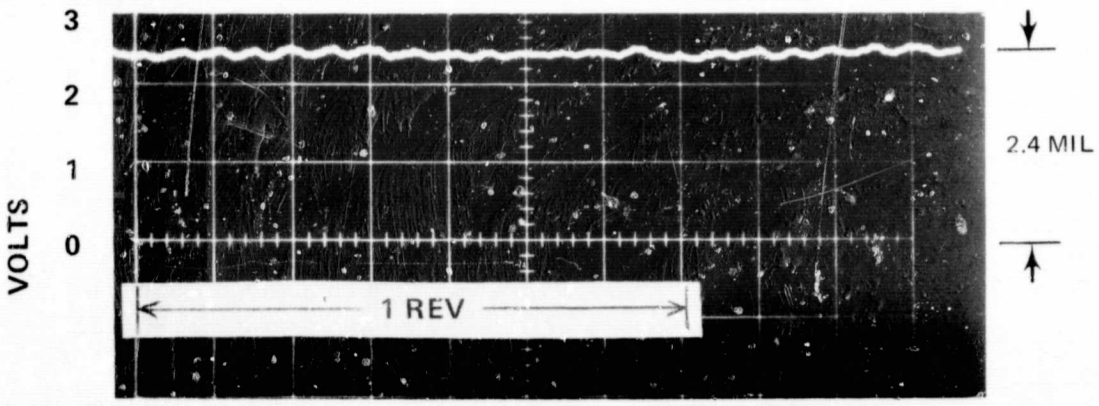

Figure 70 OC Diaphragm End Seal, Capacitance Probe No. 2 Output at 1715 RPM, Pressure Differential Approximately 1.5 PSI

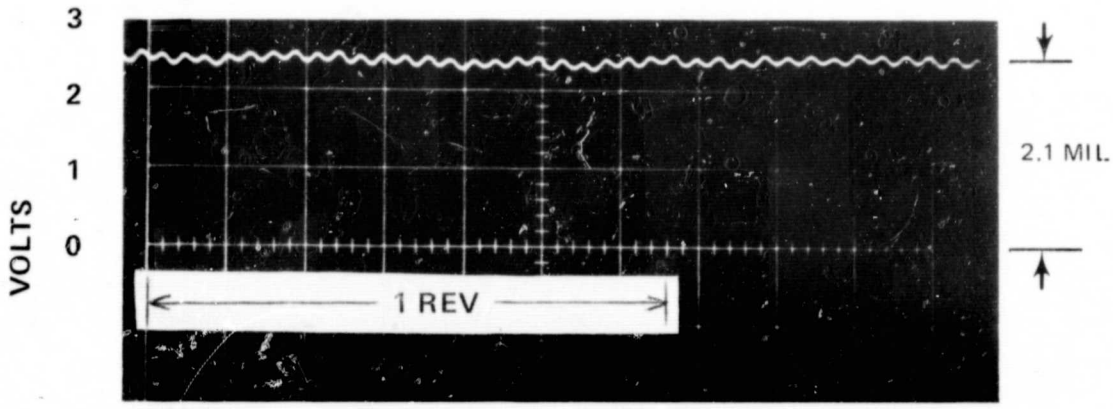

Figure 71 OC Diaphragm End Seal, Capacitance Probe No. 1 Output at 4420 RPM, Pressure Differential Approximately 1.5 PSI

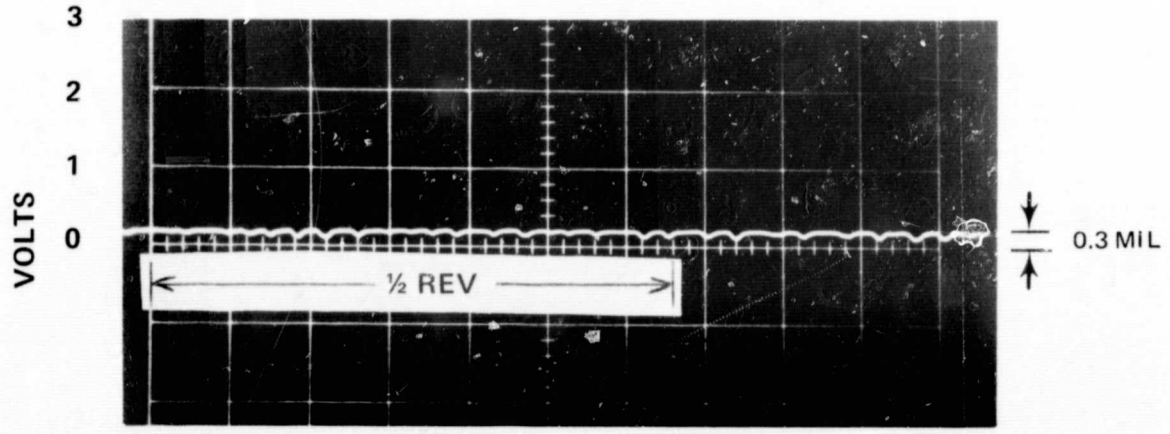

Figure 72 OC Diaphragm End Seal, Capacitance Probe No. 1 Output at 2330 RPM, Pressure Differential Approximately 1.5 PSI

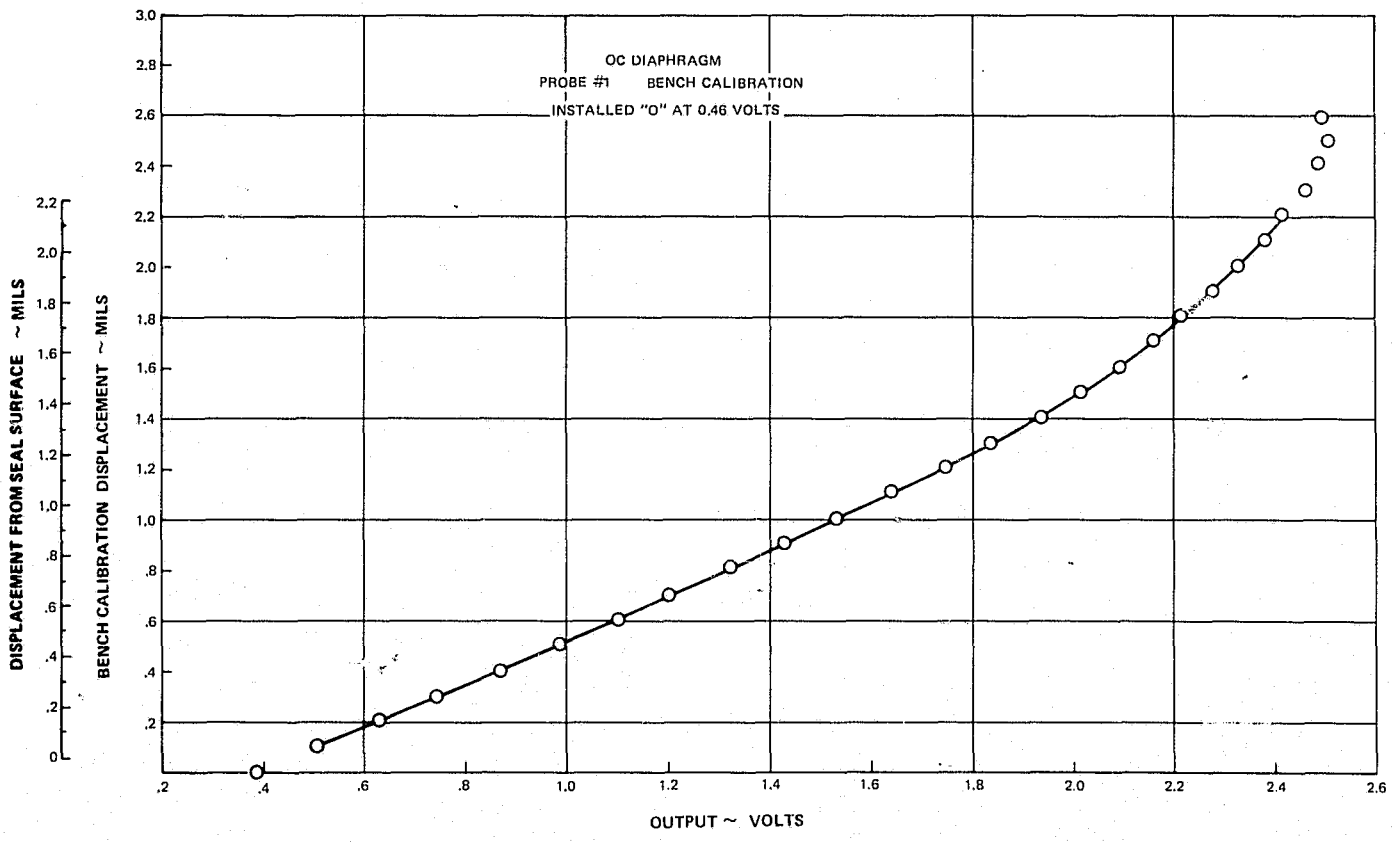

Figure 73 Bench Calibration of Probe No. 1

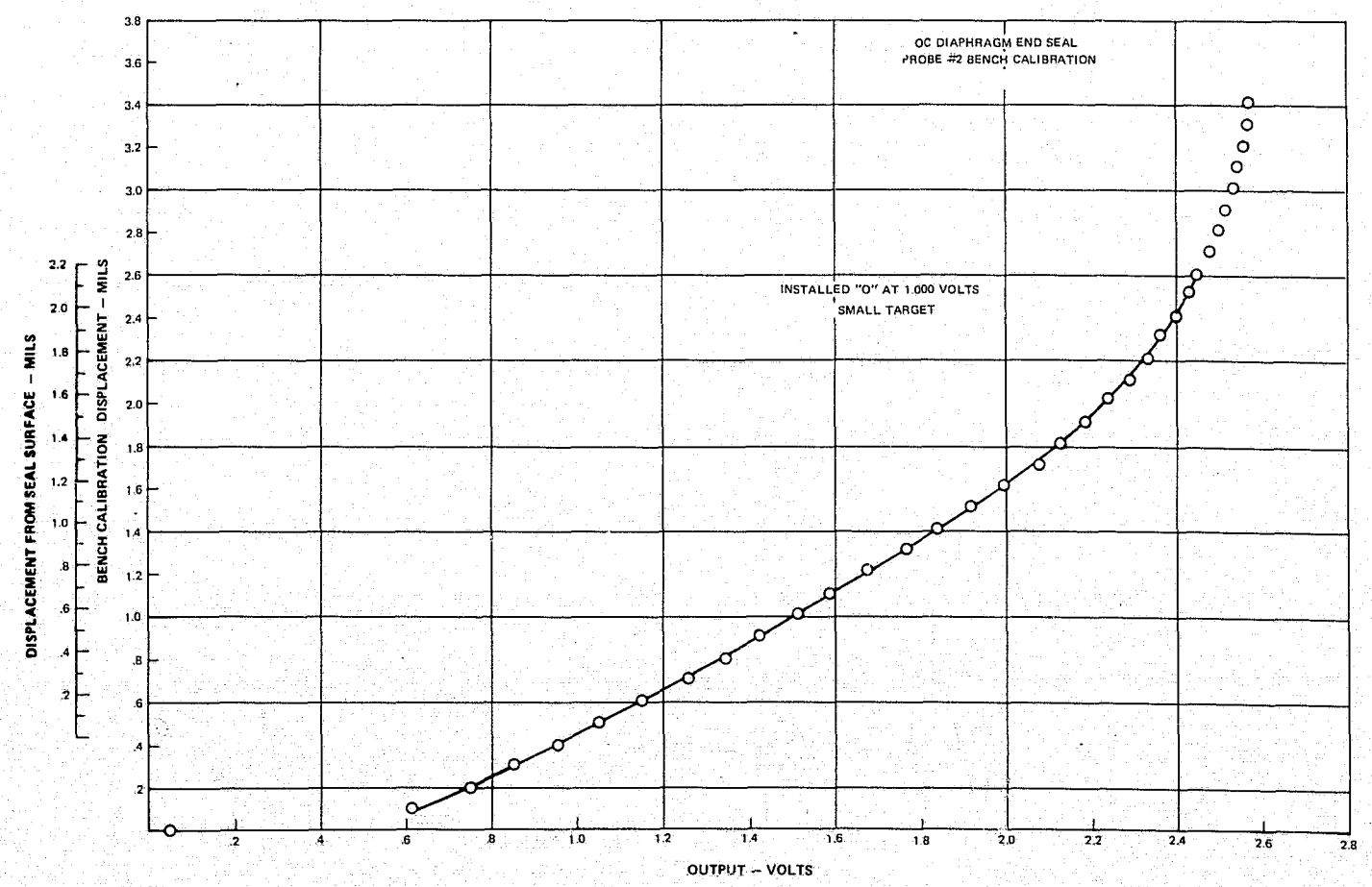

Figure 74 Bench Calibration of Probe No. 2

2. POST-TEST INSPECTION

Due to the seal-face runout (see Section II), there should have been a gap at the probe locations, but the gap did not occur uniformly around the circumference of the seal face. This lack of uniformity was most apparent in the post-test inspection, which indicated that the probes impacted with the runner and were rubbed out before the rig reached 6000 rpm. Examination of the seal face showed that significant rubbing occurred on the outside and inside edges. Other areas had light rubbing or none at all (Figures 75 and 76). There were two wear tracks caused by the two pads of the seal (Figure 77). Both wear tracks were approximately 1 to 2 mils deep, but the outer wear track was scored 4 to 6 mils deep at its outer edge, while the inner wear track was scored 3 to 5 mils deep at its inner edge. The axial runout after testing was within ± 2 mils FIR (Figure 78).

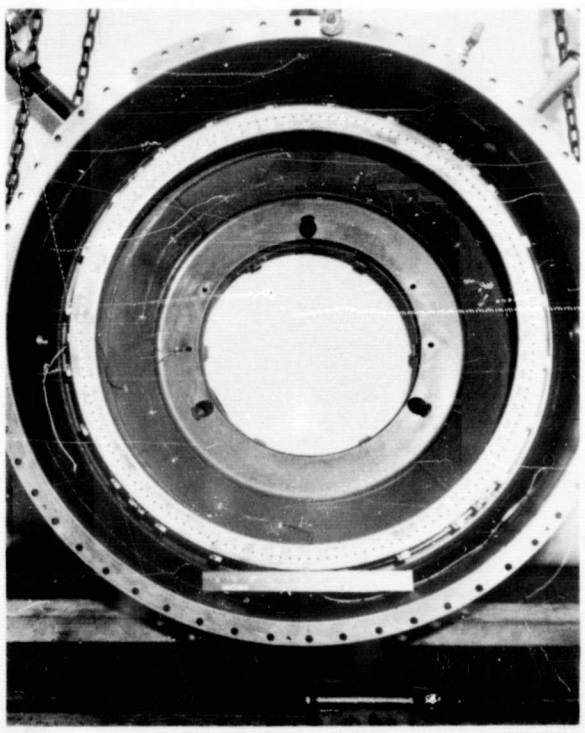

Figure 75
Seal Face after Dynamic Testing, OC Diaphragm End Seal (CN-27645)

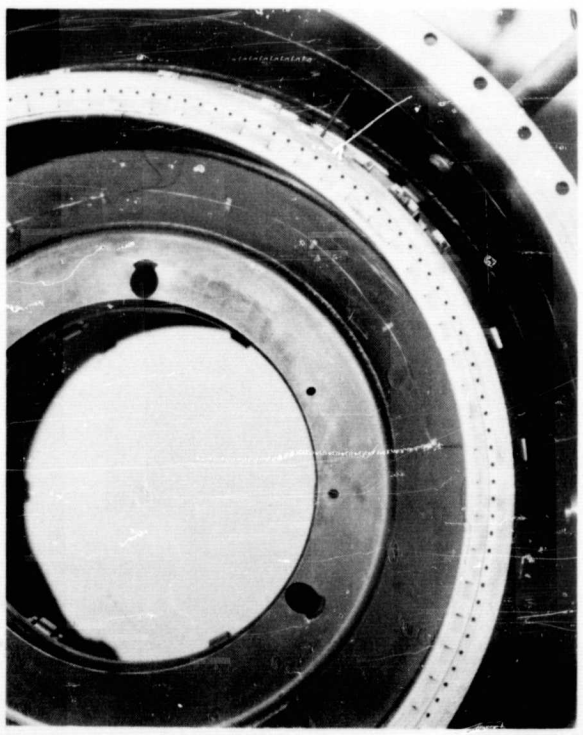

Figure 76
Close-Up View of OC Diaphragm End Seal Face after Dynamic Testing (CN-27643)

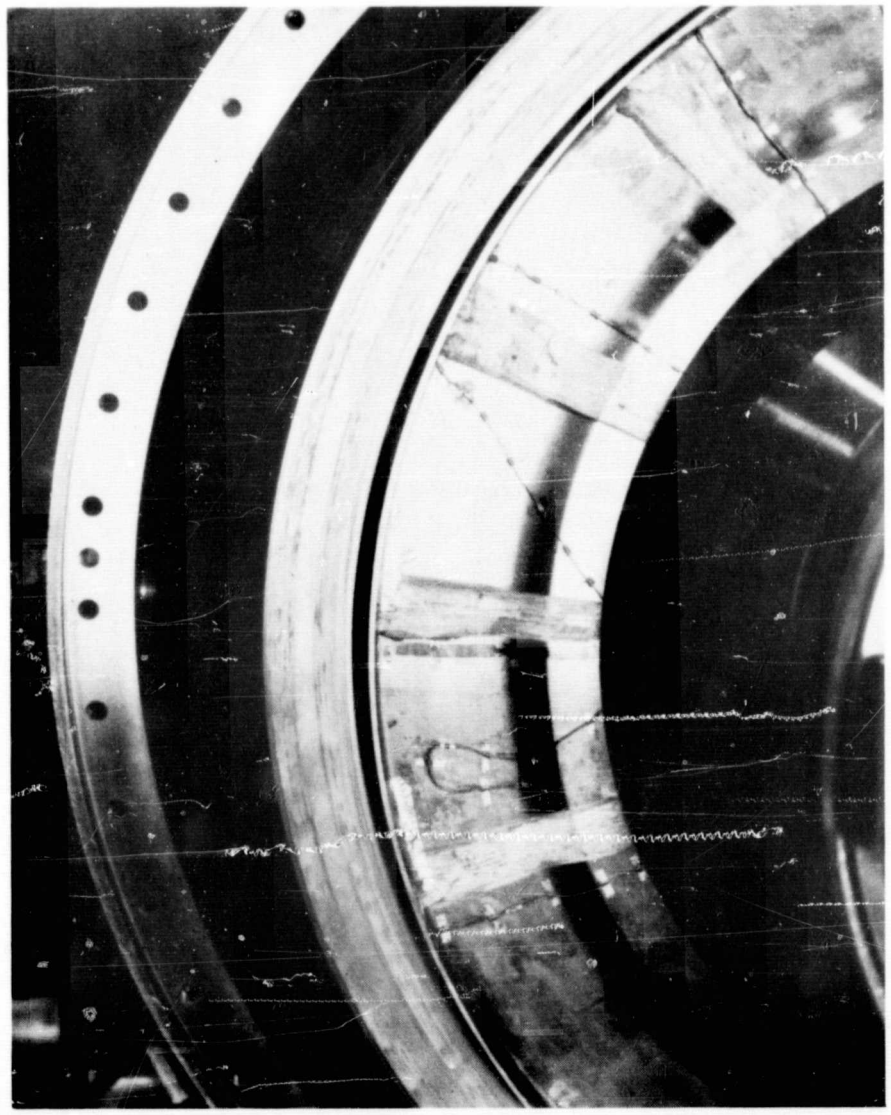

Figure 77 Wear Tracks on Face of OC Diaphragm End Seal Caused by Rayleigh Pads (XPN-13867)

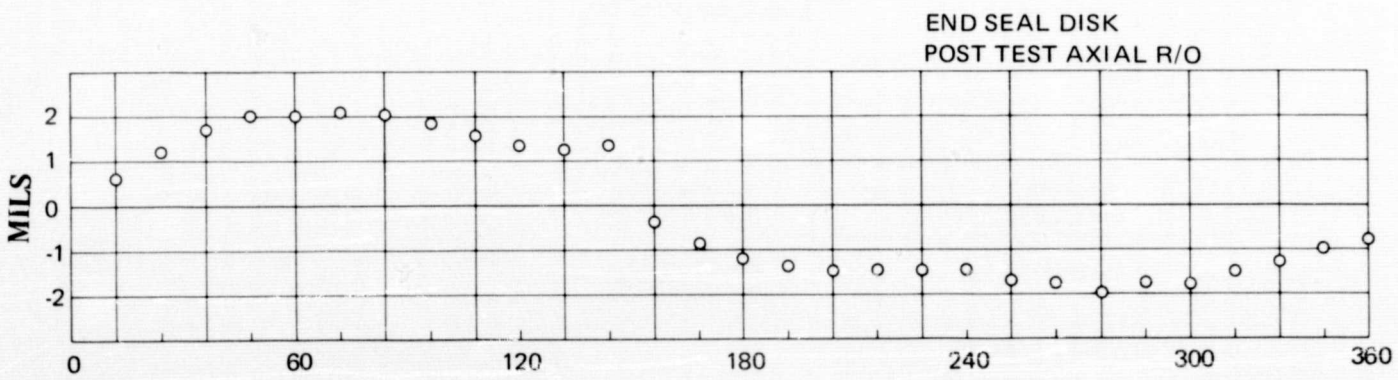

Figure 78 Post-Test Axial Runout of OC Diaphragm End Seal Runner

D. TESTING OF THE SEMIRIGID INTERSTAGE SEAL

The semirigid interstage seal was designed to operate on the same basic principle as the OC diaphragm end seal: leakage was controlled by controlling clearance. Primary sealing was accomplished at the seal face, which consisted of a single land. This land had a spiral-groove, inherently compensated orifice profile, and it acted as a bearing and seal combination (Figures 79 through 82).

The primary seal ring was pre-loaded with 16 helical coil springs to ensure contact at start and to permit the development of separating air films at speeds under 30 ft/sec. Both the seal face and the runner were hardcoated with chrome carbide for compatibility at high temperature and resistance to wear. This material was identical to the material used for the OC diaphragm seal.

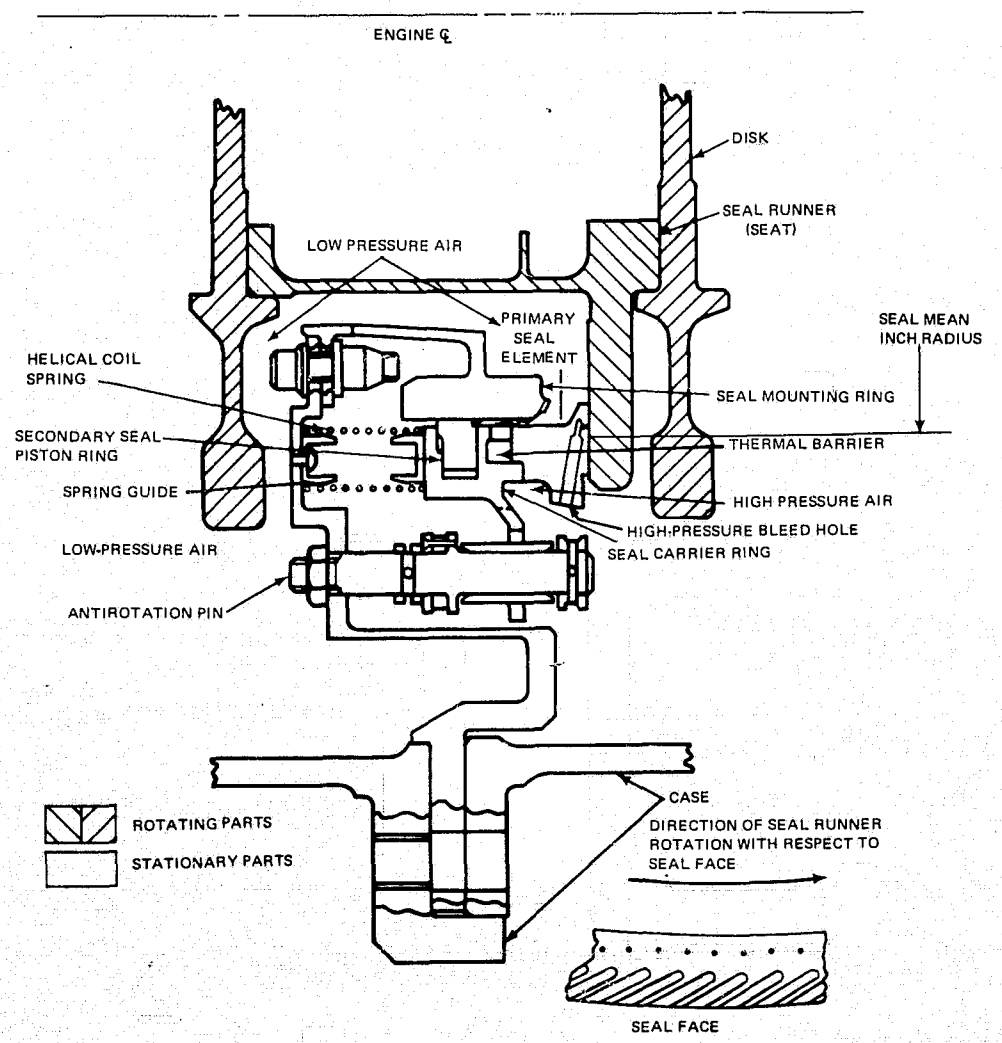

Figure 79 Schematic of Semirigid Interstage Seal

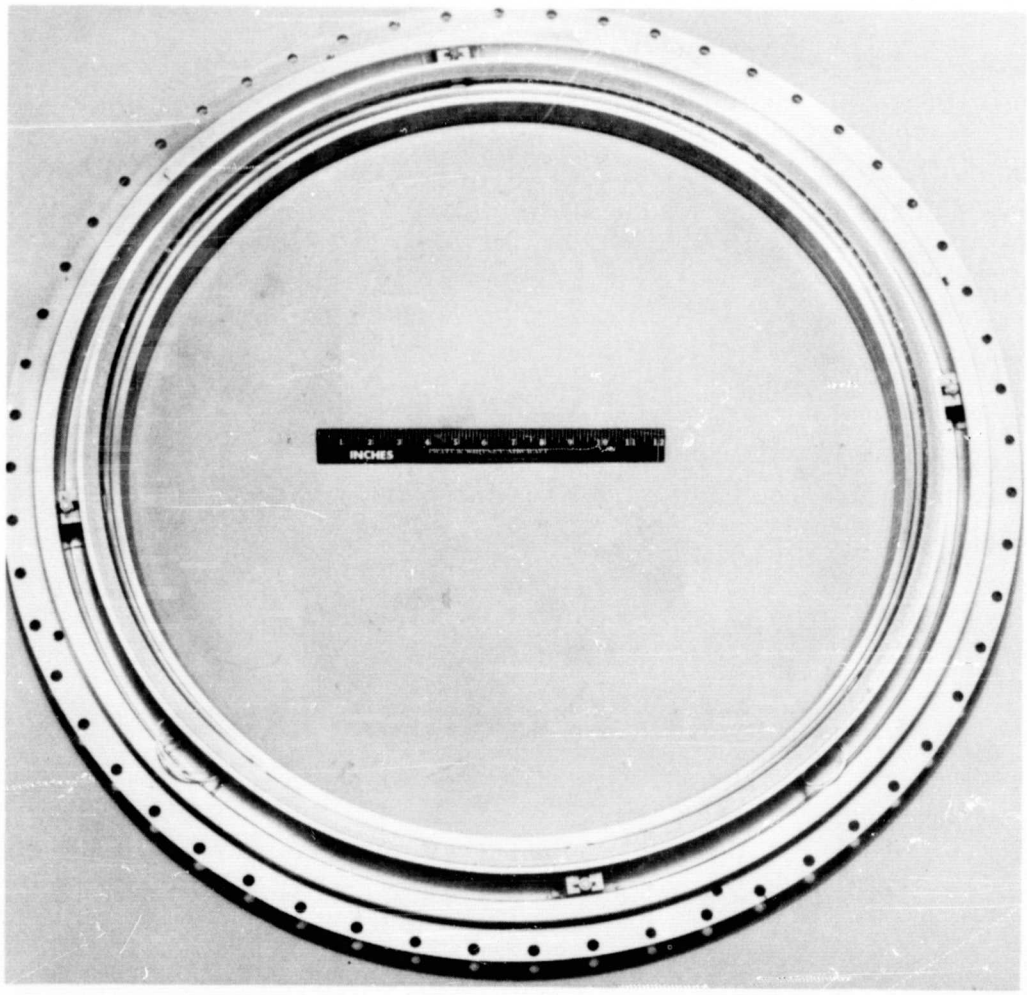

Figure 80 Semirigid Interstage Seal (CN-20084)

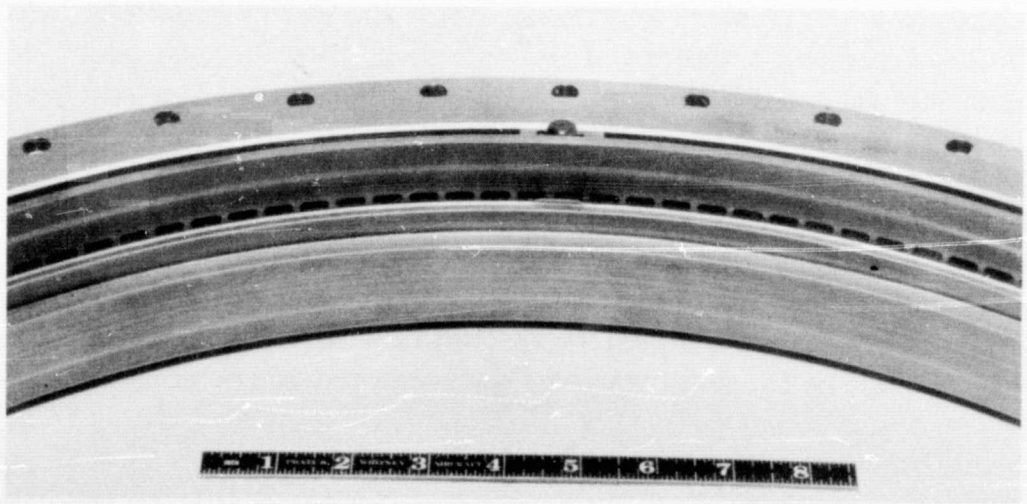

Figure 81 Close-Up of Semirigid Interstage Seal ID (CN-20085)

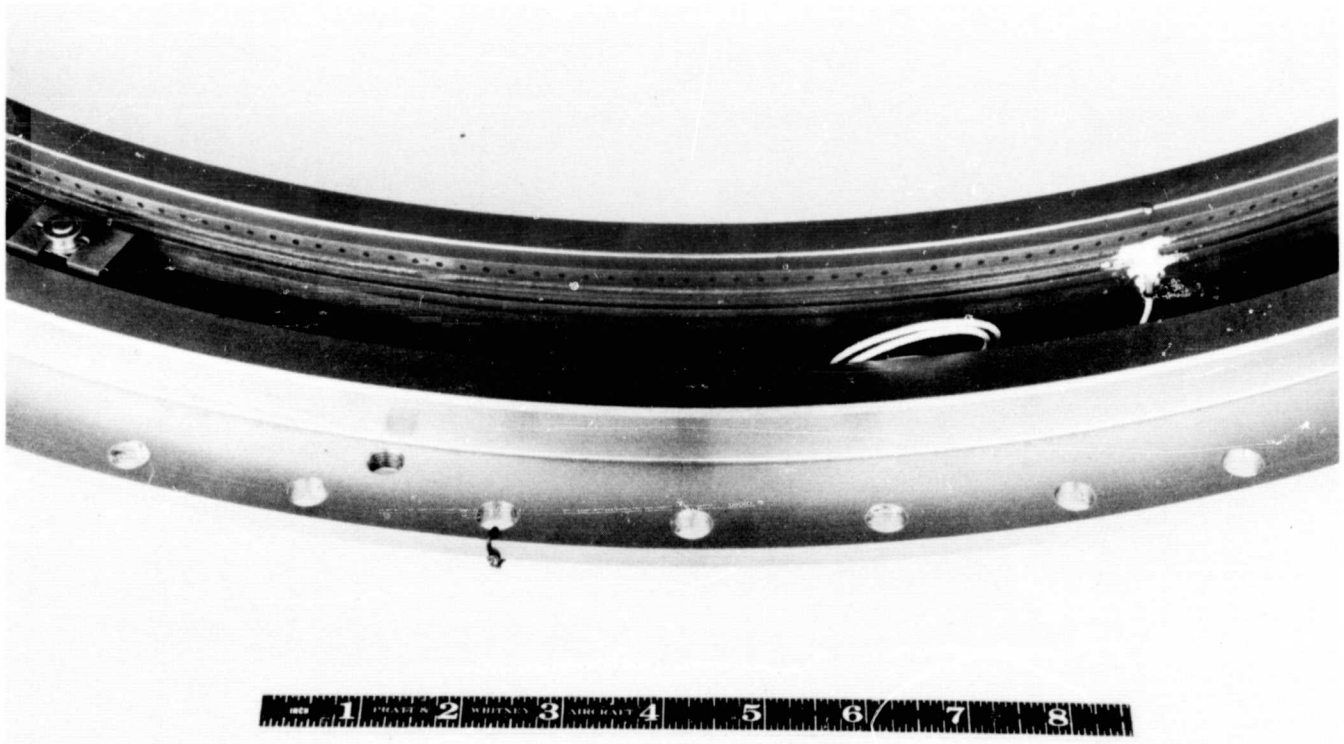

Figure 82 Close of Semirigid Interstage Seal OD (CN-20086)

1. ROOM TEMPERATURE DYNAMIC TEST

Static testing had revealed that the seal face had not lifted off from the runner hydrostatically. For this reason, the dynamic test program was based on the hydrodynamic-lift features of the seal. This program called for immediate acceleration to 3800 rpm (470 ft/sec) before establishing a low pressure differential across the seal. By limiting the dynamic testing to the hydrodynamic-lift features of the seal, the closing force was due primarily to spring-loading and was more easily supported by the reduced air-film load capacity caused by the wavy seal surface.

The seal was installed in the full-scale rig for dynamic testing and the pre-test axial runout of the seal runner was measured (Figure 83). After the rotor was installed in the rig, the seal compression was set at 0.116 inches and the rig was sent to the test stand. Before dynamic testing, seal breakaway torque (the amount of torque required to overcome friction between the seal and the runner at starting) was measured at 114 inch-pounds.

The valves were adjusted to establish a static pressure differential of 2 psi across the seal, and the main air supply was shut off. The rig was accelerated to 3900 rpm (485 ft/sec) before the main air supply was opened. The pressure differential across the seal did not reach 2 psi, indicating that losses were greater under dynamic conditions. When rotor temperatures exceeded 300°F, the run was discontinued (Figure 84) because some degree of rubbing was apparent.

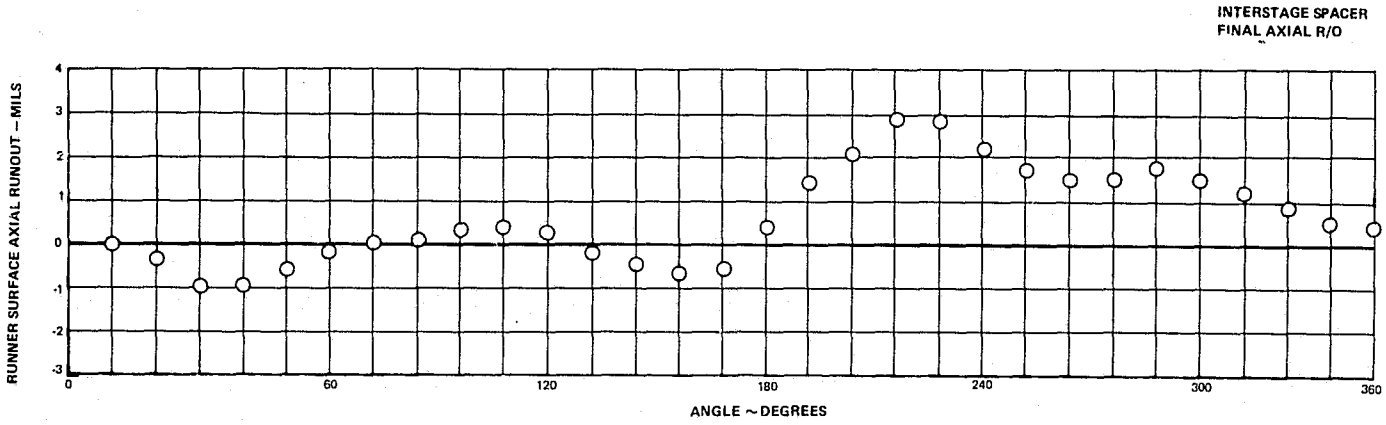

Figure 83 Pre-Test Axial Runout of Semirigid Interstage Seal

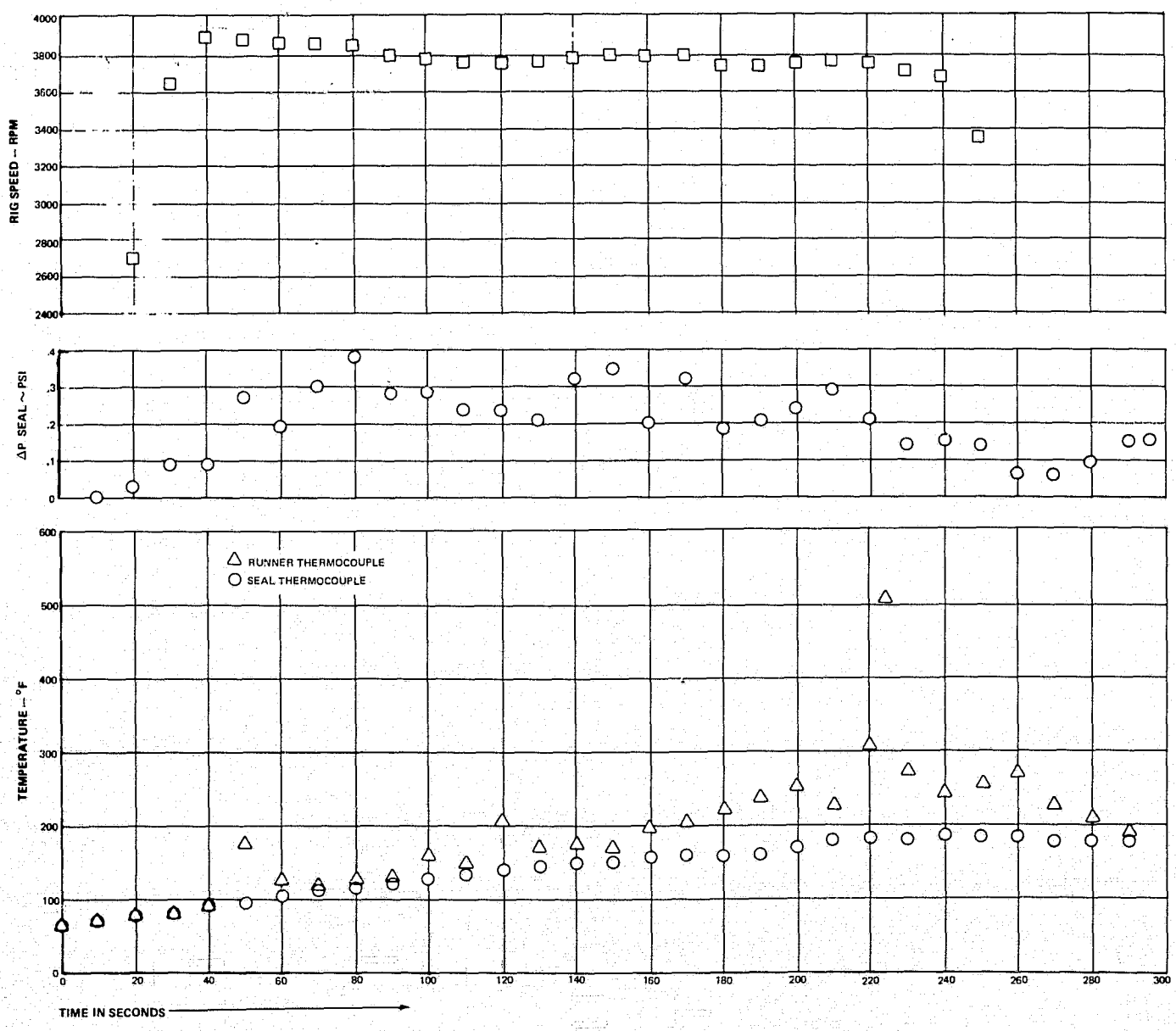

Figure 84 Speed, Pressure Differential, and Temperature vs. Time, First Test Run of Semirigid Interstage Seal

Because measured temperature were not excessive, the damage due to rubbing was assumed to be minimal, and a second run was scheduled, in which the seal pressure differential would be established before the start-up so that the seal would be cooled if initial rubbing occurred. Temperatures were automatically recorded by additional thermocouples during this test run.

The pressure differential was set at 2.22 psi and the rig was accelerated to approximately 4000 rpm (497 ft/sec). The observed temperatures of the seal and the rotor showed a very rapid rise, and the pressure differential dropped to about 0.13 psi. The second test was discontinued after a run of 1 minute, 48 seconds. The visual readout equipment did not respond to rapid temperature excursions, and the actual temperatures of the seal and runner could not be determined, but indications were that they may have exceeded 500°F.

Before the automatically-recorded data were reduced, a third test run was made in an attempt to reach surface speeds which would produce maximum air-film development. As in the second run, a low pressure differential of 2 psi was established across the seal and the rig was rapidly accelerated to approximately 4000 rpm. The pressure differential dropped off, but no sharp spikes in temperature were apparent. Rig speed was held within 3800-4200 rpm for about four minutes. All observed temperatures were stable, with the maximum around 250°F. The rig speed was increased to over 5900 rpm (733 ft/sec), where thermal spikes occurred and the run was discontinued.

When the automatically recorded data was reduced, it became apparent that, during the second run, one of the previously unrecorded thermocouples indicated a temperature spike in excess of 1325°F. Similar temperatures were recorded during the third test run at high speeds.

2. POST-TEST EXAMINATION

After the rig had been pulled from the stand, the seal and runner were removed for inspection. The wear track on the rotor was relatively uniform, 8 to 9 mils deep. The interstage seal face showed considerable wear, with most of the hardface material rubbed off. Spiral grooves were still apparent on some of the deeper valleys of the surface, and the heavy wear on the runner and seal, combined with the high temperatures, indicated that the seal rubbed. The wear patterns on the rotor are illustrated in Figure 85, and the wear patterns of the seal are shown in Figure 86. The post-test axial runout of the runner is shown in Figure 87.

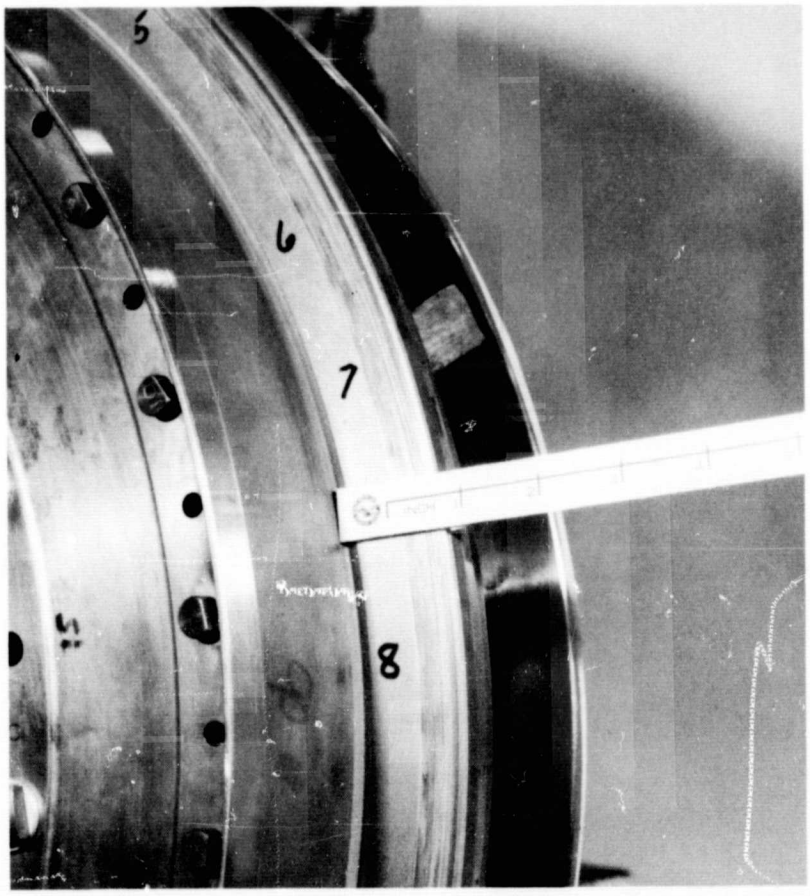

Figure 85

Wear Patterns on Rotor
after Dynamic Testing
(XPN-11207)

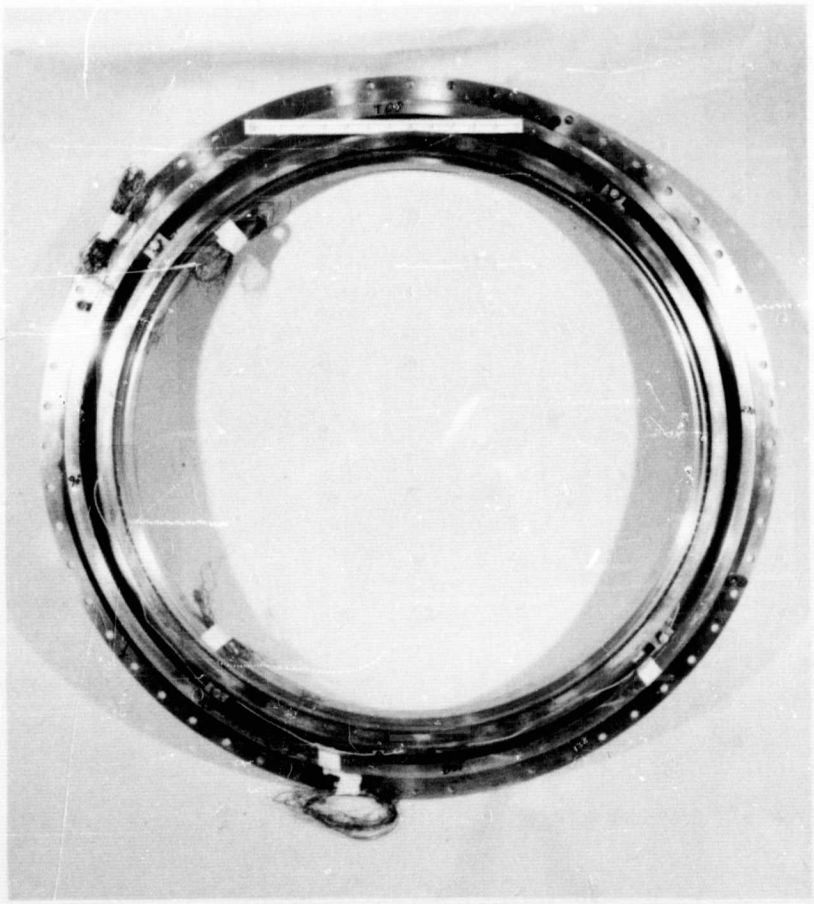

Figure 86

Wear Patterns on Seal
after Dynamic Testing
(XPN-11206)

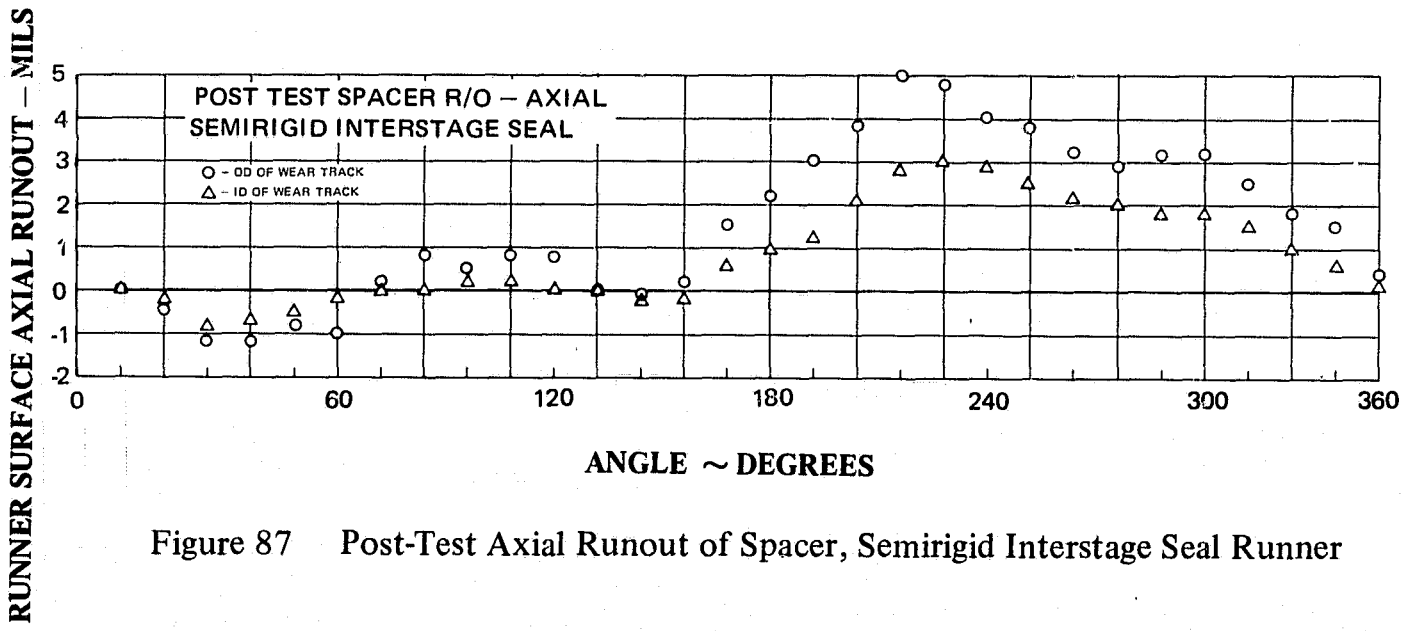

Figure 87 Post-Test Axial Runout of Spacer, Semirigid Interstage Seal Runner

V. SELF-ACTING COMPRESSOR SEAL DESIGN AND ANALYSIS

A. INTRODUCTION

The contractor has conducted design and performance analyses for each of two seal designs as specified in the Task V work statement. The first seal design, designated Design A, was created by converting the semirigid interstage seal of Tasks I and II from a "hybrid" primary seal configuration to a "self-acting" seal. The second seal design, referred to as Design B, was furnished by the National Aeronautics and Space Administration Program Manager and is a self-acting end seal.

The form and function of the self-acting seals of Task V represent a significant departure from the hybrid seals of Tasks I and II. The primary seal face of a self-acting seal is divided into a sealing region and a self-acting air bearing region. The sealing region, usually referred to as the seal dam, occupies a relatively small fraction of the seal face. The pressure differential across the seal controls the pressure distribution over the seal dam. Seal dam pressure distribution is relatively insensitive to linear or angular displacement of the seal face.

The self-acting air bearing may be located in either the high-pressure or the low-pressure region of the seal face or, as in Design B, may be located in both regions. The air bearing generates an average pressure or "load capacity" in the air film, which is relatively insensitive to angular displacement of the seal face. The self-acting seal stiffness characteristic makes control of air film thickness potentially less difficult than it was using the hybrid seals of Tasks I and II.

B. SELF-ACTING INTERSTAGE SEAL, DESIGN A

The original primary seal design for the semirigid interstage seal was a hybrid design in which a spiral groove self-acting air bearing operates in combination with an orifice-fed air bearing pressurized from the high-pressure side of the seal. The contractor recommends that the seal be converted to a purely self-acting design by enlarging the orifice feed holes to make the pressure drop through the holes negligible and connecting the holes with a 0.050 inch wide by 0.030 inch deep annular groove in the seal face. The self-acting bearing region is then bounded by the outer edge of the seal face and the annular groove. The groove position makes the bearing region 0.350 inch wide. The bearing has high-pressure air along both edges and the spiral grooves pump air from the outer edge of the bearing to the inner edge. The seal is shown in Figure 88.

Analysis of the seal is described in four parts: Primary seal analysis, Force and Moment Balance, Dynamic Analysis, and Seal Optimization.

1. PRIMARY SEAL ANALYSIS

The primary seal analysis was conducted by computing the seal dam leakage and load capacity and the spiral groove load capacity in separate steps. The load capacity values are combined to find the total primary seal load capacity or opening force for force balance purposes.

a. Analysis of Seal Dam Load Capacity

Seal dam load capacity curves for parallel and non-parallel film boundaries are presented in Figures 89,90 and 91. It was decided that a variation in seal dam width should be included in the design analysis of the Design A self-acting seal. Reoperation of an existing seal assembly placed constraints on the selection of a seal dam width, and the practical upper and lower limits to dam width were found to be 0.050 inches and 0.025 inches, respectively. Selection of a seal dam width was narrowed to a choice between those two values.

The parallel film boundary load curves were obtained directly from a fluid flow computer program created by the National Aeronautics and Space Administration for this purpose (Reference 5). The curve irregularities in the region of a one mil film thickness at high pressures are characteristic of a flow regime transition from laminar to turbulent. Entrance and exit pressure loss effects are also included in the National Aeronautics and Space Administration computer program. The seal dam load capacity for film boundary angles of two and three milliradians (converging flow) were found using a simplified laminar flow analysis in which the percent increase of the tilted load over the parallel load was determined. The tilted load capacities curves shown reflect this percent increase over the parallel load curves obtained from the NASA computer program.

Although the 50-mil dam load curves exhibit a higher stiffness, selection of a final dam width and balance diameter was deferred until the effect of dam width on total primary film load capacity could be determined.

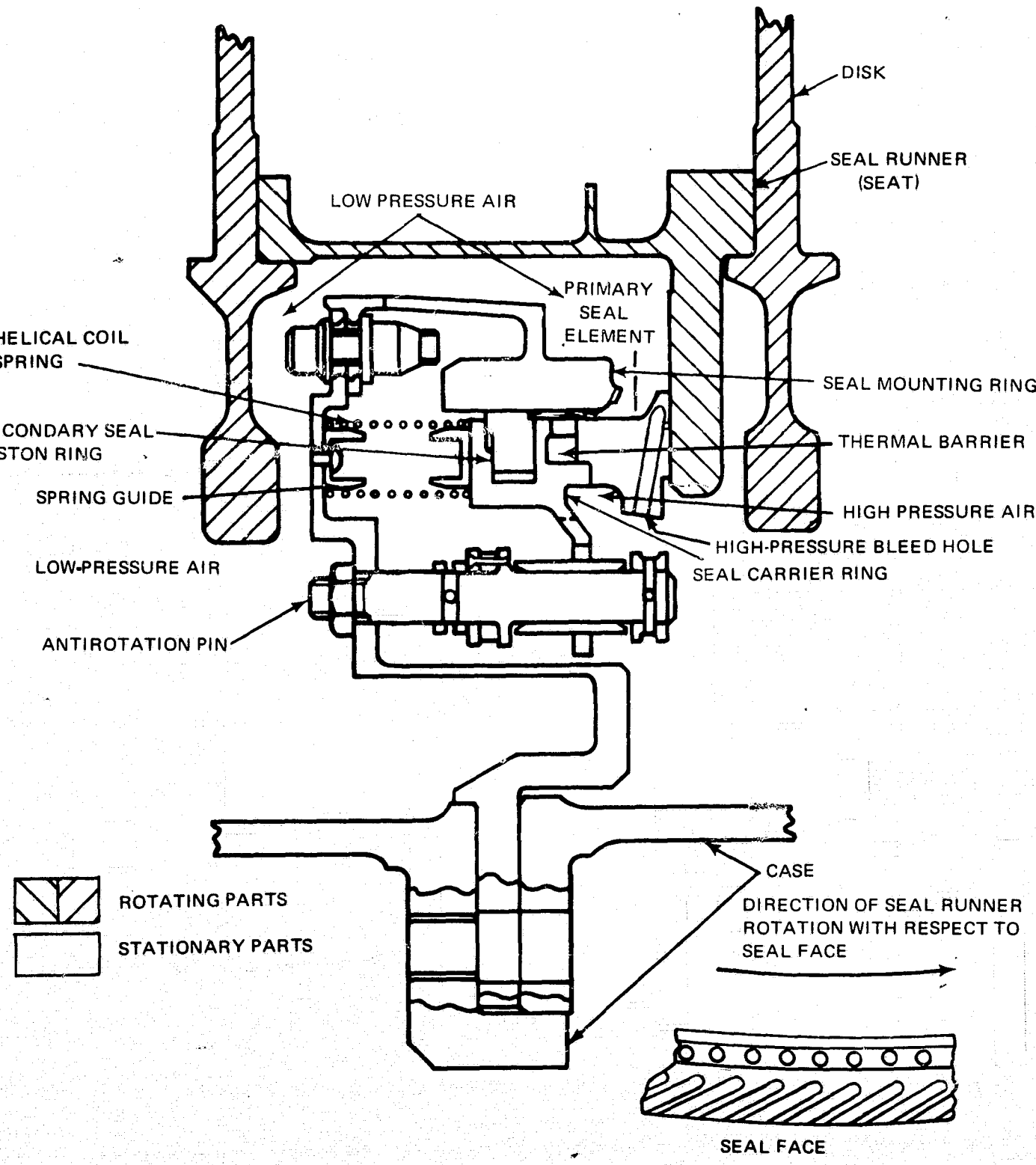

Figure 88 Self-Acting Interstage Seal, Design A

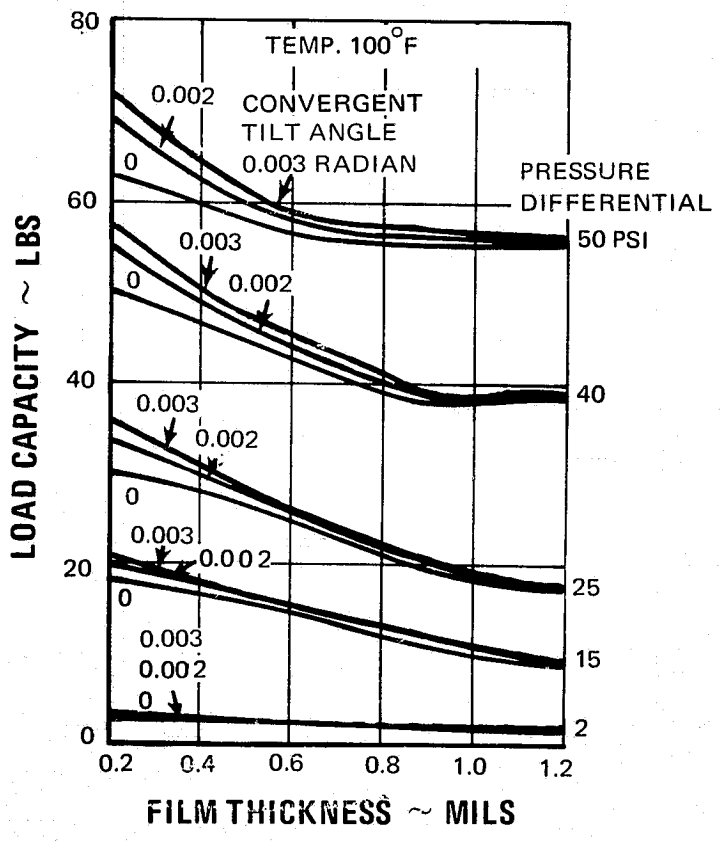

Figure 89 Load Capacity of the 25 Mil Seal Dam at 100°F

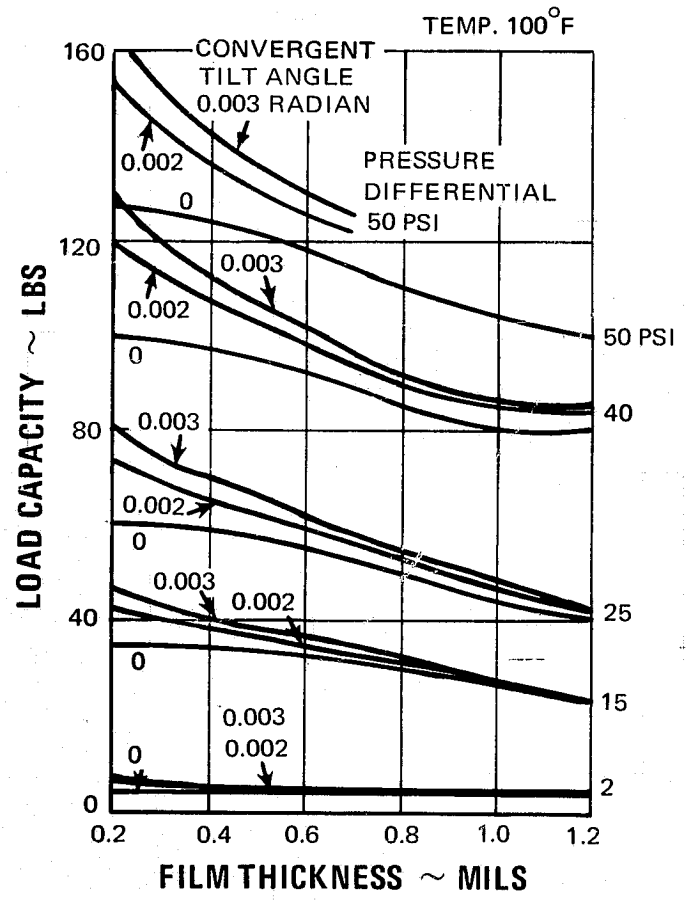

Figure 90 Load Capacity of the 50 Mil Seal Dam at 100°F

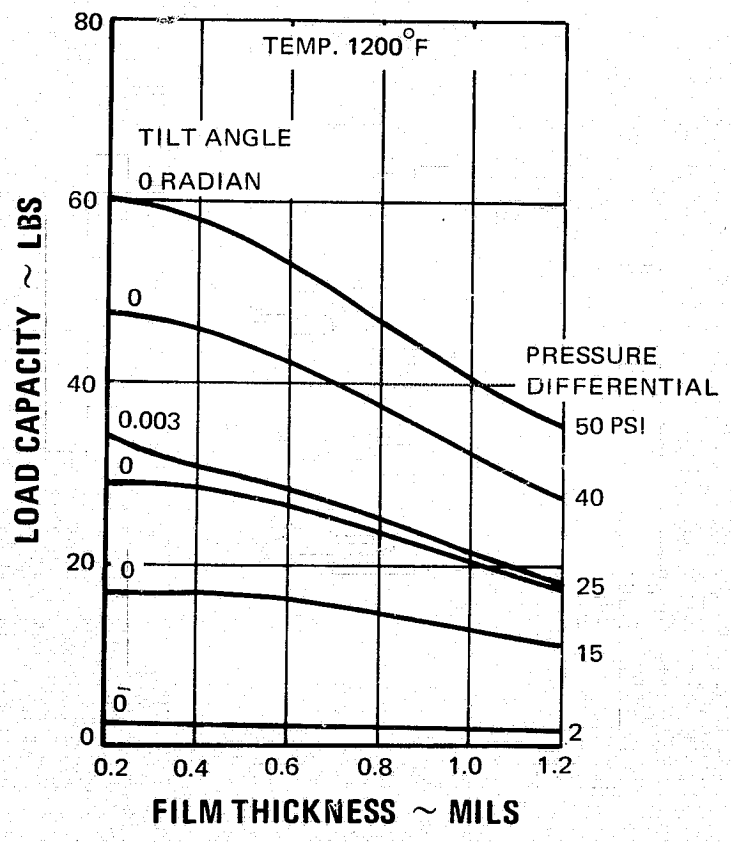

Figure 91 Load Capacity of the 25 Mil Seal Dam at 1200°F

b. Selection of Spiral Groove Bearing Geometry

The geometry of the self-acting semirigid seal was analyzed to determine the optimum groove length and groove depth (see References 6, 7, 8, and 9). The groove angle measured from a line normal to the direction of motion was 72 degrees for all cases analyzed.

The effect of groove length on load capacity is shown in Figure 92 for groove lengths equal to 70,80, and 90 percent of face width (groove length is measured normal to the direction of motion). Since the nominal operating film thickness for the seal is 0.4 to 0.7 mils, it is apparent from Figure 92 that a groove length equal to 80 percent of the face width provides the highest load capacity.

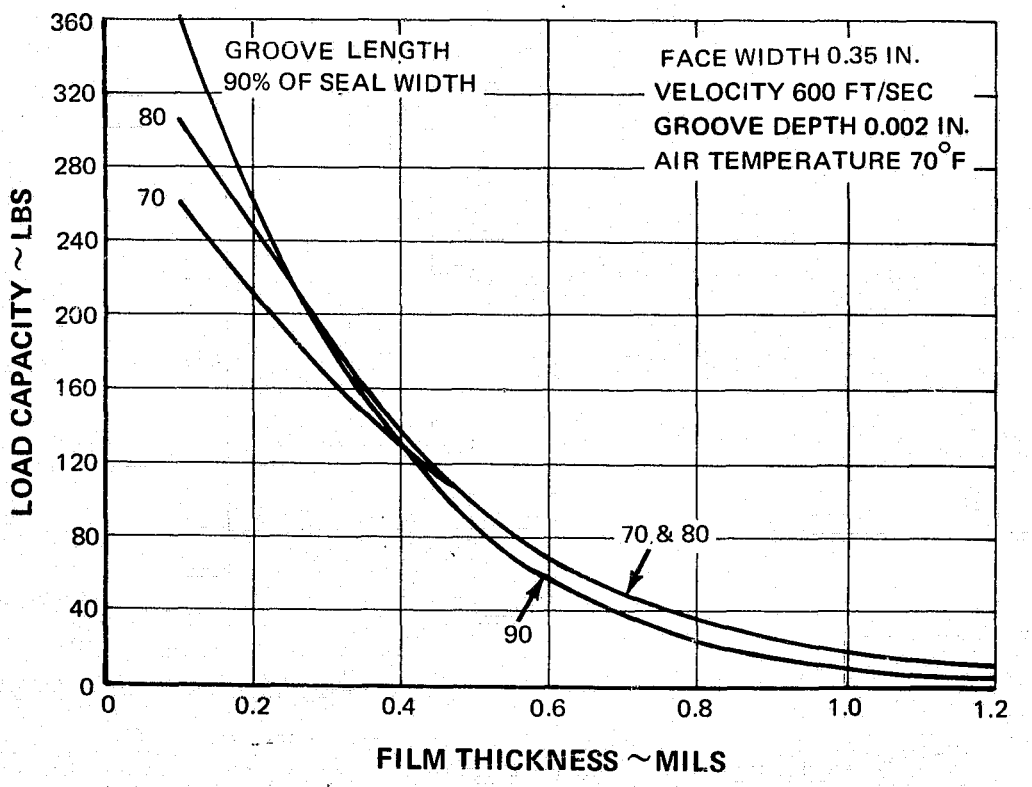

Figure 92 Effect of Groove Length on the Load Capacity of Seal Design A

With a groove length of 0.28 inch (80 percent of the face width of 0.35 inch), the effect of groove depth on load capacity was determined. The results of this analysis are shown in Figure 93 for groove depths of 0.001, 0.002, and 0.003 inch. For film thicknesses from 0.4 to 0.7 mils, it is apparent that a groove depth of 0.002 inch provides the optimum load capacity. Below a film thickness of 0.4 mil, a groove depth of 0.001 inch would provide substantially higher load capacity, but the seal will not normally operate at such a low film thickness. Furthermore, a depth as small as 0.001 inch would easily be destroyed by any small amount of rubbing.

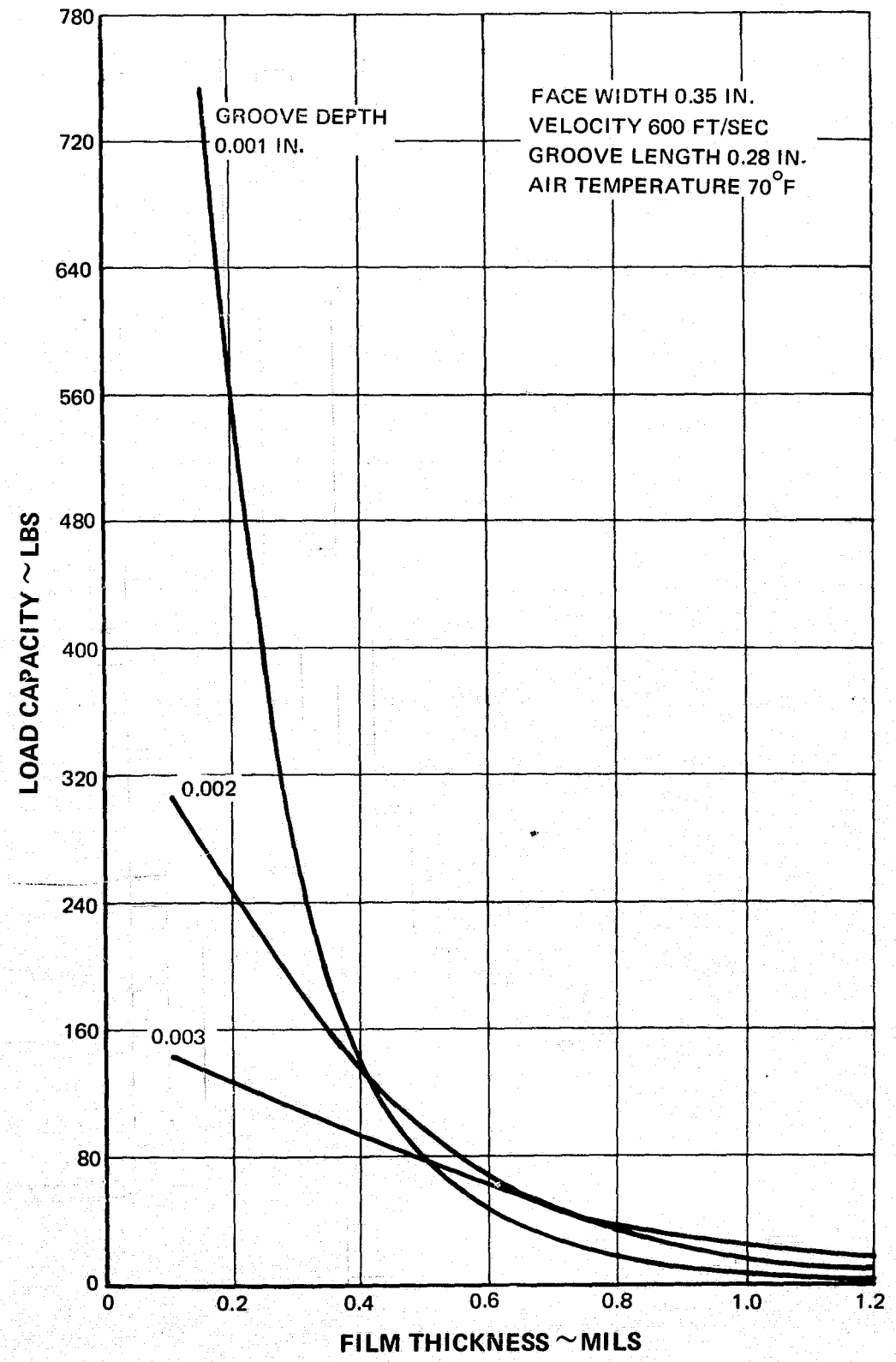

Figure 93 Effect of Groove Depth on the Load Capacity of Seal Design A

c. Analysis of Spiral Groove Bearing Load Capacity

Using the selected groove dimensions, the spiral groove bearing load capacity was calculated for a range of speeds and film thicknesses at air temperatures of 100°F, 680°F, and 1200°F. Curves of load capacity variation with film thickness at the upper and lower temperature extremes are shown in Figures 94 and 95. It is apparent from these figures that increasing velocity and increasing air temperature increases the air film load capacity and stiffness in the spiral groove region of the primary seal (see also Reference 3).

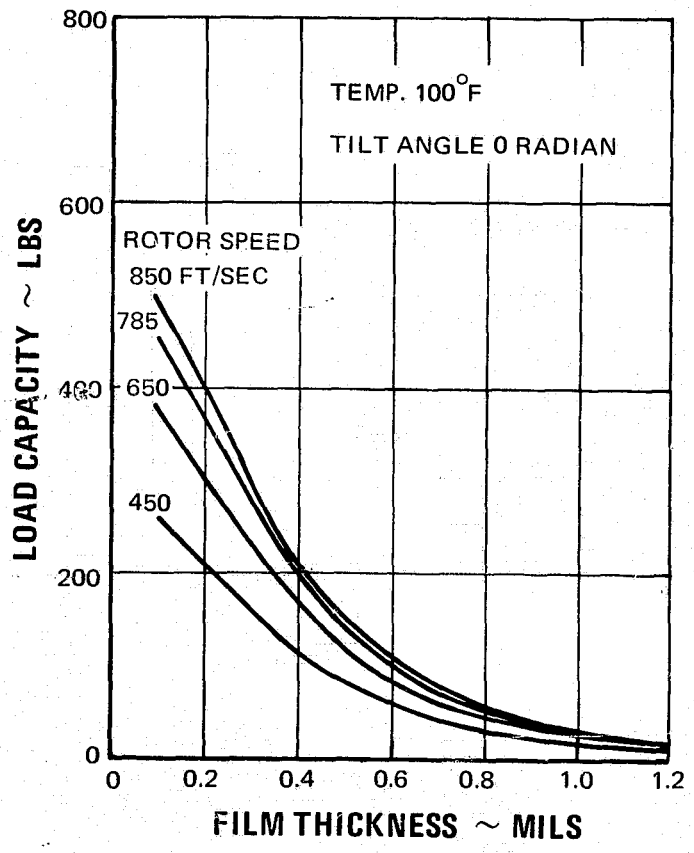

Figure 94 Load Capacity of the Spiral Groove Bearing at 100°F

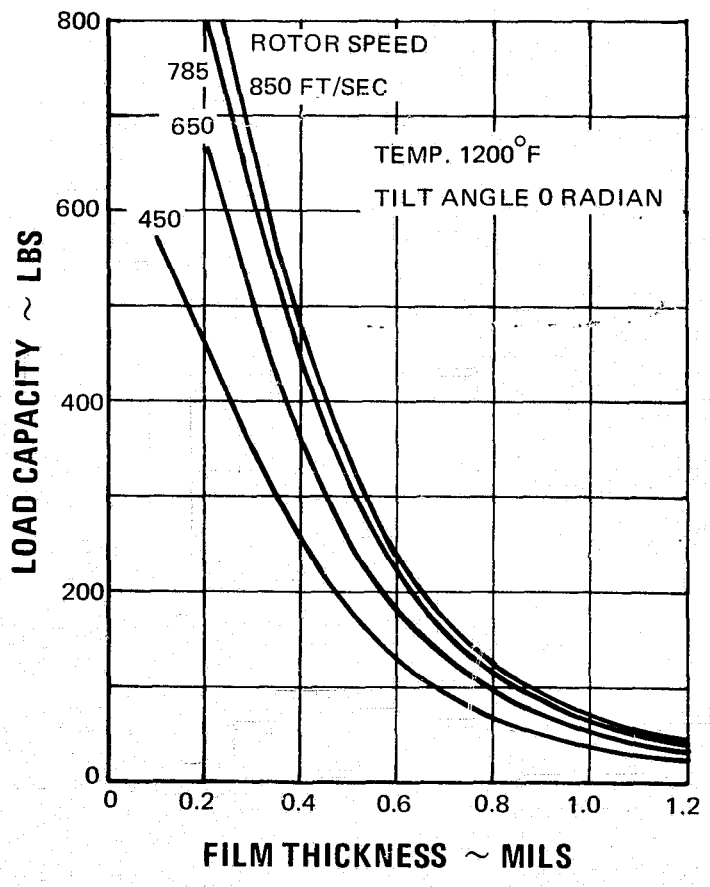

Figure 95 Load Capacity of the Sprial Groove Bearing at 1200°F

The change in spiral groove load capacity due to a three milliradian tilt angle is shown in Figure 96. The load capacity increases with a positive tilt angle (converging flow). In contrast to the tilted dam load curves, tilted groove load curves do not extend below 0.6 mil film thickness. Since the seal dam is closer to the apex of the tilt angle, the mean operating film thickness of the dam will be smaller than that of the mean groove film thickness.

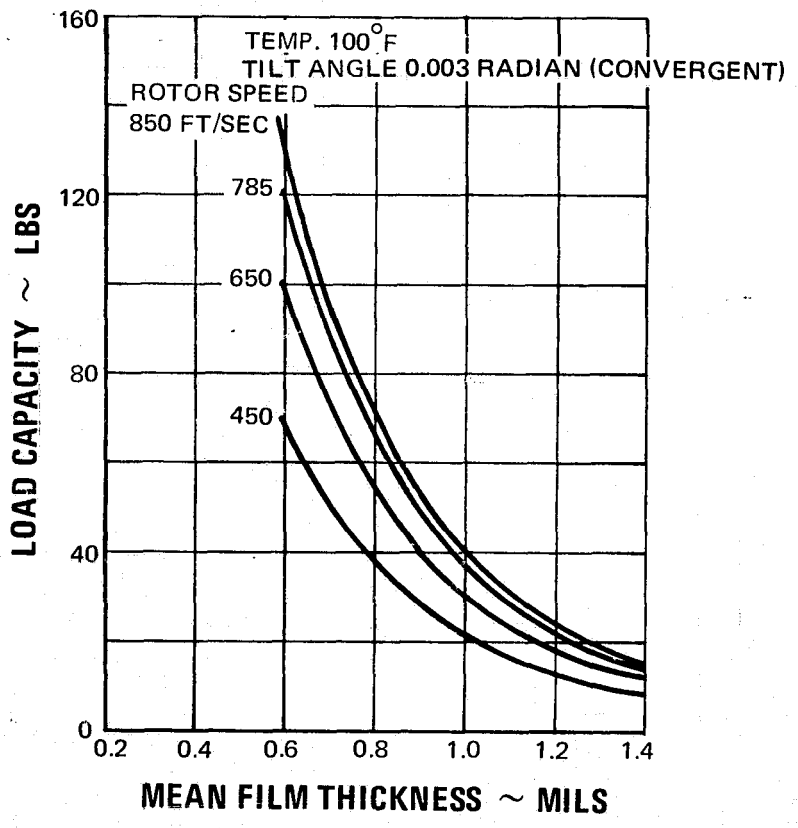

Figure 96 Load Capacity of the Spiral Groove Bearing at 100°F and a 3 Milliradian Tilt Angle

d. Primary Seal Total Load Capacity Curves

Determination of the total opening force developed by the primary seal air film during operation is accomplished by the addition of the spiral groove and seal dam load capacity curves. A set of total load curves, for a specific dam width and operating temperature, consists of four speed curves at six different pressures, or twenty-four separate curves. Since presentation of all the total load curves in this report is impractical, only the high-pressure low-temperature condition is shown in Figure 97. Total load capacity was also examined at non-parallel film boundary conditions. Film angles of 2 and 3 milliradians were analyzed and Figure 98 illustrates the primary seal load capacity at a 3 milliradian film angle.

The double scale gives the mean film thickness for both the seal dam and the spiral groove bearing. Figure 99 shows how the difference in operational film thicknesses was arrived at for both dam widths and tilt angles.

For convenience, the difference in film thickness was considered to be 0.5 and 0.7 mils for the 2 and 3 milliradian film angles respectively, at both dam widths. The double scale for the film thickness reflects this difference.

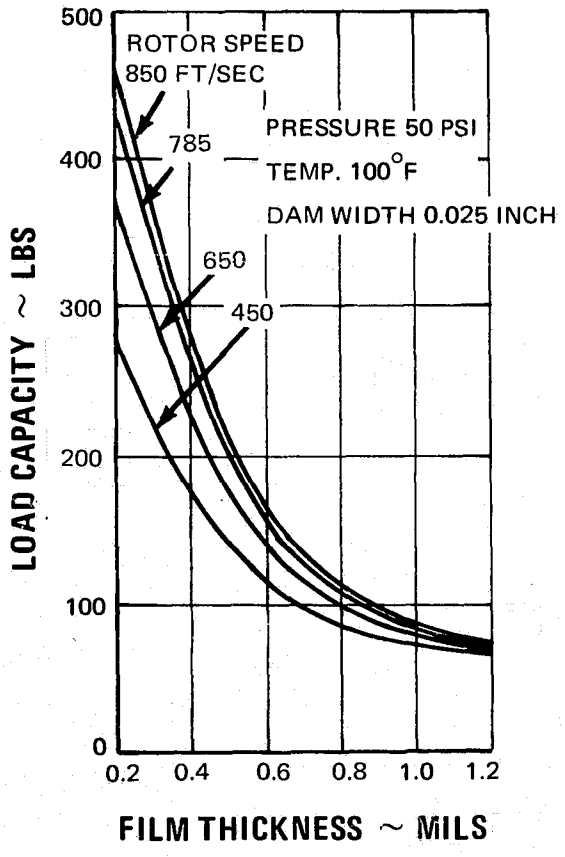

Figure 97 Typical Primary Film Total Load Capacity

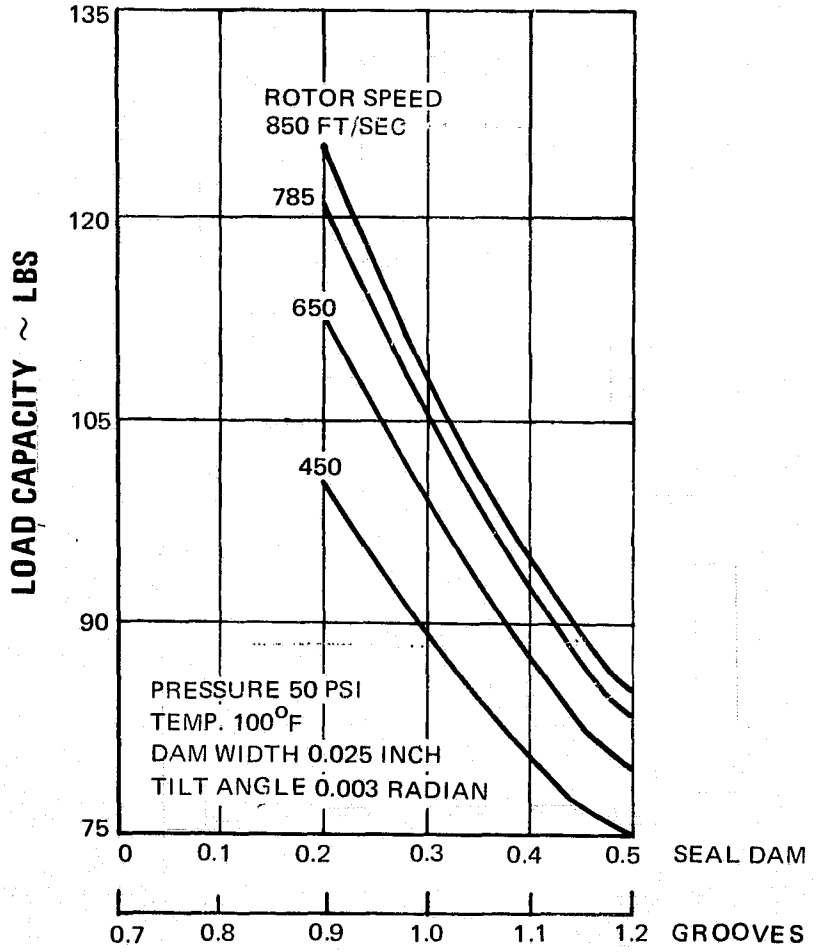

Figure 98 Primary Film Total Load Capacity at 100°F and a 3 Milliradian Tilt Angle

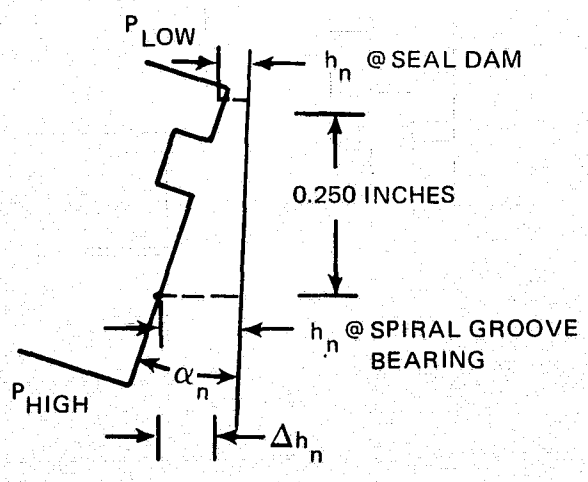

DAM WIDTH = 0.050 INCHES

$\alpha_1 = 0.002$; $\Delta h_1 = (0.25)(0.002) = 0.0005$ INCHES

$\alpha_2 = 0.003$; $\Delta h_2 = (0.25)(0.003) = 0.00075$ INCHES

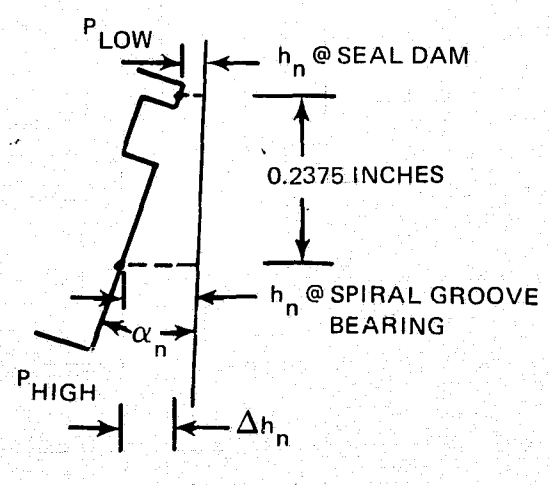

DAM WIDTH = 0.025 INCHES

$\Delta h_1 = (0.2375)(0.002) = 0.00048$

$\Delta h_2 = (0.2375)(0.003) = 0.00071$

Figure 99 Film Thickness Variation with Tilt Angle

2. FORCE AND MOMENT BALANCE

Axial forces on the seal are properly balanced when the film thickness generated at key operating conditions provides a maximum tolerance to conical distortion of seal surfaces and to runout of the rotor. The closing forces applied to the seal by the coil springs and by static pressure forces, which are determined by the size of the secondary seal diameter or "balance diameter," serve to control the mean film thickness of the primary seal.

In order to explore the optimization problem, equilibrium film thickness values were found for two values of spring force (30 and 60 pounds), two values of unbalance ratio (A_H/A_T = 0.6 and 0.8), two values of dam width (0.025 and 0.050 inch) and two values of pressure differentials (2 and 50 psi). A_T is the area of the seal; and A_H is the area between the balance diameter and the outer diameter of the dam. Table I lists the equilibrium film thickness which corresponds to all combinations of the above variables at selected temperature speed, and angular distortion levels. The mean film thickness indicated for a given angular distortion value is the mean thickness at the seal dam.

Moments on the seal are balanced by adjusting the axial position of the nosepiece centroid relative to the center of radial pressure load on the nosepiece. A small amount of material must be removed from the nosepiece to convert the seal to a self-acting configuration, and additional material removal is required at the opposite end of the nosepiece to return the centroid to its proper location.

3. DYNAMIC ANALYSIS

Film thickness disturbances produced by a 0.004 inch full indicator reading runout of the seal rotor have been calculated for all seal operating conditions. Typical calculations are discussed in Part I of this report. Figure 100 describes the film thickness variation due to a 4-mil runout. The film stiffness was assumed to be linear and no saddle shaped or higher order distortion was assumed to be present on runner surfaces.

Table I presents values for minimum film thickness which were found by subtracting the film thickness variation due to rotor runout from the mean film thickness found by the axial force balance analysis. The slope of the primary seal total load capacity curve at a given mean film thickness was used to define the film stiffness.

Dam Width (mils)	Pressure Drop (psi)	Temp (°F)	Percent Unbalance	Spring Force (lbs)	Tilt Angle (rads)	Total Closing Force (lbs)	450 Mean Film (mils)	ft/sec Min Film (mils)	650 Mean Film (mils)	ft/sec Min Film (mils)	785 Mean Film (mils)	ft/sec Min Film (mils)	850 Mean Film (mils)	ft/sec Min Film (mils)
50	2	100	60	30	0	34.9	.85	.66	.96	.42	1.05	-.05	1.09	-.51
25	2	100	60	30	0	32.5	.8	.67	.91	.58	.98	.40	1.0	.3
50	50	100	60	30	0	153.8	.71	.626	.81	.61	.85	.53	.875	.485
25	50	100	60	30	0	91.9	.75	.635	.85	.56	.92	.42	.95	.33
50	2	100	80	30	0	36.6	.84	.66	.95	.42	1.0	0	1.03	-.47
25	2	100	80	30	0	33.3	.79	.665	.90	.58	.97	.41	.99	.31
50	50	100	80	30	0	195.	.535	.485	.62	.51	.67	.51	.69	.51
25	50	100	80	30	0	112.5	.62	.548	.72	.55	.77	.51	.80	.50
50	2	100	60	60	0	64.9	.60	.53	.72	.56	.77	.505	.80	.48
25	2	100	60	60	0	62.5	.58	.524	.69	.53	.75	.50	.77	.47
50	50	100	60	60	0	183.8	.58	.52	.66	.545	.71	.535	.73	.51
25	50	100	60	60	0	121.9	.57	.51	.67	.53	.73	.50	.75	.475
50	2	100	80	60	0	66.6	.58	.51	.69	.54	.75	.51	.775	.495
25	2	100	80	60	0	63.3	.58	.524	.69	.53	.75	.50	.77	.47
50	50	100	80	60	0	225.0	.44	.398	.53	.447	.58	.45	.60	.45
25	50	100	80	60	0	142.5	.49	.446	.59	.49	.65	.49	.67	.475
50	50	680	60	30	0	153.8					.86	.685		
25	50	680	60	30	0	91.9					.88	.67		
50	50	680	80	30	0	195.0					.74	.63		
25	50	680	80	30	0	112.5					.82	.655		
50	50	680	60	60	0	183.8					.77	.64		
25	50	680	60	60	0	121.9					.78	.63		
50	50	680	80	60	0	225.0					.67	.578		
25	50	680	80	b0	0	142.5					.72	.60		
50	25	1200	60	30	0	91.9							1.12	.80
25	25	1200	60	30	0	79.5							1.05	.76
50	25	1200	80	30	0	112.5							1.04	.76
25	25	1200	80	30	0	71.							1.09	.77
50	25	1200	60	60	0	121.9							.97	.70
25	25	1200	60	60	0	90.9							.97	.73
50	25	1200	80	60	0	142.5							.88	.69
25	25	1200	80	60	0	101							.94	.72
50	50	100	60	30	.002	197					.56	.20	.58	.135
25	50	100	60	30	.002	95.					.49	.105	.51	.06
50	50	100	80	30	.002	199.					.32	.14	.34	.12
25	50	100	80	30	.002	116.					.35	.08	.38	.07
50	50	100	60	60	.002	187.					.375	.135	395	.115
25	50	100	60	60	.002	125.					.30	.07	.33	.075
50	50	100	80	60	.002	229.					.22	.10	.24	.10
25	50	100	80	60	.002	146.					.225	.08	.25	.055
50	50	100	60	30	.003	159.1					.49	.01	.51	-.05

FOLDOUT FRAME 1

50	25	1200	60	30	0	91.9			1.12	.80	
25	25	1200	60	30	0	79.5			1.05	.76	
50	25	1200	80	30	0	112.5			1.04	.76	
25	25	1200	80	30	0	71.			1.09	.77	
50	25	1200	60	60	0	121.9			.97	.70	
25	25	1200	60	60	0	90.9			.97	.73	
50	25	1200	80	60	0	142.5			.88	.69	
25	25	1200	80	60	0	101			.94	.72	
50	50	100	60	30	.002	197	.56	.20	.58	.135	
25	50	100	60	30	.002	95.	.49	.105	.51	.06	
50	50	100	80	30	.002	199.	.32	.14	.34	.12	
25	50	100	80	30	.002	116.	.35	.08	.38	.07	
50	50	100	60	60	.002	187.	.375	.135	395	.115	
25	50	100	60	60	.002	125.	.30	.07	.33	.075	
50	50	100	80	60	.002	229.	.22	.10	.24	.10	
25	50	100	80	60	.002	146.	.225	.08	.25	.055	
50	50	100	60	30	.003	159.1	.49	.01	.51	-.05	
25	50	100	60	30	.003	97.2	.375	-.035	.39	-.09	
50	50	100	80	30	.003	200.	.245	.075	27	.08	
25	50	100	80	30	.003	117.8	.23	-.10	.26	-.13	
50	50	100	60	60	.003	189.1	.29	.06	.32	.05	
25	50	100	60	60	.003	127.2	.165	-.095	.18	-.12	
50	50	100	80	60	.003	230.3	.14	-.03	.16	-.03	
25	50	100	80	60	.003	147.8	.065	-.195	.09	-.21	
50	50	680	60	30	.003	159.1	.49	.17			
25	50	680	60	30	.003	97.2	.42	.13			
50	50	680	80	30	.003	200	.29	.12			
25	50	680	80	30	.003	117.8	.315	.095			
50	50	680	60	60	.003	189.1	.34	.14			
25	50	680	60	60	.003	127.2	.27	.075			
50	50	680	80	60	.003	230.3	.205	.09			
25	50	680	80	60	.003	147.8	.20	.045			
50	25	1200	60	30	.003	94.6			.65	.18	
25	25	1200	60	30	.003	63.6			.62	.12	
50	25	1200	80	30	.003	115.0			.50	.12	
25	25	1200	80	30	.003	73.9			.55	.10	
50	25	1200	60	60	.003	124.6			.44	.14	
25	25	1200	60	60	.003	93.6			.42	.10	
50	25	1200	80	60	.003	145.0			.35	.12	
25	25	1200	80	60	.003	103.9			.37	.10	

FOLDOUT FRAME 2

PW

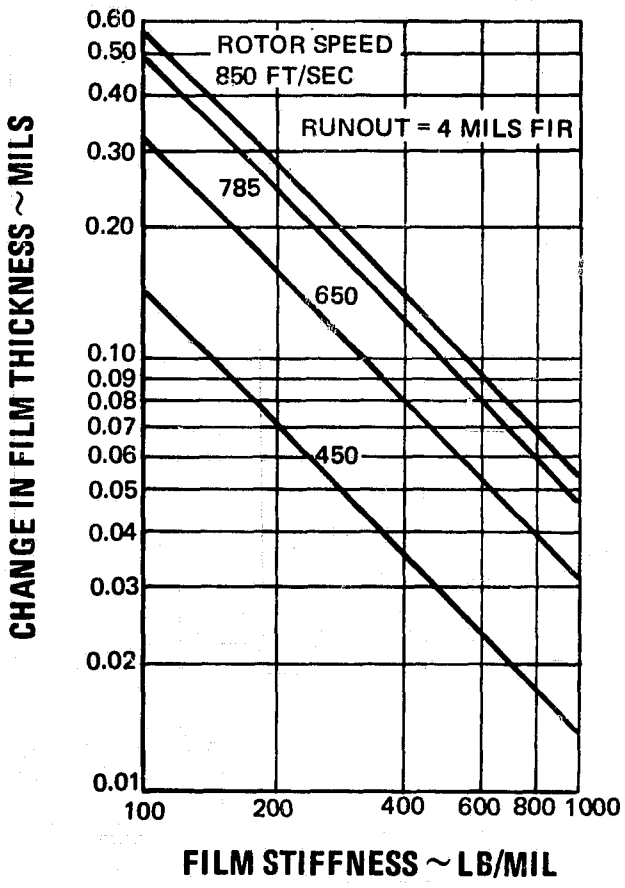

Figure 100 Film Thickness Variation Due to Rotor Runout

4. SEAL DESIGN AND OPTIMIZATION

Selection of a seal dam width was complicated by the differences between parallel and tilt conditions. At parallel film conditions, the 25-mil dam has the more desirable operating film thicknesses. The stiffness of its total load curves is higher, as evidenced by the difference between mean and minimum film thickness. Specifically, at certain operating conditions the 50-mil dam will contact, whereas the 25-mil dam has an acceptable film thickness. However, at the tilted conditions the 50-mil dam appears to have the same advantages that the 25-mil dam had at the parallel conditions. At 100°F and 3 milliradians tilt, seal contact is likely. However, at 2 milliradian tilt, which is more likely at 100°F, no contact occurs. It should be noted that at tilt conditions the film thicknesses shown are the seal dam film thicknesses, and that the grooves run 0.5 to 0.7 mils further from the runner. It appears some contact at tilted conditions is inevitable with either dam width. Since only the dam will contact, and not the grooves, the 25 mil dam width was chosen because it will be less affected by contact. In addition, at parallel conditions the 25 mil dam will have the best operating film thickness.

Selection of a combination of spring force and percent unbalance was based on two prime considerations. First, the stiffness of the total load curve must be sufficient to prevent contact. Due to dynamic effects, contact will occur when the dynamic change in film thickness exceeds the mean film value. The film thickness values predicted in the table indicate an unbalance of 80 percent would satisfy the first condition.

Second, the initial rubbing, which will occur during start-up, must be held to a minimum. Start-up will occur at low pressure differentials. Since unbalance at low pressures has little or no effect on closing force, the second consideration is unaffected by the 80 percent unbalance. Spring force, however, is significant. The 30-pound spring force will allow the seal to lift off sooner than the higher spring force. Therefore, the initial rubbing will be short during start-up.

Figures 101, 102, and 103 contain the leakage curves for 100°F, 680°F, and 1200°F. Plotted over the leakage curves are the mean operating films for each speed. The resulting cross plot gives a good visualization of what the leakage and film thickness would be for any speed and pressure. In addition, the 100°F curve has cross plots for tilted operation. The points shown are the mean seal dam film thickness.

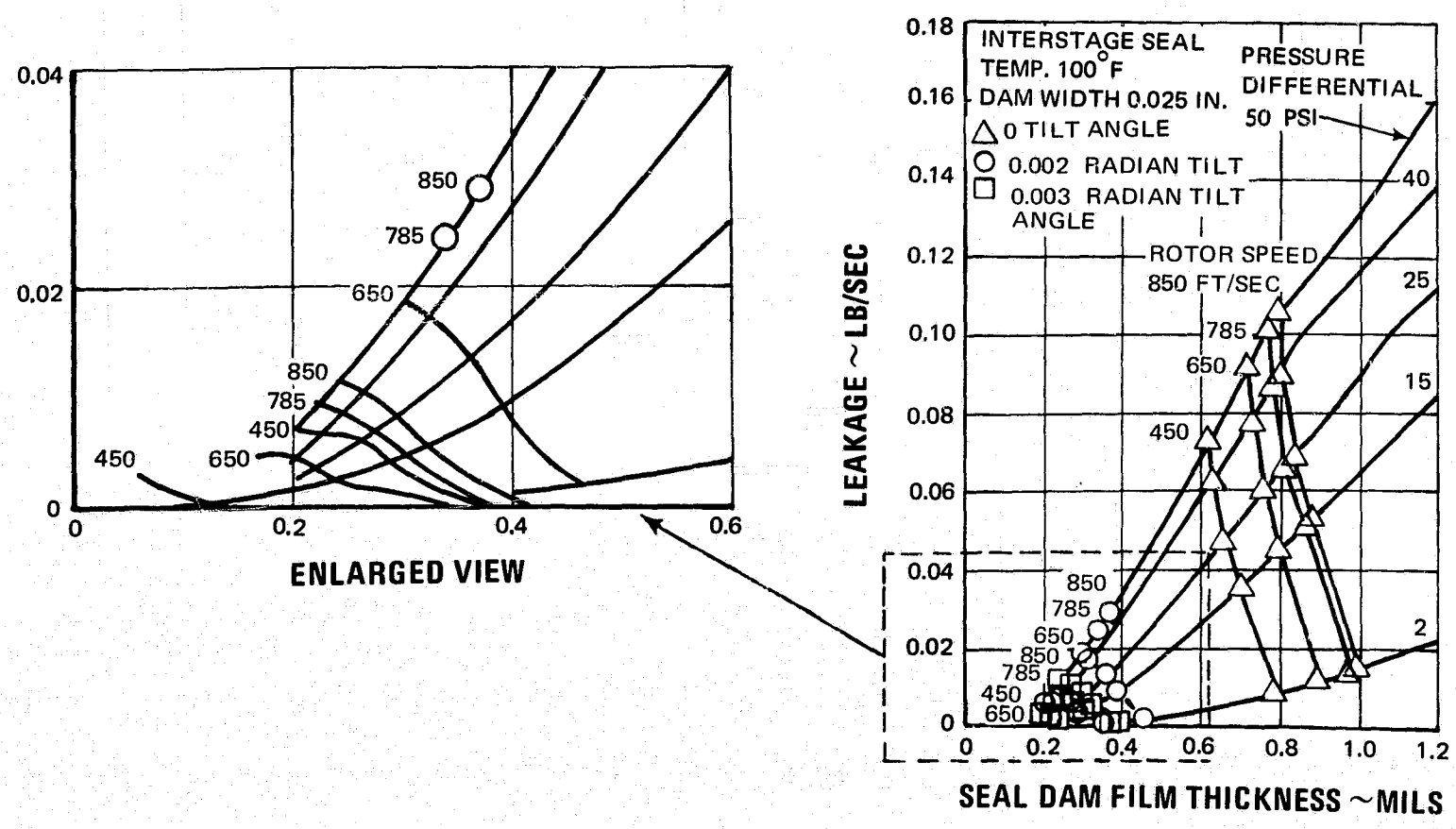

Figure 101 Seal Performance at 100°F with Parallel and Tilted Film Boundaries

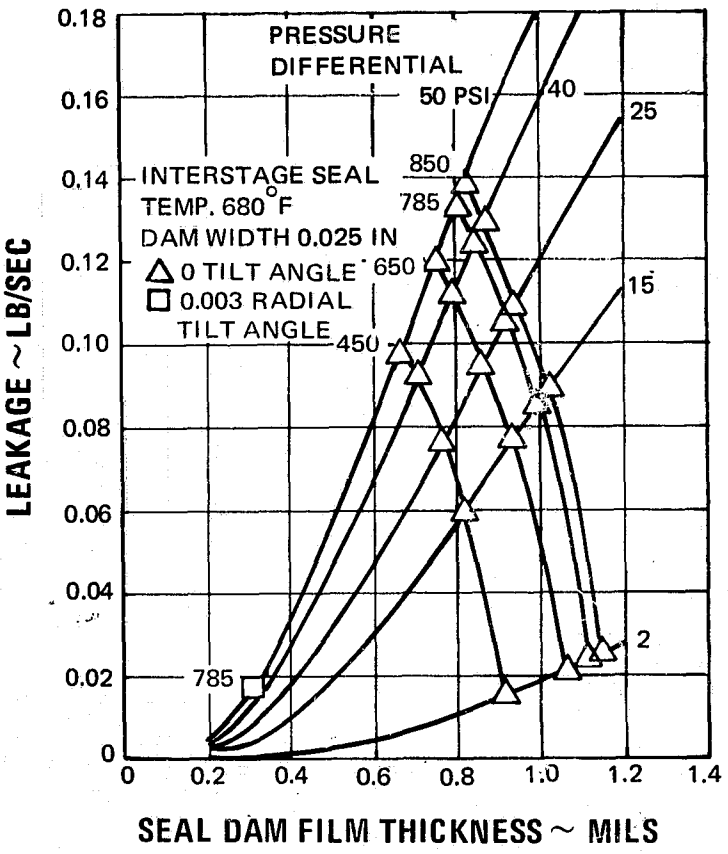

Figure 102 Seal Performance at 680°F with Parallel Film Boundaries and with a 3 Milliradian Tilt at Take-off Conditions

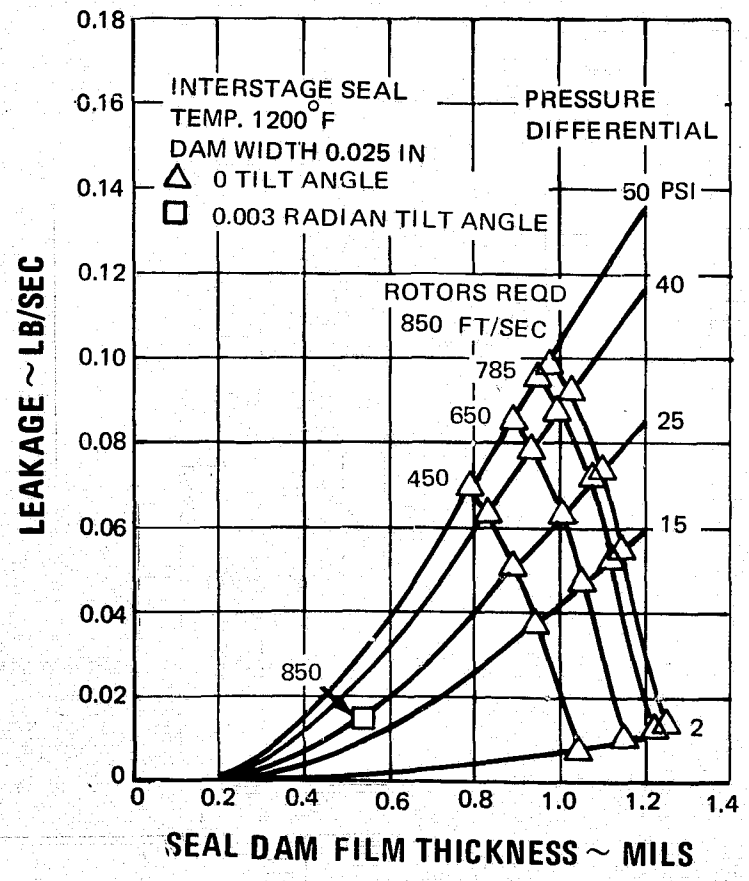

Figure 103 Seal Performance at 1200°F with Parallel Film Boundaries and with a 3 Milliradian Tilt at Take-off Conditions

C. SELF-ACTING END SEAL, DESIGN B

The Design B end seal employs a double row of Rayleigh step self-acting bearing pads to generate primary seal load capacity. Figure 104 illustrates the mechanical arrangement of the seal. The contractor conducted an analysis which defines the theoretical performance of a seal designed according to drawings furnished by the National Aeronautics and Space Administration program manager. The analysis has identified several design modifications which should be made to improve the force and moment balance of the seal. Extensive optimization studies of the Design B seal, however, were beyond the scope of the Task V work statement. Presentation of the Design B analysis follows the format used in presenting the Design A analysis.

1. PRIMARY SEAL ANALYSIS

The primary seal configuration for the Design B seal is made up of 180 Rayleigh step bearing pads, 90 pads on each side of a 0.060 wide seal dam. Each pad is approximately 0.685 inches long and 0.260 inches wide. The shallow recess in each pad is 0.400 inches long, 0.200 inches wide and 0.0006 deep. Deep radial grooves carrying seal leakage air into and away from the seal dam are located between each pad. The radial grooves and pad recesses are cut into the surface of the seal runner while the circumferential grooves separating the self-acting bearings from the seal dam are cut into graphitic carbon segments in the nosepiece assembly. Seal dam and bearing pad regions were analyzed separately followed by the construction of combined load capacity curves which define the primary seal opening force variation with film thickness for several film angles and a wide range of operating conditions.

a. Seal Dam Load Capacity

Seal dam load capacity and leakage was calculated using the same methods employed in Design A calculations. Figures 105 and 106 represent seal dam load capacity variation with film thickness at several film angle values and temperature levels.

b. Bearing Load Capacity

Rayleigh step bearing load capacity was calculated using the same computer program (Reference 5) that was used to calculate performance characteristics of the hybrid Rayleigh step primary seal for the one-side floated-shoe seals. Figures 107 and 108 illustrate the variation in load capacity with film thickness and speed for parallel and tilted film boundaries. When film angles of 0.002 radians or greater are encountered, the row of step bearings on the high film thickness side of the seal dam have negligible load capacity. The tilted Rayleigh step bearing load capacity is plotted with reference to the film thickness at the center of the row of step bearings on the low film thickness side of the seal dam (not the film thickness at the center of the primary seal face).

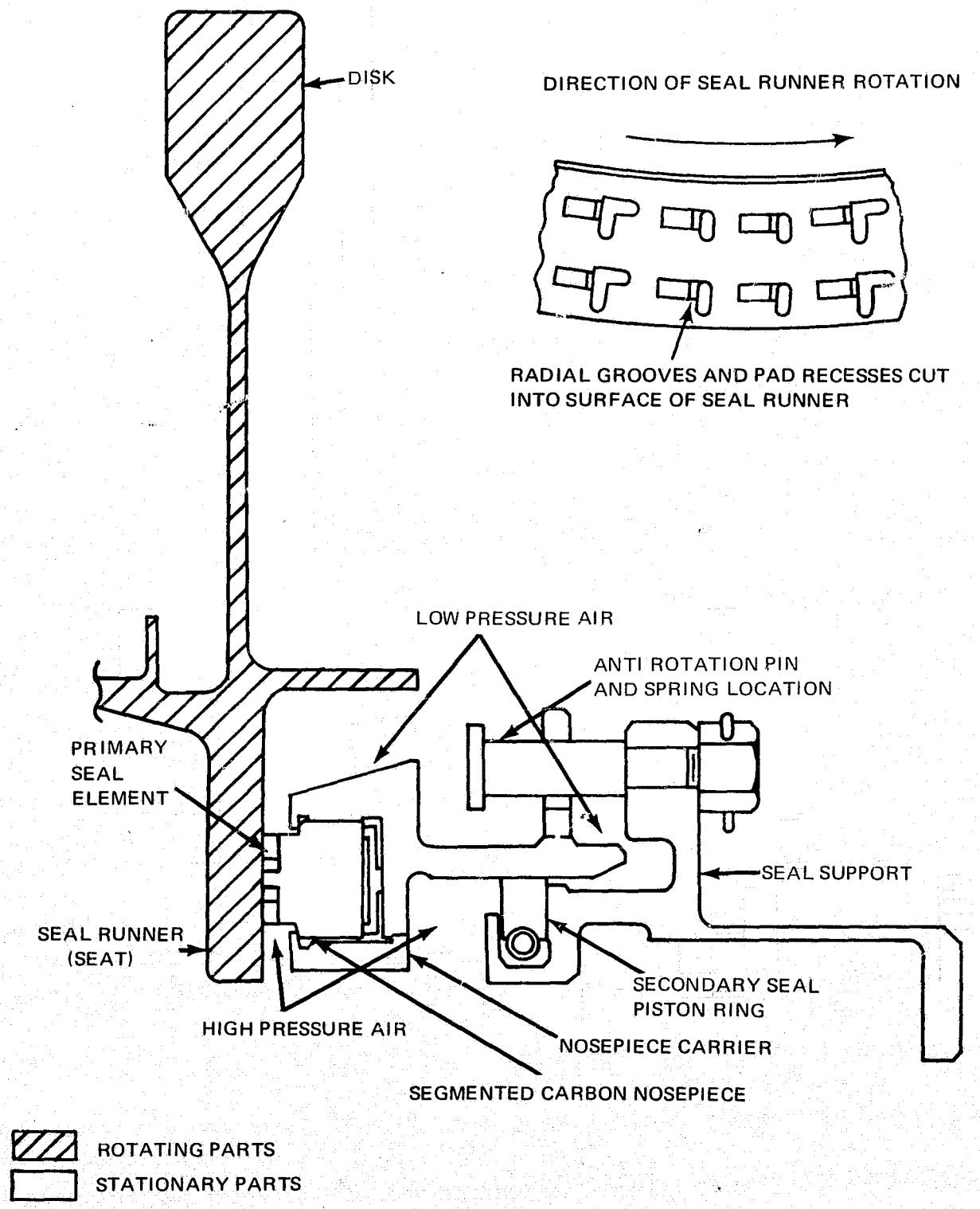

Figure 104 Self-Acting End Seal, Design B

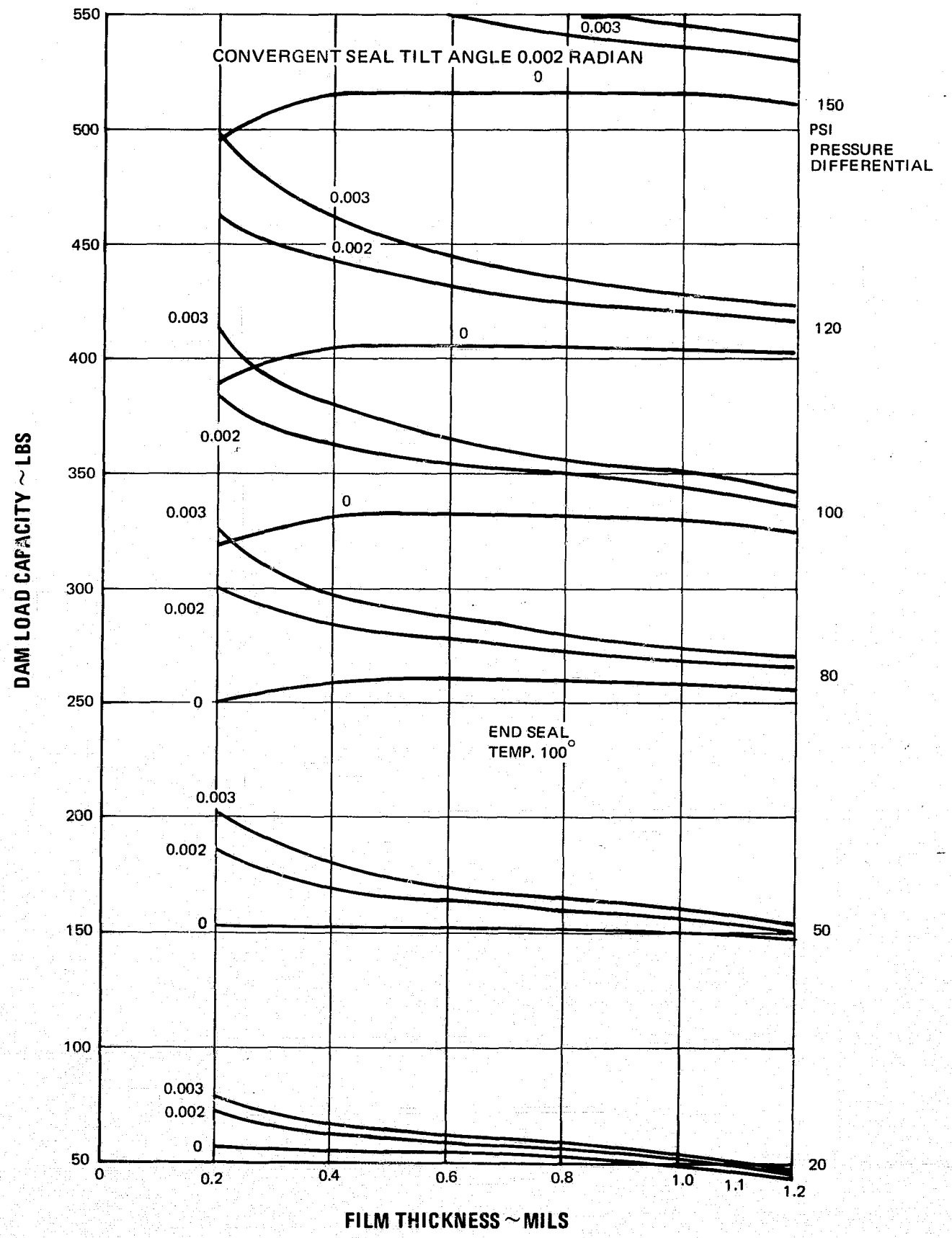

Figure 105 Seal Dam Load Capacity at 100°F

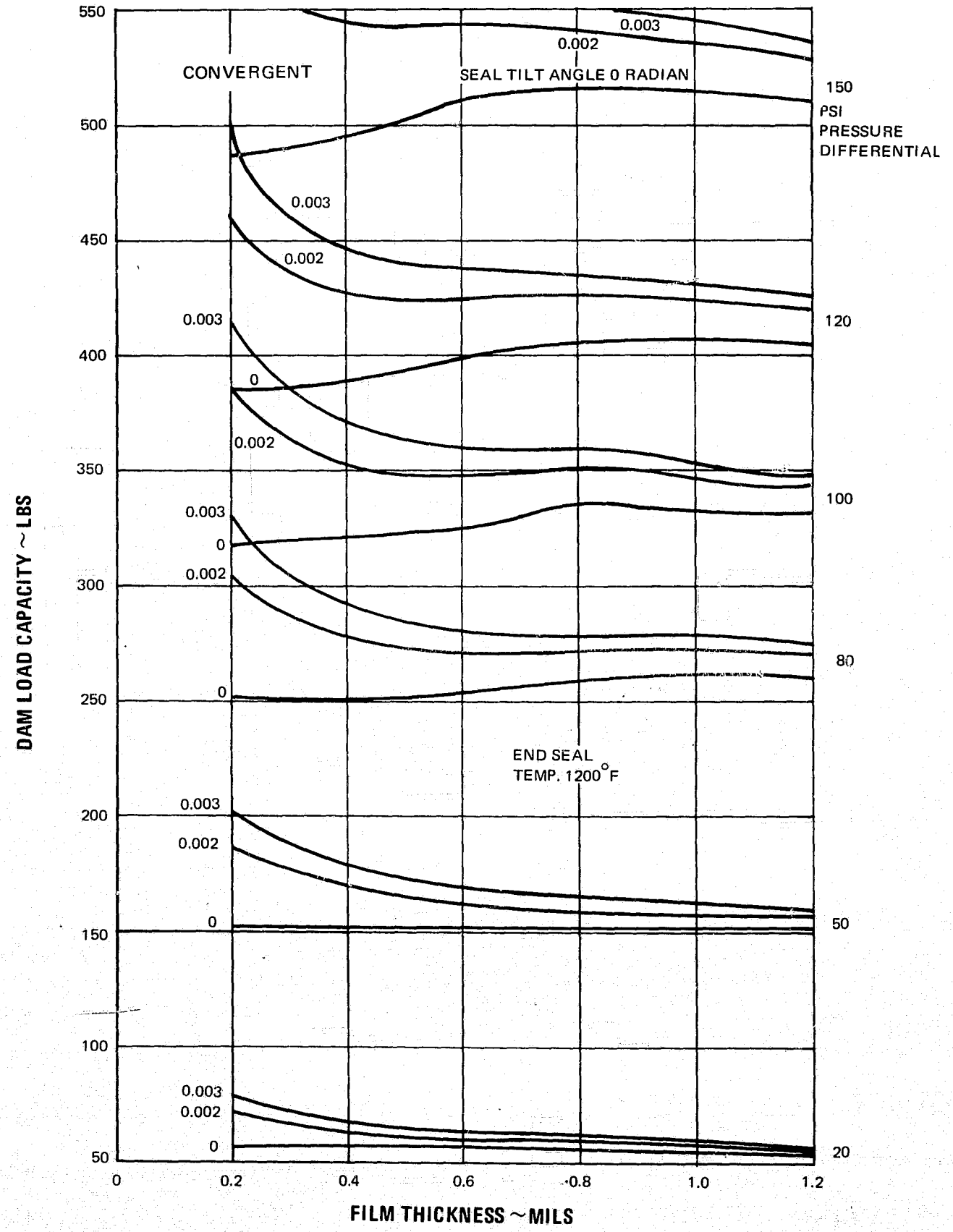

Figure 106 Seal Dam Load Capacity at 1200°F

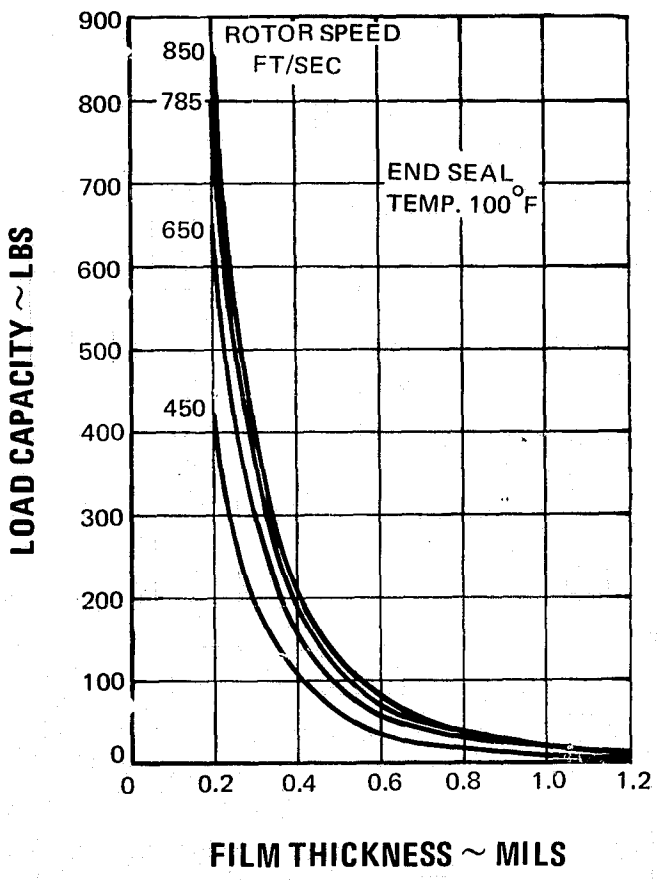

Figure 107 Load Capacity of the Step Bearing at 100°F

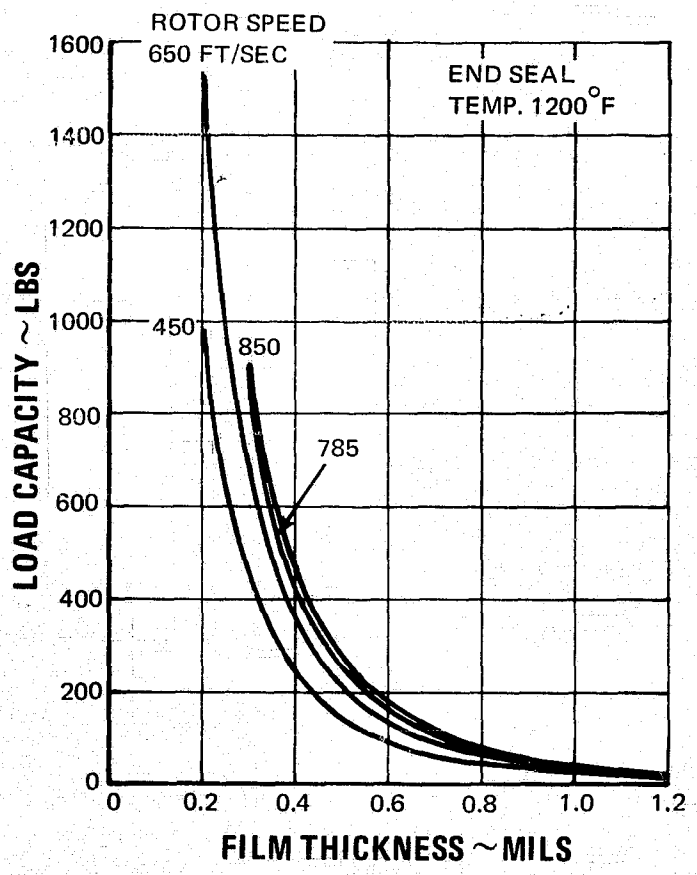

Figure 108 Load Capacity of the Step Bearing at 1200°F

c. Primary Seal Total Load Capacity

The total opening force generated in the primary seal air film was found for many combinations of speed, pressure, temperature, film angle, and film thickness. Figures 109 and 110 represent typical total load capacity curves. The load capacity curves for a convergent film angle are plotted with reference to the film thickness at the inner row of step bearings and also with reference to the seal dam film thickness. The bearing film thickness is 0.0005 inch and 0.0007 inch less than the seal film thickness at 0.002 and 0.003 radian film angles, respectively.

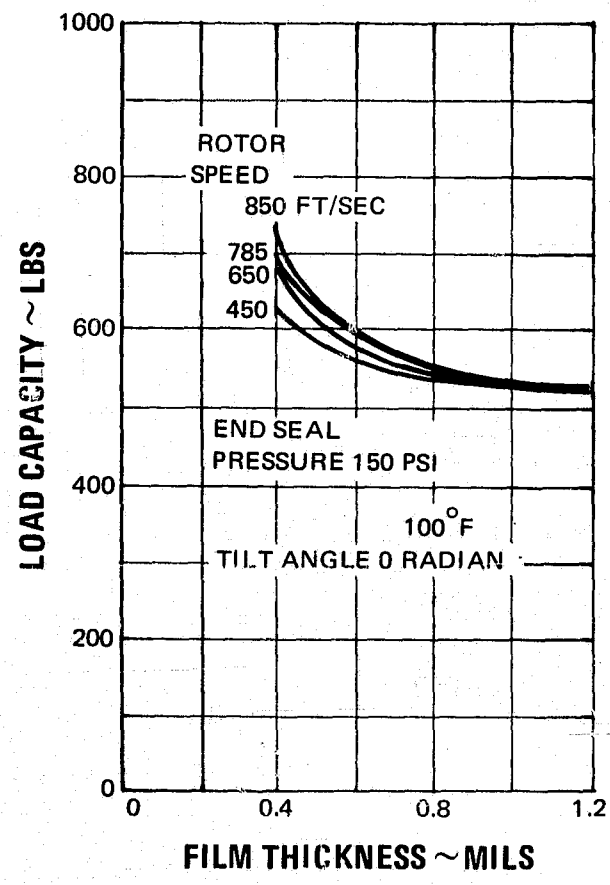

Figure 109 Typical Primary Film Total Load Capacity at Tilt Angle of 0 Radians

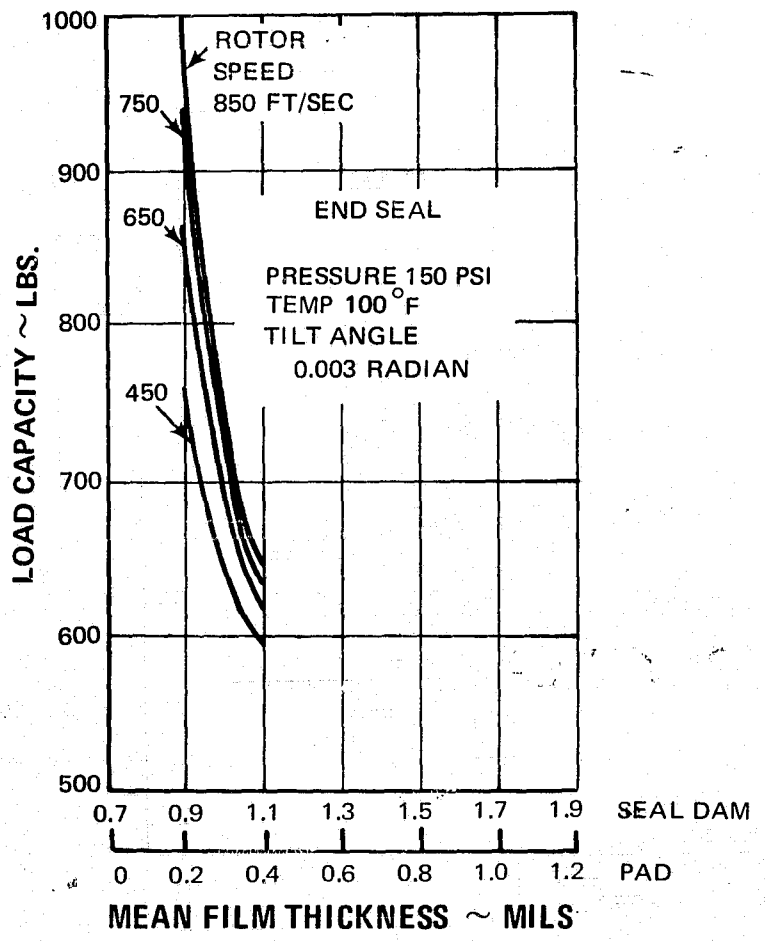

Figure 110 Typical Primary Film Total Load Capacity at Tilt Angle of 0.003 Radians

2. FORCE AND MOMENT BALANCE

The static pressure induced closing force on the nosepiece assembly is regulated by the seal balance diameter. The balance diameter specified on the seal drawings represents a balance ratio, A_H/A_T, of 0.639. A coil spring closing force of 45 pounds was selected by the contractor. The spring force must be high enough to yield adequate film stiffness during low pressure operation, yet low enough to avoid excessive rubbing contact and heat generation during start-up. A_T is the area of the seal; and A_H is the area between the balance diameter and the outer diameter of the dam.

With total closing force values established by the above considerations, equilibrium film thickness values were found using the primary film total load capacity curves described in the preceding section. The mean film thickness values determined by this analysis were combined with seal leakage curves to produce the seal performance maps shown in Figures 111, 112, and 113.

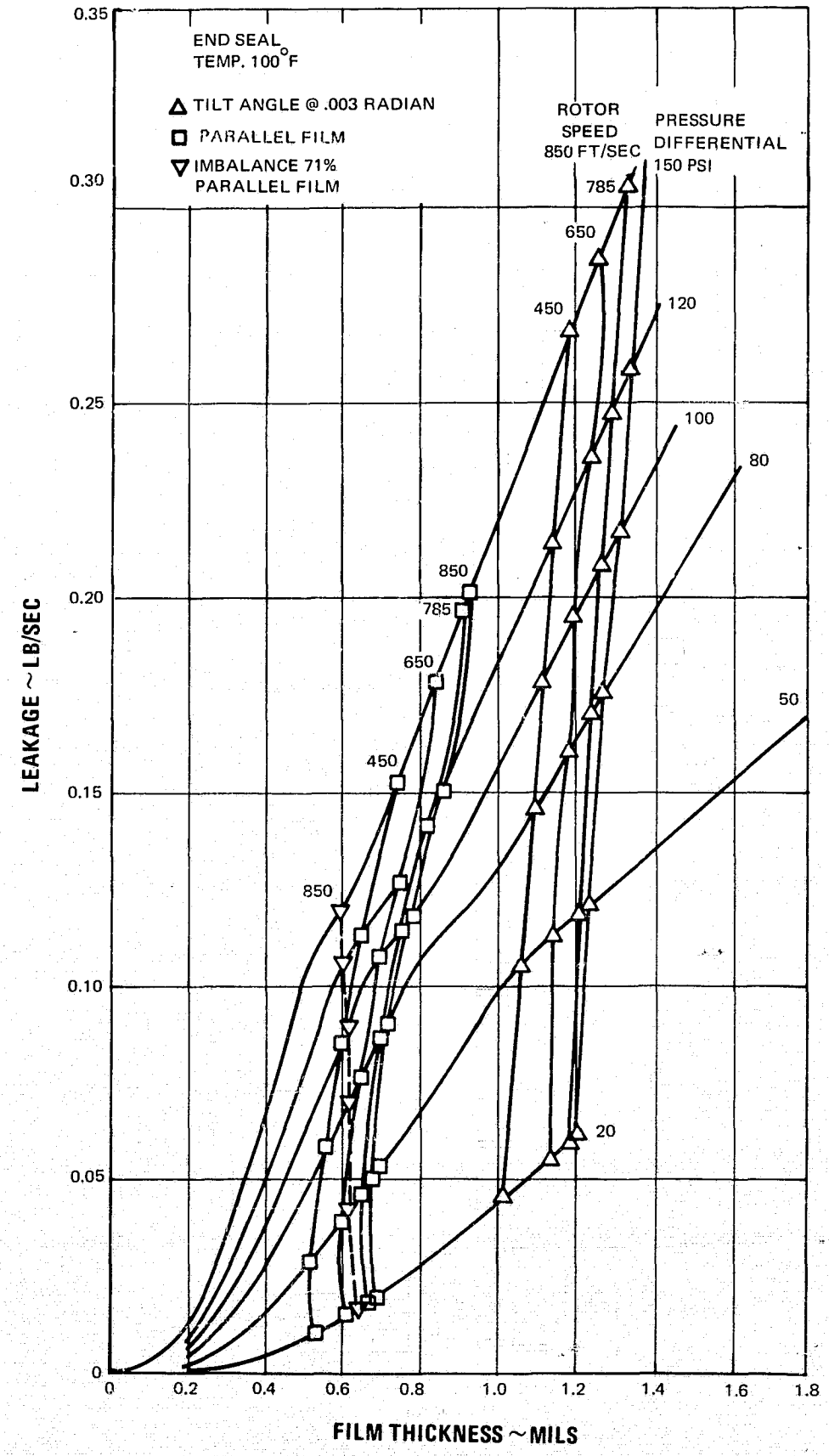

Figure 111 Seal Performance at 100°F with Parallel and Tilted Film Boundaries

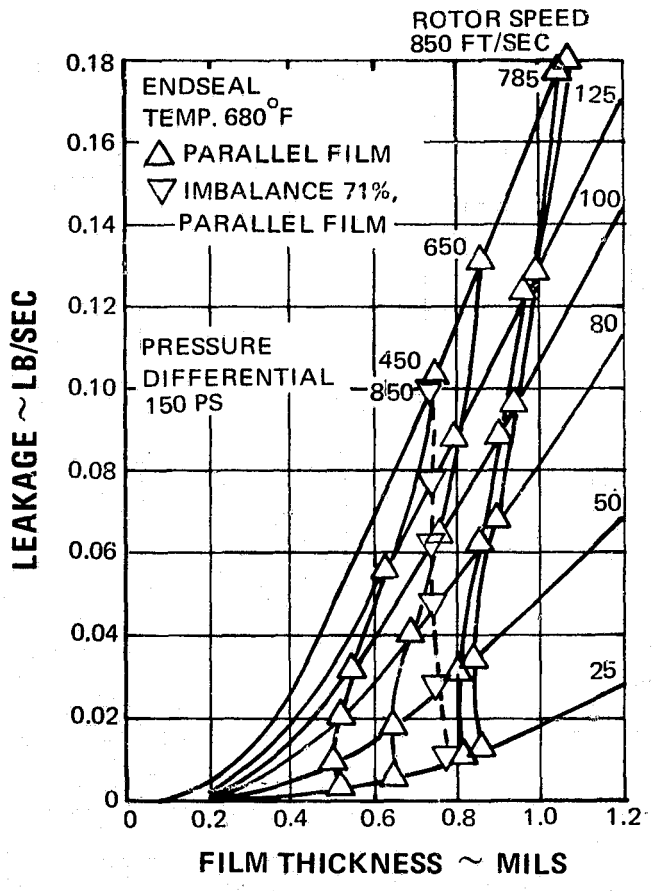

Figure 112 Seal Performance at 680°F with Parallel Film Boundaries and with a 3 Milliradian Tilt at Take-off Condition

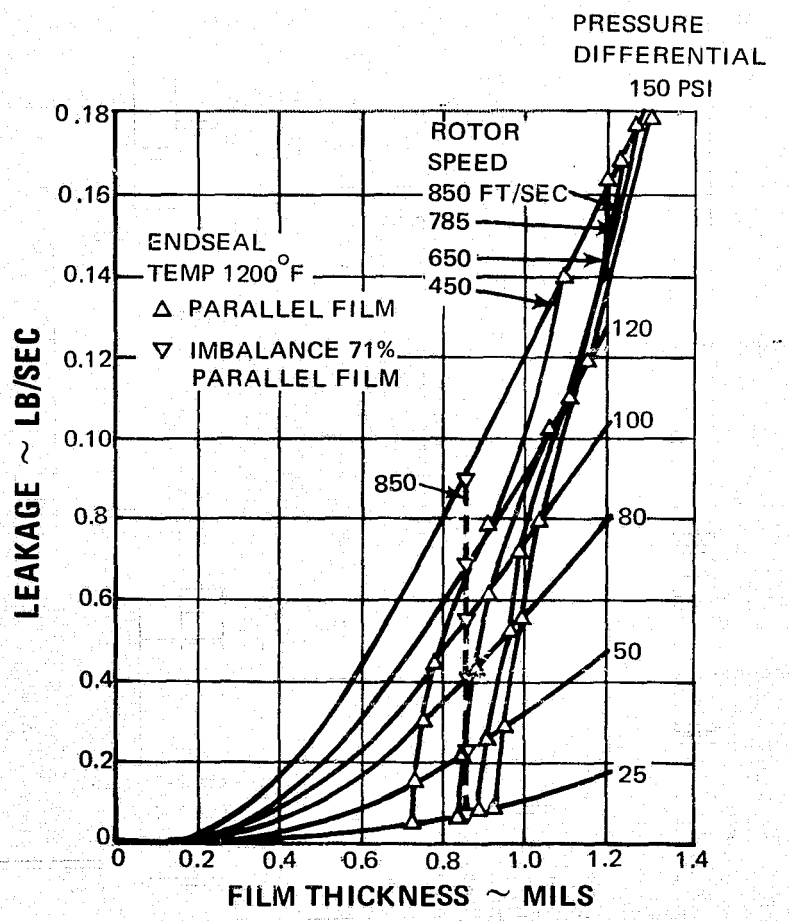

Figure 113 Seal Performance at 1200°F with Parallel Film Boundaries and with a 3 Milliradian Tilt at Take-off Conditions

Figure 111 also shows the effect of a 0.003 radian film angle on film thickness and leakage.

It became apparent during the analysis of the seal that an increase in the seal balance ratio would improve seal performance at the upper pressure levels. The contractor recommends that the balance ratio be changed to 0.71. The seal performance maps indicate the effect of a 0.71 balance ratio on seal film thickness and leakage at the 850 ft/sec speed level. The contractor also recommends an increase in the flow area through the radial grooves which carry seal leakage into and away from the seal dam to allow for the higher leakage of a tilted film.

Moment loads on the seal nosepiece assembly are controlled by the nosepiece centroid position relative to the center of radial pressure loads on the nosepiece. The pressure center location on the Design B seal varies with the axial position of the nosepiece relative to the seal support, so that a zero-moment load is possible at only one nosepiece position. Since the allowable axial travel must be 0.20 inch to either side of nominal, the radial center of pressure is shifted 0.10 inch to either side of nominal and the total moment on the seal is at least 2,000 inch-lbs in either direction. The problem is further complicated by the need to move the nosepiece centroid 0.080 inch closer to the seal face to minimize the moment when the nosepiece position is at either extreme. Assuming that the nosepiece centroid location is optimized, the angular displacement of the nosepiece under a 2000 inch-lb moment is 0.0015 radian. The pressure-induced film angle would then be a significant function of the allowable angle, and the amount of thermal distortion tolerated during seal operation would be severly limited.

3. DYNAMIC ANALYSIS

The weight of the carbon nosepiece segments was estimated to be two pounds, the weight of the nosepiece ring is approximately 14 pounds. A complete nosepiece assembly has a total weight of 16 pounds. Figure 114 indicates the effect of a 0.004-inch full indicator reading run-out of the rotor on the primary film thickness as a function of film stiffness and operating speed (see Reference 2).

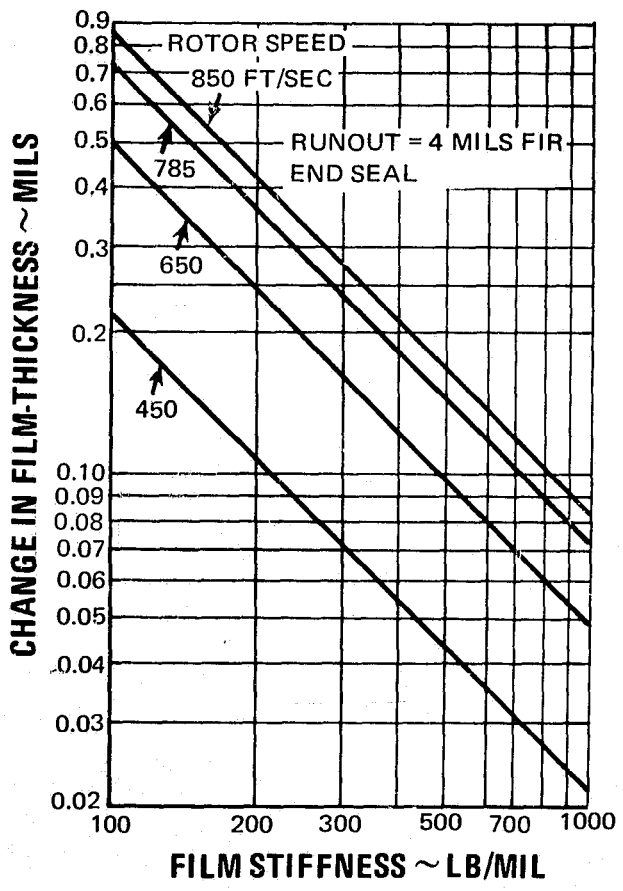

Figure 114 Film Thickness Variation Due to Rotor Runout

D. RUNNER FABRICATION

Two seal runners for the self-acting Design B seal of Task V were fabricated under Task VI for use in and end seal location. Seal surfaces were machined for the application of hard-facing (chrome carbide or equivalent), but were not hard-faced. Both runners were manufactured flat and true within practical tolerances to represent the best practice expected in an aircraft engine. The completed seal runners were shipped to the manufacturer of the Design B seal in accordance with instructions from the NASA Project Manager. Photographs of the fully machined seal runners are shown in Figures 115 and 116. The manufacture of seal design B under another contract will complete the runner fabrication by machining the self-acting pad geometry on the inner surface. Testing of this self-acting seal is not within the scope of this contract.

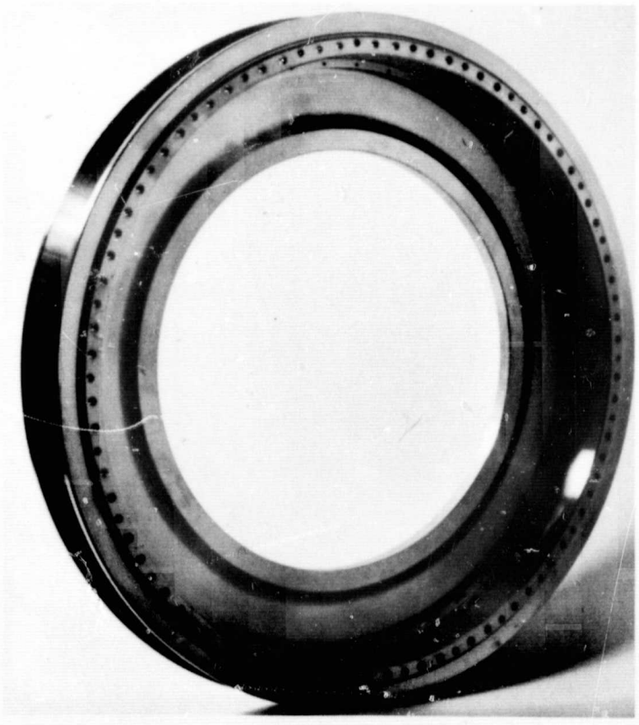

Figure 115 Front View of Runner for Design B Seal (XPN-14116)

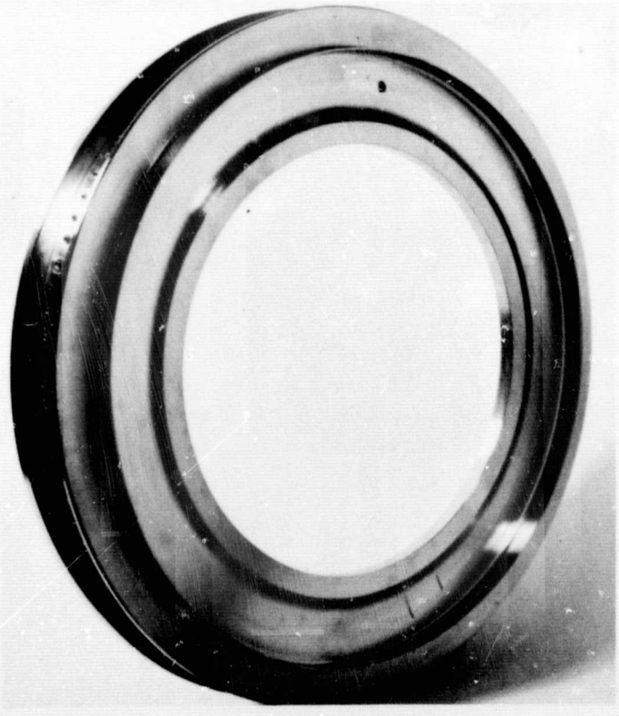

Figure 116 Rear View of Runner for Design B Seal (XPN-14117)

PRECEDING PAGE BLANK NOT FILMED

VI. COMPRESSOR STATOR PIVOT BUSHING AND SEAL CONCEPT FEASIBILITY ANALYSIS

A. SUMMARY

A feasibility analysis program was conducted on stator vane pivot bushing and seal concepts for application in compressors for advanced air-breathing propulsion systems. The first phase of this program consisted of preliminary analysis and screening of various seal concepts prior to the selection of concepts for the detailed feasibility analysis. The analytical effort included a comparison of the selected concepts to current practive, and all calculations, analyses, and drawings necessary to establish the feasibility of the selected concepts. This analytical program was subcontracted to Mechanical Technology, Incorporated, of Latham, New York, and the principal investigators there were Dr. D. F. Wilcock, Dr. H. S. Cheng, and Mr. J. Bjerklie. Pratt & Whitney Aircraft closely monitored the analytical program, as required by the NASA contract, and prepared the final feasibility designs on the basis of the concepts which had been designed and analyzed by Mechanical Technology, Incorporated.

In the screening study (Reference 2) 12 different concepts were examined for the vane pivot bushing and seal designs. Because of excessive leakage, the effects of dirt, the effects of load deflection, inherent reliability, weight, space, design simplicity, and other considerations, ten of the concepts were discarded, leaving only the bellows-loaded seal and the spherical-seat seal. Before the final feasibility analyses, several variations of these two concepts were explored. Finding that none of these variations provided a significant advantage over the original concepts, feasibility analyses were only conducted on the single-bellows and the spherical-seat seals.

The feasibility analyses showed that both the single-bellows seal and the spherical-seat seal had the potential to provide substantial improvements over the baseline seal, and also showed that the problem areas of the two seals would be very similar. The results of the feasibility analyses are summarized in Table II, which also includes the characteristics of the baseline vane pivot seal in use at the time of the study.

Both the single-bellows seal and the spherical-seat seal were considered to be feasible and adequate for final design and testing under Task IV. However, before submitting these two designs to NASA, Pratt & Whitney Aircraft modified the designs to make them more practical for aircraft engine applications without making changes in the basic seal concepts shown on the drawings submitted by Mechanical Technology, Incorporated. The final designs were submitted to NASA on 19 May 1966, and approval to proceed with Task IV was granted in a letter from NASA on 31 May 1966.

TABLE II

SUMMARY OF THE FEASIBILITY ANALYSES

	Single-Bellows Seal	Spherical-Seat Seal	Present Seal
Leakage at 135 psi (scfm)	0.00079	0.0004	0.0077
Wear rate	Low on flame plate	Extremely low	Very low
Required torque less bending moment effect (in-lbs)	1.53	0.54	3.8
Seal diameter (in)	0.509	0.527	0.5
Seal weight (lbs/pivot seal)	0.025	0.025	0.025
Unproven materials		Carbon at 1200°F	Not suitabe at 1200°F
Effect of dirt	Increase in leakage	None	Increase in leakage and wear
Effect of cocking	Absorbed by bellows	Must reseat	Increased leakage
Separate parts for assembly	7	7	5
Ability to be installed as a cartridge	Possible for bellows assembly	Separate parts	Separate Parts
Replacement of seals and seats	Separate	In matched pairs	Separate
Potential problems	Effect of dirt on wear and leakage. Bellows integrity	Ability to remain properly seated when cocked. Carbon integrity	

B. SCREENING STUDY

The stators of high-pressure compressors for advanced engines will probably incorporate variable vane stagger. The number of stages which will require variable vanes is as yet unknown, but the number of variable vanes in a given engine will probably exceed 500. Each variable vane requires a pivot which penetrates the compressor wall, and even a small amount of leakage out of each could represent a sizeable efficiency loss.

This section discusses the design and screening of a number of vane pivot concepts. Some of these were in the original proposal and others were conceived later. All of the seal designs were compared to a baseline seal which had been built and tested by Pratt & Whitney Aircraft prior to the start of this contract. That design (shown in Figure 117) was originated as a first modification of a seal being used in test engines at that time. Leakage measurements on the baseline seal provided a basis on which the new seal concepts could be adjudged as probably better or probably worse than the baseline seal.

The seal concepts considered in the screening study are listed below:

Belleville washer	Internal Actuation
Coned carbon rings with gaps	External covers
Fractured carbon rings	Bellows-Loaded face seal
Metal spring	Spring-loaded spherical-seat seal
Seal packing	Close-clearance bushing
Lamiflex	Multiple labyrinth

Of these concepts, only the ones in the left-hand column were included in the proposal: the others were conceived later. All of the concepts are shown in Figure 118. Variations in each basic seal type were examined when there appeared to be an advantage in a slightly different design, but the first screening was done on the basic concepts only.

The screening considered three basic factors in seal concept acceptability: leakage rate, functional considerations, and application considerations. Since the basic goal of the program was to reduce leakage, any candidate that could not lead to low leakage was discarded. Tolerance to dirt, tolerance to load deflections, and the effects of temperature were the three main parts of the functional considerations. If a candidate were considered poor in this respect, it was discarded. Finally, the application considerations of weight, space, actuation power, design simplicity, and servicing were considered. In all cases, the candidate concepts were compared to the baseline seal.

Two concepts emerged from the screening study as the most promising candidates. They were the spherical-seat face seal and the bellows-loaded face seal. Both of these concepts were recommended and accepted for final feasibility analysis.

Primary sealing in the spherical-seat face seal is accomplished by the convex seal bearing against a concave seat. The two surfaces are kept in compression by a helical spring and by the thrust load created by the high pressure within the compressor.

In the bellows-loaded face seal, primary sealing is accomplished by a flat face seal bearing against the end of a bushing, which is installed in the outer shroud with an interference fit. The thrust loads created by air pressure, spring forces, and bellows forces are carried by a thrust bearing located at the tip of the vane.

A description of the screening study follows, and each of the basic factors governing seal concept acceptability is discussed.

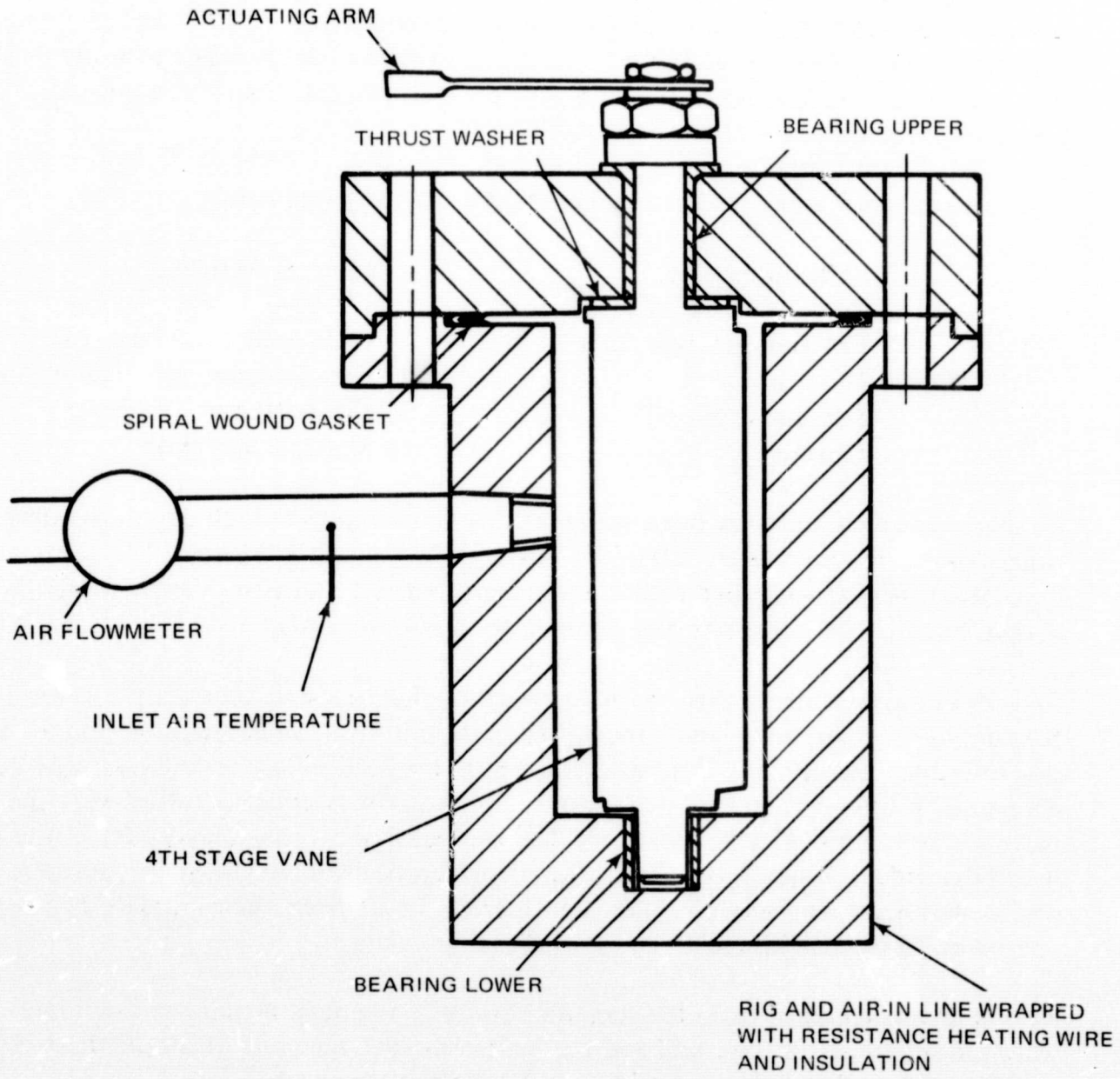

Figure 117 Baseline Vane Pivot Seal in Test Rig

FOLDOUT FRAME 1

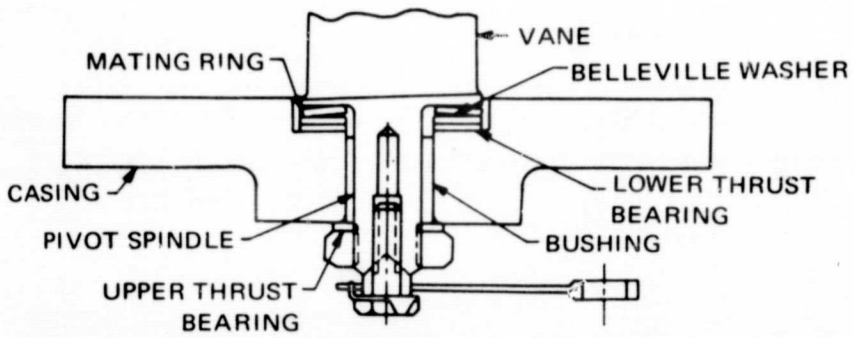

BELLEVILLE WASHER TYPE SEAL FOR COMPRESSOR STATOR VANE PIVOT BUSHING AND SEAL

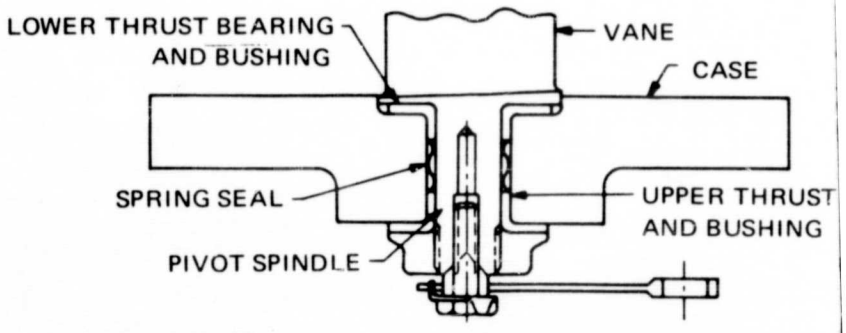

METAL SPRING SEAL FOR COMPRESSOR STATOR VANE BUSHING AND SEAL

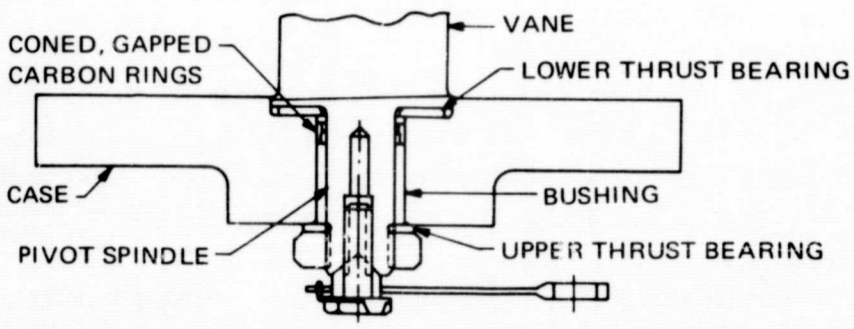

CONED CARBON RING SEAL FOR COMPRESSOR STATOR VANE PIVOT BUSHING AND SEAL

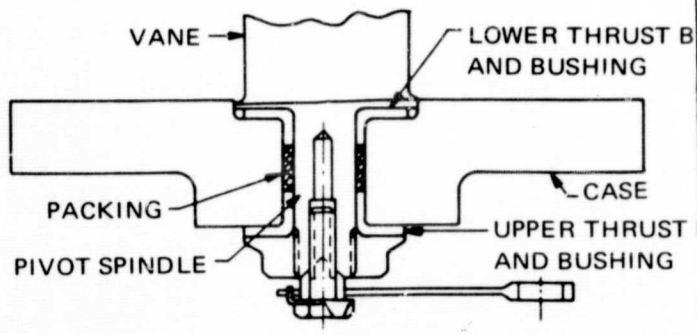

PACKING SEALS FOR COMPRESSOR STATOR VANE PIVOT BUSHING AND SEAL

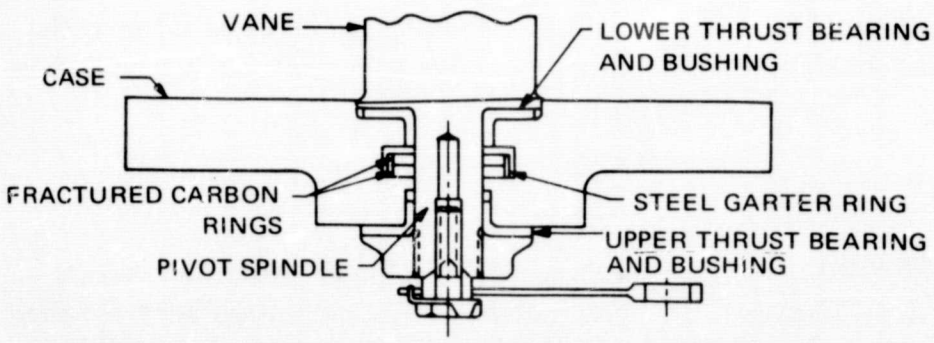

FRACTURED CARBON RING SEAL FOR COMPRESSOR STATOR VANE PIVOT BUSHING AND SEAL

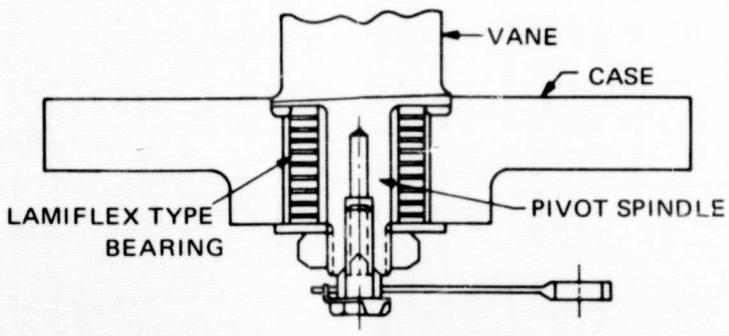

LAMIFLEX TYPE BEARING FOR COMPRESSOR STATOR VANE PIVOT BUSHING AND SEAL

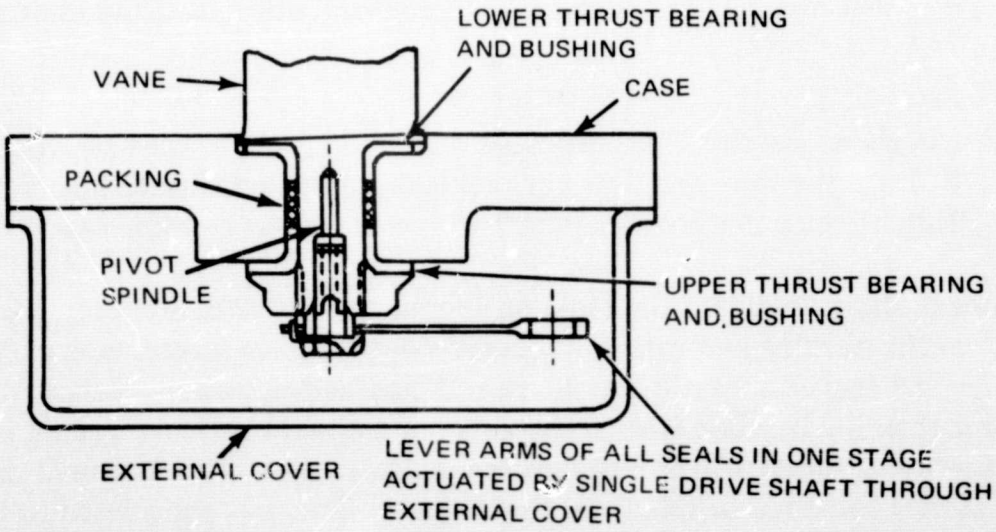

EXTERNAL COVER FOR COMPRESSOR STATOR VANE PIVOT BUSHING AND SEAL

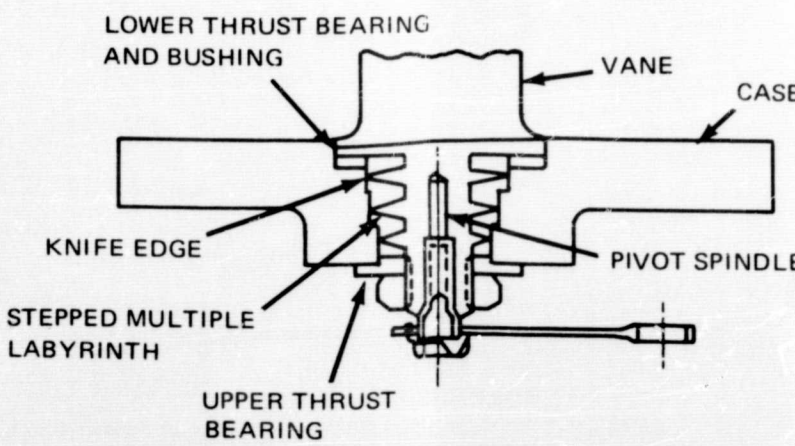

MULTIPLE LABYRINTH SEAL FOR COMPRESSOR STATOR VANE PIVOT BUSHING AND SEAL

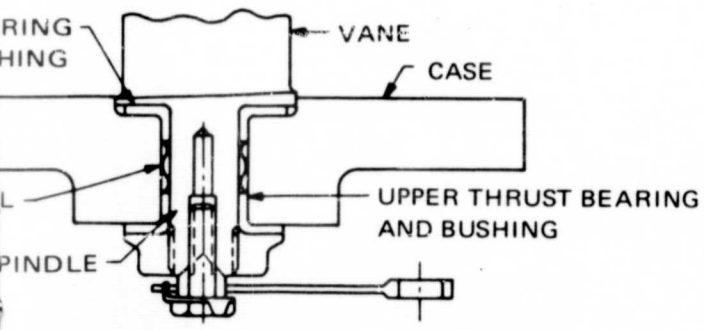

ING SEAL FOR COMPRESSOR STATOR VANE
BUSHING AND SEAL

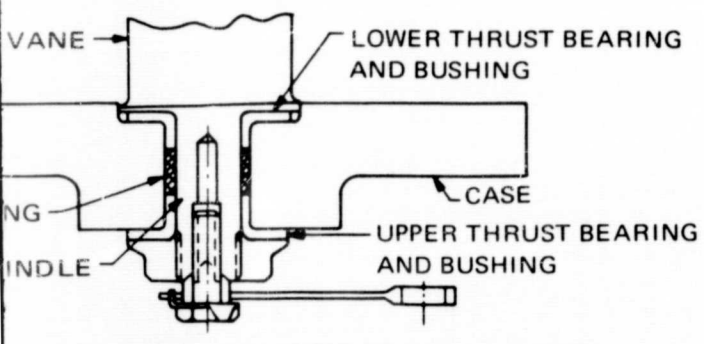

EALS FOR COMPRESSOR STATOR VANE PIVOT
BUSHING AND SEAL

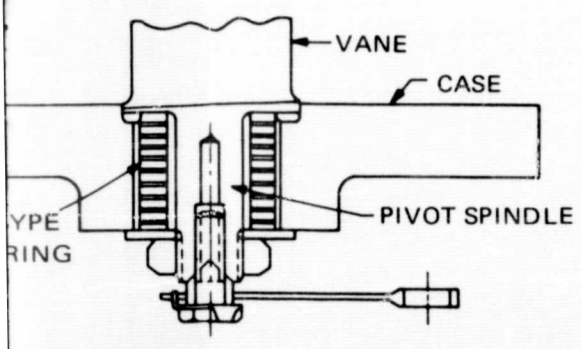

TYPE BEARING FOR COMPRESSOR STATOR
VANE PIVOT BUSHING AND SEAL

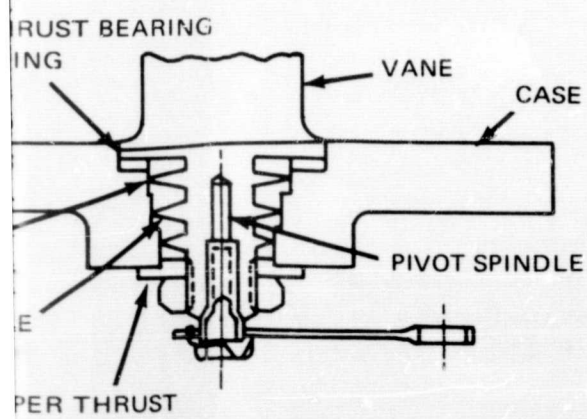

E LABYRINTH SEAL FOR COMPRESSOR STATOR
VANE PIVOT BUSHING AND SEAL

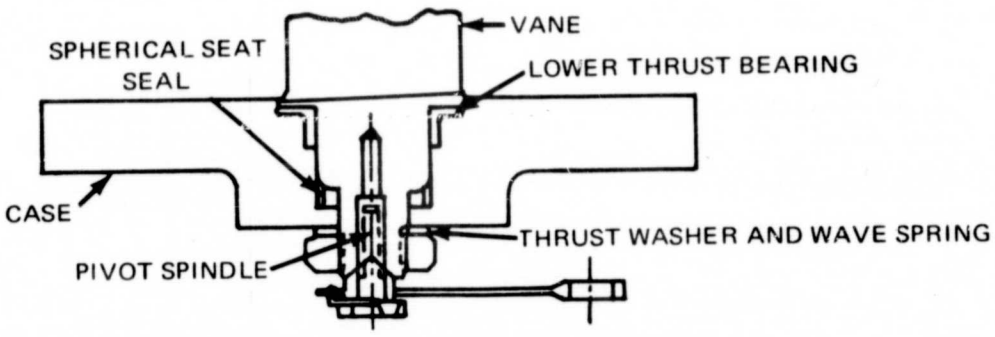

SPRING-LOADED SPHERICAL-SEAT SEAL FOR COMPRESSOR
STATOR VANE PIVOT BUSHING AND SEAL

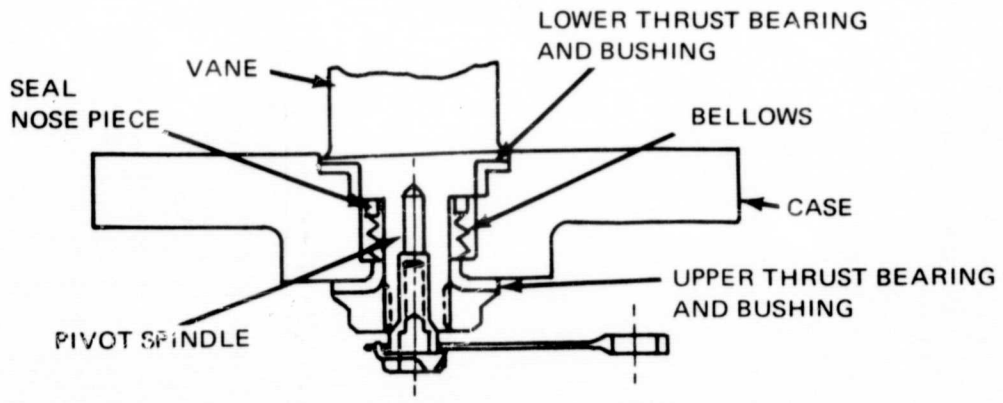

BELLOWS-LOADED FACE SEAL FOR COMPRESSOR
STATOR VANE PIVOT BUSHING AND SEAL

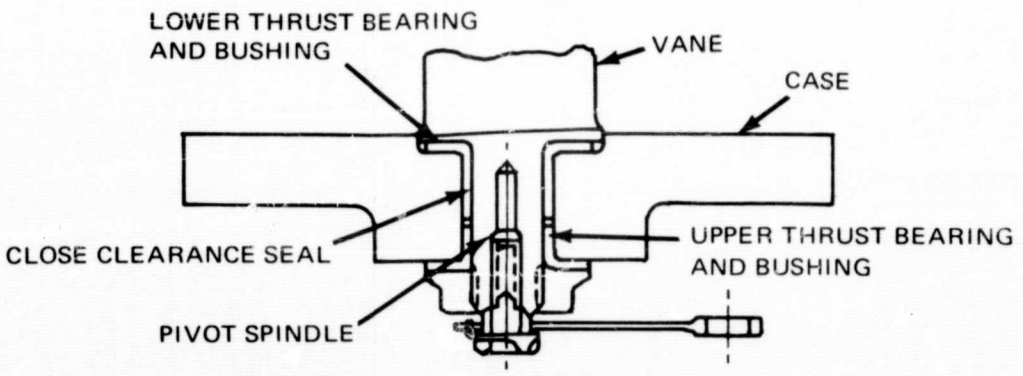

CLOSE CLEARANCE TYPE SEAL FOR COMPRESSOR
STATOR VANE PIVOT BUSHING AND SEAL

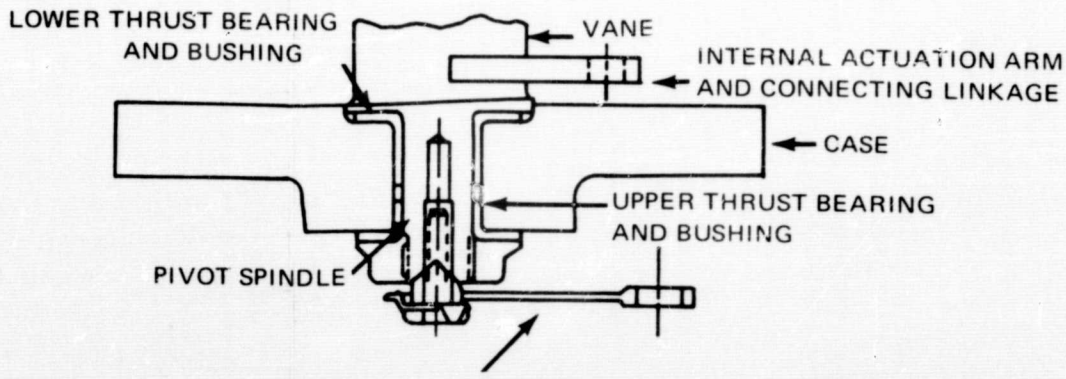

INTERNAL ACTUATION FOR COMPRESSOR
STATOR VANE PIVOT BUSHING AND SEAL

Figure 118 Vane Pivot Seal Concepts

1. LEAKAGE RATE CONSIDERATIONS

The belleville washer and the coned carbon ring with gaps were discarded because it could not be shown that their leakage would have been as low as that of the baseline seal. The belleville washer concept would have had two leakage paths past the washer. Each path would have been short, and the effective clearance would not have been any less than the clearance in the baseline design. The coned carbon ring with gaps would have had more leakage at a single gap than the total leakage for the baseline design.

Pratt & Whitney Aircraft had measured the leakage of the baseline seal prior to the screening study, and had found it to be less than 0.004 scfm at 94 psi and 400°F for static conditions. The loading on the thrust washer, including initial torquing plus pressure load, was about 95 pounds. The leakage rate was used to calculate the effective gap width of each of two leakage paths, resulting in a calculated gap of 0.088 mils.

To compare these measurements with the belleville washer, the actuating torque had to be the same for both designs. Because the length of the lever arm was the same for both designs, and because the friction coefficient was expected to be the same for both designs, the loading on the belleville washer had to be the same (95 pounds). With this loading, the effective gap between the washer and the seal would have been approximately the same as the scale of roughness. Assuming a 63-microinch finish and a gap length equal to approximately one tenth of a washer thickness, the calculated leakage for an unloaded vane was about 0.054 scfm, more than an order of magnitude greater than the baseline leakage.

The gaps in the coned carbon ring could have been as much as 0.010 inch. Calculations showed that leakage through such a gap could be as much as 0.1 scfm at the same conditions as the baseline test. That amount was considered to be much too large to permit further consideration of the coned carbon ring.

2. FUNCTIONAL CONSIDERATIONS

The principal functional considerations for these seals were the effects of dirt, the effects of load deflections, and the effects of temperature. These effects were examined both for their immediate impact on the design's sealing ability and for their effect on reliability. Six seals were eliminated because of functional considerations: the fractured carbon ring, the metal seal, the close-clearance bushing, the lamiflex seal, internal actuation, and the multiple labyrinth seal.

With the baseline seal, there was the possibility that dirt could get into the seal, encouraging the vane to cock. Because the vane could be cocked, leakage could be quite high when the vane was loaded. Both of these possibilities posed problems for the baseline seal.

The close-clearance bushing exhibited the same problems. In this case, however, the presence of particles between the bushing and vane pivot could contribute to severe wear because of the close clearance, and also could seriously increase the actuation power. Hence, this design was rated as poorer than the baseline seal. Reliability, as defined for the screening study, refers to the possibility of failure of the seal during vane actuation. The fractured carbon ring, by its very nature, consisted of relatively fragile parts. This was considered to be sufficent to rate it poorer than the baseline seal.

The metal spring seal depended on a close fit between the pivot and the spring for sealing. This meant that it would rub. Rubbing was expected to lead to wear and eventual penetration of the spring material, especially since dirt could also be deposited in the seal. Because of the rubbing and dirt problem, this design was rated as worse than the baseline design.

The lamiflex seal depended for its operation on an elastomeric material bonding a number of metallic washers. The stack of washers plus elastomer extended for most of the length of the pivot. However, the inner portion of the seal could be subjected to temperatures approaching 1200°F, the compressor exit temperature. Thus, at least a portion of some of the pivot seals would be exposed to temperatures considerably above the usable temperature of any available elastomer. Consequently, some of the pivots would not be reliable.

Internal actuation had the potential to reduce leakage, simply by reducing the number of compressor wall penetrations. However, internal actuation would necessitate the use of a linkage exposed to hot oxidizing gases. Also, the actuating torque would have to be transmitted to the inner linkage through a limited number of vanes, potentially causing excessive stresses and deflections.

Multiple labyrinths could conceivably make a good seal, but there would have to be a large number of segments for effective sealing. Because the available space was small, the segments of the labyrinth would have to be made of thin sheet stock, only a few thousandths of an inch thick. If the vane cocked under load, the segments would probably rub. If rubbing occurred, the segments would wear, would probably bend, and generally unknown effects could take place. Consequently, the seal was not considered to be reliable. The labyrinth seal was therefore rated a little lower than the baseline seal.

3. APPLICATION CONSIDERATIONS

After eliminating eight concepts because of leakage rates or functional considerations, the four remaining concepts were the packed seal, external covers, bellows-loaded face seal, and the spring-loaded spherical-seat seal. Application considerations for these seals included weight, space, actuation power, design simplicity, assembly, and servicing. None of these considerations was important enough by itself to eliminate one of the four remaining seal concepts. However, it was felt that if a concept displayed improved leakage and an acceptable functional level, then logistic considerations would show which of the candidates was likely to be the best.

Except for the external covers, the weights of the remaining concepts were about the same. The external cover required a separate pressure cover outside of the actuators and pivots. However, it was probably the most straightforward way of keeping leakage low. Its disadvantages were that it rated poorly on weight, space, and servicing. The space requirements for the other three systems were all about the same.

Of these three remaining systems, only the packed seal was found to require higher actuating power than the baseline seal. Calculations indicated the possibility of low friction after the seal had been worn in, but past experience contradicts these results, indicating that actuation power might well be too high to be acceptable.

The packed seal also exhibited a difficult assembly and servicing requirement. The baseline seal was torqued down during assembly, so that the unloaded actuating torque was 1.5 in-lb. The packed seal also required preloading by torquing the seal during assembly. However, the sealing ability of the packed seal depended on the packing pressure against the vane shaft. The compressor pressure load would not markedly assist the sealing, as it does for the baseline seal. Thus, leakage past the packed seal would be slightly more sensitive to initial adjustment.

The packed seal would have to be worn in without loss of sealing ability. This too, would complicate the assembly and servicing, since wearing in would have to occur before final installation.

Bellows-loaded face seals do not have to be preloaded by torque adjustment: they can be assembled as a cartridge. Thus, they represent a gain in assembly and in servicing ease.

The spring-loaded spherical-seat seal likewise did not need to be adjusted on installation. However, its assembly was more complicated because one part of the seal must be firmly attached to the vane shaft. These two effects tended to counterbalance each other, so far as assembly and servicing were concerned. Consequently, this seal was rated equal to the baseline seal.

C. DESIGN VARIATIONS

Design variations involved refinement of the concepts and review for comments and suggestions with seal manufacturers. The final feasibility designs were prepared in the light of these comments.

A sketch of a single-bellow seal design (shown in Figure 119) was sent to several manufacturers for comments and recommendations. One seal manufacturer responded with the sketch shown in Figure 120. This design incorporated a housing over the seal rather than trapping the pivot between the engine case flanges. Also in this design aluminum oxide or tungsten carbide was used rather than graphite as the face material. These materials were considered as alternatives to graphite or boron nitride, but they have much higher coefficients of friction. Because the seal manufacturer recommended the use of a larger bellows, it was decided that for the final feasibility design further consideration would be given to a machined bellows of only one half or one convolution. This was made necessary because of the tight circumferential spacing of the vane pivots at a given stage.

Figure 121 shows another version of the bellows-loaded face seal, incorporating the thrust face at a point on the pivot shaft further from the primary gas path. Some thermal advantage could be achieved by this relocation, because the temperature would be between 50 and 100°F cooler than at the inside. This much of a temperature advantage could make a graphite coating more feasible. There would be no advantage gained for the other candidate face materials. A similar scheme was considered for the spherical-seat seal.

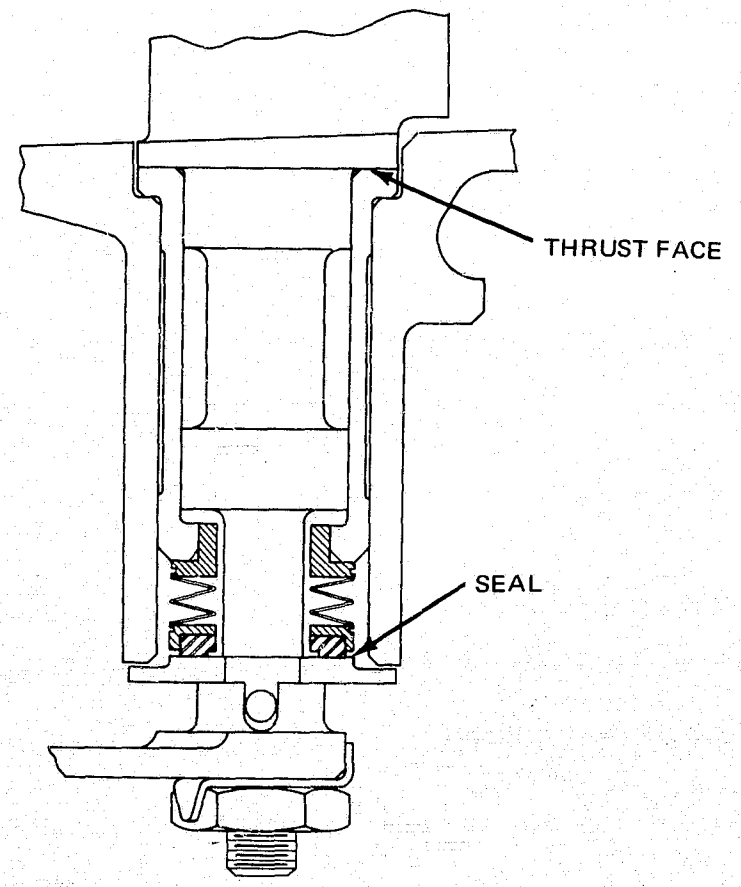

Figure 119 Single-Bellows Seal

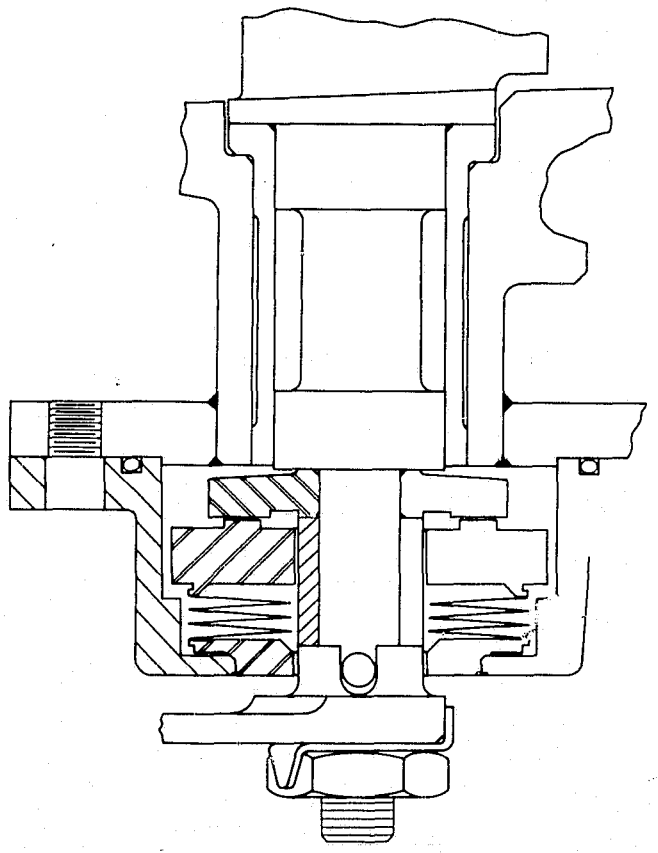

Figure 120 Single-Bellows Seal

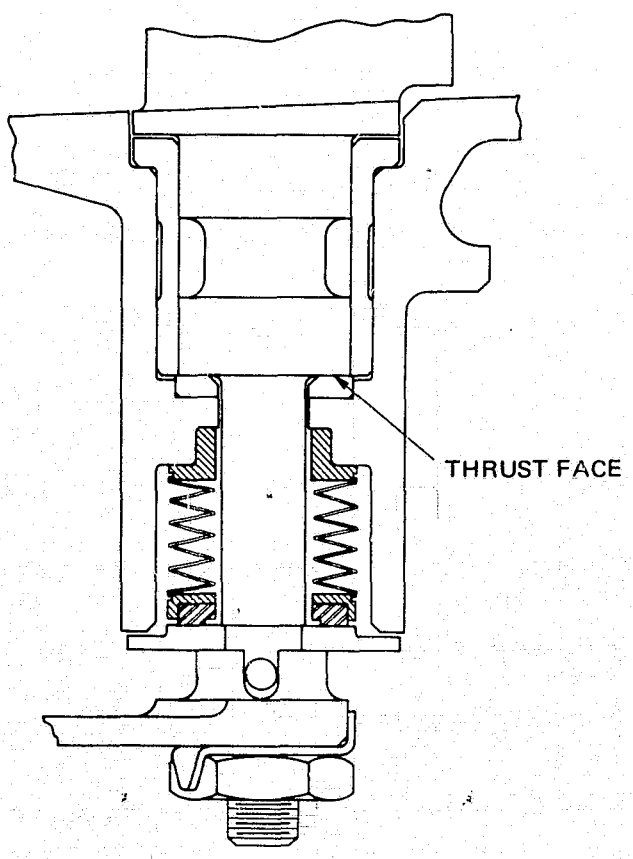

Figure 121 Single-Bellows Seal, Relocated Thrust Face

Taking into consideration the results of the screening study, the comments of the seal vendors, and the possibilities reviewed in the design variation studies, three seal designs were recommended to NASA for final feasibility analysis. These three designs were the spherical-seat face seal (Figure 122), the single-bellows face seal (Figure 123), and the double-bellows face seal (Figure 124). On October 7, 1965, NASA approved the final feasibility studies for the spherical-seat face seal and the single-bellows face seal. These feasibility studies are discussed in the next two sections.

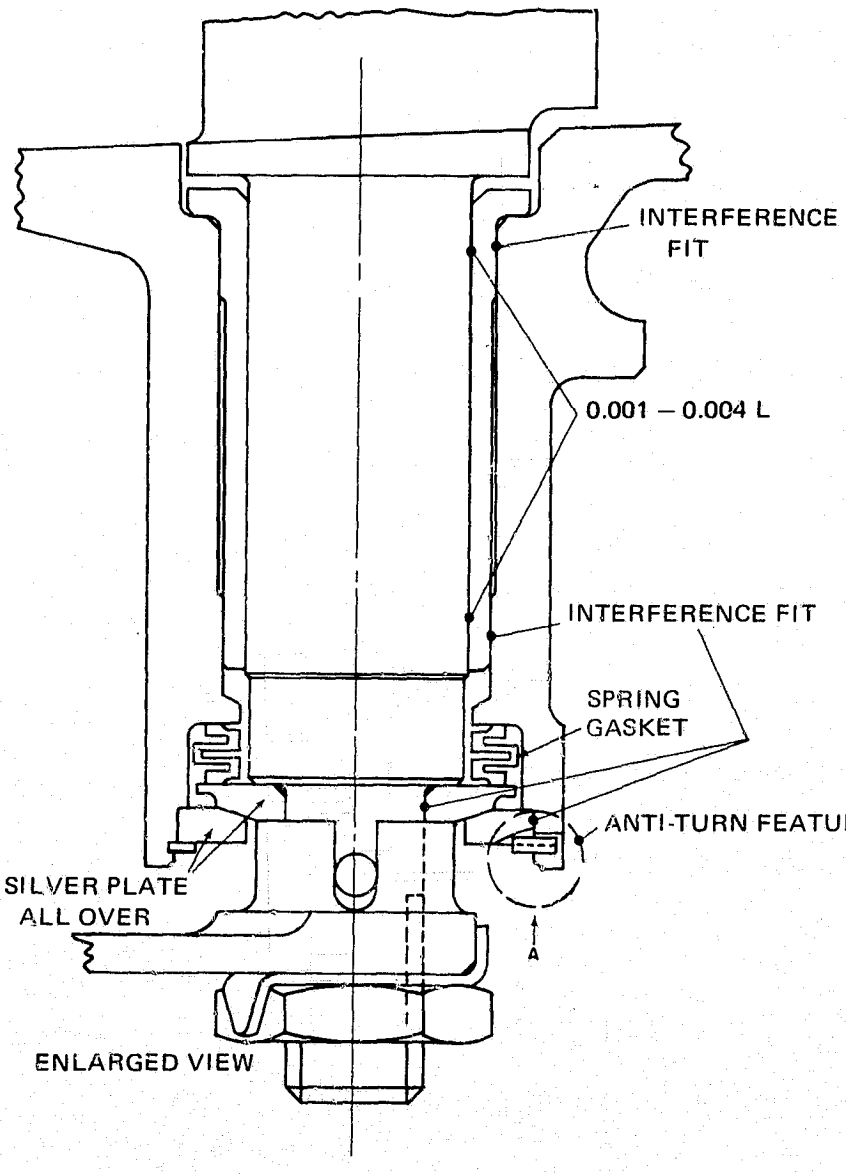

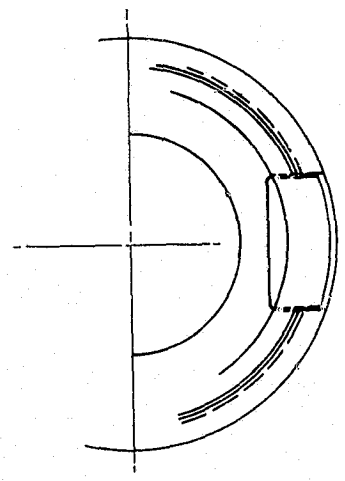

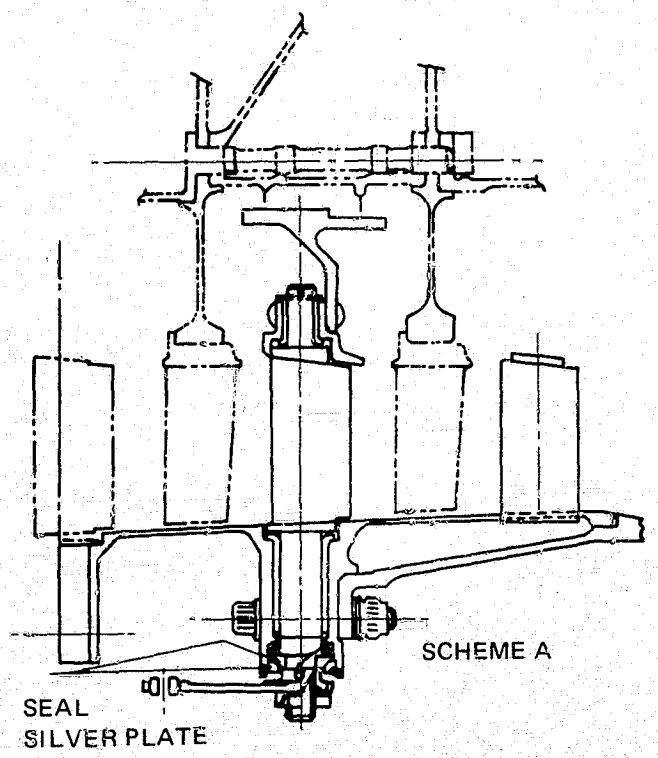

DESCRIPTION

SCHEME A – SPHERICAL SEAT FACE SEAL

IN THIS DESIGN THE PRIMARY SEAL IS EFFECTED BY A SPRING-LOADED SPHERICAL SEAT FACE SEAL. THE SPHERICAL FACE ALSO ACTS AS A THRUST BEARING TO ABSORB THE SEATING FORCE OF THE SKINNER SPRING PLUS THE THRUST LOAD CREATED BY THE AIR PRESSURE ACTING ON THE VANE. BOTH OF THE SPHERICAL SURFACES WILL BE PLATED WITH A MATERIAL HAVING A LOW COEFFICIENT OF FRICTION TO REDUCE ACTUATING TORQUE AND PREVENT GALLING.

Figure 122 Spherical-Seat Face Seal

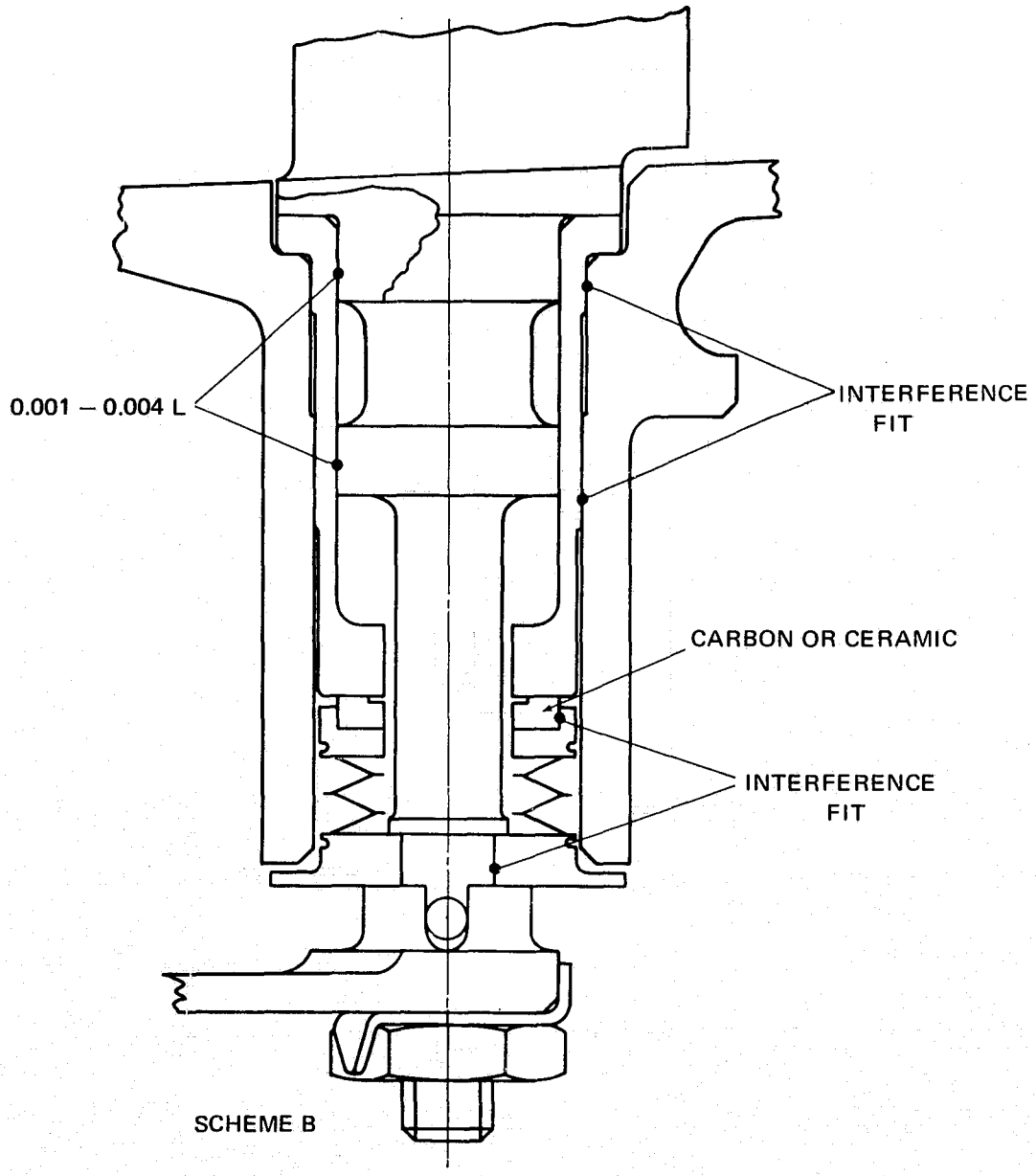

SCHEME B

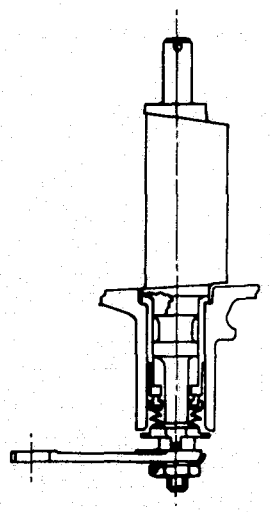

SCHEME B

DESCRIPTION

SCHEME B – SINGLE BELLOWS FACE SEAL

THIS DESIGN IS SIMILAR TO THE DOUBLE BELLOWS SEAL, EXCEPT THAT ONLY ONE SEALING FACE IS BELLOWS SUPPORTED. THE OTHER SEALING FACE IS FORMED BY THE END OF A BUSHING WHICH IS INSTALLED IN THE OUTER SHROUD WITH AN INTERFERENCE FIT. THE MAIN ADVANTAGE OF THIS DESIGN OVER THE DOUBLE BELLOWS DESIGN IS THAT IT HAS FEWER PARTS.

Figure 123 Single-Bellows Face Seal

30

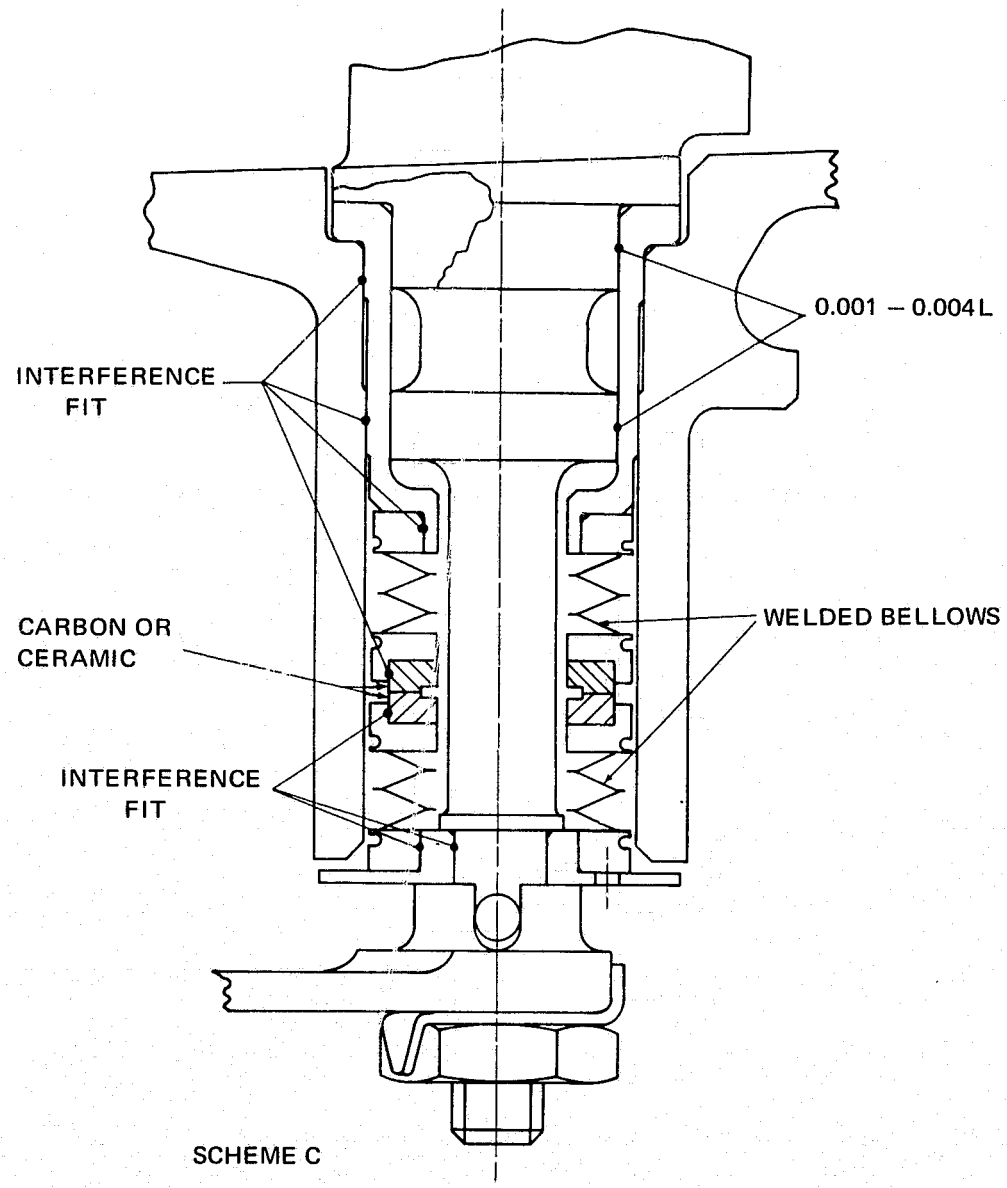

SCHEME C

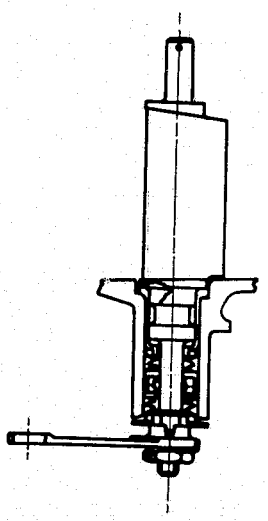

SCHEME C

DESCRIPTION

SCHEME C – DOUBLE BELLOWS FACE SEAL

THIS DESIGN OFFERS MAXIMUM TOLERANCE TO DEFLECTIONS IN THAT BOTH SEALING SURFACES ARE SUPPORTED BY A WELDED METAL BELLOWS. THE SEAL PIECES ARE MADE OF A MATERIAL SUCH AS CARBON OR CERAMIC AND ARE RETAINED IN THE BELLOWS ASSEMBLY BY AN INTERFERENCE FIT. THE THRUST LOADS CREATED BY AIR PRESSURE AND SPRING FORCES ARE CARRIED BY A THRUST BEARING LOCATED AT THE TIP OF THE VANE.

Figure 124 Double-Bellows Face Seal

D. FEASIBILITY ANALYSIS OF THE SINGLE–BELLOWS FACE SEAL

The single-bellows face seal offers a potential leakage advantage over other seal configurations. As adapted to the vane pivot, it offers a relatively simple solution to the problem of preventing leakage of compressed air out of the compressor through the compressor wall. Such a design consists of relatively simple components, which can be fabricated at moderate cost. The seal can be made small enough to fit any vane location in the compressor and pressure balanced to accommodate any pressure level. Because of this versatility, the seal can be used over the whole compressor, or merely at the high-pressure stages, as desired.

The design of the single-bellows face seal is shown in Figure 123. It has a flat seal face held in contact with its seat at all times by the spring action of a lightly loaded bellows. The seat against which the seal face rides is mounted as a separate piece to minimize distortion. The seal is formed between a seat fastened to the shaft and a face seal (nose) held to the housing by a bellows. The high pressure is on the outside of the bellows. The thrust caused by the internal pressure of the compressor is taken up on a thrust collar located at the compressor wall.

1. LEAKAGE CALCULATIONS

The leakage for this seal can be estimated using conventional equations for purely viscous flow. The leakage rate through a slit is

$$m = \frac{h^3}{24 \mu b} \rho_2 P_2 \left[1 - \left(\frac{P_1}{P_2} \right)^2 \right]$$

where

- m = mass flow rate per unit width (lb-sec/in^2)
- μ_2 = mass density of the upstream gas (lb-sec^2/in^4)
- P_2 = pressure of the upstream gas (lb/in^2)
- P_1 = pressure of the downstream gas (lb/in^2)
- h = gap film thickness (inches)
- μ = viscosity of the upstream gas (lb-sec/in^2)
- b = leakage path length (inches)

The leakage path thickness in the case of two closely fitting surfaces is taken here to be twice the rms waviness (B) of the surfaces. Then

$$m = \frac{8\,B^3\,\rho_2\,P_2}{24\,\mu\,b}\left[1-\left(\frac{P_1}{P_2}\right)^2\right] = \frac{8\,B^3\,\rho_2}{24\,\mu\,b}\left(\frac{P_2+P_1}{P_2}\right)\Delta P$$

where $\Delta P = P_2 - P_1$

The leakage rate for the vane pivot seal can be calculated using the mean circumference of the seal,

$$R' = \frac{R_o + R_i}{2}$$

where

R_o = outer radius of seal, inches

R_i = inner radius of seal, inches

Then,

w = g x 2 π R ′m pounds per second

$$= \frac{2\pi\,g\,B^3\,\rho_2}{3\,\mu\,b}\,R'\left(\frac{P_2+P_1}{P_2}\right)\Delta P = \frac{2\pi}{3}\,g\,\frac{B^3\,R'}{\mu\,b}\left(\frac{P_2+P_1}{P_2}\right)\Delta P\,\frac{P_2}{R\,T_2}$$

where

g = acceleration due to gravity (in/sec^2)

R = gas constant (in^2/°R − sec^2)

T_2 = seal inlet gas temperature (°R)

Then to find the volumetric flow at standard conditions,

$$V = \frac{w \times 60}{\rho}$$

where ρ = density of air at standard conditions, or

$$\rho \approx 0.00237\ \frac{lb_f\ sec^2}{ft^4}$$

Using the following input for contract-specified test rig conditions,

B = (3 helium light bands) = $3 \times 11.6 \times 10^{-6}$ inches

ΔP = 135 psi

$R' = \frac{0.75}{4}$ inches

$b = \frac{0.25}{4}$ inches

μ = .039 cp = 5.65×10^{-9} lb-sec/in^2

g = 386^2 in/sec^2

P_2 = 150 psia

P_1 = 15 psia

T_2 = 1200°F = 1660 °R

R = 246500^2 in^2/°R-sec^2

Flow rate is:

w = 9.86×10^{-7} lb/sec

V = 0.00079 scfm

2. ACTUATION TORQUE

The torque required to move the actuator could only be estimated, since accurate friction coefficients were not known. However, the friction coefficient of tungsten carbide against aluminum oxide was assumed to be 0.3, and torque was obtained as follows:

$$T = 0.3\, R_{m\,SEAL}\, (F_{THRUST} + F_{SEAL}) + \text{bending moment effect, inch-pounds}$$

where

$R_{m\,SEAL}$ is the mean radius of the thrust collar and seal

$$T = 1.53 \text{ in-lbs} + \text{bending moment effect}$$

under test rig cruise conditions. This was based on current design dimensions, $\Delta P = 135$ psi, and seal pressure = 12 psi due to the bellows.

3. LIFE

The seal materials chosen were tungsten carbide running against aluminum oxide, for which wear data had been obtained at Union Carbide (Reference 10) as follows for 500 psi face pressure:

- rotated part, 43×10^{-6} inches/1000 feet of rubbed distance
- stationary part, 12×10^{-6} inches/1000 feet of rubbed distance

Therefore, where t = operating time in minutes (for 2000 hours), anticipated wear is

$$55 \times 10^{-6} \frac{\frac{2(20)}{\text{CPM} \times 360} \times 2\pi \times R' \times t}{1000} = 720 \times 10^{-6} \text{ inch}$$

Of the various other material combinations reported by Union Carbide the best combination would reduce total wear to 400×10^{-6} inches. Either of these figures is much less than the thickness of the flame-sprayed coating, but considerably more than the uneveness left on the finished surfaces without flame-sprayed coatings. Hence, it becomes a matter of judgment as to which surface combination to use. The wear rates were calculated for 2000 hours of ± 20 degree cycling at 10 cycles per minute and for the 500 psi test load condition. This is undoubtedly a higher number of cycles than will actually be encountered, the pressure is nearly 2 times as high as will be used, and the real cyclic rate will probably be closer to an average of 1/2 cycle per minute for the full period. Therefore it appeared that either material combination would be sufficient. Mechanical Technology Incorporated gathered data on tungsten carbide against aluminum oxide and found the combination to be good for long wear. This familiarity lent confidence in choosing this combination for this application.

4. COMPARISON WITH CURRENT VANE PIVOT SEAL PRACTICE

a. Size and Weight

Each seal assembly extends radially outward about 2 inches from the outside of the compressor wall. The distance from the outer surface of the seal to the inside wall of the housing is about 0.55 inch. The weight of the seal, exclusive of vane pivot shaft, actuator arm and bolt, and housing is 0.025 pound, about the same as the weight of the baseline seal. It should be noted that the baseline seal, while being used for comparison, was not designed for or used under the conditions specified for the work under this contract.

b. Design Simplicity

The complete unit is assembled in seven parts, considering the actuator assembly and tie-down bolt as one part, the bellows-seal assembly as one part, and not counting the vane pivot shaft or housing.

Steps in assembly are as follows:

- Drop in bellows-seal assembly, press to fit.
- Insert housing bushing inside of housing. Thrust collar is part of the bushing.
- Insert vane pivot shaft with seat cylinder attached through housing from the inside.
- Place lower spring guide, spring, and upper spring guide.
- Assemble actuator on shaft.
- Install and tighten bolt on shaft. This will load the thrust collar against the housing, and compress the bellows slightly to make a good seat at the face seal.

Disassembly can be accomplished by using the same steps in reverse. Servicing will consist of inspection for wear and distortion on thrust collar and face, and seal face and seat. The parts can be replaced as necessary, and need not be used as matched parts or in matched pairs.

The basic material used throughout the seal is Inconel X-750. However, several parts require coatings, inserts, or other structural material. The basic requirements of the materials at various points in the seal assembly are to retain dimensional stability at temperatures as high as 1200°F to provide good wear life at high temperature while in slight motion, to have a relatively low coefficient of friction at high temperature and high load, and to be capable of forming a very good static seal between parts at high temperature.

To accomplish these tasks, the following materials and coatings are used:

- Silver plate on all statically mating parts
- Seal face: 0.0025 to 0.003 inch thick aluminim oxide
- Seal seat: 0.0025 to 0.003 inch thick tungsten carbide (LW-5)

The bellows is Inconel X-750 or 718. The actuator arm, spring and spring guide are AMS 5616. The self-locking nut is AMS 5735. All other parts are Inconel X-750.

The clearances, tolerances, and finishes in specific parts must be held quite closely. The seal face and seat is to be finished to a flatness of 3 helium light bands. The parts that fit over the shaft are 0.0002 inch to 0.0006 inch loose. Stationary mating surfaces are given a 32 microinch (rms) finish. The seal seat has a slight interference fit with the seat housing to ensure zero leakage between them.

The coating materials, use of the bellows, and better finishes represent the main difference between this seal and the baseline seal.

c. Tolerance to Foreign Particles and Load Deflections

Overall tolerance to dirt and cocking for the single-bellows seal appear to be good. The seal face and seat are kept in a mating position at all times so that dirt can not ordinarily get between them. The loading force is about 0.9 pound. The required impact to separate the two faces, therefore, is over 1000 g's. This is such a high level that it will never be enountered in an operational engine.

Since the surfaces are not exactly mated (the helium light bands flatness corresponds to 34.8 x 10^{-6} inches (variation) there is a possibility that dirt particles up to 69.6 x 10^{-6} inches diameter can become deposited in the seal. This, then could cause the gap to increase by that amount as the seal rotates. The leakage could then go as high as 8 times the quoted flow. This is still much less than present leakage values. Dirt particles that could get in the gap will tend to be worked out by the reversing motion of the seal face as the actuator moves back and forth. Since the surface materials are very hard, the probability of developing scratches is very low. The wear particles of the surface materials are probably the hardest that will be encountered. These, of course, should be small enough to polish the surfaces as they are being worked out rather than causing damage.

The bellows has good bending flexibility so that a cocked attitude of the shaft should have no effect on the ability of the seal faces to mate.. If there is any cocking or misalignment, there will be a tendency for the seal to ride off-center. However, this will only slightly reduce the effective length of the slit rather than cause any serious departure from design performance.

The baseline seal does not use finishes as smooth as those on the bellows-loaded face seal, so larger dirt particles can enter and causing scratching and wear. Also, the baseline seal can become unseated when cocked, so leakage rates with the baseline seal are unavoidably higher than for the new design, and wear can be greater.

d. Reliability

Overall reliability considerations, other than those above, depend largely upon the integrity of the bellows, the flame-sprayed coatings, and the electrofilm coatings. Past experience with similar coatings, has been satisfactory, but design reliability can only be proven by testing. The life and wear of the coatings have already been discussed. The installation of the bellows is predicated upon advice from bellows manufacturers. It has been stated that externally pressurized bellows offer less problem with squirming, and therefore less problem with proper mating, than with internal pressurization. The pressure-induced stress in the walls of the bellows is always less than 17,000 psi. The 0.0001-percent creep/hour of Inconel X at 1200°F is about 62,000 psi, fully heat treated, thereby realizing sufficient safety factor to account for some bending, squirming and compression-induced stresses.

It is concluded that the only unknown design aspect for overall reliability is the life of the electrofilm coating. Other points, although better understood, need experimental verification, too. These would include integrity of the flame-plated material; the bellows integrity; the

ability of the silver plated parts to resist galling; and the ability of the loaded face seal to resist opening with shock load and cocking loads, and to withstand the action of very small dirt particles which may tend to wear surfaces and open the seal.

e. Air Leakage Rate and Actuation Torque

The calculated leakage of the single-bellows face seal was 0.00079 scfm at a pressure drop of 135 psi, or about 0.0004 scfm at 94 psi. The measured leakage of the baseline seal was 0.004 scfm at 94 psi, which make it appear that leakage past the bellows-loaded face seal would be as much as an order of magnitude lower than that of the baseline seal.

The measured actuating torque for the baseline design when no pressure is applied is 1.5 in-lb. The calculated torque required when pressure (but no bending load) is applied is 3.8 in-lb for an assumed friction coefficient of 0.1. This compares to 1.53 in-lb calculated torque requirement (without bending moment effects) for the new design.

E. FEASIBILITY ANALYSIS OF THE SPHERICAL–SEAT FACE SEAL

The spherical-seat face seal for the vane pivot offers excellent sealing properties at the expense of requiring very fine finishes. This vane sealing method can be utilized anywhere along the compressor.

The design of the spherical seat face seal is shown in Figure 122. It combines the thrust face and seal face and does not require a bellows. A spring is used to keep the two faces together at all times. The spherical geometry, combined with the lack of radial restraint on the seal permits it to seek its own alignment and therefore stay seated even though there may be some shifting of the axis as a bending moment is applied to the vane. The seal is formed between the spherically concave seat located in the housing and the spherically convex seal held to the shaft. This surface is also the thrust bearing for the vane: the loading due to compressor pressure is taken by the seal. The seat is not tightly confined perpendicular to the vane axis. This permits motion required to keep the sphere seated, as a bending movement is applied to the vane. The high pressure is on the outer diameter of the seal surface. Materials selection appeared to be the biggest technical problem.

1. LEAKAGE

The leakage for this seal is somewhat more difficult to analyze than for the bellows-loaded face seal. The finish is better for the spherical surface and is lapped to fit the seat almost perfectly. If the seal is well seated, an estimate can be made using the rms finish as the half width of the slot. This gives a calculated leakage of about 1/2 of that for the bellows loaded face seal, or V = 0.0004 scfm at engine conditions. The probable degree of non-seating with this seal is unknown, since there will be friction tending to prevent proper seating. If unseating does actually occur, the leakage rate of this seal will exceed that of the bellows face seal. This effect can be properly evaluated only by testing.

2. ACTUATION TORQUE

The torque requirement for actuation was estimated using an assumed friction coefficient of 0.1 for carbon against tungsten carbide and 0.2 for silver against silver.

Thus

$T = 0.1 \times R_m \times F_{THRUST}$ + bending moment effects = 0.54 in-lb + bending moment effects

This is an approximate value for actuation torque under test rig cruise conditions.

3. LIFE

The wear rate on the thrust bearing could not be calculated directly. However, it had been reported by the vendor that the grade of graphite used here will last 2000 hours when Pv is less than 15,000, where P is in psi and v is in ft/min.

The conditions estimated for service of this seal are 20 degrees of rotation at 10 cycles per minute. The thrust force to be taken up is approximately the area inside the outer edge of the seal times the pressure differential

$$F = \pi R_0^2 \Delta P \text{ pounds}$$

where R_0 is the outer radius of the high pressure zone.

Then

$$P_{THRUST} = \frac{\pi R_0^2 \Delta P}{\pi (r_0^2 - r_i^2)} = 210 \text{ psi for cruise conditions,}$$

where r referes to the thrust face. v can be taken as the mean rubbing speed of the seal, or

$$v = CPM \left(\frac{2a_{TOTAL}}{360} \right) \left(2\pi R' \right) = 0.218 \text{ ft/min}$$

where $R' = \frac{r_0 - r_i}{2}$

a_{TOTAL} = rotation angle, degrees

therefore

$$P_{THRUST} v = 46$$

This number is so low that there should be no questions about reaching 2000 hours life in the test rig. However, wear due to oxidation could be significant.

The loading on this seal is such that the mean $P_{THRUST} v$ for the carbon is much lower than the recommended upper limit. Therefore, wear should be satisfactory for this seal.

There are no wearing surfaces in this seal made up of one ceramic against another. This fact reduces the uncertainties of allowable wear rate to just that which the Purebon 56-HT can take.

4. COMPARISON WITH CURRENT VANE PIVOT SEAL PRACTICE

a. Size and Weight

The complete assembly extends about 2 inches radially outward from the inside of the compressor wall. The distance from the outer surface of the seal to the inside wall of the seal housing is 0.65 inch. The weight of an individual seal assembly, exclusive of vane pivot shaft, actuator arm and bolt, and seal housing is 0.025 pound. These sizes and weights are comparable to those for the baseline seal.

b. Design Simplicity

The complete unit is assembled in seven parts, considering the actuator lever and tie-down bolt as one part, considering the seal and retainer ring as one part, and not counting the shaft. Assembly is accomplished as follows.

- Press in housing bushing.
- Drop in seat and retainer ring until it seats against housing shoulder.
- Press seal onto vane pivot shaft.
- Insert vane pivot shaft through housing from the inside.
- Place spring guide and springs over shaft.
- Assemble actuator on shaft.
- Install and tighten bolt on shaft. This will load the seat to the housing shoulder, thereby making a stationary seal between the primary seal and the housing.

Disassembly is accomplished by reversing the above operations. All faces and seats would be inspected for wear and replaced as necessary . The spherical seat and seal face will have to be replaced as matched pairs.

The basic material of construction is Inconel X-750. As for the single-bellows seal, however, several faces and surfaces have to be of other materials. The spherical seat will be a shaped carbon mass held in its retainer ring. The seal itself is flame-plated with 0.0025-inch to 0.003-inch thick tungsten carbide (Linde LW-5). All Inconel parts required to form a static seal are plated with silver.

Required fits and clearances for a properly functioning seal are as follows:

- Seal: 2 microinch (rms) finish
- Seal and seat lapped together

The main complication of this seal over the baseline seal is the use of very good finishes on the sealing parts. Some simplification exists with the new design in that the seal also serves as the thrust collar, a separate part in the present design.

c. Tolerance to Foreign Particles and Load Deflections

This seal resists the action of cocking and misalignment by utilizing a spherical seal and seat. The friction coefficient between the two parts is low, so there will be a great tendency to remain seated with only a small applied force from slight spring compression. Any external

vibration will assist in achieving such seating. The force tending to keep the two parts seated is three pounds, but this must act at an angle as low as 22 degrees. This provides centering forces as low as 1.2 pounds. However, the friction force resisting centering is 0.32 pounds, with a friction coefficient of 0.1. These values appear to be satisfactory for centering and resistance to tilting with cocking loads.

The finishes specified should keep dirt out of the face seal, even down to a particle diameter of 4×10^{-6} inch. The effect of such small particles on the seal, if they should enter, would be two-fold: a tendency to separate the faces and a tendency to imbed in the carbon. Neither effect would be serious, since the increased leakage of such a small lift is negligible as far as absolute amount is concerned, and small imbedded particles will not seriously affect either wear or leakage.

The baseline seal has a much rougher finish than the spherical-seat seal, so large dirt particles can enter and cause scratching and wear. Also, the baseline seal can become unseated when cocked, so leakage rates and wear are unavoidably higher in the present design than for this new design.

d. Reliability

Overall reliability will depend on the integrity of the carbon inserts, the flame plating, and the ability of the silver plate to resist galling. Past experience of a general sort is available on all of these, but little specific information is available. Basically, it appears that the overall reliability should be good. The design aspects requiring experimental verification are life of the carbon inserts at 1200°F, flame plate integrity, the ability of the seal to remain seated, and the action of small dirt particles on wear and leakage.

e. Air Leakage Rate and Actuation Torque

The estimated leakage rate of the new design is 0.0004 scfm at test conditions, or about 0.0002 scfm at 94 psi pressure differential. This is 1/20 of that measured for the baseline design at 94 psi.

The calculated torque requirement is 0.54 in-lb (without bending moment effects) for the new design, compared to 3.8 in-lb calculated for the baseline design without bending moment effects.

VII. PIVOT BUSHING AND SEAL EXPERIMENTAL EVALUATION

A. BACKGROUND

This phase of the program provided for final design and procurement of bushings and seals, design and fabrication of a test rig, and experimental evaluation of bushing and seal assemblies. The final design of the two selected concepts (a single-bellows seal and a spherical-seat seal) included all calculations, material determinations, analyses, and drawings necessary for optimization, procurement, and experimental evaluation.

A single-vane test rig was designed and fabricated to evaluate the two selected pivot bushing and seal designs under simulated operating conditions for the last compressor stage. The vane and actuating mechanisms were applicable to current advanced engine practice.

The pivot bushing and seal assemblies were calibrated in incremental steps over the full pressure and temperature range, with a maximum pressure of 135 psi and a maximum temperature of 1200°F.

The seals were subjected to a test program which simulated take-off for 20 hours and cruise for 20 hours. Later, the seals were subjected to a cyclic endurance run of 40 hours. The take-off and cruise simulations provided conditions typical of advanced engine designs through duplication of:

- Compressor stage air temperatures
- Supporting structure geometry
- Supporting structure temperatures
- Pivot movements as required for the vanes
- Pivot loading (mechanical loading was used to simulate air loading)
- Compressor stage pressure drop

The pivot movement was 13 degrees at 9.6 cycles per minute. The pivot loading included a vibratory load superimposed on the steady load and equal to approximately ±15 percent of the steady load.

B. SEAL DESIGN

1. SINGLE-BELLOWS VANE PIVOT SEAL

The final design layout of the single-bellows vane pivot seal is shown in Figure 125. It is a flat face seal mounted on a bellows to keep it free from distortion. With a slight load on the bellows, its spring action holds the seal face in contact with the seal seat at all times. The seat is pressed onto the vane trunnion shaft and the bellows seal assembly is pressed into the housing. High-pressure air is on the outside of the bellows. A radial thrust caused by the internal pressure of the compressor is taken up on a thrust collar located at the compressor wall.

The seal face of the bellows assembly has a nominal outside diameter of 0.500 inch and a surface width of 0.100 inch. A flame-sprayed hardface deposited on this surface is lapped to a flatness of 20 microinches and a surface finish of 5 microinches (arithmetic average). The seal face (or nosepiece) is welded to the bellows, which has an outside diameter of 0.500 inch and an inside diameter of 0.300 inch. The bellows is constructed from 5-mil sheet stock, and welded into 15 single-ply convolutions. In turn, the bellows is welded to an adapter containing puller holes so that the assembly may be pulled into the seal housing on its snap diameter and seated against a shoulder. The seal's nominal free length from the adapter seat to the seal face is 0.541 inch, and it has a nominal operating length of 0.536 inch. The maximum bellows face loads are 4.25 pounds at 0.534 inch and 0.55 pound at 0.538 inch.

A flame-sprayed hardface is applied to the seal seat and lapped to the same specifications as the bellows seal face. The combination vane sleeve and seal seat is pressed onto the simulated vane and finish ground on the outer surface. There is no hardcoat on this journal surface. The simulated vane bending moment is supported by the vane sleeve and a bushing installed in the seal housing. The radial thrust loading is supported by a thrust collar at the base of the vane bearing against the top of the bushing. The bushing is installed in the seal housing with a press fit, and the inner surface is then finish ground. The clearance between the bushing and the vane sleeve when the vane is not loaded is 0.001 to 0.004 loose.

Material selections for the single-bellows seal are tabulated in Table III.

TABLE III
MATERIAL SELECTIONS FOR THE SINGLE-BELLOWS SEAL

Simulated Vane	AMS 5663 (Inco 718)
Vane Sleeve/Seal Seat	
Base Material	AMS 5663 (Inco 718)
Seal Seat Hardcoat	
Unit 3	Tungsten Carbide (Linde LW5)
Unit 4	Chrome Carbide (Linde LC1C)
Bellows Seal Assembly	
Seal Face Base Material	AMS 5664 (Inco 600)
Seal Face Hardcoat	

TABLE III (CONT'D)

Unit 3	Tungsten Carbide (Linde LW5)
Unit 4	Chrome Carbide (Linde LC1C)
Bellows	AMS 5542 (Inco 750)
Bushing	AMS 5387 (Haynes Stellite 6B)

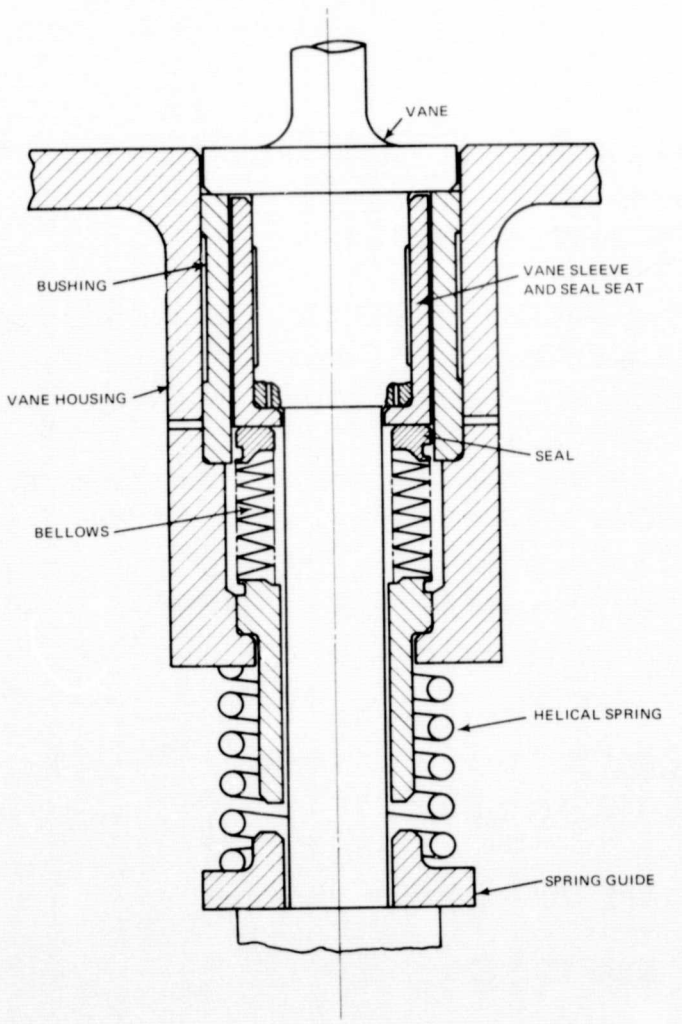

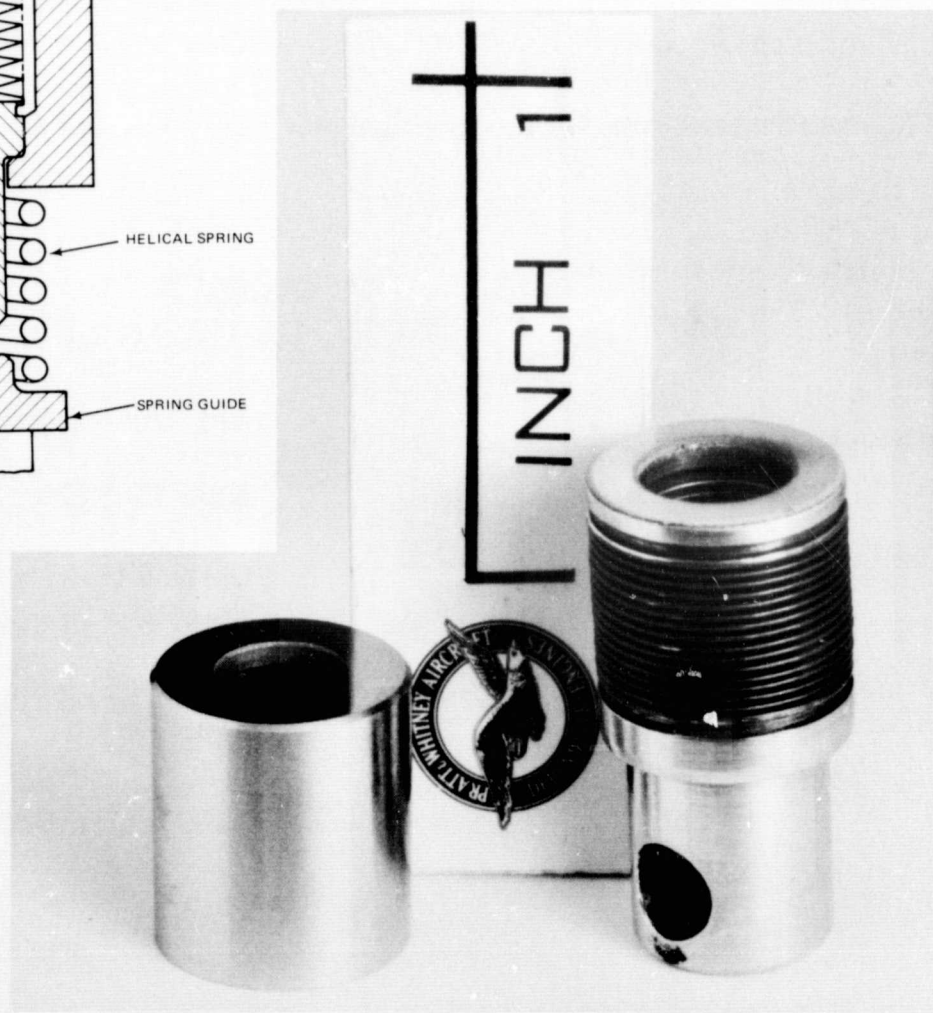

Figure 125 Single-Bellows Vane Pivot Seal (XP-9777)

2. SPHERICAL-SEAT VANE PIVOT SEAL

The final design layout of the spherical-seat vane pivot seal is shown in Figure 126. It differs from the single-bellows configuration in that it combines the thrust face and seal face. Sealing is accomplished by seating a convex seal face in a concave seal seat. A second seal interface occurs between the flat surface of the spherical seat and the base of the seal housing. A helical spring outside the seal housing and concentric with it keeps the seal surfaces in contact at all times. High-pressure air is on the outside of the seal. Radial thrust caused by the internal pressure of the compressor is transmitted through the spherical seal and seat to the seal housing.

The combination vane sleeve and spherical seal is pressed onto the simulated vane rod trunnion shaft. The outer surface of the vane rod is silver plated in this area prior to installation to facilitate installation of the sleeve and to seal the interface.

The seal seat is dropped into the housing with no radial retention. This allows the seat to align with the seal when the vane cocks under a bending load. The nominal radius of the spherical mating surfaces is 0.4060 inch. A flame-sprayed hardface is applied to the spherical seal and to the base of the seal housing. Both hardface surfaces are lapped. The spherical seal is lapped to the spherical seat at assembly. Clearance between the sleeve and bushing is specified to be 0.001 to 0.004 inch loose.

The material selections for the spherical-seat vane pivot seal are listed in Table IV.

TABLE IV
MATERIAL SELECTIONS FOR THE SPHERICAL-SEAT SEAL

Simulated Vane	AMS 5663 (Inco 718)
Vane Sleeve/Spherical Seal	
Base Material	AMS 5663 (Inco 718)
Seal Hardcoat	
Unit 5	Chrome Carbide (Linde LC1C)
Unit 6	Tungsten Carbide (Linde LW5)
Spherical Seat	
Unit 5	Carbon 56HT (Pure Carbon)
Unit 6	AMS 5387 (Haynes Stellite 6B)
Seal Housing	
Base Material	AMS 5646 (SST)
Hardcoat	
Unit 5	Chrome Carbide (Linde LC1C)
Unit 6	Tungsten Carbide (Linde LW5)

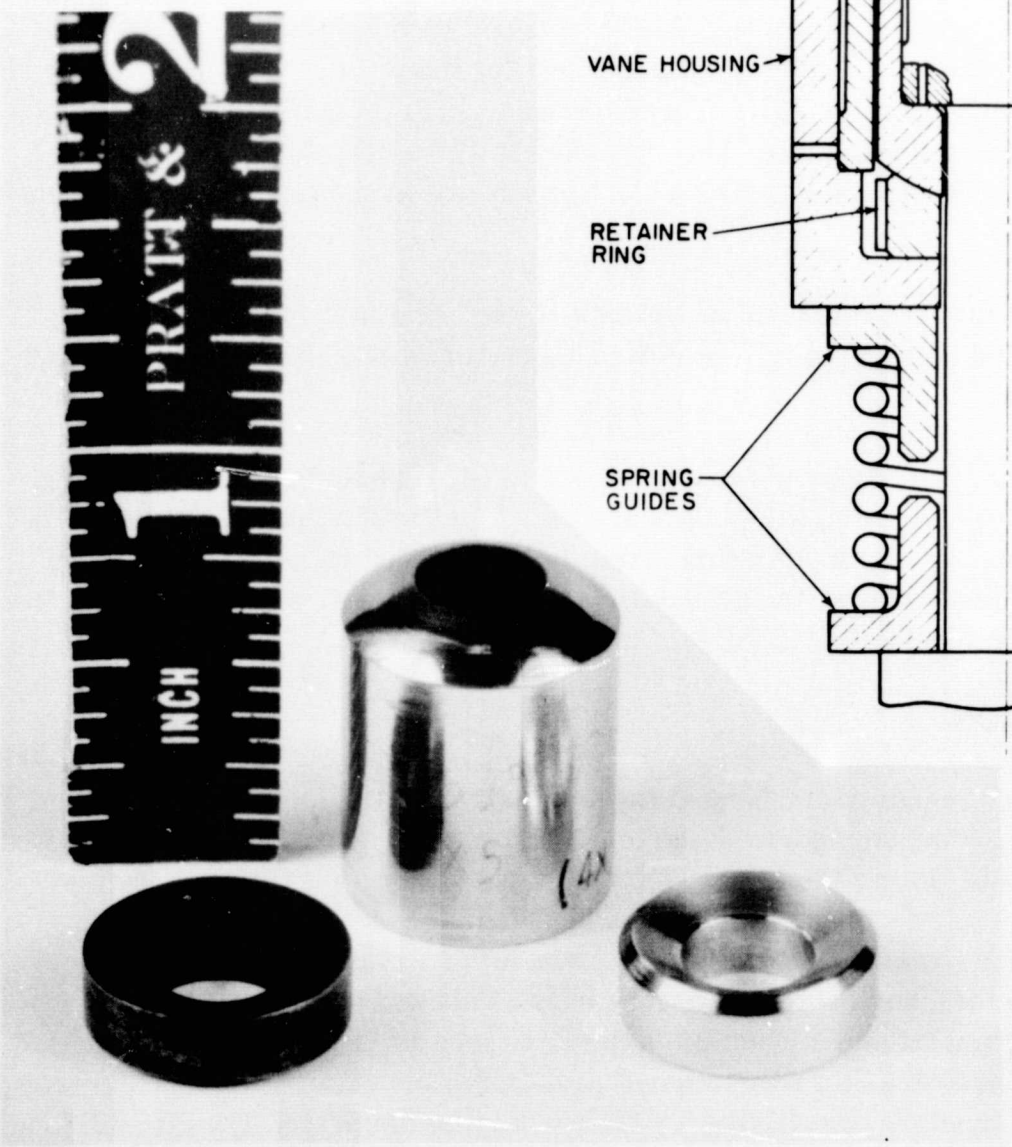

Figure 126 Spherical-Seal Vane Pivot Seal (XPN-13118)

C. TEST EQUIPMENT

1. RIG DESCRIPTION

The test rig (shown in Figure 127) was a small stainless-steel body with a hollow cylindrical core into which the simulated vane rod was inserted. The smaller test seal housing containing the seals was bolted to the rig. In line with and perpendicular to the vane rod was a push rod and bellows assembly. This assembly was contained in a small pressure chamber bolted to the rig. A steady-state bending moment was imposed on the vane rod by displacing a cam installed on an 1800-rpm motor mounted on a lead-screw slide. A vibratory component equal to 15 percent of the steady-state load was superimposed on the vane by rotating the cam. Two cams were used for this purpose, one to simulate cruise, the other for take-off. The displacement of the cam was transmitted to the vane rod through the push rod. The bellows assembly in the pressure chamber provided a seal for the push rod entering the rig chamber. Since the bellows would have been overstressed at high pressure differentials, air of equal pressure was admitted around it. The air leaked to the atmosphere around the shaft, providing cooling. The flow was appreciable, but was not in the test leakage measurement circuit.

The simulated vane rod trunnion shaft passed through the test seal housing to the outside of the rig, where it was linked to a 9.6 rpm motor. This motor cycled the test seals through a 13° angular oscillation.

Three electric immersion Calrod heaters were embedded in the rig housing to maintain the required air temperature surrounding the simulated vane. Later in the program, it was found necessary to supplement these with three strap heaters bolted to the outside of the rig. No attempt was made to preheat the air entering the test chamber, since the leakage rates were expected to be small.

2. INSTRUMENTATION

The basic instrumentation remained unchanged throughout the testing program. However, there was a need to make some changes over the initially proposed instrumentation discussed here. These changes will be pointed out in the later discussion on rig shake-down testing.

In the original test scheme shown in Figure 127, test seal leakage was to be measured upstream of the rig by monitoring total airflow into the test cavity. This was to be accomplished with the use of a capillary flowmeter and a water manometer to measure the pressure differential across the flowmeter. The flowmeter was designed to measure the expected low seal leakage, and was made of a steel capillary tube having a 0.008-inch inner diameter. The 20-inch long tube was brazed into end fittings and supported by an external shell. The laminar flow through the tube was directly proportional to the pressure drop.

Rig cavity pressure and balance-chamber pressure were measured with standard pressure gauges. Strain gauges were utilized to measure vane pivot actuation forces and vane deflection loading. The push rod used to transmit the static vane-bending moment and the superimposed vibratory load is shown in Figure 128 with a close-up view of the strain gauge installation.

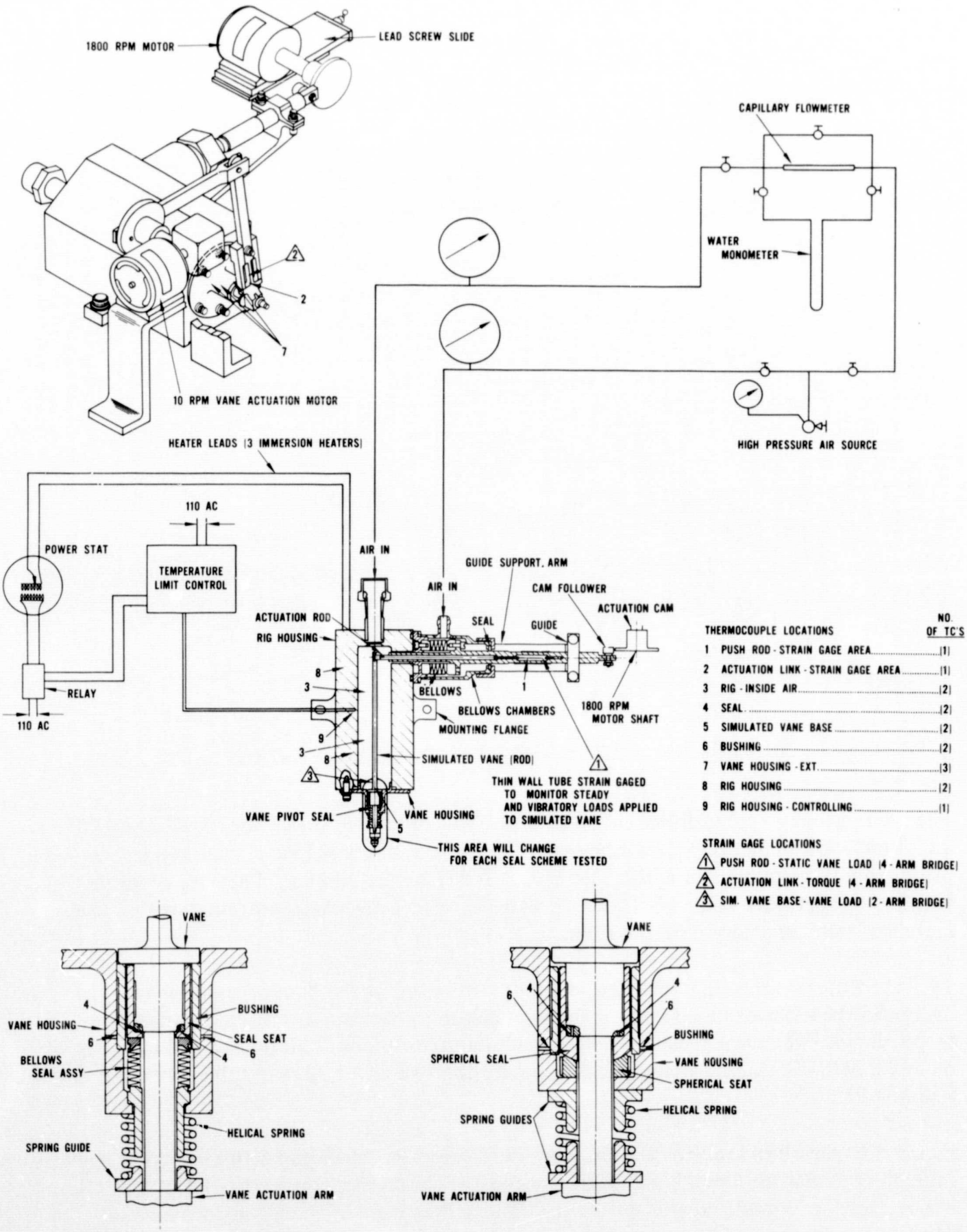

THERMOCOUPLE LOCATIONS	NO. OF TC'S
1 PUSH ROD - STRAIN GAGE AREA	(1)
2 ACTUATION LINK - STRAIN GAGE AREA	(1)
3 RIG - INSIDE AIR	(2)
4 SEAL	(2)
5 SIMULATED VANE BASE	(2)
6 BUSHING	(2)
7 VANE HOUSING - EXT.	(3)
8 RIG HOUSING	(2)
9 RIG HOUSING - CONTROLLING	(1)

STRAIN GAGE LOCATIONS

(1) PUSH ROD - STATIC VANE LOAD (4 - ARM BRIDGE)

(2) ACTUATION LINK - TORQUE (4 - ARM BRIDGE)

(3) SIM. VANE BASE - VANE LOAD (2 - ARM BRIDGE)

Figure 127 Schematic of the Original Design of the Stator Pivot Seal Test Rig (XP-82625)

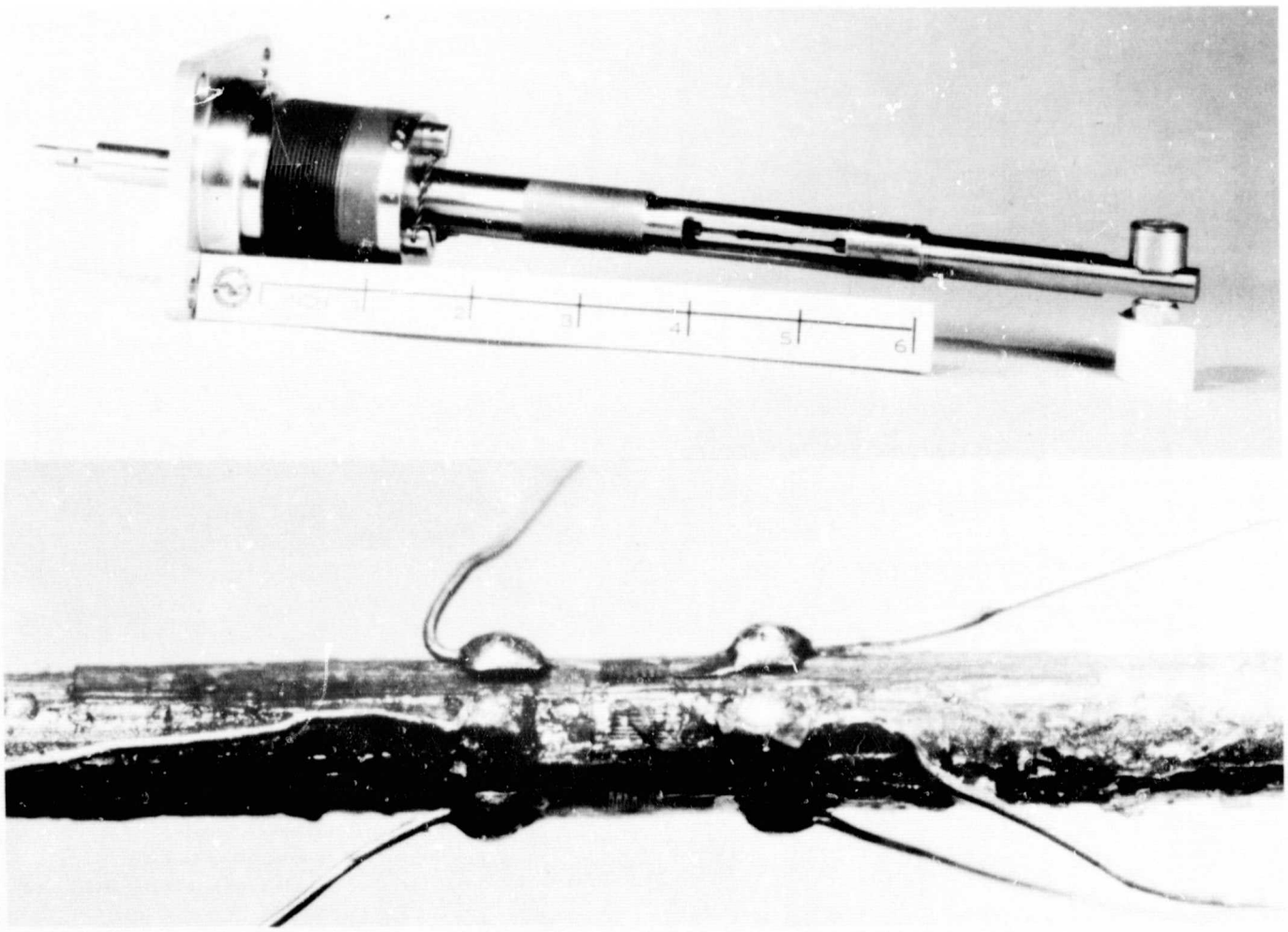

Figure 128 Push Rod and 25X View of Strain Gauge (XP-78644, XP-80223)

The strain gauges were installed in a four-arm bridge mounted on a tube (0.042 inch OD by 0.038 inch ID) to measure the steady-state load to the simulated vane. The gauges were made from Constantan foil with a grid size of 0.015 by 0.020 inch. They are accurate within a temperature range of -100°F to +400°F. The gauges were installed so that they measured pure axial strain on the tube.

Two dynamic strain gauges installed in a two-arm bridge at the base of the vane rod measured the vibratory load and served as a backup to the four-arm bridge installed on the push rod. The dynamic gauges were made of nichrome-base alloy, and had a grid size of 0.062 by 0.125 inch. A simulated vane with the two-arm bridge installed is shown in Figure 129.

Figure 130 shows the vane actuation link. A four-arm bridge strain gauge was used to measure vane pivot actuation forces. The bridge was installed at a location where the cross section was reduced to provide greater sensitivity. The gauges were made of a nichrome-base alloy, and had a grid size of 0.062 by 0.067 inch.

The gauges of all three installations were commercial gauges manufactured by the Budd Company. Prior to installation, each assembly was calibrated over its expected load range. The

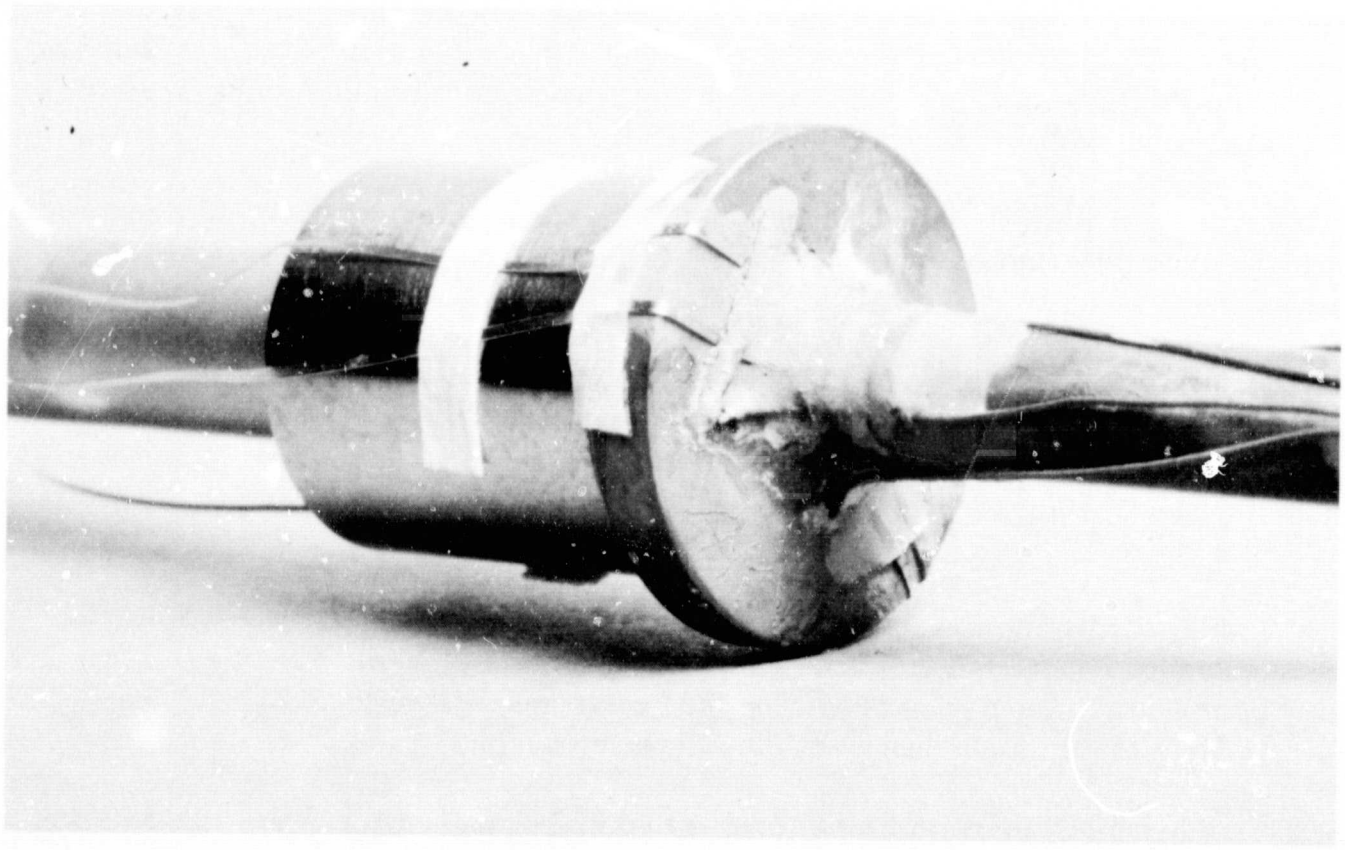

Figure 129 Bridge Installation on Simulated Vane (XP-80137)

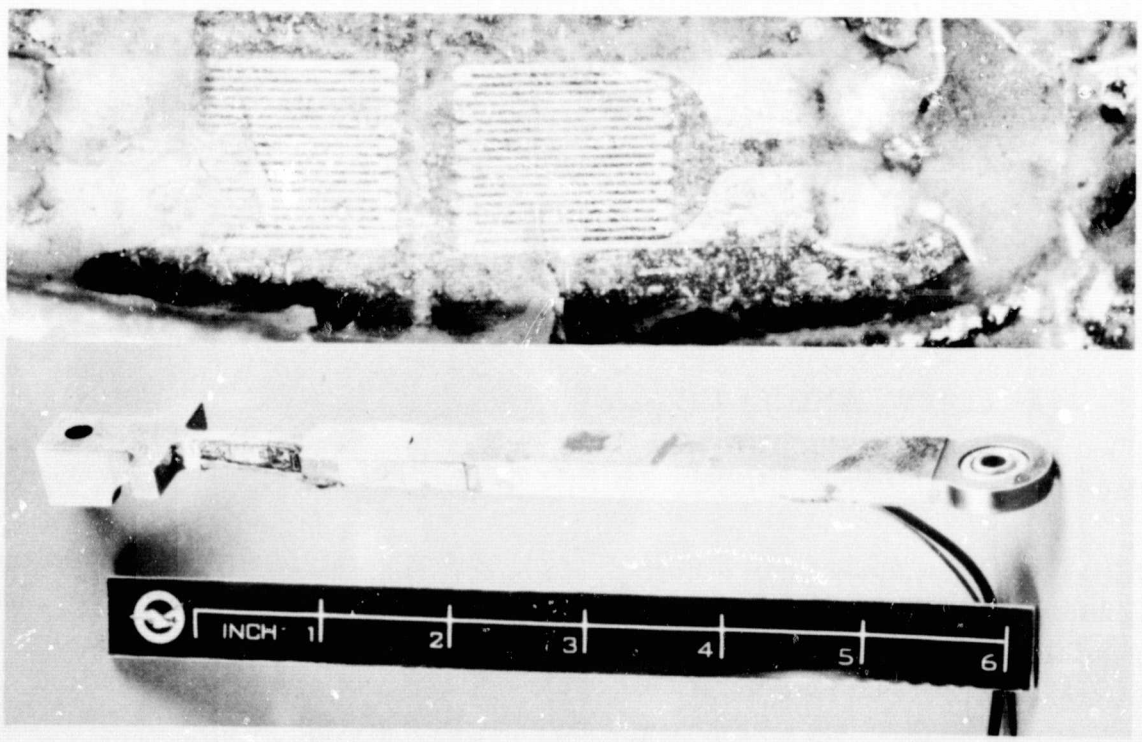

Figure 130 Strain Gauge and Vane Actuation Link (XP-80487, XP-80488)

lead work for the bridge at the vane base was coiled to allow the vane rod to be rotated. Leads from that location were then passed through ceramic inserts in the seal housing. A high-temperature enamel was used to seal the holes in the housing and inserts. Sketches of the gauge installations are shown in Figure 131.

Temperatures of the seal, bushing, and rig housing were measured with grounded immersion-welded junction thermocouples. Seal temperatures were measured with two Chromel-Alumel thermocouples, constructed of 0.010-inch diameter stainless-steel sheathed wire. The leads were nickel-gold brazed to the vane sleeve seat and brought out through holes in the vane housing. The holes were sealed with cement. Thermocouples at the base of the simulated vane were similarly installed, except that they were attached by resistance-welding the thermocouple tip to the surface, and were not immersion welded. The thermocouples at the seal and vane base were replaced with 0.020-inch diameter sheathed wire whenever the 0.010-inch wire failed.

Seal bushing temperatures were monitored by two grounded immersion-welded junction thermocouples constructed of 0.020-inch diameter stainless-steel sheathed wire. These were inserted in holes through the seal housing and bottommed against the bushing. They were furnace brazed in the same manner as the seal thermocouples.

Seal housing temperatures were monitored with 0.032-inch diameter sheathed wire. The junctions were resistance-welded to the housing surface and displaced axially and radially around the surface.

Air temperatures in the test cavity were sensed by two Chromel-Alumel bare-wire junction thermocouples. The thermocouples were constructed of 0.062-inch diameter sheathed wire and passed through holes in the rig housing. These thermocouples were also nickel-gold brazed into place.

Three grounded immersion-welded thermocouples brazed into blind holes measured the rig housing temperature. The wire size for these thermocouples was 0.062-inch diameter.

All of the thermocouples were connected to a potentiometer for temperature readout. Figure 132 shows the instrumentation and control panel, as well as a rear view of the panel with the test rig and associated hardware mounted.

3. RIG SHAKEDOWN AND MODIFICATION

a. Test Unit 1

The first test unit was made up of a single-bellows seal assembly, the vane rod and sleeve assembly, and the seal housing and bushing assembly. The unit was assembled and installed in the rig to determine the integrity of the rig. Bending loads were applied to the simulated vane while the vane was rotated through its 13° cycle. The rig was pressurized and leak checked. Air losses were extremely high, beyond the capacity of the capillary flowmeter. It was found that much of the leakage was passing through the instrumentation lead holes through the seal housing and through the snap diameter at the bellows. After disassembly, it was also

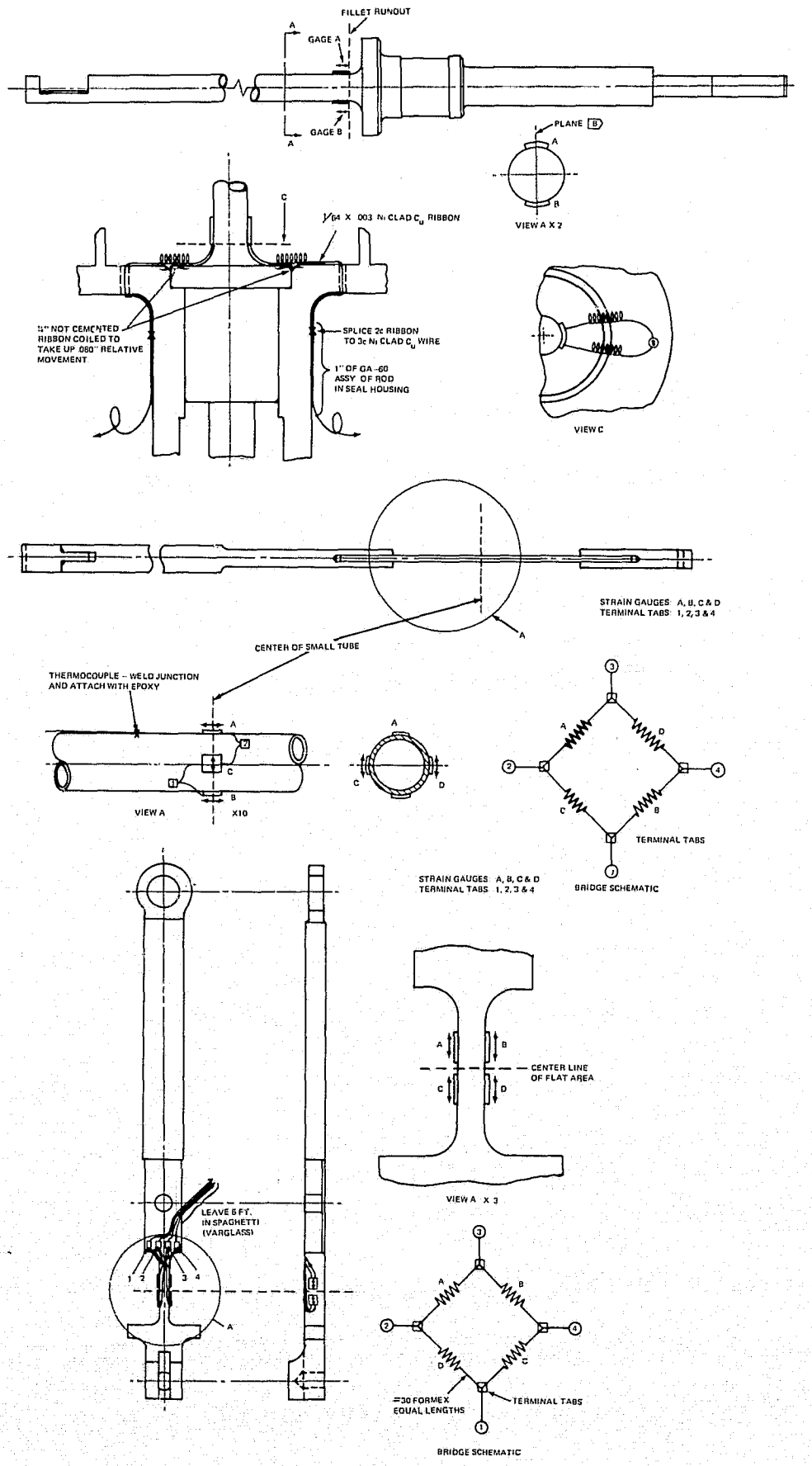

Figure 131 Schematic of Strain Gauge Installations

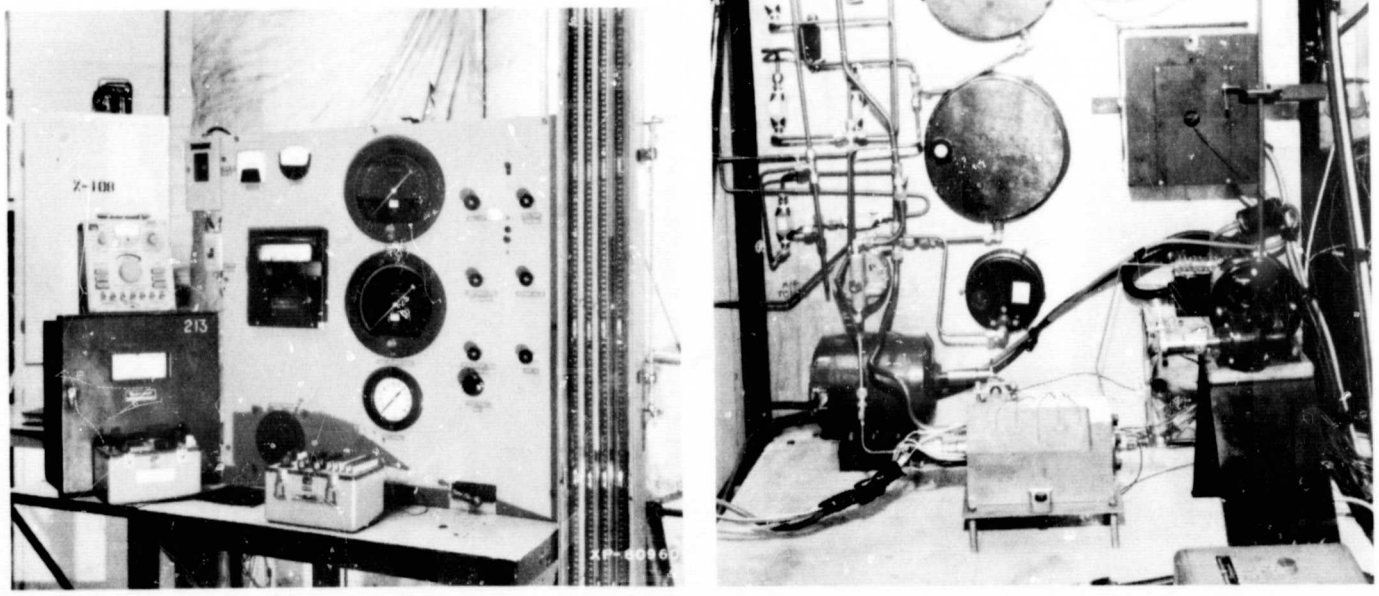

Figure 132 Front and Back Views of Test Stand Set-Up (XP-80959, XP-80960)

found that air was also leaking through instrumentation holes in the vane rod and between the vane sleeve and vane rod.

The four-arm bridge strain gauge installation on the push rod was found to be faulty in its operation. It was judged that too much internal friction made the gauge readings unreliable. This gauge was not used on later builds, since accurate readings were available from the strain gauge at the vane base.

All other instrumentation and mechanical workings of the rig functioned properly during this brief test run.

b. Test Unit 2

To reduce the excessive leakage experienced with Test Unit 1, four modifications were incorporated in Test Unit 2 and all later test units.

- The bellows seal assembly snap diameter was silver plated.
- The vane rod was silver plated at the sleeve interface.
- Silver braze was flowed around the seal thermocouples to seal the pass-through holes.
- As shown in Figure 133, a soft stainless steel tube was brazed into the housing so that thermocouple leads could be sealed at a low-temperature location.

Test Unit 2 used a spherical-seat seal. The seal was installed in the rig and subjected to a calibration program which ran for a little more than 11 hours. The program encompassed a

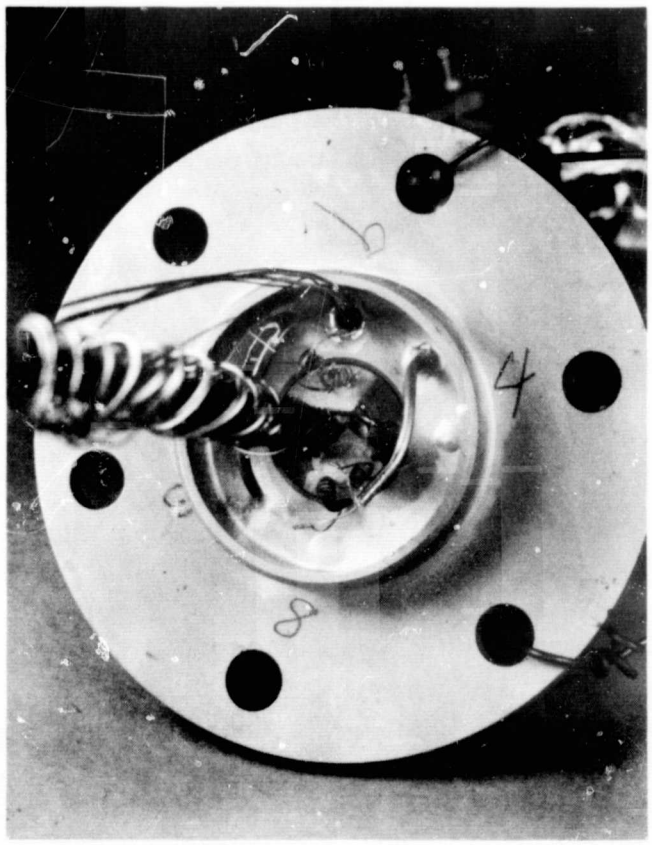

Figure 133 Stainless Steel Tube for Thermocouple Leads (XP-82624)

pressure range from 20 to 135 psi and a temperature range from room temperature to 1200°F. Simulated cruise and sea-level take-off conditions accounted for the 40 hours of endurance testing, which consisted of alternating five-hour periods of cruise and take-off. This program was performed to determine the rig's performance for extended periods of running under endurance testing conditions.

When the testing had been completed, the test-seal leakage path was sealed off with a flat plate, and the rig was recalibrated. Leakage during the recalibration was approximately the same as that experienced with the test seal in place, indicating that the rig static seals were not satisfactory. Leakage was also noted around the leads for the test-cavity air thermocouples.

During the testing of the seal, the commercial strain gauges at the base of the simulated vane provided poor service under the bending and vibratory loading, especially at elevated temperatures. The test program was interrupted several times for repairs to the gauges, and it was finally necessary to replace the gauges with new ones having a grid size of 0.125 by 0.188 inch. The gauge location was moved up the rod to a position approximately 1.5 inches above the base. The new location was chosen to reduce the strains on the gauges in order to extend their fatigue lives. The new gauges had previously shown good reliability under vibratory load at high temperatures.

During the testing, thermal growth of the support arm attached to the rig body caused a misalignment of the actuation rod. In turn, the misalignment caused considerable rubbing against

the balance chamber metal seal and resulted in severe wear on the rod. As the wear progressed, large airflows past the seal limited the rig's capacity to reach the higher pressure points. The situation was corrected by removing the support arm from the rig housing and designing a support which was independent of the rig. To reduce excessive air leakage in the balance chamber, a teflon seal was fabricated to replace the metal seal.

To eliminate the air losses around the rig-cavity thermocouples, the rig housing around the pass-through holes was machined to provide lips around each hole. The stainless-steel sheaths of the thermocouple wire were welded to the lip.

The flange seal seats of the rig housing were modified to accept new silver-plated all-metal V seals as replacements to the spiral-wound static seals.

c. Test Unit 3

Test Unit 3 assembled with a single-bellows seal, and was tested for leaks with room-temperature air. Even though significant improvement was noted, the leakage past the new static seals and through minute cracks in the welded and brazed areas was still excessive in comparison to the very low leakage rates expected from the test seals. It became apparent that it would be impractical to measure seal leakage by measuring total airflow into the rig.

An improved scheme was designed to measure only the air losses past the test seal. It is shown schematically in Figures 134 and 135. Leakage past the test seal was to flow around the vane rod shaft and be collected in a sealed cylinder. A bellows was provided to allow the vane actuation link to oscillate. The collected gasses then flowed to a flow meter vented to the atmosphere, making the pressure drop across the leakage collector essentially zero.

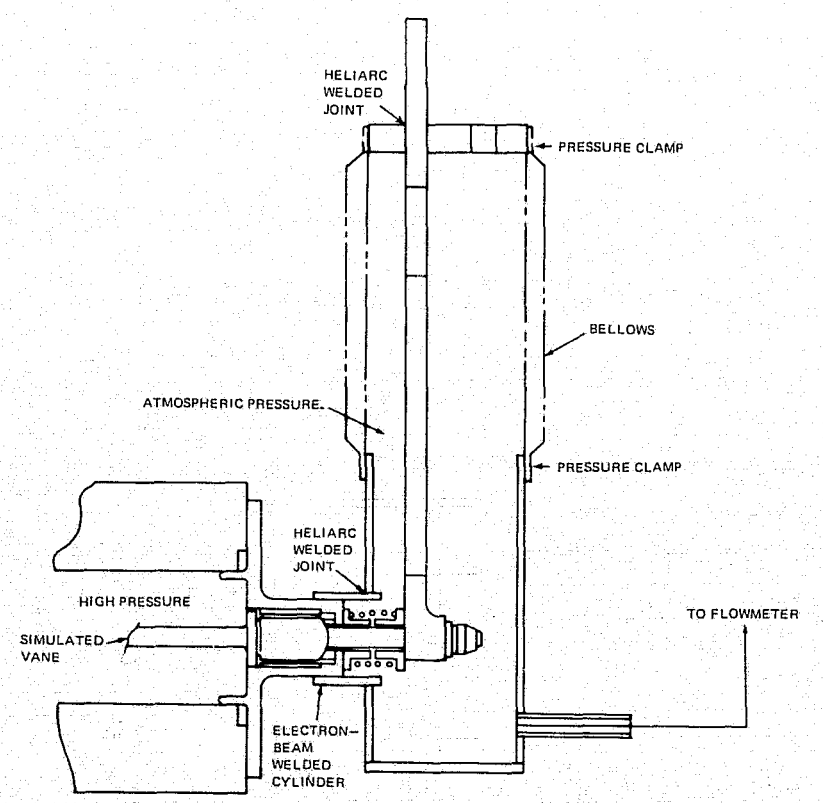

Figure 134 Improved Scheme for Measuring Leakage Past Task IV Seals

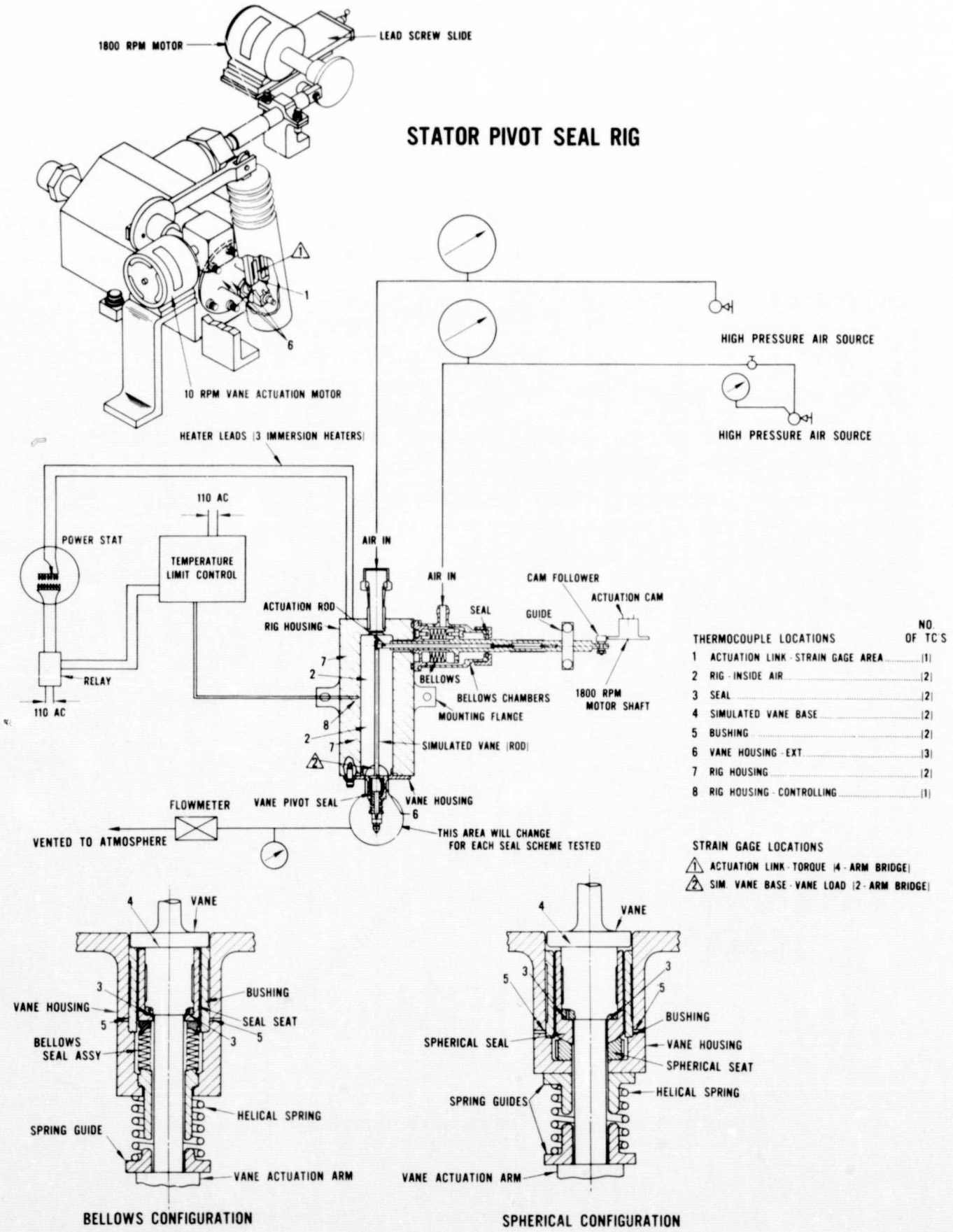

Figure 135 Schematic of the Improved Design of the Stator Pivot Seal Test Rig

Test Unit 3 was reassembled with this new scheme and installed in the rig. To check the system, it was first pressurized with a helium tracer to 2 psig on the downstream side of test seal. A mass spectrometer indicated that the system's leakage was less than the minimum detectable with the spectrometer (5×10^{-8} cc/sec). The rig was then pressurized with the helium tracer to a pressure of 90 psig, but the leakage remained less than 5×10^{-8} cc/sec. Seal testing commenced with this unit, and is discussed in Section E "Test Results". Figure 136 shows the test unit installed in the rig.

Since the strain gauges on the vane actuation link were temperature limited, the link was reoperated to remove them from the area of the higher heat source.

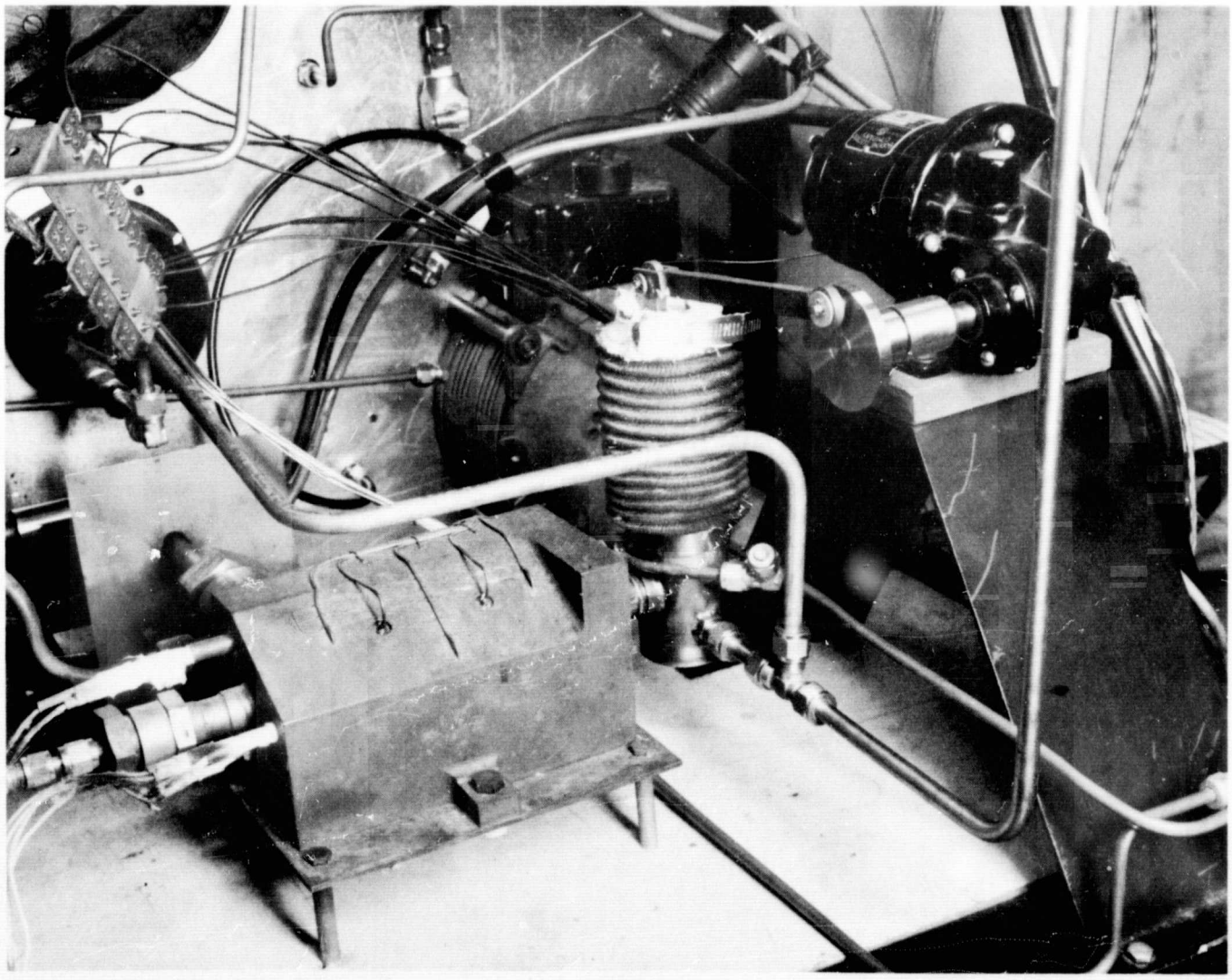

Figure 136 Improved Design of the Stator Pivot Seal Test Rig

D. TEST CONDITIONS

The experimental evaluation of the four variable-stator pivot seals was conducted under conditions which simulated the final compressor stage of an advanced engine. Each seal was calibrated in increments over the full pressure and temperature range, with a maximum pressure drop of 135 psi across the seals and a maximum air temperature of 1200°F. One seal of each design was endurance tested for 40 hours.

Table V illustrates the calibration program to which the seals were subjected. At each temperature level the seals were pressurized through the range indicated. Throughout the calibration a pivot movement of 13° was executed at a rate of 9.6 cycles per minute. During the entire calibration of Test Unit 3, a vane bending moment of 30 in-lbs was applied. For Test Units 4, 5, and 6, the vane bending moment was reduced to a more realistic value of 10 in-lbs at the 1000°F and 1200°F test points. In addition to the steady-state vane bending moment, a vibratory load equal to ±15 percent of the steady-state load was applied to the simulated vane.

Each test point illustrated in the table was held for 15 minutes, at which time the data was recorded. The test schedule includes operation of the seal at conditions simulating sea-level take-off and cruise.

TABLE V

CALIBRATION SCHEDULE FOR STATOR PIVOT SEALS

Rig Air Temperature (°F)	Seal Pressure Differential (psi) 20	40	60	80	100	120	135
Room Temperature	X	X	X	X	X	X	X
200	X	X	X	X	X	X	X
400		X	X	X	X	X	X
600		X	X	X	X	X	X[1]
800		X	X	X	X	X	
1000		X[2]	X	X	X	X[2]	
1200			X[3]	X	X[2]		
Room Temperature	X	X	X	X	X	X	X

[1]Sea-level take-off

[2]Point added for Test Unites 4, 5, and 6

[3]Cruise

The vane pivot seals were subjected to an endurance run of 40 hours duration. The program provided for 20 hours at simulated take-off conditions followed by 20 hours at simulated cruise conditions. During the endurance test, the vane was actuated through the 13° pivot

movement at the rate of 9.6 cycles per minute. Vane bending moments were 30 in-lbs for sea-level take-off and 10 in-lbs for cruise conditions. A vibratory load equal to ±15 percent of the steady-state vane bending moment was superimposed on the steady-state load.

Seal leakage rates were found to be so low during endurance testing that the only means available to measure them was the use of a bubble flowmeter and a stop watch. Flow rates were taken during the course of a 15-minute time interval and averaged to provide a seal leakage data point. The remaining experimental data was recorded at 15-minute intervals.

E. TEST RESULTS

1. SINGLE-BELLOWS VANE PIVOT SEAL

a. Test Unit 3

A dimensional inspection determined that all details of Test Unit 3 (the first unit for test) were acceptable for test. There were no serious deviations on the critical parts. The hardcoat selected for this test was tungsten carbide (Linde LW5) on both the bellows seal face and the seal seat. The seal face had been lapped to a flatness of less than 1 helium light band and a surface finish of 5 to 8 microinches arithmetic average. The seal seat had a flatness of 2 helium light bands and a surface finish of 3 microinches arithmetic average. The relatively high surface-finish value for the seal face was caused by some porosity in the hardcoat. The bellows spring rate was 232 lb/in, while the bellows compression varied from 0.0247 inch on one side to 0.0227 inch on the other side. The variation in bellows compression indicated a slight run-out on the seal face. Clearance between the bushing and vane sleeve was 0.003 inch.

The test seal was assembled, installed in the rig, and calibrated. Seal losses were lower than the range of the flowmeter, a ¼-inch diameter Tri-flat tube with a nylon float. This flowmeter was replaced later during the calibration program with a bubble flowmeter and stop watch. Some seal losses were measureable with the latter arrangement. The results of the calibration program are shown in Table VI. Seal leakage was measureable at the two highest temperatures (1000°F and 1200°F) and at the second room-temperature calibration. Vane bending moment was held constant at 30 in-lbs throughout the calibration. Total running time for the seal calibration test was 14.5 hours.

TABLE VI

CALIBRATION OF TEST UNIT 3

	Pressure													
	20		40		60		80		100		130		135	
AIR TEMP. °F	Leakage (SCFM)	Torque (IN-LBS)	Leakage (SCFM)	Torque (IN-LBS)	Leakage (SCFM)	Torque (IN-LBS)	Leakage (SCFM)	Torque (IN-LBS)	Leakage (SCFM)	Torque (IN-LBS)	Leakage (SCFM)	Torque (IN-LBS)	Leakage (SCFM)	Torque (IN-LBS)
Room Temp.	*	6	*	6	*	6	*	6	*	6	*	4	*	3
200	*	3	*	3	*	3	*	3	*	2	*	2	*	2
400			*	2	*	2	*	2	*	2	*	1.6	*	1.6
680			*	3.2	*	2	*	2	*	2	*	2	*	2.4
800			*	4.8	*	4.8	*	6.4	*	8	*	8		
1000					*	7.2	*	7.2	0.100	7.2				
1200					0.031	6.4	0.052	6.4						
ROOM TEMP	*	20+	0.00023	20+	0.0014	20+	0.007	20+	0.011	20+	0.014	18.4	0.0177	17.6

*Less than Capability of instrumentation

Vane Bending Load - 30 in-lbs Static
- ±4.5 in-lbs superimposed at 1725 cps.

Vane Actuation - $\pm 6.5^{o}$ at 9.6 cpm

After calibration, the test unit was endurance tested for 40 hours, beginning with 20 hours at sea-level take-off conditions. Leakage at start-up was high, but dropped rapidly as the debris between the seal interface worked itself out and the seal seated.

Failure of the cam follower bearing interrupted the sea-level take-off test. The first failure occurred at the end of 4.5 hours and the second occurred at the end of 4.75 hours. The seal leakage was a little higher on restart after both incidents.

Leakage in general was very low throughout the sea-level take-off test, running about 0.00069, which compares very favorably with the analytical predictions of 0.00079. The results of the endurance test are shown in Figure 137. Seal leakage at cruise conditions ran about 0.0002 scfm. At several points on the curves of Figure 137, the data points are missing or show extremely low leakage. The data at these points are considered to be unreliable because there were several bubbles in the flowmeter at once.

The torque required to actuate the vane during the endurance test is shown in Figure 138. It was considered to be too high, and indicated an extremely high coefficient of friction. An analysis to determine the cause of the high torque is presented in Section F "Torque Analysis".

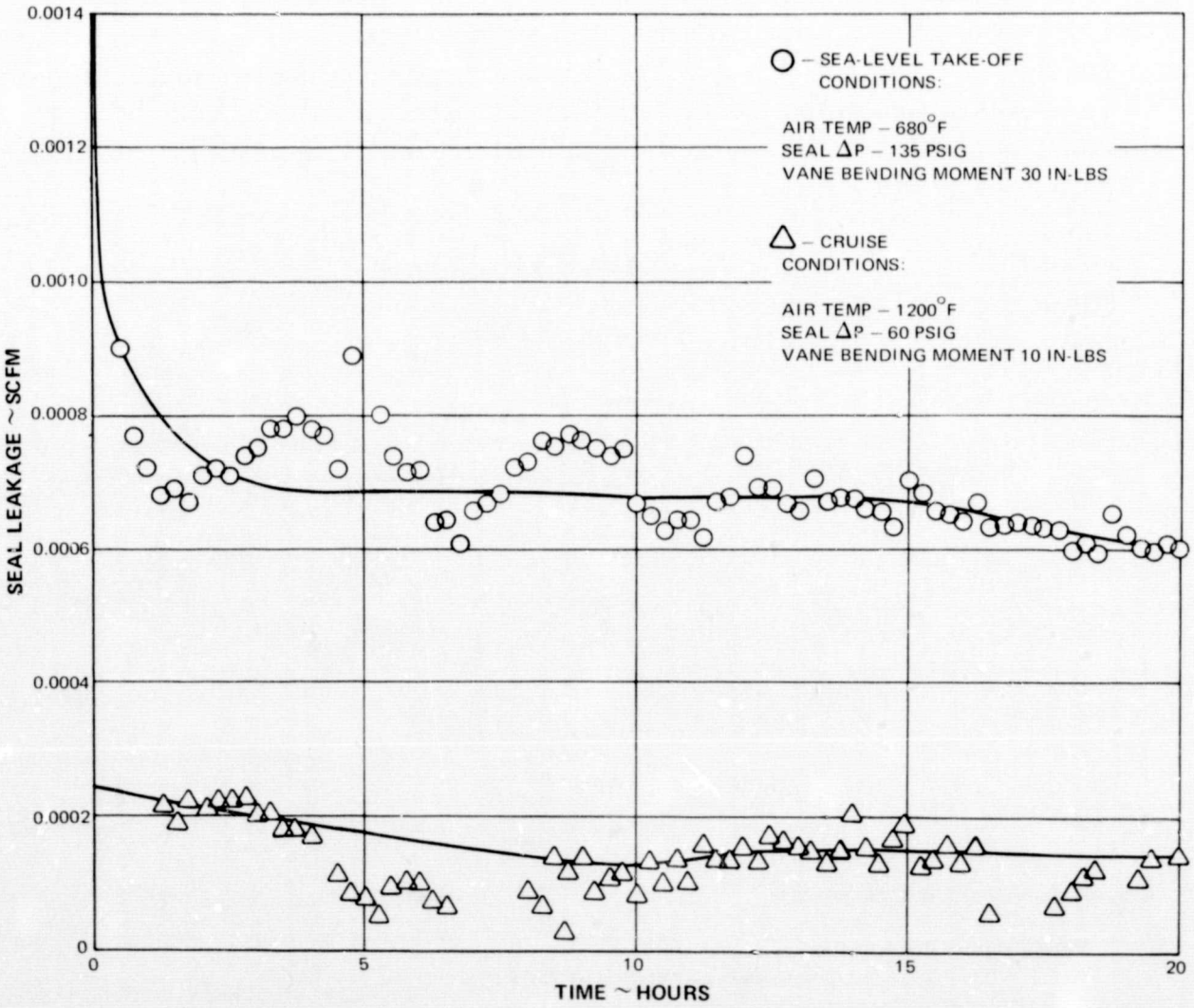

Figure 137 Air Leakage Past the Single-Bellows Vane Pivot Seal (Test Unit 3)

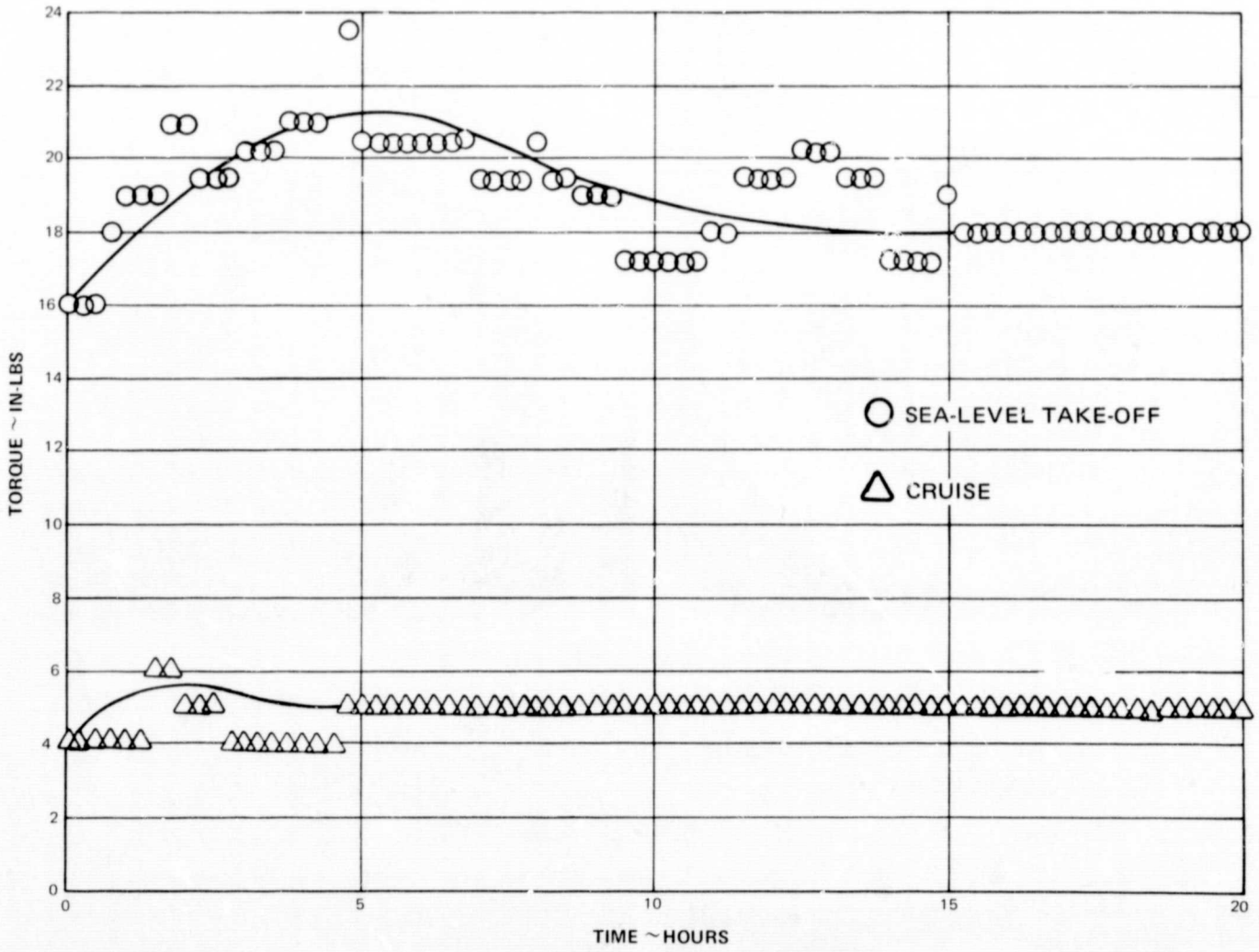

Figure 138 Actuation Torque for the Single-Bellows Vane Pivot Seal (Test Unit 3)

On disassembly, a visual examination of the parts revealed some scoring and heat discoloration on the mating seal surfaces, as shown in Figures 139 through 142. Sample temperatures recorded during the endurance test are shown in Figures 143 and 144.

An examination of the bushing and vane sleeve bearing surfaces showed more severe scoring than had been evident on the seal surfaces. The bearing surfaces are shown in Figure 145. No measurable wear was found on the bearing surface or the seal surfaces.

The requirements and specifications of Test Unit 3 are summarized in Table VII.

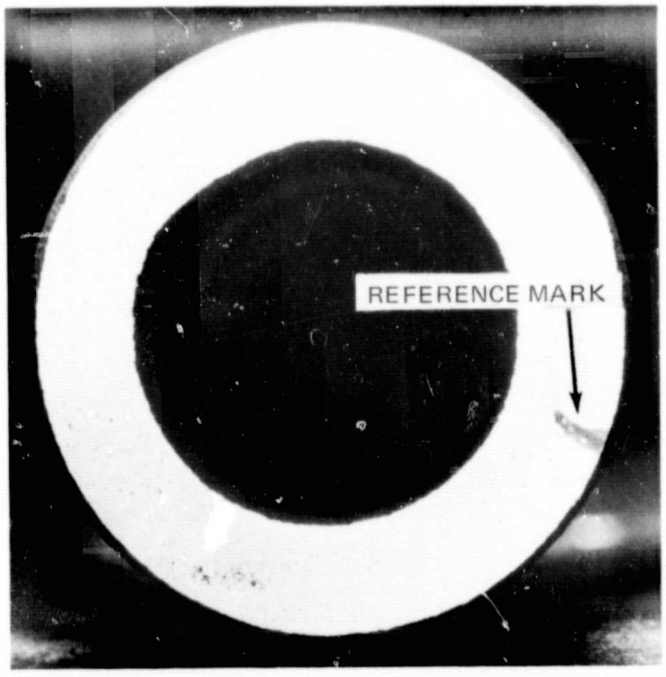

Figure 139 Condition of Hardface Seal Surface of Test Unit 3 Before Test (XP-84759)

Figure 140 Condition of Hardface Seal Surface of Test Unit 3 After Test (XP-90811)

Figure 141 Condition of Hardface Seat Surface of Test Unit 3 Before Test (XP-83425)

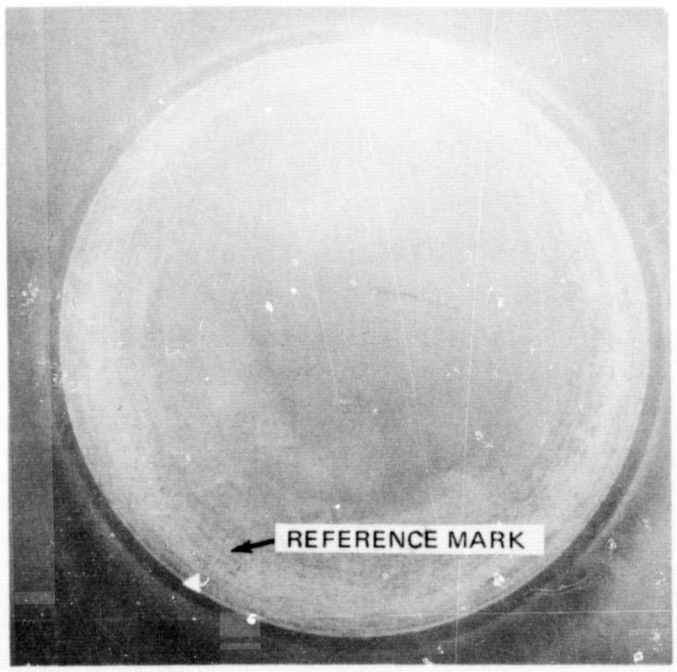

Figure 142 Condition of Hardface Seat Surface of Test Unit 3 After Test (XP-90810)

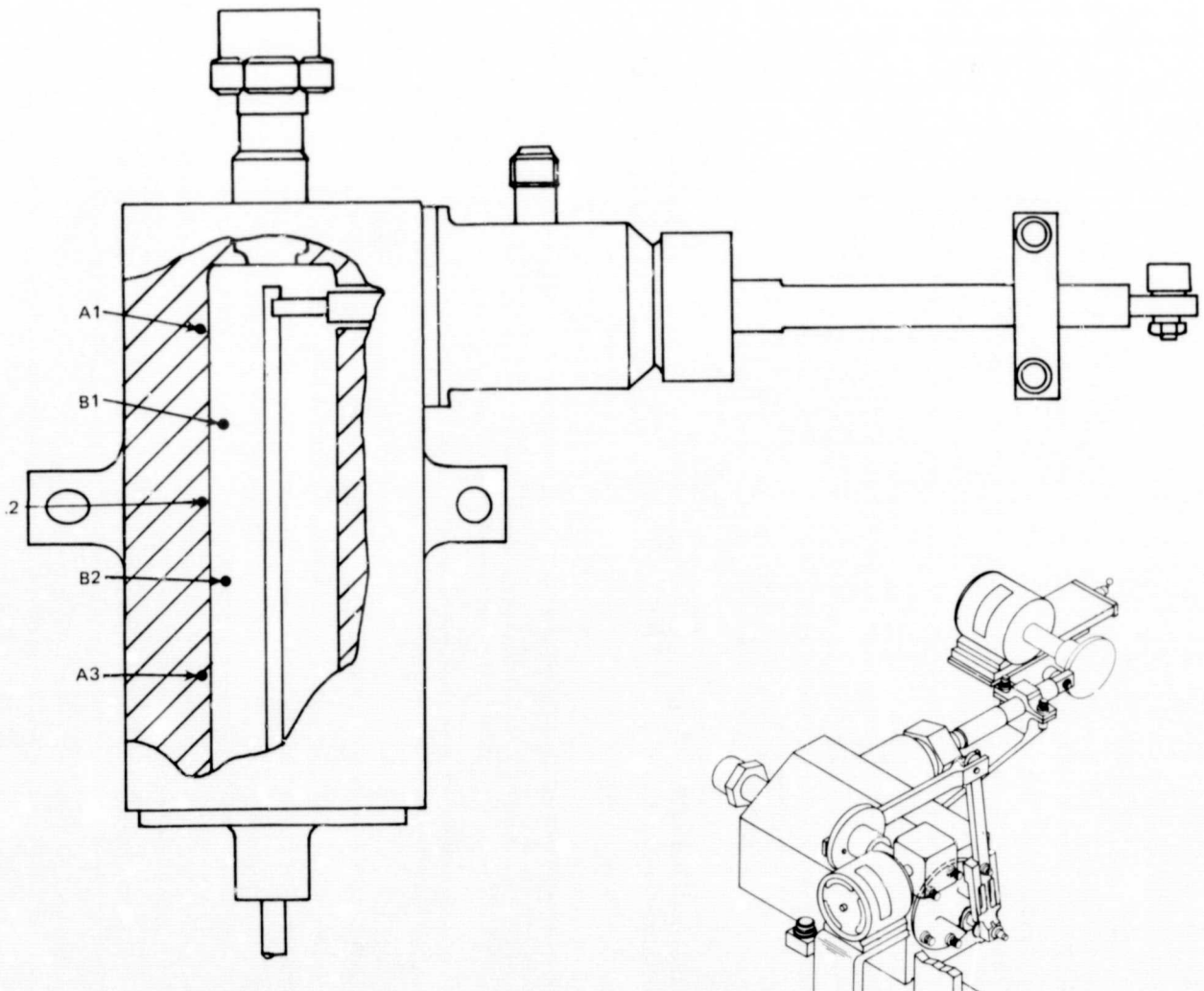

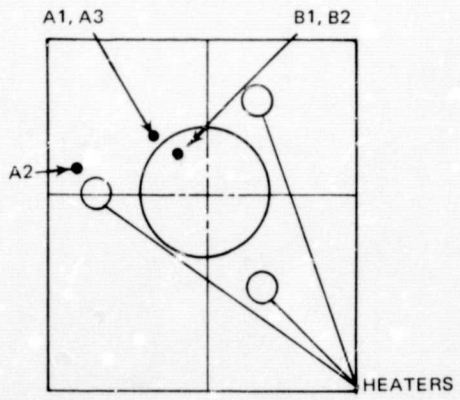

Angular Location of Thermocouples and Heaters

THERMOCOUPLE	TEMPERATURE AT SLTO (°F)	TEMPERATURE AT CRUISE (°F)
HOUSING T/C 1	685	1225
HOUSING T/C 2	755	1250
HOUSING T/C 3	745	1195
RIG AIR T/C 1	680	1230
RIG AIR T/C 2	720	1205

Figure 143 Schematic of Rig Housing Showing Thermocouple and Heater Locations and Temperatures

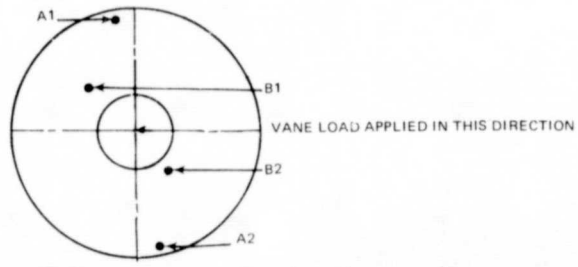

Angular Location of Seal Thermocouples and Vane Base Thermocouples

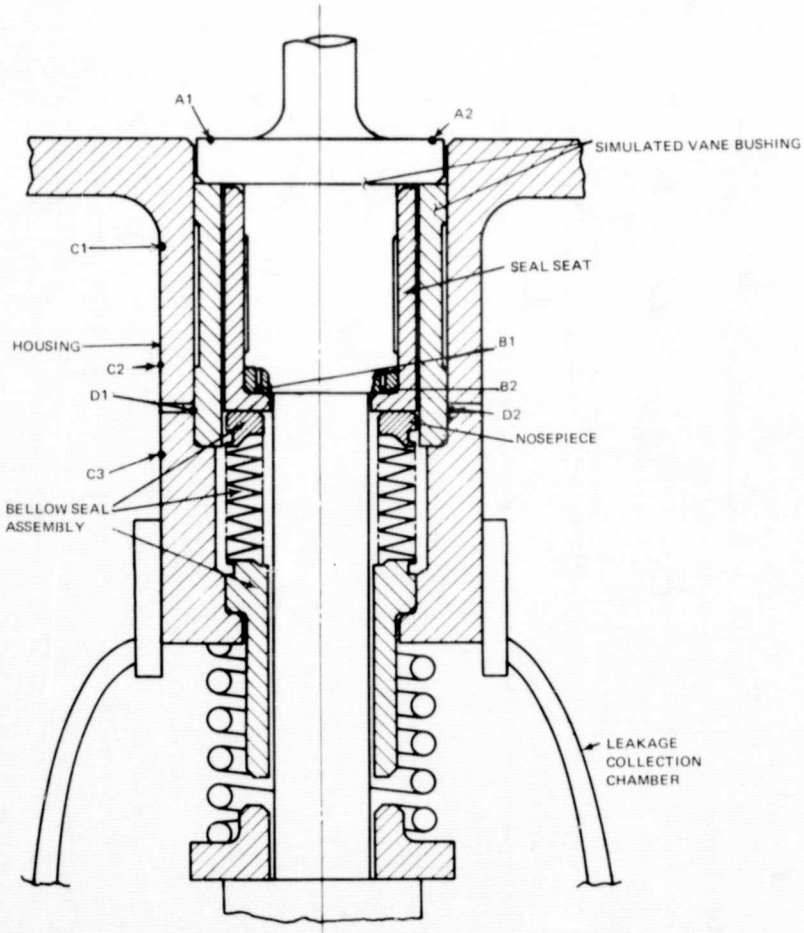

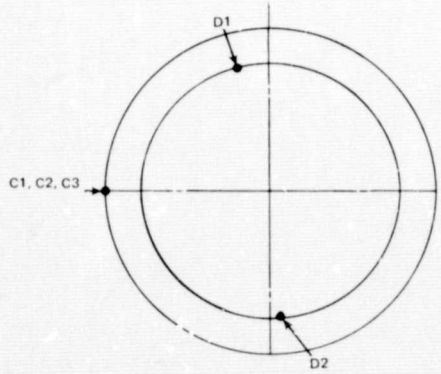

Angular Location of Bushing Thermocouples and Housing Thermocouples

THERMOCOUPLE	TEMPERATURE AT SLTO (°F)	TEMPERATURE AT CRUISE (°F)
VANE T/C A1	615	960
VANE T/C A2	615	965
SEAL T/C B1	650	1005
SEAL T/C B2	570	875
HOUSING T/C C1	570	890
HOUSING T/C C2	540	840
HOUSING T/C C3	500	780
BUSHING T/C D1	525	815
BUSHING T/C D2	530	800

Figure 144 Schematic of Single-Bellows Test Seal Showing Thermocouple Locations and Sample Temperatures During Endurance Testing

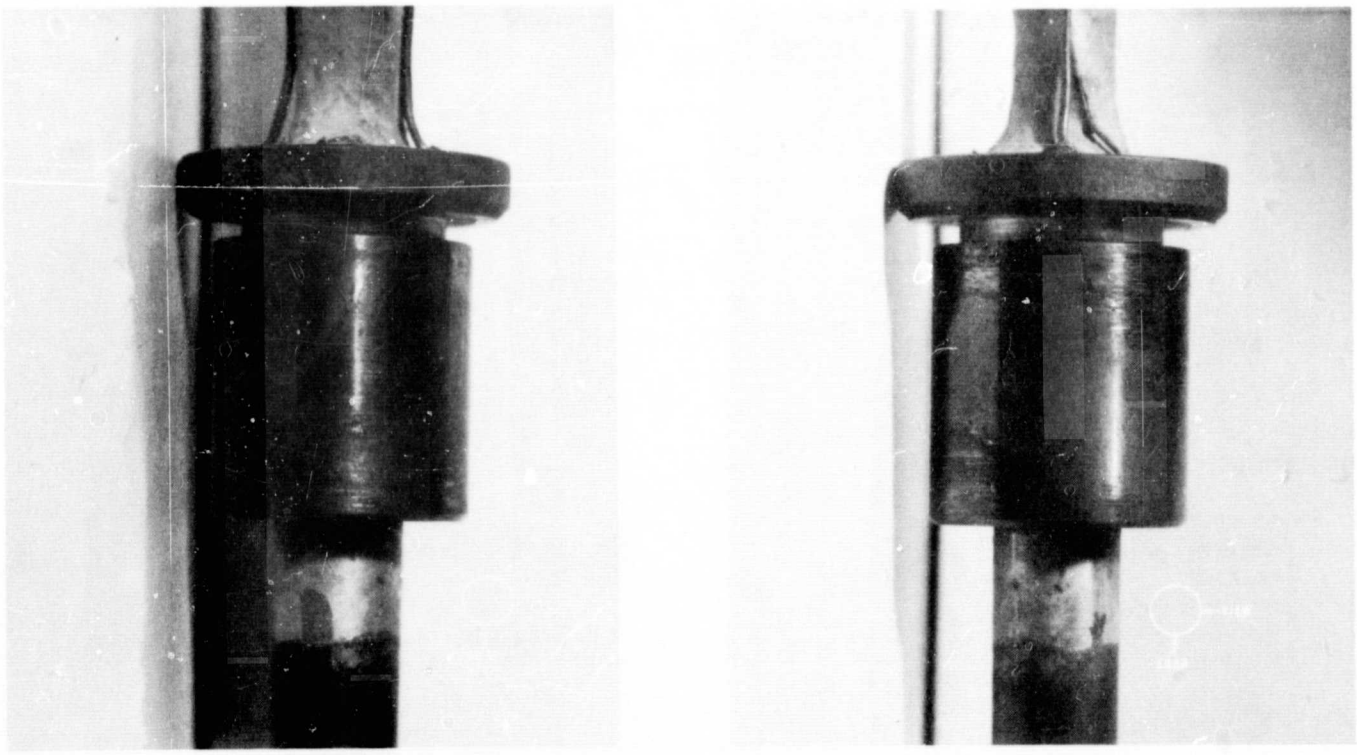

Figure 145 Seal Seat Bearing Area After Test Showing Scoring (Load and Viewing Directions Indicated on Each Frame) (XP-90806, XP-90807, XP-90808, XP-90809)

TABLE VII
OPERATING CONDITIONS AND REQUIREMENTS FOR TEST UNIT NO. 3

CALIBRATION (14.5 HOURS)

Seal Pressure Differential (psi)	Test Description
20 - 135	7 points at room temp. and 200°F
40 - 135	6 points at 400°F - 680°F
40 - 120	5 points at 800°F
60 - 80	2 points at 1200°F
60 - 100	3 points at 1000°F
20 - 135	7 points at room temperatures

ENDURANCE

Cruise (20 hours)	
Simulated vane loading	10 inch pounds ±15% vibratory
Seal ΔP	135 psig at 1200°F
Sea-Level Take-Off (20 hours)	
Simulated vane loading	30 inch pounds ±15% vibratory
Seal ΔP	60 psig at 680°F

SPECIFICATIONS

Bellows Seal Assembly

Nosepiece	
Substrate	AMS 5665
Surface treatment	Tungsten carbide
Finish, multidirectional	5-8 microinches AA before test, lightly second after
Flatness, helium light bands	<1 before test, not measurable after **
Bellows	
Material	AMS 5542
Spring rate (lbs/in)	232
Assembled compression (in)	0.0227 - 0.0247
Bellows Seal Seat	
Material	AMS 5663
Surface treatment (seal face)	Tungsten carbide
Finish, multidirectional	3 microinches AA before test, lightly scored after
Flatness, helium light band	<2 before test, not measurable after **

*Rig air temperatures
**Not measurable due to non-reflectivity of surface

b. Test Unit 4

The bellows seal selected for this build was hardfaced with chrome carbide (Linde (LCIC) as was the mating seal seat. The hardface surface on the bellows was lapped flat to 1 helium light band with a finish of 1 microinch arithmetic average. The seal seat was lapped to a flatness less than 2 light bands with a finish of 3 microinches arithmetic average. The bellows spring rate was measured to be 250 lb/in, and the assembly compression of the bellows was 0.022 to 0.028 inch. Clearance between the bushing and the vane sleeve was 0.003 inch.

The test unit was installed in the rig and underwent a calibration test program. Seal leakage calibration curves are provided in Figure 146. It is apparent from the curves that some seal run-in was required before the leakage fell below the design forecast of 0.00079 scfm at sea-level take-off conditions. The vane actuation torque recorded at each of the test points is tabulated in Table VIII. Like Test Unit 3, the actuation torque for Test Unit 4 was considered to be too high.

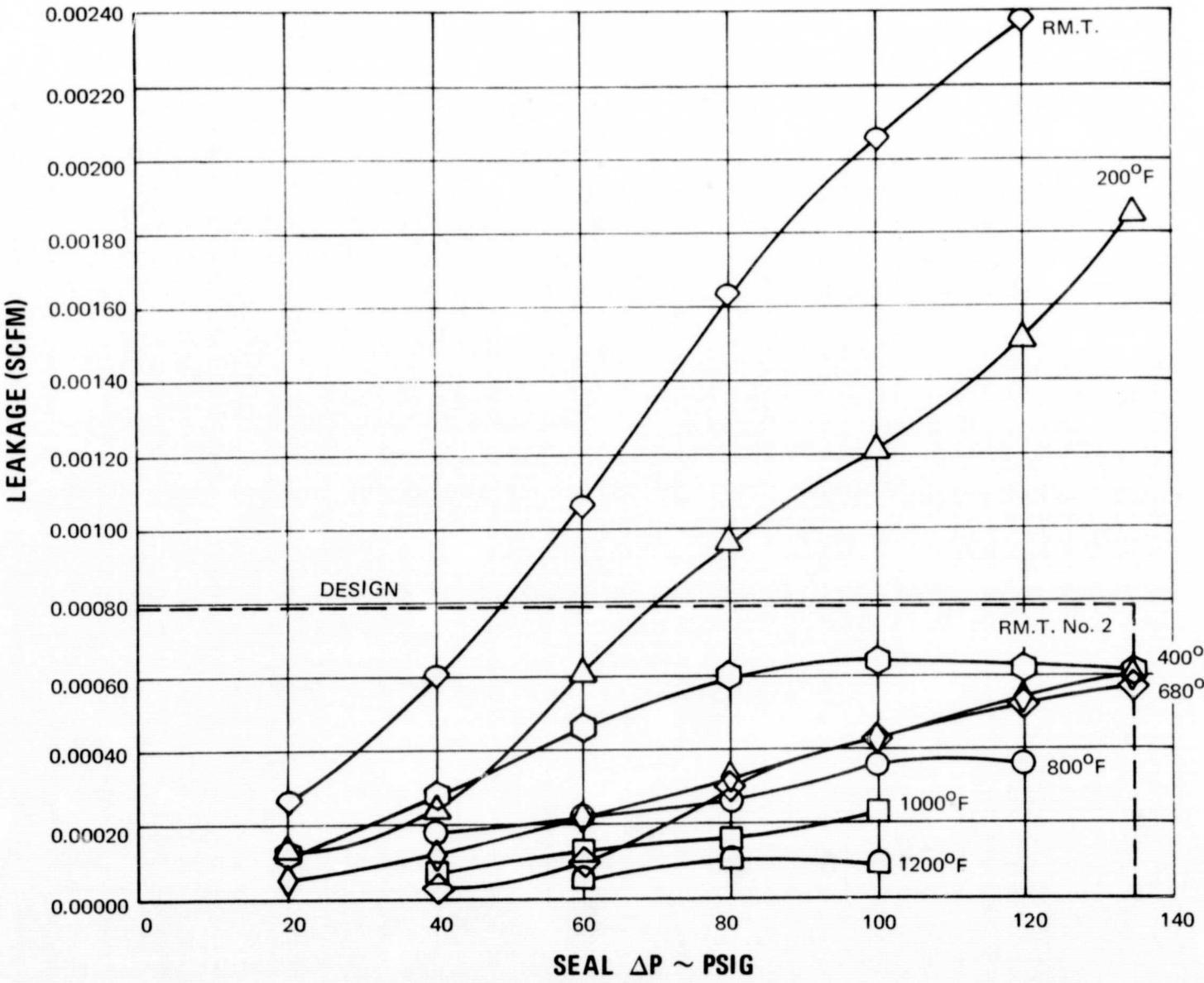

Figure 146 Seal Leakage Calibration on the Single-Bellows Vane Pivot Seal (Test Unit 4)

TABLE VIII
CALIBRATION SCHEDULE AND ACTUATION TORQUE FOR TEST UNIT 4

Rig Air Temperature (°F)	Seal Pressure Differential (psi) 20	40	60	80	100	120	125
Room Temperature	8.3	9.0	9.0	11.6	11.3	10.5	11.3
200	13.5	12.4	12.0	9.0	8.3	7.5	8.6
400		9.5	8.5	9.5	9.5	8.5	9.5
680		11.3	10.9	13.1	13.1	13.9	13.5
800		15.0	14.5	13.0	14.0	13.5	
1000		3.6	3.7	4.2	4.8	5.0	
1200			4.4	4.8	5.2		
Room Temperature	19.5	15.0	15.5	15.5	16.0	16.0	15.0

Except for the runs at 1000°F and 1200°F, the steady-state vane bending moment was 30 in-lb. For those two runs, the vane bending moment was reduced to 10 in-lb. In all cases, a vibratory load of ± 15 percent of the steady-state load was applied to the vane.

Upon completion of the test, the seal was disassembled and examined. It was noted that with the reduced vane moment load at high temperatures, the contact areas on the vane sleeve and bushing were less than the same areas of Test Unit 3. This was found to be true with Test Units 5 and 6 also. Figure 147 shows the wear pattern on the vane sleeve. The wear pattern was typical of all units tested.

Profile traces taken axially along the sleeve journal and bushing journal revealed no measureable wear in the contact area, but did exhibit light scoring. Similarly, traces were taken across the sealing surfaces of the seat and bellows assembly. Some grooves were evident in the bellows face: they varied from 0.03 to 0.09 mils deep. A wear track approximately 0.050 mils deep was noted in the seat. Figures 148 through 151 are pretest and posttest comparison photographs of the sealing surfaces of the bellows seal and seat.

Table VIII summarizes the requirements and specifications of Test Unit 4.

TABLE IX
OPERATING CONDITIONS AND REQUIREMENTS FOR
TEST UNIT NO. 4

CALIBRATION (14.5 HOURS)

Seal Pressure Differential (psi)	Test Description	Vane Load (in-lb)
20 - 135	7 points at room temp. and 200°F*	30
40 - 135	6 points at 400°F – 680°F	30
40 - 120	5 points at 800°F	30
40 - 120	5 points at 1000°F	10
60 - 100	3 points at 1200°F	10
20 - 135	7 points at room temperature	30

SPECIFICATIONS

Bellows Seal Assembly

Nosepiece	
Substrate	AMS 5665
Surface treatment	Chrome carbide
Finish, multidirectional	1 microinches AA before test, lightly scored after, wear track 0.000050 inches deep
Flatness, helium light bands	< 1 before test, not measurable after**
Bellows	
Material	AMS 5542
Spring rate (lbs/in)	250
Assembled compression (in)	0.022 - 0.028
Bellows Seal Seat	
Material	AMS 5663
Surface treatment (seal face)	Chrome carbide
Finish, multidirectional	3 microinches AA before test, lightly scored after 0.00003 to 0.00009 inches deep
Flatness, helium light band	<2 before test, not measurable after**

*Rig air temperatures
**Not measurable due to non-reflectivity of surface

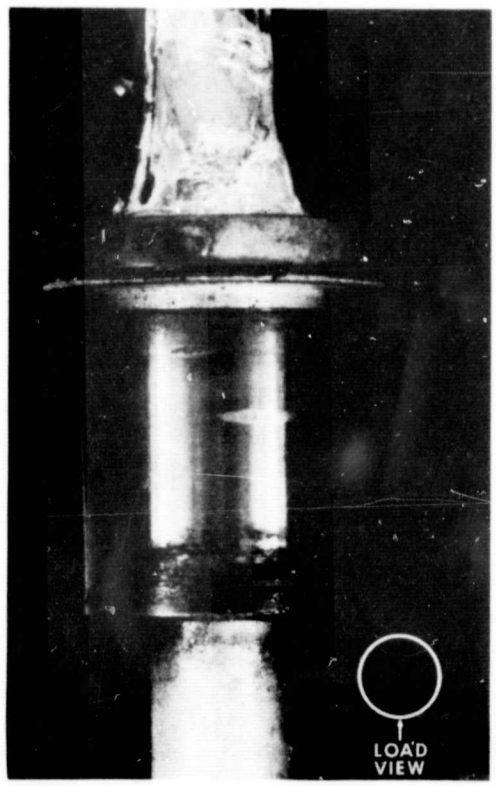

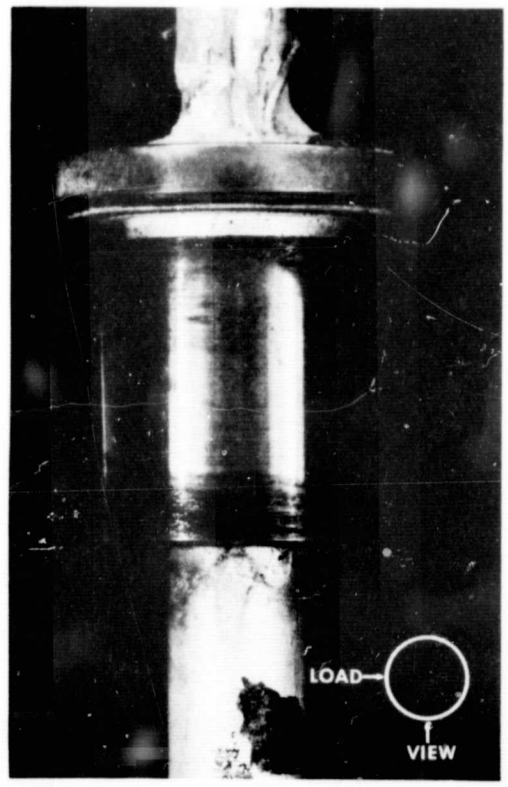

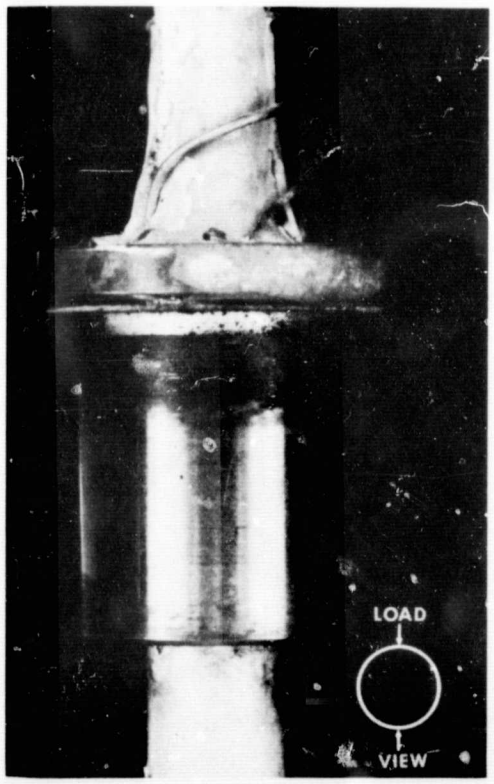

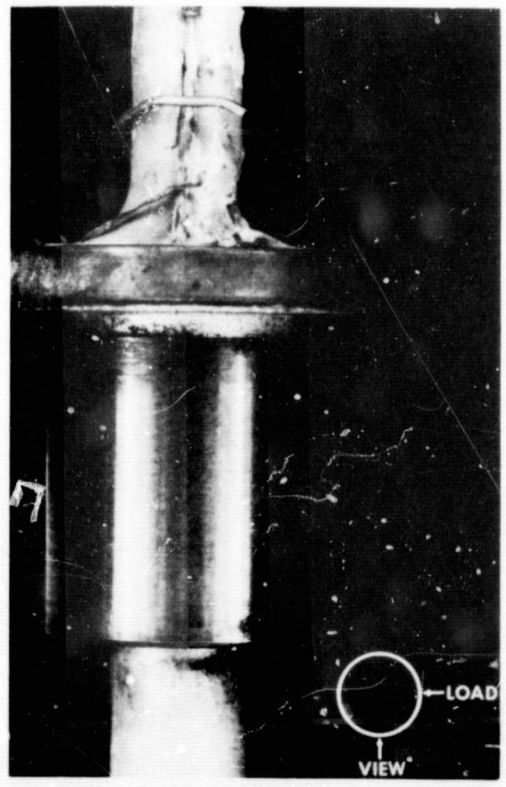

Figure 147 Test Unit 4 Seal Seat Bearing Area Showing Scoring After Test (Load and Viewing Directions Indicated on Each Frame) (XP-93267, XP-93268, XP-93269, XP-93270)

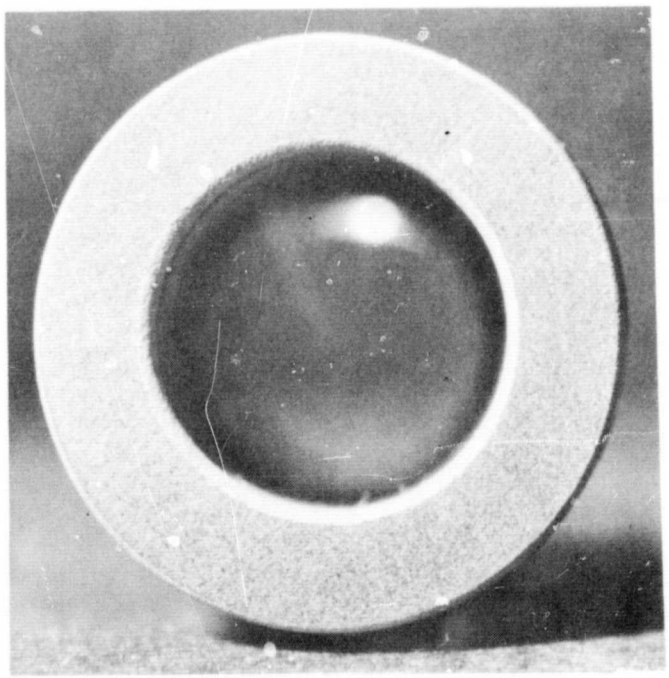

Figure 148 Condition of Hardface Seal Surface of Test Unit 4 Before Test (XP-90407)

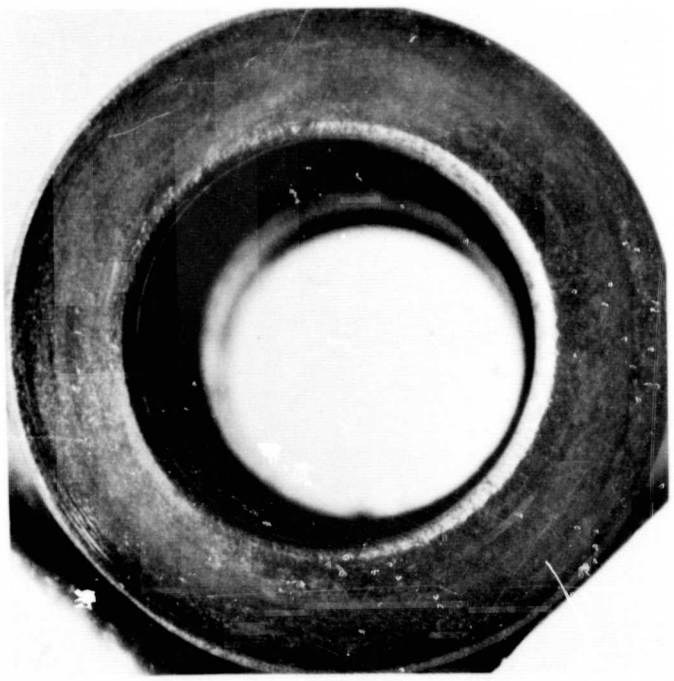

Figure 149 Condition of Hardface Seal Surface of Test Unit 4 After Test (XPN-1113)

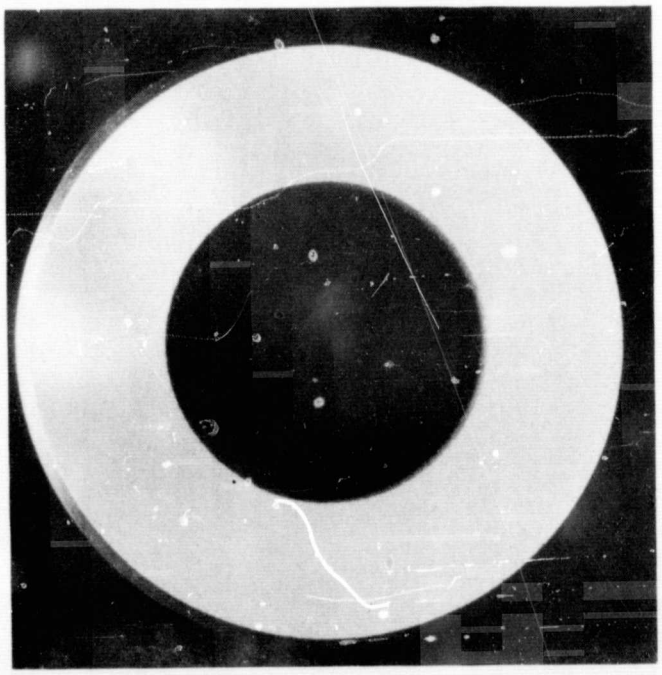

Figure 150 Condition of Hardface Seat Surface of Test Unit 4 Before Test (XP-83424)

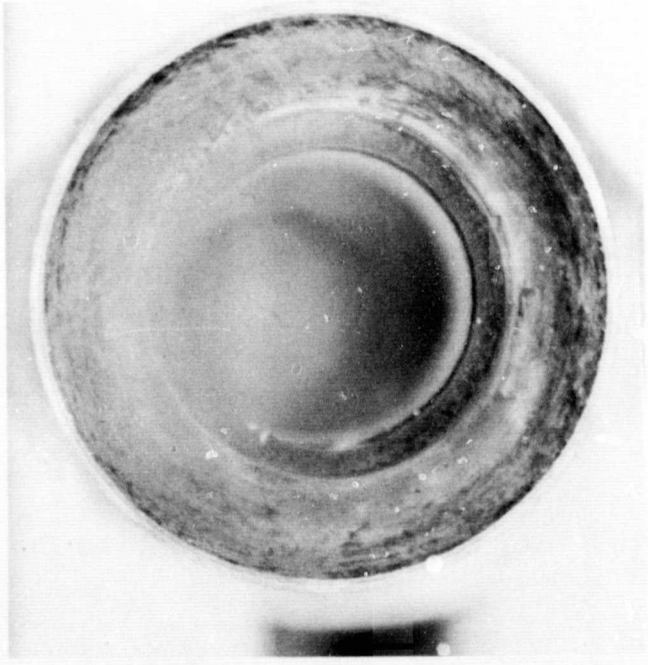

Figure 151 Condition of Hardface Seat Surface of Test Unit 4 After Test (XP-93271)

2. SPHERICAL-SEAT VANE PIVOT SEAL

a. Test Unit 5

For the first spherical-seat test seal, the spherical seal and seal housing were coated with chrome carbide (Linde LCIC). The spherical seat was made of high-temperature graphite (pure Carbon Company 56 HT). This material was selected because the vendor specification showed it to have good strength and oxidation properties to 1200°F.

The spherical seal and seal seat were lapped as a matched set. A pretest surface finish of 2 to 4 microinches arithmetic average was achieved on the spherical seal and a finish of 1.5 microinches arithmetic average on the spherical surface of the seat. A pretest surface finish of 3 microinches arithmetic average and a flatness less than 1 helium light band was provided on the flat surface of the seat. There was no means available to measure the surface finish at the base of the seal housing, but it was judged to be 5 to 10 microinches arithmetic average by visual comparison. Figure 152 and 153 illustrate the pretest surface conditions of the spherical seal and seat. Some slight taper was evident in the vane sleeve, and the installed clearance between the sleeve and bushing varied from 0.002 to 0.004 inch.

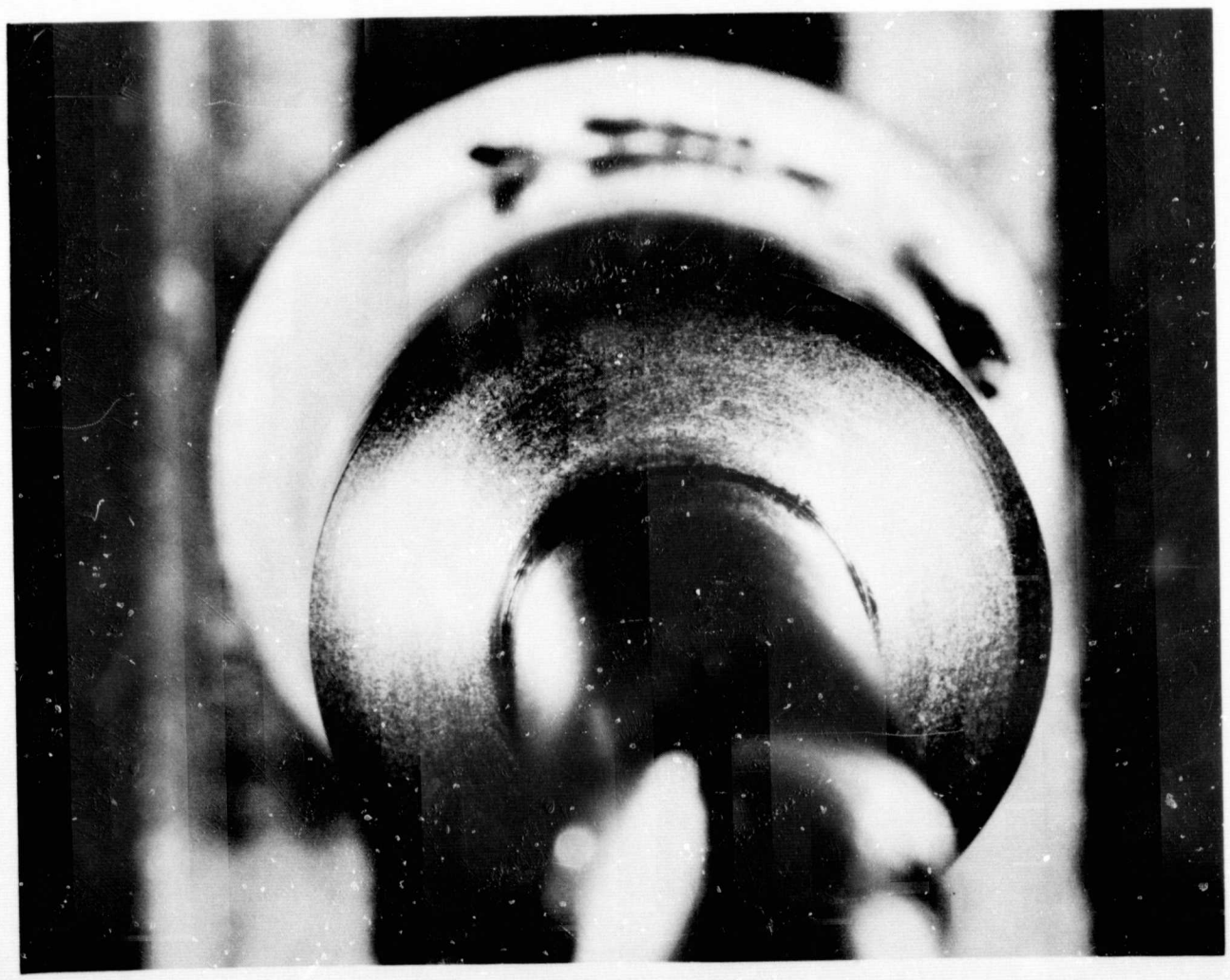

Figure 152 Condition of Hardface Seal Surface of Test Unit 5 Before Test (XP-92618)

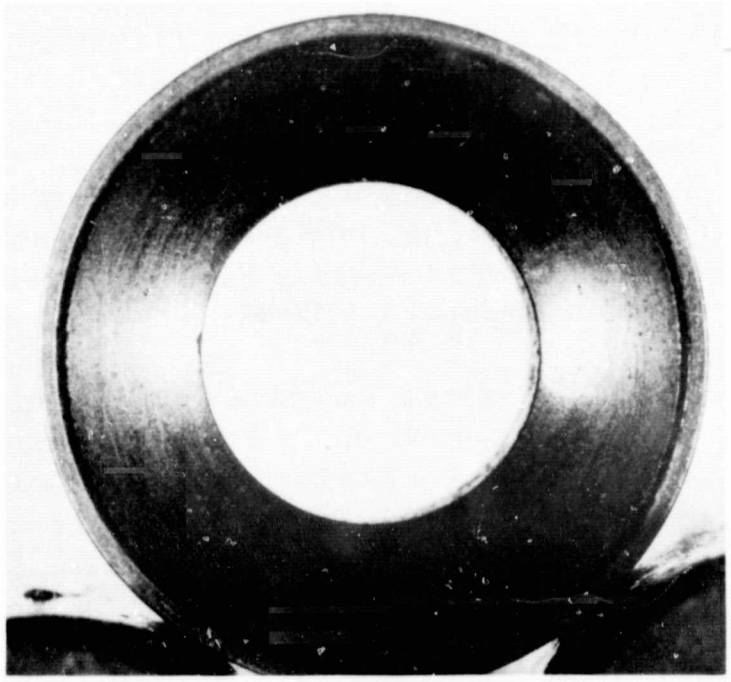

SPHERICAL SURFACE

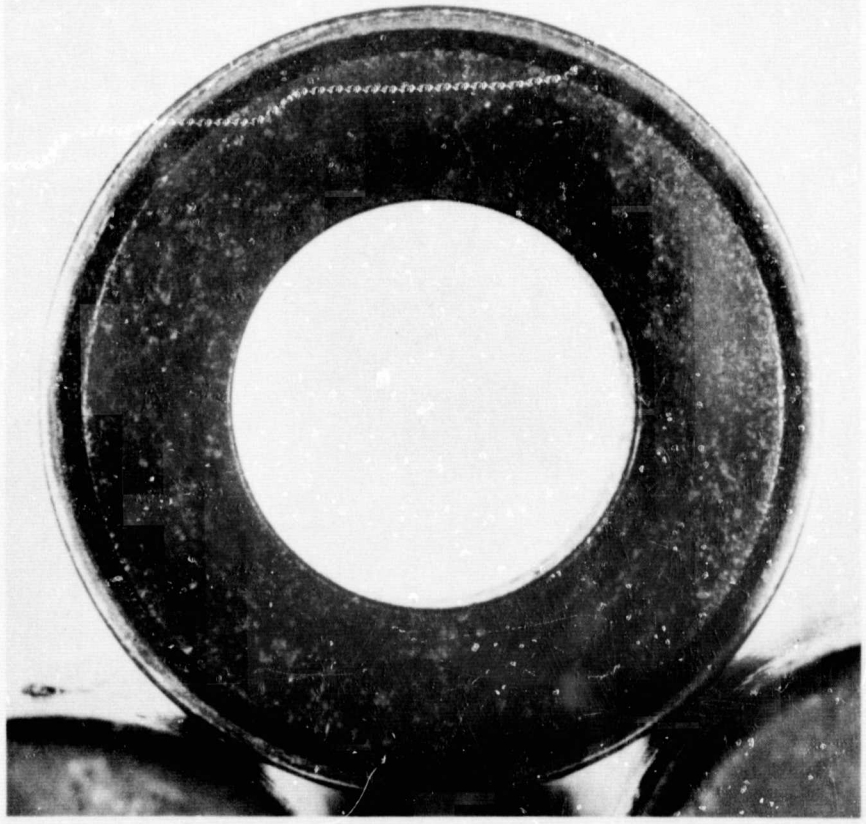

FLAT SURFACE

Figure 153 Condition of Hardface Seat Surfaces (Spherical and Flat) of Test Unit 5 Before Test (XP-92680, XP-92681)

The test unit was installed in the rig and calibration tested. The performance of this seal deteriorated as the test progressed. The design forecast for this seal predicted a leakage of 0.0004 scfm at 135 psig. It is apparent from the curves of Figure 38 that the unit's ability to seal never approached the predicted value and deteriorated as the testing progressed. Two explanations can be put forth: as the carbon seat began to oxidize and wear, the debris collected as small accumulations of carbon between the sealing surfaces, creating an air gap and providing a leakage path. Another possible explanation is that the seat failed to find a positive sealing position with the spherical seal when the vane was cocked under the bending moment. This situation was suggested when the second spherical seal (Test Unit 6) was calibrated and endurance tested. In view of the rapid deterioration in the seal's performance, the test program was discontinued after the calibration run. Table X shows the vane actuation torques recorded at each of the test points. Like the actuation torques for the single-bellows seal, the actuation torques for the spherical-seat seal were considered to be too high. The steady-state vane load was kept at 30 in-lb, except for the runs at 1000°F and 1200°F, where it was reduced to 10 in-lb.

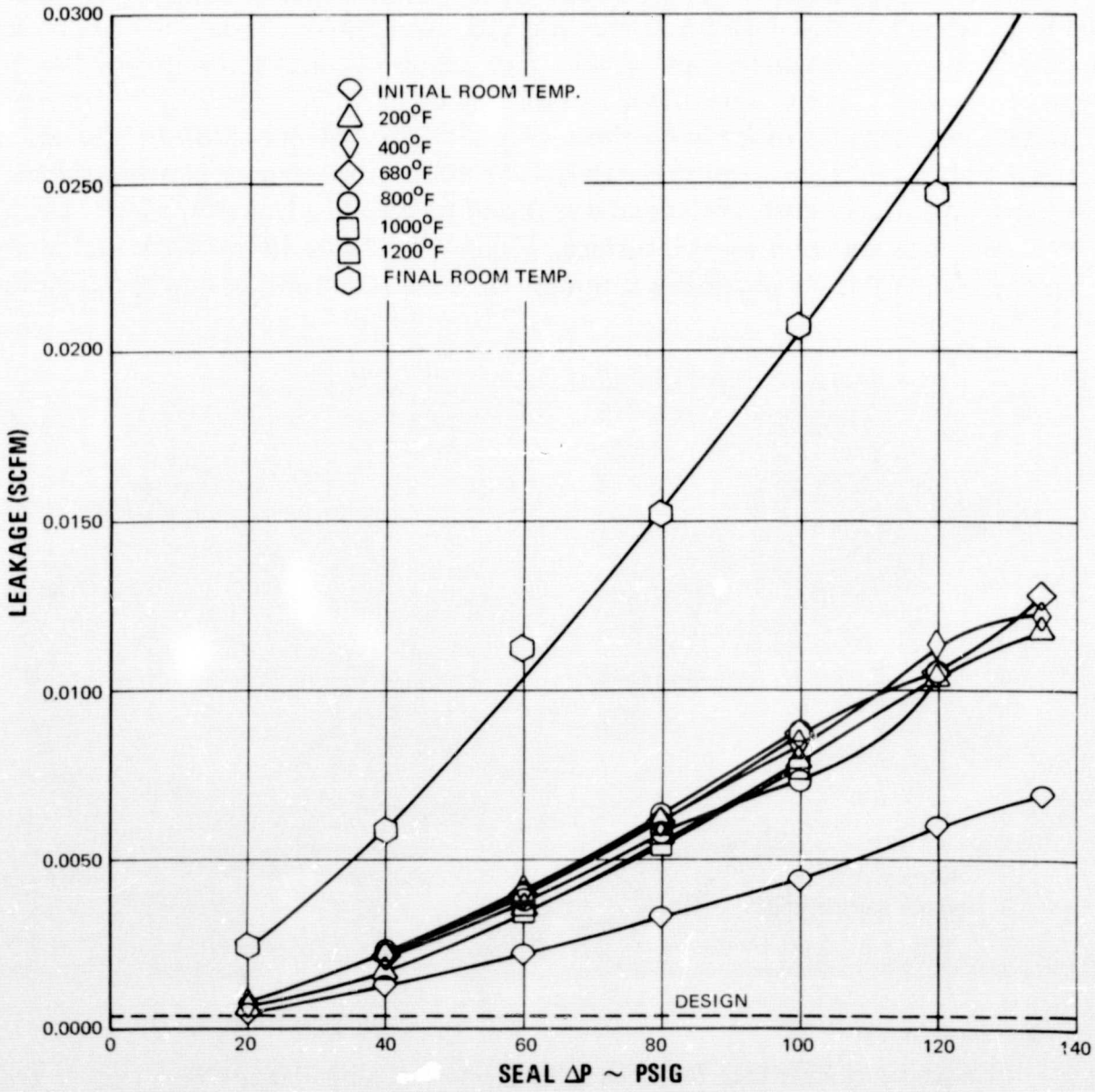

Figure 154 Air Leakage Past the Spherical-Seat Vane Pivot Seal (Test Unit 5)

TABLE X
CALIBRATION SCHEDULE AND ACTUATION TORQUE FOR TEST UNIT 5

Rig Air Temperature (°F)	Seal Pressure Differential (psi) 20	40	60	80	100	120	135
Room Temperature	15.0	15.0	15.0	15.0	15.0	15.5	16.0
200	13.5	14.0	13.0	13.5	13.0	14.0	13.5
400		13.0	13.5	12.5	12.5	13.0	13.0
680		11.5	14.0	14.0	14.0	14.0	15.0
800		14.5	16.5	17.0	17.0	17.0	
1000		6.3	7.5	6.0	6.0		
1200		6.0	4.5	4.5	4.5		
Room Temperature	14.5	14.5	14.5	15.0	16.0	16.0	16.0

After testing the seal was disassembled for inspection. It was immediately evident that the carbon spherical seat had oxidized on the sealing surfaces. Wear losses amounted to 0.16 mil in the flat surface and 0.10 mil on the spherical surface, which also was grooved. Posttest surface measurements showed that the flat surface had a finish of 12 to 36 microinches arithmetic average, while the spherical surface had a finish of 6 to 22 microinches arithmetic average. The spherical seal had picked up approximately 0.12 mil of carbon material from the mating seat. The posttest surface finish of the seal was found to be 2 to 11 microinches arithematic average. No wear was apparent on this surface. Figure 155 shows views of the seat, and Figure 156 shows the seal. Table XI provides a summary of the test conditions and specifications.

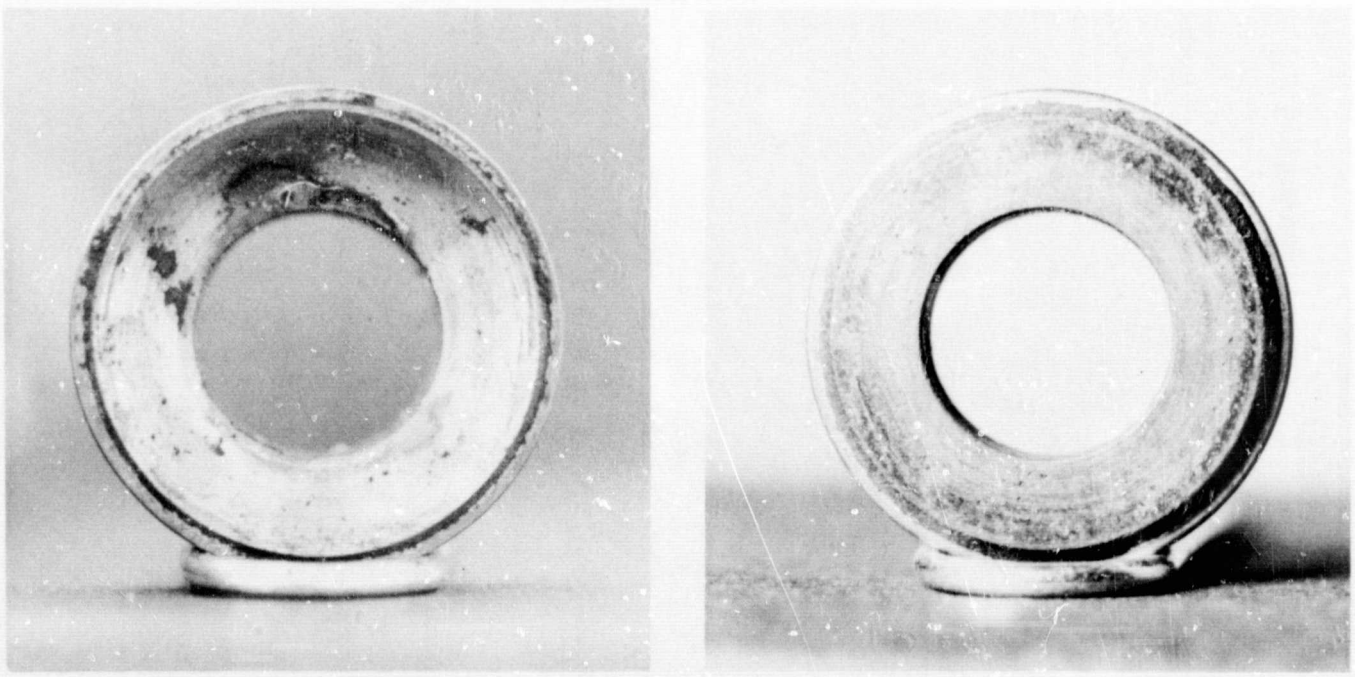

SPHERICAL SURFACE FLAT SURFACE

Figure155 Condition of Hardface Seat Surfaces (Spherical and Flat) of Test Unit 5 After Test (XP-93530, XP-93532)

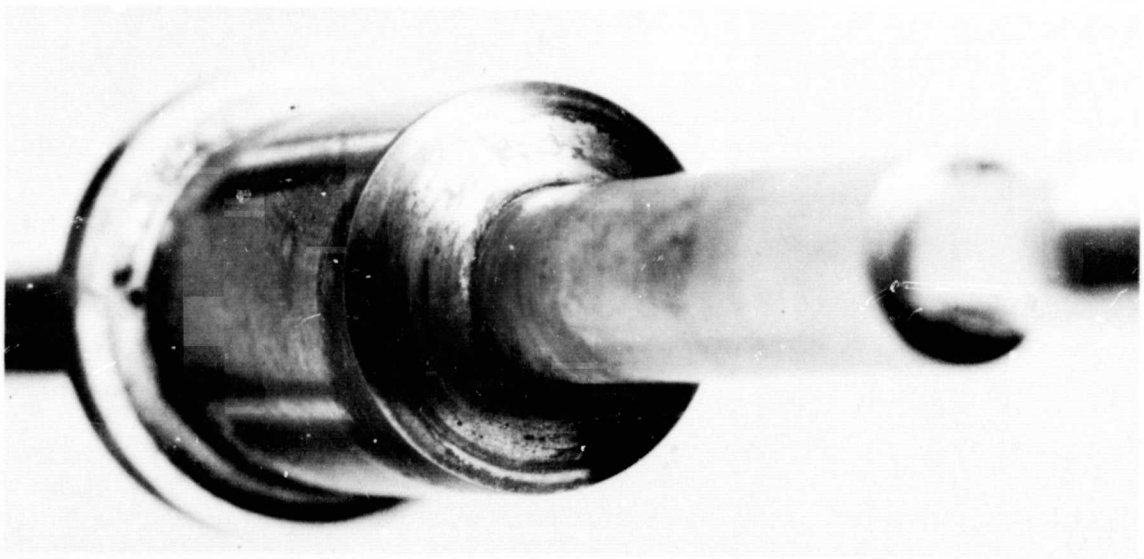

Figure 156 Condition of Hardface Seal Surface of Test Unit 5 After Test (XPN-210)

TABLE XI
OPERATING CONDITIONS AND REQUIREMENTS
FOR TEST UNIT 5

CALIBRATION (17.75 HOURS)

Seal Pressure Differential (psi)	Test Description	Vane Load (in-lb)
20 – 135	7 points at room temp, and 200°F	30
40 – 135	6 points at 400 – 680°F	30
40 – 120	5 points at 800°F	30
40 – 120	5 points at 1000°F	10
60 – 100	3 points at 1200°F	10
20 – 135	7 points at room temperature	30

SPECIFICATIONS

Spherical Seal	
Substrate	AMS 5665
Surface Treatment	Chrome Carbide
Finish (microinches)	2 – 4 AA before test, 2 – 11 AA after test
Wear (mils)	0.12 material buildup
Seat Spherical Surface	
Material	Graphite, Pure Carbon Company 56HT
Finish (microinches)	1.5 AA before test, 6 – 22 AA after test, with deeper grooves
Wear (mils)	No measureable wear
Seat Flat Surface	
Material	Graphite, Pure Carbon Company 56HT
Finish (microinches)	3 AA before test, 12 – 36 AA after test
Flatness (Helium light bands)	Less than 1 before test, not measureable after test
Wear (mils)	0.16
Seal Housing	
Substrate	AMS 5646 SST
Surface Treatment	Chrome Carbide
Finish (microinches)	5 – 10 AA before test, approximately same after test

b. Test Unit 6

For the second spherical-seat seal, the seat was made of AMS 5387, a cobalt-base alloy. The seat rubbed against a tungsten carbide hardcoat deposited on the spherical seal and the seal housing. As with Test Unit 5, the seal and seat were lapped together as a matched set. The pretest surface finish on the seal was 5 microinches arithmetic average, while that on the seat was 1.5 microinches arithmetic average. The flat surface on the seal seat was lapped to a finish of 3 microinches arithmetic average and a flatness less than 1 helium light band. The hardfaces surface in the seal housing was approximately 15 to 16 microinches arithmetic average by visual comparison. The clearance between the vane sleeve and the bushing was 0.002 inch.

Although Test Unit 6 provided somewhat better sealing than Test Unit 5, its performance was still not close to the predicted leakage of 0.0004 scfm at 135 psig. Seal actuation torque remained excessively high. The total running time of the seal during calibration was 13.25 hours. Table XII and Figure 157 summarize the results of the calibration testing.

TABLE XII
CALIBRATION SCHEDULE AND ACTUATION TORQUE FOR TEST UNIT 6

Rig Air Temperature (°F)	Seal Pressure Differential (psi) 20	40	60	80	100	120	135
Room Temperature	12.8	12.0	11.3	12.5	12.5	13.0	13.0
200	13.5	13.0	13.5	12.5	13.0	14.0	14.0
400		12.0	12.0	13.0	14.0	15.0	15.0
680		13.5	13.5	15.5	18.5	20.0	20.0
800		18.0	17.3	17.3	17.3	18.0	
1000		4.0	4.0	4.0	4.0		
1200		4.1	4.1	4.1	4.8		
Room Temperature	18.5	19.0	20.0	20.0	21.0	23.1	22.8

It was from the endurance test of this seal that the inability of the seat to properly align with the seal and prevent leakage became apparent. It can be seen from the endurance data (Figure 158) that the seal performance was most erratic at sea-level take-off conditions, when the bending moment was greatest. At cruise conditions, with a relatively low bending moment, the seal performance was fairly steady, with a relatively low leakage.

The curve drawn through the sea-level take-off data points represents a limited computer effort to find an equation which best describes the test data. The equation thus determined was:

$$Y = C_i + C_2 e^x + C_3 x$$

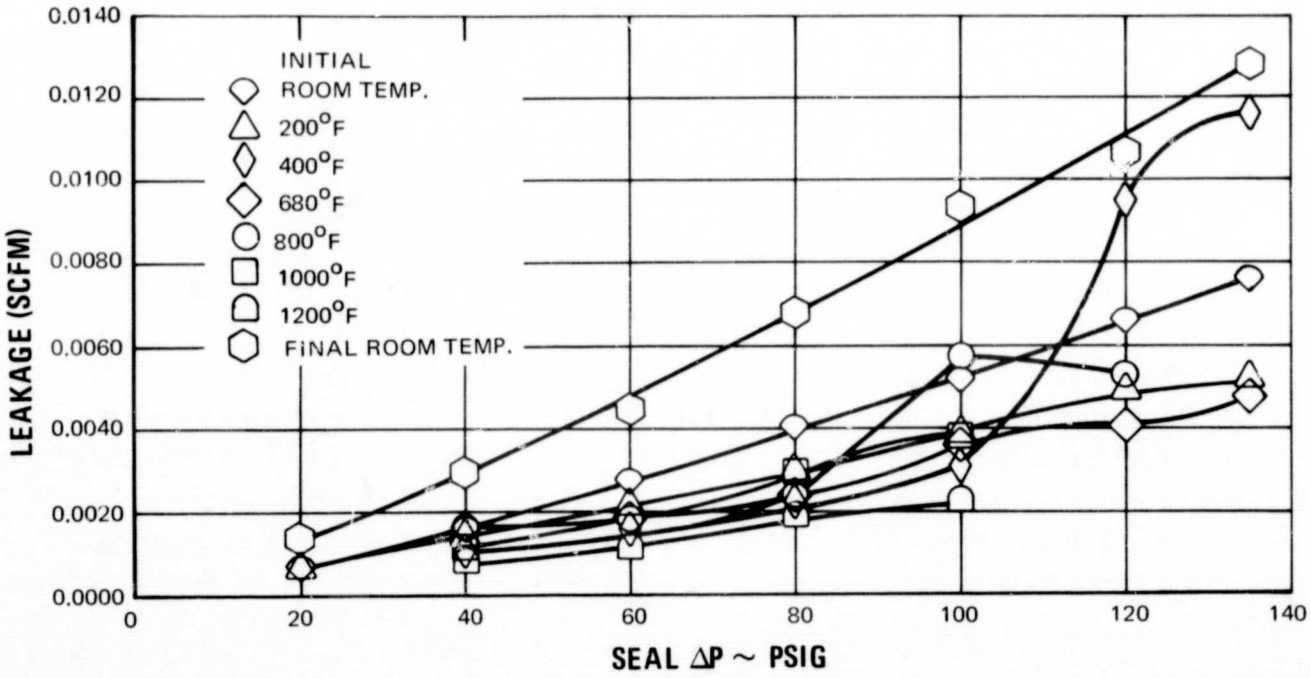

Figure 157 Air Leakage Past the Spherical-Seat Vane Pivot Seal (Test Unit 6) During Calibration Testing

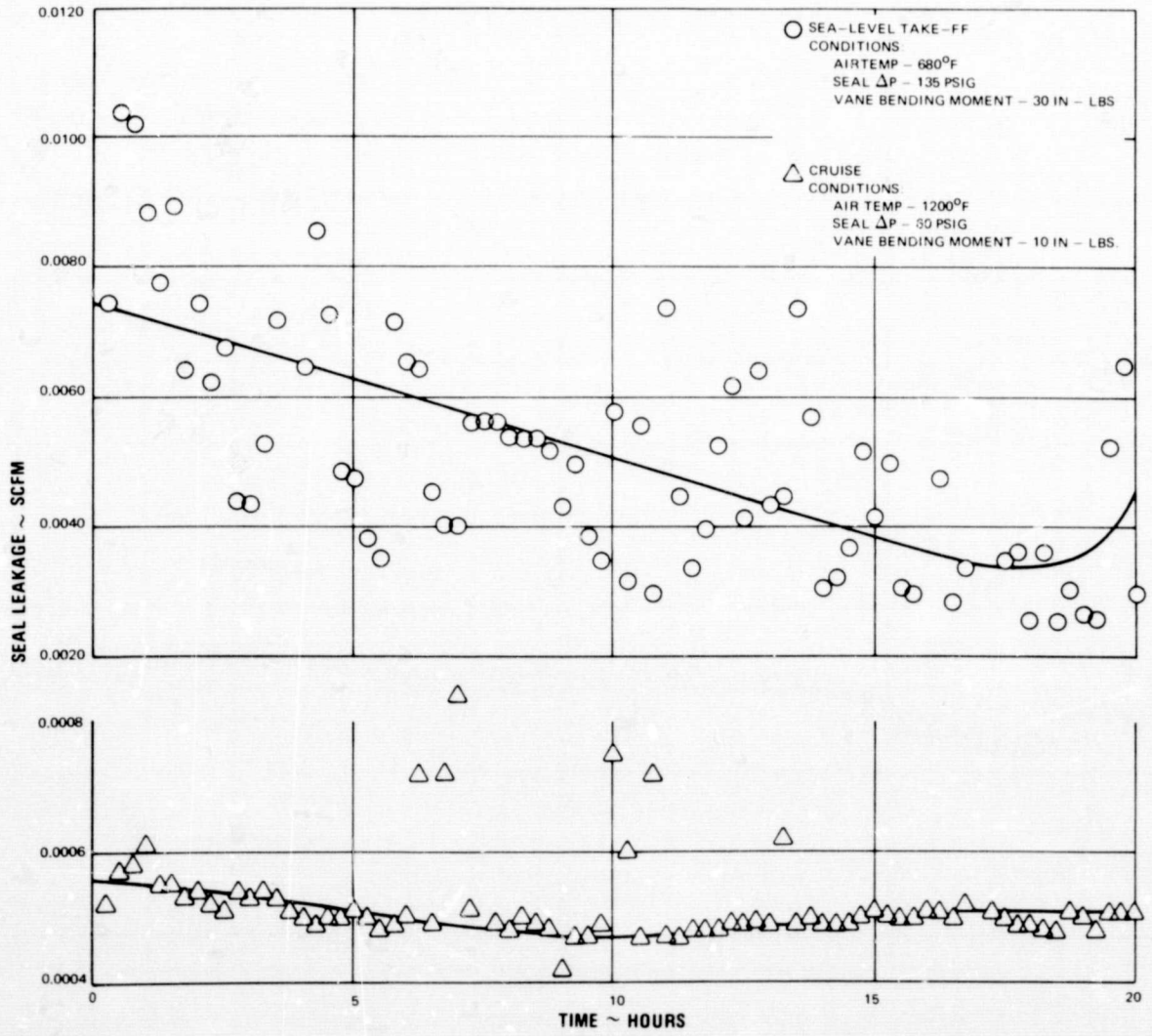

Figure 158 Air Leakage Past the Spherical-Seat Vane Pivot Seal (Test Unit 6) During Endurance Testing

where

Y = seal leakage in scfm
x = time in hours
C_1 = 7.43316×10^{-2}
C_2 = 4.12958×10^{-12}
C_3 = 2.37885×10^{-3}

Figure 159 is a plot of the vane actuation torque recorded during the endurance test. Compared with the actuation torque for the single-bellows seal (shown in Figure 138) there is not much improvement. Figure 160 is a sketch of the spherical seal assembly showing thermocouple locations and representative temperatures recorded during the endurance test.

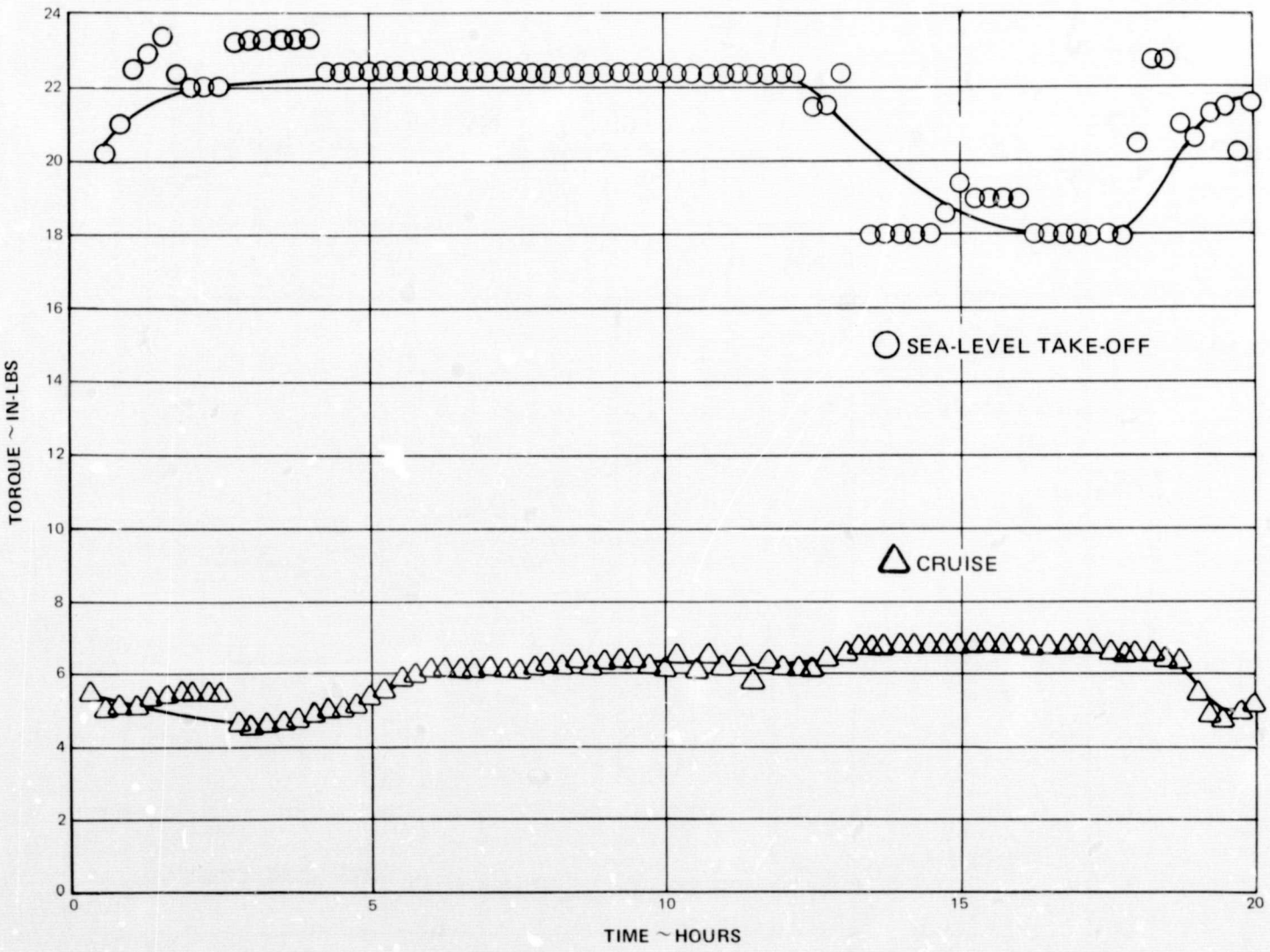

Figure 159 Actuation Torque for the Spherical-Seat Vane Pivot Seal (Test Unit 6)

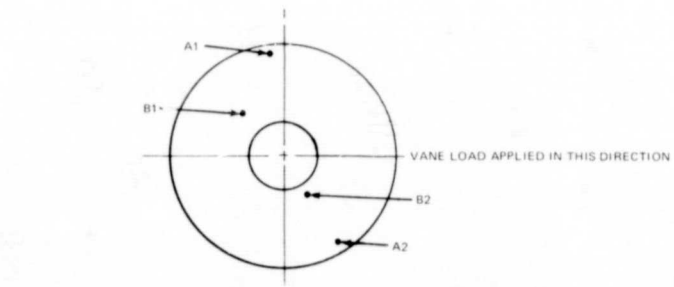

ANGULAR LOCATION OF SEAL THERMOCOUPLES AND VANE BASE THERMOCOUPLES

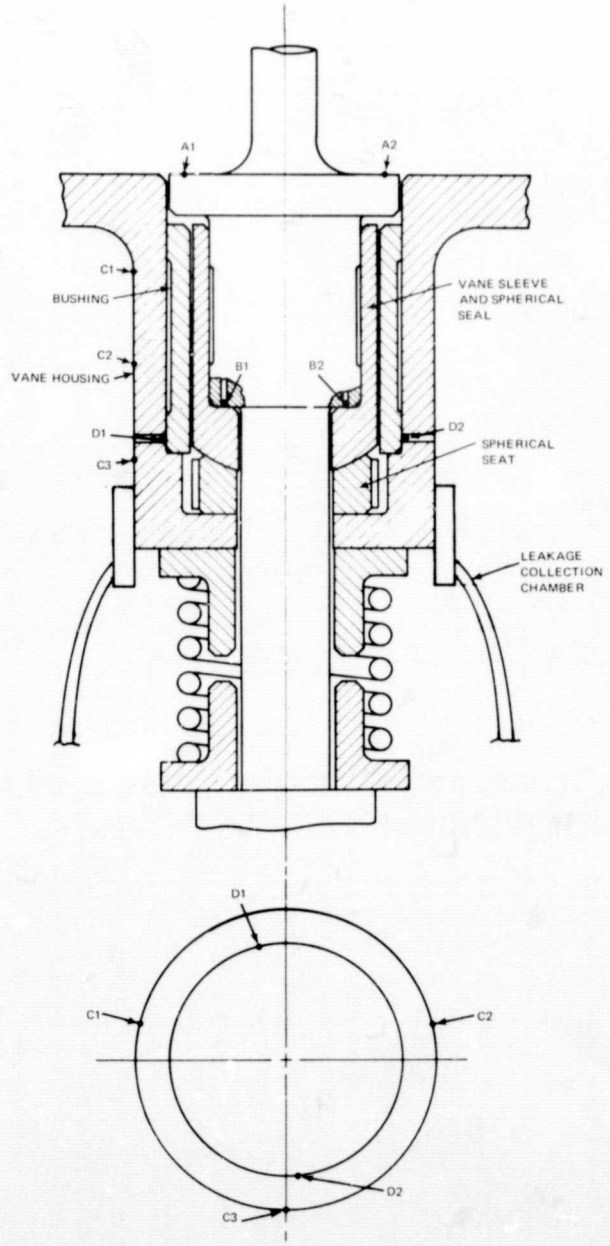

ANGULAR LOCATION OF BUSHING THERMOCOUPLES AND HOUSING THERMOCOUPLES

THERMOCOUPLE	TEMPERATURE AT SLTO (°F)	TEMPERATURE AT CRUISE (°F)
VANE T/C A1	608	997
VANE T/C A2	610	1003
SEAL T/C B1	OUT	900
SEAL T/C B2	607	989
HOUSING T/C C1	633	1042
HOUSING T/C C2	577	939
HOUSING T/C C3	OUT	OUT
BUSHING T/C D1	537	860
BUSHING T/C D2	539	856

Figure 160 Schematic of Spherical-Seat Test Seal Showing Thermocouple Locations and Sample Temperatures During Endurance Testing

After testing, the unit was disassembled and examined. Light scoring was evident on all sealing surfaces. Surface traces revealed a wear track on the spherical seal 0.14 mil deep. The mating surface on the slot was more scored than evenly worn. The deepest score mark was 0.14 mil deep. Some loose debris had also collected on this surface – an indication that an air gap existed during test. A wear track on the flat surface was approximately 0.15 mil deep. Figure 161 shows the spherical seat and Figure 162 shows the spherical seal. Table XIII provides a summary of the operating conditions and specifications for Test Unit 6.

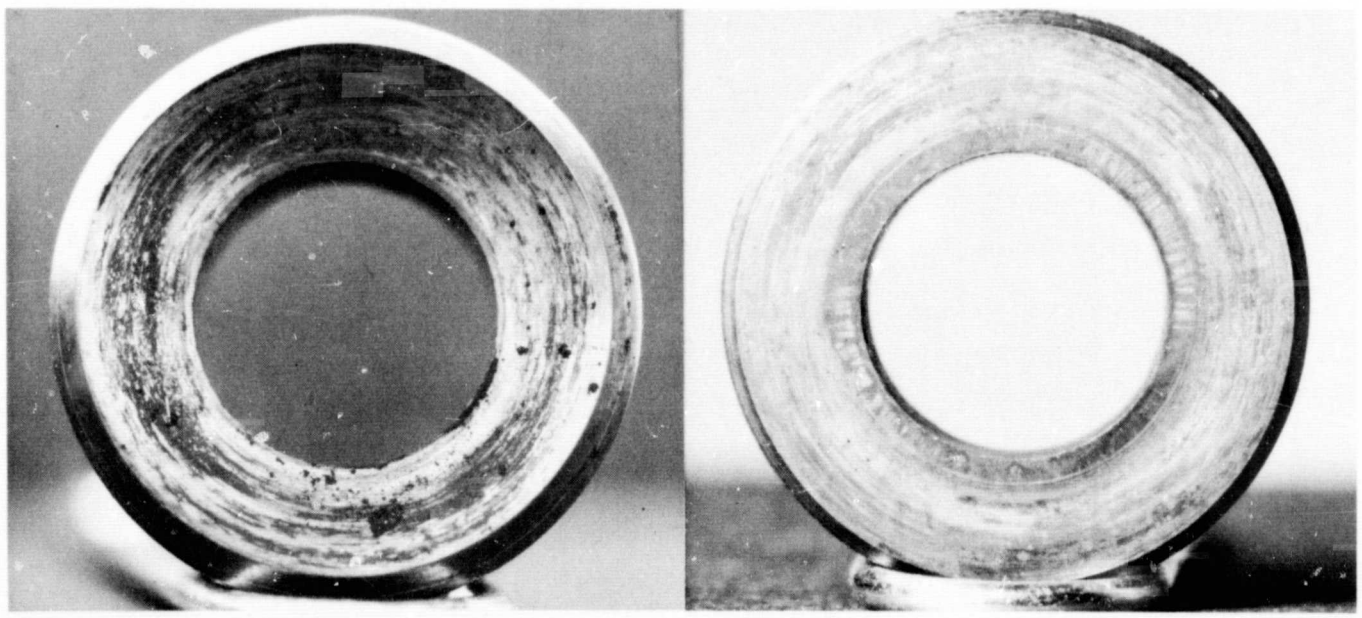

SPHERICAL SURFACE FLAT SURFACE

Figure 161 Condition of Hardface Seat Surfaces (Spherical and Flat) of Test Unit 6 After Testing (XP-93529, XP-93531)

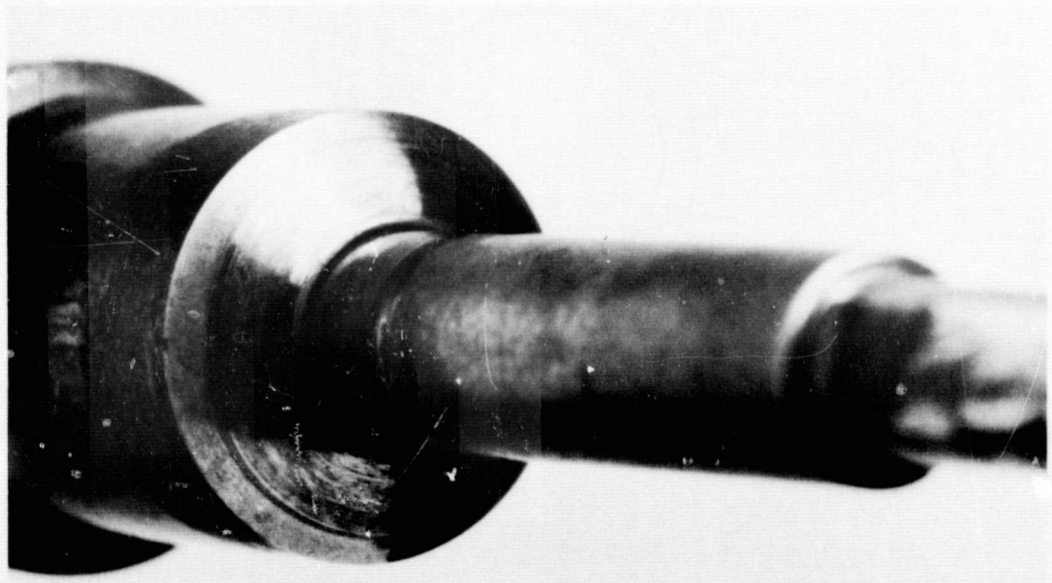

Figure 162 Condition of Hardface Seal Surface of Test Unit 6 After Testing (XPN-212)

TABLE XIII
OPERATING CONDITIONS AND REQUIREMENTS FOR TEST UNIT 6

CALIBRATION (13.25 HOURS)

Seal Pressure Differential (psi)	Test Description	Vane Load (in-lb)
20 – 135	7 points at room temp. and 200°F*	30
40 – 135	6 points at 400°F – 680°F	30
40 – 120	5 points at 800°F	30
70 – 120	5 points at 1000°F	10
60 – 100	3 points at 1200°F	10
20 – 135	7 points at room temperature	30

Endurance

Cruise (20 hours)	
Simulated vane loading	10 inch pounds ±15% vibratory
Seal △P	135 psig at 1200°F
Sea-Level Take-Off (20 hours)	
Simulated vane loading	30 inch pounds ±15% vibratory
Seal △P	60 psig at 680°F

SPECIFICATIONS

Spherical Seal Assembly	
Sperical Seal	
Substrate	AMS 5665
Surface Treatment	Tungsten Carbide
Finish, microinches	5 AA before test, 1 – 6 AA & light scoring after test
Wear, inches	0.00014
Spherical Seat	
Material	AMS 5387, cobalt base alloy
Spherical Surface	
Finish, microinches	1.5 AA before test, 16 AA after test
Wear, inches	0.00014 (deepest score mark)
Flat Surface	
Finish, microinches	3 AA before test, 4 – 7 AA after test
Flatness, helium light bands	<1 before test, not measureable after test
Wear, inches	0.00015
Seal Housing	
Substrate	AMS 5646 SST
Surface Treatment	Tungsten Carbide
Finish, microinches	15 – 16AA before test, not measureable after test

* Rig air temperatures
** Not measurable due to non-reflectivity of surface

F. TORQUE ANALYSIS

Experimental results showed that the actuation torque of the vane pivot seal was higher than had been expected. Therefore, the torque conditions in the seal were analyzed to obtain an explanation for the test results. It was found that there were three factors contributing to the high actuation torque: the seal face load caused by the compression of the bellows, the thrust-collar load caused by the pressure differentials, and the journal loads caused by the applied moment.

The friction coefficients used in calculating the torques caused by the seal face load and the thrust-collar load were obtained from a publication of the Linde Corporation. The friction coefficient used to calculate the torque caused by the moment load was obtained from data generated at Pratt & Whitney Aircraft. Torques calculated for both cruise conditions and take-off conditions agreed reasonably well with the test results, considering the inaccuracies involved in choosing friction coefficients and the location of the applied moment.

1. NOMENCLATURE

δ = bellows deflection (inches)
K = bellows spring rate (lb/inch)
F = seal face load (lb)
F_{TC} = thrust collar load (lb)
F_M = journal load (lb)
μ_B = friction coeficient at seal face
μ_{TC} = friction coefficient at thrust collar
μ_M = friction coefficient at journal
r_B = radius at which F_B acts (inches)
r_{TC} = radius at which F_{TC} acts (inches)
r_M = radius at which F_M acts (inches)
M = applied moment (in-lb)

2. ACTUATION TORQUE FROM SEAL FACE LOAD

Materials: Tungsten Carbide versus Tungsten Carbide

Cruise and takeoff

δ = 0.025 inches

K = 232 lb/in

$F_B = K\delta = 5.8$ lb

Friction Force $(F'_B) = \mu_B F_B = 0.3 \times 5.8 = 1.74$ lb
Friction Torque $= F'_B\, r_B = 1.74 \times 0.2 = 0.348$ in-lb

3. ACTUATION TORQUE FROM THRUST COLLAR LOAD

Materials: Chromium carbide versus cobalt alloy (AMS 5387)

$F_{TC} = A\,\Delta P$

$A = \pi r_B^2 = 0.125$ in^2

Cruise

ΔP = 60 psi

F_{TC} = 0.125 x 60 = 7.5 lb

Friction Force (F'_{TC}) = μ_{TC} F_{TC} = 0.2 x 7.5 = 1.5 lb

Friction Torque = F'_{TC} r_{TC} = 1.5 x 0.27 = 0.405 in-lb

Takeoff

ΔP = 135 psi

F_{TC} = 0.125 x 135 = 16.9 lb

Friction Force = 0.2 x 16.9 = 3.38 lb

Friction Torque = 3.38 x 0.27 = 0.915 in-lb

4. ACTUATION TORQUE FROM APPLIED MOMENT

Materials: Cobalt Alloy (AMS 5387) versus Inconel 718

The applied moment was resisted by the couple formed by F_M. The location at which F_M acted was determined by examining the sleeve after test. A sketch of the pivot assembly is shown in Figure 163, and the contact area is shown in Figure 164.

Cruise

Applied load at end of rod = 1.67 lb
Moment arm = 6.3 inches
Moment Load (M) = 1.67 x 6.3 = 10.5 in-lb

$$F_M = \frac{M}{0.457} = \frac{10.5}{0.457} = 23 \text{ lb}$$

Friction Force (F'_M) = μ_M F_M = 0.6 x 23 = 13.8 lb.
Friction Torque = 2 x F'_M r_M = 2 x 13.8 x 0.254 = 7.0 in-lb.

Takeoff

Applied load at end of rod = 5 lb
Moment Load = 5 x 6.3 = 31.5 in-lb

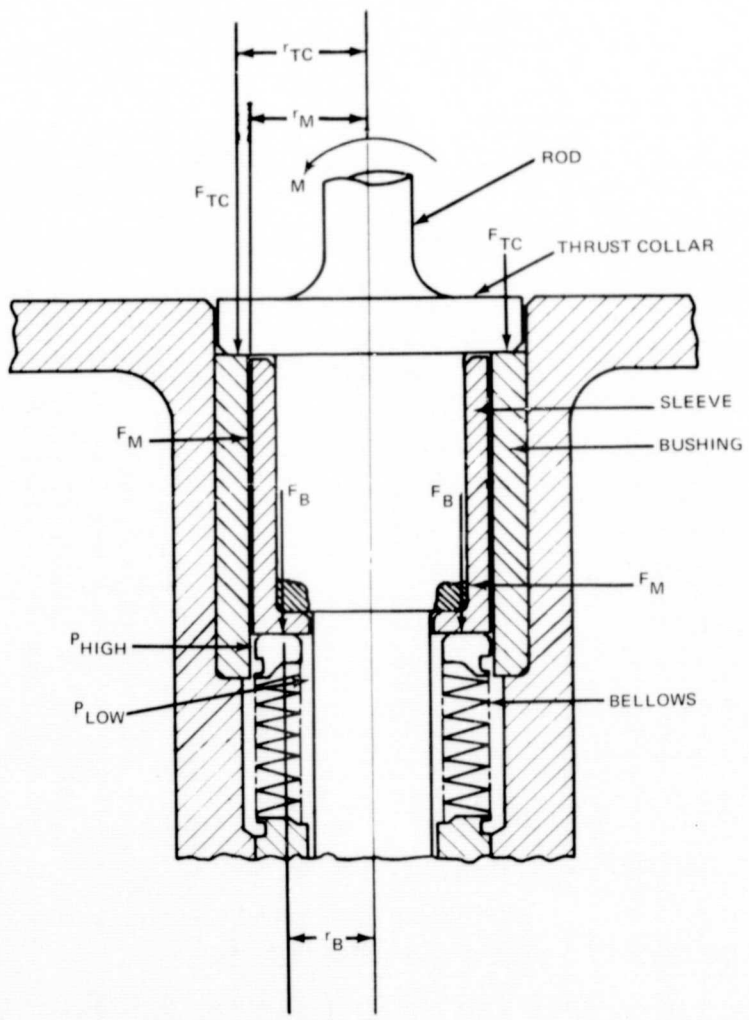

Figure 163 Loads on the Single-Bellows Vane Pivot Seal

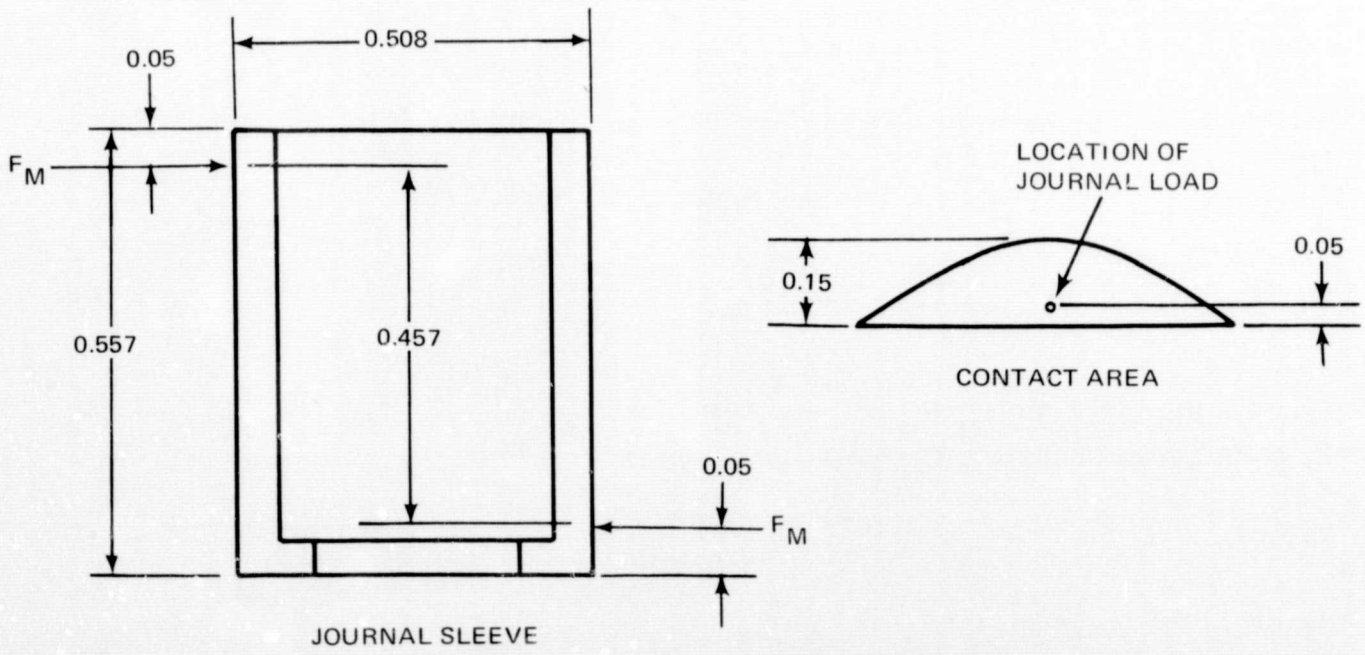

Figure164 Journal Sleeve and Contact Area for the Applied Moment on the Single-Bellows Vane Pivot Seal

$$F_M = \frac{M}{0.457} = 69.0 \text{ lb.}$$

Friction Force = 0.6 x 69 - 41.4 lb
Friction Torque = 2 x 41.4 x 0.254 = 21.0 in-lb.

Friction coefficients and torque values are summarized in Table XIV.

TABLE XIV
FRICTION COEFFICIENT AND TORQUE

	Cruise		Take-Off	
	μ	Torque (in-lb)	μ	Torque (in-lb)
Seal	0.3	0.348	0.3	0.348
Thrust Collar	0.2	0.405	0.2	0.915
Journal	0.6	7.0	0.6	21.0
Total		7.753		22.263
Test Results		5 (approx.)		18 (approx.)

Results indicate that the applied moment is the most significant contributor to the actuation torque. Since baseline tests did not include a moment load the actuation torques are considerably lower. As shown in Table XIV, the increased torques and the calculated torques agree reasonably well.

PRECEDING PAGE BLANK NOT FILMED

REFERENCES

1. Povinelli, V. P. and McKibbin, A. H. *Development of Mainshaft Seals for Advanced Air Breathing Propulsion Systems - Phase II* PWA-3933, NASA CR-72737, Pratt & Whitney Aircraft, East Hartford, Conn., June 1970

2. Hawkins, R. M., Knapp, C. A., and Waring, D. B., *Development of Compressor End Seals, Stator Interstage Seals, and Stator Pivot Seals in Advanced Air Breathing Propulsion Systems,* PWA-2752, NASA CR-54625, Pratt & Whitney Aircraft, East Hartford, Conn., January 1966

3. Hawkins, R. M., et al, *Development of Compressor End Seals, Stator Interstage Seals, and Stator Pivot Seals In Advanced Air Breathing Propulsion Systems,* PWA-3302, NASA CR-72405, Pratt & Whitney Aircraft, East Hartford, Conn., January 1968

4. Den Hartog, J. P., *Mechanical Vibrations,* 3rd edition, McGraw-Hill Book Co., Inc., N.Y., N.Y.

5. Hawkins, R. M., et al, *Development of Compressor End Seals, Stator Interstage Seals and Stator Pivot Seals in Advanced Air Breathing Propulsion Systems,* PWA-3147, Pratt & Whitney Aircraft, East Hartford, Conn., July 1967

6. Castelli, V. and Pirvics, J., "Equilibrium Characteristics of Axial-Groove Gas-Lubricated Bearings," *ASME 65-LUB-16,* (1965)

7. Castelli, V. and Pirvics, J. "Equilibrium Characteristics of Axial-Groove Gas-Lubricated Bearings," *Journal of Lubrication Technology, Trans. ASME,* Vol. 89F, 1967, pp. 177-196

8. Malanoski, S. B. and Pan, C. H. T., "The Static and Dynamic Characteristics of the Spiral Grooved Thrust Bearings, "*Journal of Basic Engineering, Trans ASME,* Vol. 87D, 1965 pp. 547-558.

9. Wildman, M., "Grooved Plate Gas Lubricated Thrust Bearings, with Special References to the Spiral Groove Bearing," Ampex Corporation, Prepared under Contract No. NoNr-3815 (00), Fluid Dynamics Branch, ONR, RR 64-1, Jan. 1964

10. Fuller, L. E., *Mating Materials in Unlubricated, High-Load Low-Speed, Wear Test at High Temperature in Air,* SAE Preprint T-43, June 1960.

11. Hawkins, R. M., et al, *Development of Compressor End Seals, Stator Interstage Seals, and Stator Pivot Seals in Advanced Air Breathing Propulsion Systems,* PWA-2875, Pratt & Whitney Aircraft, East Hartford, Conn., July 1966

12. Timoshenko, S., *Strength of Materials,* Part II, D. Van Nostrand Co., Inc. Thrid Edition, 1956

REFERENCES (Cont'd)

13. Hawkins, R. M. et al, *Development of Compressor End Seals, Stator Interstage Seals, and Stator Pivot Seals in Advanced Air-Breathing Propulsion System,* PWA-2995, Pratt & Whitney Aircraft, East Hartford, Conn., January 1967

14. Van Duyn, M. and Large, W. B. *"Rotor Stress Analysis"* United Aircraft of Canada Limited, July 1966

15. Hawkins, R. M. and McKibbin, A. H., *Development of Compressor End Seals, Stator Interstage Seals, and Stator Pivot Seals in Advanced Air Breathing Propulsion Systems,* PWA-3734, Pratt & Whitney Aircraft, East Hartford, Conn., July 1969.

BIBLIOGRAPHY

Anderson and Saunders, "Connection from an Isolated Heated Rotating Cylinder Rotating about Its Axis," *Proceedings of the Royal Society*, Series A, Vol. 217, p. 555, 1953.

Arwas, E. B. and Sternlicht, B. "Viscous Shear Compressor," Mechanical Technology Incorporated, Technical Report MTI 62TR21

Becker, K. M. and Kaye, Joseph "Measurements of Diabatic Flow in an Annulus with an Inner Rotating Cylinder", *J. Heat Transfer, Trans. ASME, 84,* 97-105, May 1962.

Bjorkland, "*Heat Transfer from Rotating Bodies - Single Cylinders and Concentric Cylinders*", Technical Report No. 34, Dep't. of Mechanical Engineering. Stanford University. 1957.

Bjorkland and Kays, "*Heat Transfer Between Concentric Rotating Cylinders*", ASME Paper No. 58-A-99. 1958.

Buckley, D. H. and Johnson R. L., "Friction and Wear of Hexagonal Metals and Alloys as Related to Crystal Structure and Lattice Parameters in Vacuum", *ASLE Trans.* 9, 121-135 (1966)

Castelli, V. and Shapiro, W. "Improved Method for Numerical Solutions of the General Incompressible Fluid Film Lubrication Problem", *Journal of Lubrication Technology, Trans. ASME,* Vol. 89F, 1967, pp. 211-218.

Cheng, H.S., Chow, C.Y., and Murray, S. *Gas Bearing Design Methods* Vol. I, Mechanical Technology Incorporated Technical Report, MTI 65TR5-I.

Cheng, H., Chow, C., and Murray, F. S. "*The Hydrodynamic Gas Journal Bearing and The Hydrodynamic Gas Thrust Bearing*" Vol. I, MTI-65TR5-II, Mechanical Technology Inc., Latham, N. Y., 1965.

Daily, J. W. and Nece, R. E. "Chamber Dimension Effects on Induced Flow and Frictional Resistance of Enclosed Rotating Discs", *J. Basic Engineering, Trans. ASME,* Vol. 82, p. 217, 1960.

Den Hartog, J. P. *Advanced Strength of Materials,* McGraw-Hill Book Co., Inc., N.Y., N. Y., 1952

Eckert, E. R. and Drake, R. M. Jr. *Heat and Mass Transfer,* McGraw-Hill Book Co., New York, 1959

Fuller, Dudley D., *Theory and Practice of Lubrication for Engineers,* John Wiley & Sons, Inc., New York, 1956

Grassam, N. S. and Powell, J. W. *Gas Lubricated Bearings,* Butterworth, Inc., London, 1964

BIBLIOGRAPHY (CONT'D)

Hsing, F. and Chiang, T. "Discharge Coefficient of Orifices and Nozzles," *Mechanical Technology Inc. Technical Memo MTI-65TM7.*

Jakob, Max and Hawkins, George, *Elements of Heat Transfer,* third edition, John Wiley & Sons, Inc., New York, 1958.

Kalnins, A., "Analysis of Shell of Revolution Subject to Symmetrical and Nonsymmetrical Loads," *Journal of Applied Mechanics,* Sept. 1964

Keenan, J. H. and Kaye, J. *Gas Tables,* John Wiley & Sons, New York 1961

Lave, J. H., "Hydrostatic Gas Bearings," California Institute of Technology Progress Report No. 20-353 Pasadena, 1958

Love, A.E.H., *The Mathematical Theory of Elasticity,* Fourth Edition, Dover Press, 1944

Lund, J. W., "Gas Bearing Design Methods Vol. 2, "Mechanical Technology Incorporated Technical Report, MTI 65-TR5-II.

McAdams, W. H. *Heat Transmission,* 3rd edition. New York: McGraw-Hill, 1954

Pinkus, Oscar and Sternlicht, Berno, *Theory of Hydrodynamic Lubrication,* McGraw-Hill Book Co., New York, 1961

Rabinowicz, E. *Friction and Wear of Materials,* John Wiley & Sons, Inc. New York, 1965

Roark, R. J. *Formular for Stress and Strain,* Third Edition, McGraw-Hill Book Co., Inc., N. Y., N. Y., 1954

R. P. I. and M. T. I., "Design of Gas Bearings," Vol. I

Schlichting, H., *Boundary Layer Theory,* Fourth Edition, McGraw-Hill, New York, 1960

Shapiro, A. H., *The Dynamics and Thermodynamics of Compressible Fluid Flow,* Vol. 1, The Ronald Press Co., New York, 1953

Sokolnickoff, I. S., *Mathematical Theory of Elasticity,* Second Edition, McGraw-Hill Book Co., Inc., N. Y., N. Y., 1956

Tang, I. C., and Gross, W. A. "Analysis and Design of Externally Pressurized Gas Bearings". *ASLE Transactions,* Vol. 5, pp. 261-284. 1962

BIBLIOGRAPHY (CONT'D)

Theodorsen, T. and Reiger, A., "Experiments on Drag of Revolving Discs, Cylinders, and Streamline Rods of High Speeds," *NACA Transactions,* Vol. 796

Whitley, S. and Williams, L. G. "Principles of Gas-Lubricated Shaft Seals", *Journal of Mechanical Engineering Science,* Vol. 4, No. 2, 1962

LIST OF SYMBOLS

Upper Case Symbols

A	diameter to inner toroidal center of OC diaphragm seal (inches)
B	diameter to outer toroidal center of OC diaphragm seal (inches)
B	surface flatness (helium light bands)
C	diameter to semitoroidal center of OC diaphragm seal (inches)
C	radial clearance between rotor and seal ring (inches)
C	labyrinth discharge coefficient (dimensionless)
C_D	orifice discharge coefficient (dimensionless)
C_d	orifice discharge coefficient (dimensionless)
C_m	radial clearance or manufactured (inches)
C_{A1}, C_{A2}	influence coefficients associated with α_n
C_{B1}, C_{B2}	influence coefficients associated with β_n
C_{U1}, C_{U2}	influence coefficients associated with U_n
C_{V1} C_{V2}	influence coefficients associated with V_n
C_1	damping rate (lb-sec/in/in of circumference)
C_1, C_2, C_3	carrier, seal ring, and runner displacement respectively (inch)
C_1.... C_5	force moment arms (inch)
D	diameter (inches)
E	modulus of elasticity (lb/in^2)
F	seal face load (lbs)
F_M	journal load (lbs)
F_s	sum of horizontal pressure forces on segment (lbs)
F_s	helical coil spring force (lb/in)
F_v	sum of vertical pressure forces or segment (lbs)
F_{TC}	thrust collar load (lbs)
F_{s1}, F_{s2}	C and O diaphragm spring reactions (lb/in)
F_f	friction force (lbs)
F_f	coefficient of friction (dimensionless)
F_o	carrier axial pressure load (lb/in)
F_y	carrier radial pressure load (lb/in)
F_{r1}	net gas force change due to tolerance @ take-off (lbs)
F_{r2}	net gas force change due to tolerance @ cruise (lbs)
F_1, F_2, F_3.... F_x, F_y	force vectors (lb/in)
G	modulus of rigidity (lb/in^2), shear modulus of elasticity (lb/in^2)
G	orifice flow (dimensionless) = $m\sqrt{RT/\pi}\, a^2\, pnC_d$
I	area moment of inertia (in^4)
J	thermal conversion factor = 12 x 778 (in-lb/Btu)
K	bellows spring rate (lb/in)
K_s	static gas film stiffness (lb/in/in)
K_{ss}	axial gas film stiffness (lb/in/in)
K^*_s	axial gas film stiffness per unit area ($lb/in/in^2$)
K^*_r	bending stiffness of seal ring = $\frac{EI}{R^2}$ (in-lb/in-radian)

K^*_{ss}	OC diaphragm stiffness (lb/in/in)
K_1, K_2, K_3	spring constants (lb/in)
K_2	spring diaphragm stiffness (lb/in)
K_3	gas film stiffness (lb/in)
L	width of flow path (inches)
L	air film shear = $\mu(U/h)$
M	applied moment to simulated vane (in-lb)
M, M_1, M_2 .... etc	moment (in-lb/in)
M_c	residual moment due to "C" diaphragm tolerance (in-lbs/in)
M_o	residual moment due to "O" diaphragm tolerance (in-lbs/in)
M_{oc}	combined residual moment due to tolerance = $M_o + M_e$ (in-lb/in)
M_R	carrier residual moment (in-lb/in)
M_{res}	residual moment (in-lb/in)
N	rotor speed (RPM)
Q, Q_1, Q_2	weight flow rate (lb/sec)
$\bar{Q}$	seal leakage flow rate (dimensionless) = $\frac{12\,\mu\,RT}{p^2 h^3}\,Q$
R	gas constant ($in^2/°R\text{-}sec^2$)
R	radius (in.)
R_i	seal inner radius (inch)
R_o	seal outer radius (inch)
$R_{m\ SEAL}$	mean radius of thrust collar and seal (inch)
R′	mean radius of seal = $\frac{R_i + R_o}{2}$ (inch)
S	seal ring radius (inches)
T, T_1, T_2, etc.	temperature (°R or °F)
T	tension load (lb)
T	actuation torque (in-lb)
T_R	surface temperature of rotor (°F)
T_S	surface temperature of segment (°F)
ΔT	temperature change across thickness (°F)
U	velocity (in/sec)
V	mean-velocity in vibration excursion (ft/sec)
V	volumetric flow (SCFM)
$W, W_1, W_2 W_3, W_4$	seal or bearing reactions (lb/in)
$\bar{W}, \bar{W}_1, \bar{W}_2$	dimensionless seal or bearing loads
X	coordinate axis
X_1, X_2, X_3	tolerance dimension (inches)
X_1, X_2, X_3	displacement (inches)
Y	coordinate axis
Y	outside diameter of OC seal primary face (inches)
Z	coordinate axis

Lower Case Symbols

a	orifice radius (inches)
a′	½ length of shoe segment of 3.6 inches (inches)
α	thermal coefficient (in/in/° F)
α_n	angular runner deformation (radians)
α_r	thermal expansion coefficient of rotor (in/in-°F)
α_s	thermal expansion coefficient of segment (in/in-°F)
b	leakage flow path length (inches)
$b_1 \ldots b_4$	width dimension (inches)
c	pad length (inches)
$c_1, c_2, c_3 \ldots$	segment pressure force moment area (inches)
d	distance from c diaphragm edge to seal face (inches)
f	friction coefficient (dimensionless)
g	gravitational constant (in/sec^2)
g	mass flow through double knife edge (lbs-sec/in.)
h, h_o, h_1 ....etc	film thickness (inches)
h_{min}	minimum gas film thickness (inch)
$h_{T\,min}$	combined mode minimum film thickness (inch)
$h_{R\,min}$	minimum film thickness resulting from residual moments (inch)
h_{RM}	mean film thickness resulting from residual moments (inch)
k	ratio of air specific heat
k_f	stiffness of air film (lb/in)
k_s	support stiffness (lb/in)
l	net change in axial film thickness (inches)
m	mass flow per unit length (lb-sec/in^2)
m_1, m_2	mass flow through leakage path at downstream and upstream sections per orifice, respectively (lb-sec/in)
m_3	mass flow rate through orifice (lb-sec/in)
m_1	carrier mass (lb-sec^2/in)
m_2	seal ring mass (lb-sec^2/in)
n	number of orifice holes
n	operational mode (1, 2, 3, ... etc)
p, p_1, p_2 .... etc.	pressure (psi)
p_i	intermediate step pressures (psi)
p_j	arbitrary pressure in equation $r_{ij} = \frac{p_i}{p_j}$
q	heat generation (Btu/unit time)
r_B	radius at which F_B acts (inches)
r_M	radius at which F_M acts (inches)
r_{TC}	radius at which F_{TC} acts (inches)
r_{ij}	pressure ratio = p_i/p_j
r_{i1}, r_{i2}	pressure ratio defined by $\frac{p_i}{p_1}$ and $\frac{p_i}{p_2}$, respectively

t	thickness (inches)
t	radial depth of segment (inches)
u	axial thermal displacement (inches)
u_1	transverse seal ring displacement (inches)
u_2	transverse carrier displacement (inches)
u_n	dynamic seal ring transverse response to runner deformations α_n and ϵ_n (inches)
v	radial thermal displacement (inches)
υ	vena contracta coefficient (dimensionless)
w	flow rate (lb/sec)
$\bar{x}_c$	dimensionless center of pressure = $\frac{Xc}{b}$
x^*	centroid, x coordinates (inch)
x_f	center of pressure = $b\bar{x}_c$ (inches)
x^f	centroid, x coordinate (in)
x_1, x_2, x_3	rigid body displacements (inches)
y_f	distance from seal face to primary element centroid (inches)
y^f	centroid "Y" coordinate (inches)
y_1, y_2, y_3	force moment arms (inch)

Greek Symbols

α	seal tilt angle (radians)
α	coefficient of thermal expansion (in/in/°F)
α_n	dynamic seal ring angular response to runner deformation ϵ_n and δ_n
β_n	static seal ring angular response to seal ring deformation τ_n and η_n
δ	thermal radial mismatch (inches)
δ	initial transverse deformation of rotor surface (inches)
δ	bellows deflection (inches)
δ	carrier excursion (inches)
δ_b	radius increase due to thermal bowing (inches)
δ_c	centrifugal growth (inches)
δ_f	frequency amplitude (inches)
δ_n	dynamic seal ring transverse response (inches)
δ_n	nth component of dimensionless, initial transverse rotor deformation. (inches)
δ_t	differential growth due to temperature and material differences (inches)
ϵ	initial angular rotor deformation (radians)
ϵ_n	nth component of initial angular rotor deformation (inches)
τ	initial angular deformation of seal ring (radians)
τ_n	nth component of initial angular deformation of seal ring (inches)
θ	seal tilt angle due to restraining effect of OC springs (radians)
θ	angle of carrier rotation (radians)
ν	frequency (rad/sec)
ν_1, ν_2	critical system frequency (rad/sec)
ν_o	operating frequency (rad/sec)
ν_{n1}, ν_{n2}	natural frequencies of flexible seal ring (rad/sec)
λ_y	bearing compressibility number, $6\mu Vb/ph^2$
μ	viscosity (lb-sec/in^2)
μ_B	friction coefficient at seal face
μ_M	friction coefficient at journal
μ_{TC}	friction coefficient at thrust collar
μ_2	mass density of the upstream gas (lb-sec^2/in^4)
ξ	angular deflection of seal (radians)
$\rho, \rho_1, \rho_2 \ldots$	mass density (lb-sec^2/in^4)
σ_B	bending stress of C diaphragm (psi)
σ_t	direct stress of C diaphragm (psi)
ϕ	net angle between rotor and seal ring (radians)
ω	angular speed (rad/sec)
ω_n *	ratio of unit dynamic load to film stiffness (dimensionless)